

CR-184100

January 28, 1991

RI/RD 91-114

BLADE TIP RUBBING STRESS PREDICTION

FINAL REPORT

PREPARED FOR:

NASA-MARSHALL SPACE FLIGHT CENTER

CONTACT: NAS8-36361

**ORIGINAL CONTAINS
COLOR ILLUSTRATIONS**

(NASA-CR-184100) BLADE TIP RUBBING STRESS
PREDICTION Final Report (Rockwell
International Corp.) 172 p CSCL 13I

N91-18435

Unclass

G3/37 0332838



Rockwell International

Rocketdyne Division

6633 Canoga Avenue
Canoga Park, CA 91303



Rockwell International

Rocketdyne Division
6633 Canoga Avenue
Canoga Park, California 91304

BLADE TIP RUBBING STRESS PREDICTION

FINAL REPORT

PREPARED UNDER CONTRACT NAS8-36361
FOR GEORGE C. MARSHALL SPACE FLIGHT CENTER
MARSHALL SPACE FLIGHT CENTER, ALABAMA 35812

28 JANUARY 1991

PREPARED BY:

GARY DAVIS
TURBOMACHINERY STRUCTURAL
ANALYSIS

RAY CLOUGH
ADVANCED ROTATING
MACHINERY PROJECTS

APPROVED BY:

R.F. SUTTON
MANAGER, ADVANCED
ROTATING MACHINERY PROJECTS

A. CSOMOR
PROGRAM MANAGER

Table of Contents

FORWARD.....	i-1
ABSTRACT.....	i-2
List of Figures.....	i-3
List of Tables.....	i-7
1.0 INTRODUCTION.....	1.0-1
2.0 TECHNICAL DISCUSSION.....	2.1-1
2.1 ANALYTICAL MODEL.....	2.1-1
2.1.1 Parametric Analysis.....	2.1-2
2.1.1.1 Method of Solution.....	2.1-3
2.1.2 Discussion of Results.....	2.1-10
2.1.3 Conclusions Drawn from Model.....	2.1-12
2.2 EXPERIMENTAL VERIFICATION.....	2.2-1
2.2.1 Facility Description.....	2.2-1
2.2.2 Whirligig Tester.....	2.2-2
2.2.2.1 Bearing Preload System.....	2.2-2
2.2.2.2 Squeeze Film Dampers.....	2.2-2
2.2.2.3 Bearing Coolant and Lubrication System.....	2.2-3
2.2.2.4 Main Supports.....	2.2-3
2.2.2.5 Labrinth Seal.....	2.2-3
2.2.2.6 Slip Ring.....	2.2-3
2.2.3 Turbine Disk and Blades.....	2.2-4
2.2.4 Tip Seal Test Module.....	2.2-4
2.2.5 Test Article.....	2.2-5
2.2.6 Instrumentation.....	2.2-5
2.2.6.1 Whirlig Operations Monitoring Data.....	2.2-5
2.2.6.2 High-frequency Test Instrumentation.....	2.2-6
2.2.6.3 Turbine Blade Strain Gage Installation.....	2.2-6
2.3 TEST PROGRAM.....	2.3-1
2.3.1 Goal of Test.....	2.3-1
2.3.2 Test Procedure.....	2.3-2
2.3.2.1 Whirlig Operation.....	2.3-2
2.3.2.2 Test Module Operation.....	2.3-3
2.3.2.3 Test Plan.....	2.3-3
2.4 TEST RESULTS.....	2.4-1
2.4.1 Summary.....	2.4-1
2.4.2 Shaft Speed versus Time.....	2.4-1
2.4.3 Strain Gage Data Processing.....	2.4-1
2.4.4 Compressed Time-History Data.....	2.4-2
2.4.5 Strain Levels versus Speed.....	2.4-3
2.4.6 Expanded Time-History Data.....	2.4-3
2.4.7 Frequency Domain Data.....	2.4-4
2.4.8 Post Test Hardware Inspection.....	2.4-5
2.4.9 Correlation of Rub Inspection with Strain Data.....	2.4-6
2.4.10 Rub Angle.....	2.4-7

2.4.11 Comparison to SSME Hardware.....	2.4-7
2.4.12 Blade Damping.....	2.4-7
2.4.13 Blade Natural Frequencies.....	2.4-8
2.5 TEST/ANALYSIS CORRELATION.....	2.5-1
3.0 CONCLUSIONS AND RECOMMENDATIONS.....	3.0-1
3.1 CONCLUSIONS.....	3.0-1
3.2 RECOMMENDATIONS FOR FURTHER WORK.....	3.0-1

FOREWORD

Investigations of the problem of turbine blade cracking have not yielded completely satisfactory explanations of the phenomenon. One hypothesized cause is the rubbing of the turbine blade tips against the tip seals. This problem has not been fully investigated, and the current program constitutes an effort to examine the magnitude of stresses produced by blade tip rubbing, and to determine if tip rubbing is a likely contributor to blade cracking. This program was conducted for NASA Marshall Space Flight Center under Contract Number NAS8-36361.

The program was divided into two phases. In Phase I, the important parameters were defined and an analytical model of the rubbing of a turbine blade against its tip seal was created. In Phase II, a test apparatus was designed and constructed to simulate the rubbing condition in a turbine, and to gather strain gage data to confirm the predicted blade strain response. The test was conducted using an existing dynamic diagnostic device, commonly known as the "whirligig", configured to use an SSME HPFTP turbine disk and blades. A bolt-on module designed and built expressly for this test program forced a simulated tip-seal against the tips of the spinning turbine blades. Strain gage data was acquired from gages applied to the surface of the blades, and this data was compared to the analytical predictions.

ABSTRACT

An analytical model was constructed to predict the magnitude of stresses produced by rubbing a turbine blade against its tip seal. This model used a linearized approach to the problem, after a parametric study found that the non-linear effects were of insignificant magnitude. The important parameters input to the model were: the arc through which rubbing occurs, the turbine rotor speed, normal force exerted on the blade, and the rubbing coefficient of friction. Since it is not possible to exactly specify some of these parameters, values were entered into the model which bracket likely values.

The form of the forcing function was another variable which was impossible to specify precisely, but the assumption of a half-sine wave with a period equal to the duration of the rub was taken as realistic assumption.

The analytical model predicted resonances between harmonics of the forcing function decomposition and known harmonics of the blade. Thus it seemed probable that blade tip rubbing could be at least a contributor to the blade-cracking phenomenon.

A full-scale, full-speed test conducted on the SSME HPFTP Whirligig Tester was conducted at speeds between 33,000 and 28,000 RPM to confirm analytical predictions.

List of Figures

Fig 2.1-1. SSME HPFTP Turbine Blade Finite Element Model.....	2.1-16
Fig 2.1-2. Half-sine Wave Forcing Function.....	2.1-17
Fig 2.1-3. SSME HPFTP Turbine Blade Campbell Diagram....	2.1-18
Fig 2.1-4. Stress Time History of Excited Blade.....	2.1-19
Fig 2.1-5. Space Plot.....	2.1-20
Fig 2.1-6. Displacement vs Shaft Speed.....	2.1-21
Fig 2.1-7. Displacement vs Shaft Speed.....	2.1-21
Fig 2.1-8. Displacement vs Shaft Speed.....	2.1-21
Fig 2.1-9. Fourier Transform of Forcing Function.....	2.1-22
Fig 2.1-10. Campbell Diagram Showing Resonance with Forcing Function.....	2.1-23
Fig 2.1-11. Amplitudes of Resonant Harmonics vs Contact Arc.....	2.1-24
Fig 2.1-12. Critical Speed/Arc Summary.....	2.1-25
Fig 2.2-1. Cross-section of SSME HPFTP Whirligig.....	2.2-9
Fig 2.2-2. Overview of Whirligig Plumbing System.....	2.2-10
Fig 2.2-3. Detail of Whirligig Plumbing System.....	2.2-11
Fig 2.2-4. Schematic Diagram of Test Module Mounted to Whirligig Base.....	2.2-12
Fig 2.2-5. Test Module Mounted to Whirligig Tester.....	2.2-13
Fig 2.2-6. Test Module Mounted to Whirligig Tester.....	2.2-14
Fig 2.2-7. Tip Rubbing Test Article.....	2.2-15
Fig 2.2-8. Strain Gage Position on Blade.....	2.2-16
Fig 2.2-9. Positions of Strain Gaged Blades in Wheel....	2.2-17
Fig 2.2-10. Wired Disk.....	2.2-18
Fig 2.2-11. Disk Showing Fir-tree Solder Tabs.....	2.2-19
Fig 2.2-12. Disk Showing Solder Tabs on Inner Curvic Boss.....	2.2-20
Fig 2.2-13. Strain Gage Applied to Turbine Blade.....	2.2-21
Fig 2.2-14. Routing Lead Wire Through Grind-out in Platform.....	2.2-22
Fig 2.2-15. Jumper Wire Connecting Gage to Wired Wheel.....	2.2-23
Fig 2.2-16. Assembled Instrumented HPFTP 1st Stage Disk.....	2.2-24
Fig 2.3-1. Test Module Control Panel.....	2.3-7
Fig 2.3-2. Seeking the Initiation of Rubbing Contact....	2.3-8
Fig 2.3-3. Dynamic Calibration Test Time-Speed Profile.....	2.3-9
Fig 2.3-4. Rubbing Test Time-Speed Profile.....	2.3-10
Fig 2.4-1. Speed Time-History.....	2.4-13
Fig 2.4-2. Compressed Time-History; 32740 Rpm.....	2.4-14
Fig 2.4-3. Compressed Time-History; 32740 Rpm.....	2.4-15
Fig 2.4-4. Strain Gage 2 Time-History vs. Speed.....	2.4-16
Fig 2.4-5. Strain Range During Rubbing; 32040 Rpm.....	2.4-17

Fig 2.4-6. Strain Range vs. Speed.....	2.4-18
Fig 2.4-7. Strain Range vs. Speed.....	2.4-19
Fig 2.4-8. Strain Range vs. Speed.....	2.4-20
Fig 2.4-9. Strain Time-History; 32740 Rpm.....	2.4-21
Fig 2.4-10. Strain Time-History; 32160 Rpm.....	2.4-22
Fig 2.4-11. Strain Time-History; 28530 Rpm.....	2.4-23
Fig 2.4-12. Strain Time-History; 31630 Rpm.....	2.4-24
Fig 2.4-13. Strain Time-History; 32040 Rpm.....	2.4-25
Fig 2.4-14. Strain Time-History; 31540 Rpm.....	2.4-26
Fig 2.4-15. Strain Time-History; 31540 Rpm.....	2.4-27
Fig 2.4-16. Strain Time-History; 32740 Rpm.....	2.4-28
Fig 2.4-17. Strain Time-History; 32740 Rpm.....	2.4-29
Fig 2.4-18. Tip Seal Accelerometer Time History - 30060 Rpm.....	2.4-30
Fig 2.4-19. Tip Seal Accelerometer Time History - 31540 Rpm.....	2.4-31
Fig 2.4-20. Tip Seal Accelerometer Time History - 32030 Rpm.....	2.4-32
Fig 2.4-21. Strain PSD During Rubbing - SG #2 - 0 to 5 Khz - 32160 Rpm.....	2.4-33
Fig 2.4-22. Strain PSD During Rubbing - SG #4 - 0 to 5 Khz - 32160 Rpm.....	2.4-34
Fig 2.4-23. Strain PSD During Rubbing - SG #5 - 0 to 5 Khz - 32160 Rpm.....	2.4-35
Fig 2.4-24. Strain PSD During Rubbing - SG #6 - 0 to 5 Khz - 32160 Rpm.....	2.4-36
Fig 2.4-25. Strain PSD During Rubbing - SG #60 - 0 to 5 Khz - 32160 Rpm.....	2.4-37
Fig 2.4-26. Strain PSD During Rubbing - SG #2 - 0 to 5 Khz - 31030 Rpm.....	2.4-38
Fig 2.4-27. Strain PSD During Rubbing - SG #4 - 0 to 5 Khz - 31030 Rpm.....	2.4-39
Fig 2.4-28. Strain PSD During Rubbing - SG #5 - 0 to 5 Khz - 31030 Rpm.....	2.4-40
Fig 2.4-29. Strain PSD During Rubbing - SG #6 - 0 to 5 Khz - 31030 Rpm.....	2.4-41
Fig 2.4-30. Strain PSD During Rubbing - SG #60 - 0 to 5 Khz - 31030 Rpm.....	2.4-42
Fig 2.4-31. Strain PSD During Rubbing - SG #2 - 0 to 5 Khz - 30560 Rpm.....	2.4-43
Fig 2.4-32. Strain PSD During Rubbing - SG #4 - 0 to 5 Khz - 30560 Rpm.....	2.4-44
Fig 2.4-33. Strain PSD During Rubbing - SG #5 - 0 to 5 Khz - 30560 Rpm.....	2.4-45
Fig 2.4-34. Strain PSD During Rubbing - SG #6 - 0 to 5 Khz - 30560 Rpm.....	2.4-46
Fig 2.4-35. Strain PSD During Rubbing - SG #60 - 0 to 5 Khz - 30560 Rpm.....	2.4-47
Fig 2.4-36. Strain PSD During Rubbing - SG #2 - 0 to 5 Khz - 30060 Rpm.....	2.4-48

Fig 2.4-37. Strain PSD During Rubbing - SG #4 - 0 to 5 Khz - 30060 Rpm.....	2.4-49
Fig 2.4-38. Strain PSD During Rubbing - SG #5 - 0 to 5 Khz - 30060 Rpm.....	2.4-50
Fig 2.4-39. Strain PSD During Rubbing - SG #6 - 0 to 5 Khz - 30060 Rpm.....	2.4-51
Fig 2.4-40. Strain PSD During Rubbing - SG #60 - 0 to 5 Khz - 30060 Rpm.....	2.4-52
Fig 2.4-41. Test Article Accelerometer PSD During Rubbing - 0 to 5 Khz.....	2.4-53
Fig 2.4-42. Test Article Accelerometer PSD During Rubbing - 0 to 5 Khz.....	2.4-54
Fig 2.4-43. Test Article Accelerometer PSD During Rubbing - 0 to 5 Khz.....	2.4-55
Fig 2.4-44. Test Article Accelerometer PSD During Rubbing - 0 to 5 Khz.....	2.4-56
Fig 2.4-45. Strain PSD During Rubbing - SG #2 - 0 to 20 Khz - 32160 Rpm.....	2.4-57
Fig 2.4-46. Strain PSD During Rubbing - SG #4 - 0 to 20 Khz - 32160 Rpm.....	2.4-58
Fig 2.4-47. Strain PSD During Rubbing - SG #5 - 0 to 20 Khz - 32160 Rpm.....	2.4-59
Fig 2.4-48. Strain PSD During Rubbing - SG #6 - 0 to 20 Khz - 32160 Rpm.....	2.4-60
Fig 2.4-49. Strain PSD During Rubbing - SG #60 - 0 to 20 Khz - 32160 Rpm.....	2.4-61
Fig 2.4-50. Strain PSD During Rubbing - SG #2 - 0 to 20 Khz - 31030 Rpm.....	2.4-62
Fig 2.4-51. Strain PSD During Rubbing - SG #4 - 0 to 20 Khz - 31030 Rpm.....	2.4-63
Fig 2.4-52. Strain PSD During Rubbing - SG #5 - 0 to 20 Khz - 31030 Rpm.....	2.4-64
Fig 2.4-53. Strain PSD During Rubbing - SG #6 - 0 to 20 Khz - 31030 Rpm.....	2.4-65
Fig 2.4-54. Strain PSD During Rubbing - SG #60 - 0 to 20 Khz - 31030 Rpm.....	2.4-66
Fig 2.4-55. Strain PSD During Rubbing - SG #2 - 0 to 20 Khz - 30560 Rpm.....	2.4-67
Fig 2.4-56. Strain PSD During Rubbing - SG #4 - 0 to 20 Khz - 30560 Rpm.....	2.4-68
Fig 2.4-57. Strain PSD During Rubbing - SG #5 - 0 to 20 Khz - 30560 Rpm.....	2.4-69
Fig 2.4-58. Strain PSD During Rubbing - SG #6 - 0 to 20 Khz - 30560 Rpm.....	2.4-70
Fig 2.4-59. Strain PSD During Rubbing - SG #60 - 0 to 20 Khz - 30560 Rpm.....	2.4-71
Fig 2.4-60. Strain PSD During Rubbing - SG #2 - 0 to 20 Khz - 30060 Rpm.....	2.4-72
Fig 2.4-61. Strain PSD During Rubbing - SG #4 - 0 to 20 Khz - 30060 Rpm.....	2.4-73

Fig 2.4-62.	Strain PSD During Rubbing - SG #5 - 0 to 20 Khz - 30060 Rpm.....	2.4-74
Fig 2.4-63.	Strain PSD During Rubbing - SG #6 - 0 to 20 Khz - 30060 Rpm.....	2.4-75
Fig 2.4-64.	Strain PSD During Rubbing - SG #60 - 0 to 20 Khz - 30060 Rpm.....	2.4-76
Fig 2.4-65.	Test Article Accelerometer PSD During Rubbing - 0 to 20 Khz.....	2.4-77
Fig 2.4-66.	Test Article Accelerometer PSD During Rubbing - 0 to 20 Khz.....	2.4-78
Fig 2.4-67.	Test Article Accelerometer PSD During Rubbing - 0 to 20 Khz.....	2.4-79
Fig 2.4-68.	Test Article Accelerometer PSD During Rubbing - 0 to 20 Khz.....	2.4-80
Fig 2.4-69.	Blade Tip Rub Marks.....	2.4-81
Fig 2.4-70.	Comparison of Test Hardware Rub Pattern with SSME Rub Pattern.....	2.4-82
Fig 2.4-71.	Comparison of Test Hardware Rub Pattern with SSME Rub Pattern.....	2.4-83
Fig 2.4-72.	Lead-Wire Debonding.....	2.4-84
Fig 2.4-73.	Correlation of Rubbing Inspection with Strain Data.....	2.4-85
Fig 2.5-1.	Stress Time-History Prediction - 5 lb. Peak Half-Sine Pulse.....	2.5-3
Fig 2.5-2.	Stress Time-History Prediction - Typical Response During Several Rub Cycles.....	2.5-4

List of Tables

Table 2.1-1. Significant Parameters.....	2.1-14
Table 2.1-2. Critical Speed and Contact Arc Combinations	2.1-15
Table 2.1-3. Normalized Radial Stress at Shank Root.....	2.1-15
Table 2.2-1. Whirligig & Test Module Instrumentation List	2.2-8
Table 2.3-1. Rotor Growth with Rotational Speed.....	2.3-6
Table 2.4-1. Shaft Speed Time-History.....	2.4-9
Table 2.4-2. Strain Range During Rubbing; 32040 Rpm.....	2.4-11
Table 2.4-3. Results of Blade Tip Inspection.....	2.4-12

1.0 INTRODUCTION

The stresses on a turbine blade are the result of several loads acting upon it. Of primary importance are the loads due to the centrifugal force and the mainstream turbine gases. Superimposed on these forces are alternating forces caused by blade wakes, coolant jets, and intermittent rubbing of the blades against the tip seals. Tip seal rubbing can be the result of intentionally small tip clearances that require rubbing to "wear in" a groove in the seal or the contact may result from radial movement of the rotor due to asymmetrical radial loading.

Blade cracking encountered in the SSME high pressure turbines revealed a need to establish the significance of tip seal rubbing on turbine blade stresses to gain the ability to analytically predict the effects of blade tip rubbing on turbine life and performance.

To accomplish this goal, it was necessary to generate an analytical model of blade tip seal rubbing to define the blade dynamics and associated stress levels, and subsequently to validate the model by conducting tests on turbine hardware.

The analytical phase of this program was aimed at understanding the parameters involved in blade tip rubbing. Initially, the problem was believed to be non-linear, but the parametric analysis led to the conclusion that the magnitude of the non-linear effects was insignificant compared to the magnitude of the linear effects, so the solution was simplified. The analysis was conducted using the SSME HPFTP first stage turbine blades, for which substantial analytical tools already existed.

The experimental phase of this program was aimed at verifying the analysis by inducing blade tip rubbing stresses in an SSME high pressure fuel turbopump first stage turbine rotor spinning at a range of speeds found in the SSME engine. An existing dynamic diagnostic test device, known as the "whirligig", was modified to allow simulation of tip seal rubbing.

Both phases of this program were designed to isolate the blade tip rubbing stresses from the other stresses acting on the turbine rotor, and with this in mind the experimental phase was conducted in a partial vacuum to eliminate the aerodynamic and thermal forces associated with actual turbine operation. The full picture of turbine blade stress is not lost, however, since superposition of the stresses from the various sources will give a realistic result.

2.0 TECHNICAL DISCUSSION

2.1 ANALYTICAL MODEL

To investigate the phenomenon of intermittent rubbing of a turbine blade against a tip seal, an analytical model was developed which utilized a finite element representation of the turbine blade. The model, pictured in Figure 2.1-1, addressed a single blade fixed at the shank root and free at the tip. The boundary conditions at the root simulate the fixity of the blade due the centrifugal loads acting through the fir tree during high speed operation. Since the flexibility of the disk actually admits motion of the blade shank, the assumption of fixity results in slight increases in both natural frequencies and stresses. However, these effects are inconsequential in regard to understanding the dynamic behavior of the blade due to tip rubbing.

To represent the rotation of a rotor about an eccentric axis, it was assumed that the blade would be in contact with the tip seal over a well-defined arc once per revolution. Only tangential friction effects were considered; therefore a tangential load was applied to the blade tip once per revolution. This load was assumed to act at a single point on the blade. The amplitude of the forcing function was set equal to the product of the normal load and the friction coefficient. The friction coefficient was constant, however the normal load was assumed to vary as a half sine wave over the duration of the rub, as shown in Figure 2.1-2. This can be expressed as:

$$F(t) = \mu N(t) = \begin{cases} \mu N \sin \frac{\pi t}{\tau_R} & , 0 < t < \tau_R \\ 0 & , \tau_R < t < \tau_R + \tau_F \end{cases} \quad (1)$$

where $F(t)$ is the forcing function, μ is the friction coefficient, $N(t)$ is the normal force τ_R is the period during which rubbing occurs, and τ_F is the period during which the blade vibrates freely. This is an entirely reasonable form for the forcing function, given the kinematics of rotation about an eccentric axis.

It was originally postulated that the blade might display non-linear behavior due to sticking of the blade tip to the seal. The preliminary analysis showed, however, that the blade tip speed due to rotation is approximately three orders of magnitude greater than that due to vibration in the first tangential bending mode, so it was concluded that the stick-slip behavior did not in fact occur. This was a very dramatic simplification in the model, since the model was now a purely linear one.

2.1.1 Parametric Analysis

Four parameters were expected to have a significant effect on the blade response: normal force, friction coefficient, shaft speed, and length of contact arc. Since it was difficult to specify exact values of these parameters, it was deemed preferable to determine the response over a range of values and then to rely on future empirical results to assist in pinpointing their actual magnitudes. Ranges for these parameters are presented in Table 2.1-1, and reflect experience with dynamic simulations of the rotor as well as known operational parameters of the pump.

A typical response analysis consisted of calculation of the steady-state solution for a specific normal force, friction coefficient, contact arc, turbine speed and point of application of the rubbing force. Since the problem was linear, linear scaling of the solutions allowed the number of cases run to be reduced. For example the response results for a given friction coefficient and normal force were linearly scaled to different values of friction coefficient and normal force. The sensitivity of the response to the point of application of the load was investigated by forcing the blade tip near the center of the airfoil, the leading edge and the trailing edge. Finally, turbine speed and contact arc were varied by changing the frequency and duration of the forcing function.

2.1.1.1 Method of Solution. The analytical and solution method employed is based on the well known modal analysis technique, and therefore the natural frequencies and mode shapes of the component to be analyzed are required as input to the program. Thus, the relationship between the finite element model needed to extract the modal characteristics and the integration program is noted. Then, the solution technique is presented.

Based on strain energy and kinetic energy considerations, the finite element formulation develops the undamped, homogeneous equations of motion in terms of physical coordinates:

$$\underline{M} \ddot{\underline{x}} + \underline{K} \underline{x} = \underline{0} \quad (2)$$

where:

\underline{M} = mass matrix

\underline{x} = displacement vector in terms of physical coordinates, and

\underline{K} = stiffness matrix.

Assuming a harmonic solution for $\underline{x}(t)$,

$$\underline{x}(t) = \underline{v} e^{i\omega t} \quad (3)$$

where

\underline{v} = eigenvector (mode shape),

$i = \{-1\}^{.5}$, and

ω = circular frequency (square root of the eigenvalue).

This results in the eigenvalue problem

$$\left\{ \begin{array}{c} \underline{K} \\ \underline{\quad} \end{array} - \omega^2 \begin{array}{c} \underline{M} \\ \underline{\quad} \end{array} \right\} \underline{v} = \underline{0} \quad (4)$$

For nontrivial solutions of \underline{v} , the eigenvalues must satisfy the characteristic equation

$$\det \left\{ \begin{array}{c} \underline{K} \\ \underline{\quad} \end{array} - \omega^2 \begin{array}{c} \underline{M} \\ \underline{\quad} \end{array} \right\} = \underline{0} \quad (5)$$

In this case, the stiffness and mass characteristics of the blade were obtained from an existing, in-house, three-dimensional finite element model (ANSYS code) of the HPFTP first-stage turbine blade, shown in Figure 2.1-1. To lessen the time and cost of the modal extraction, a reduced subspace iteration technique was used. The master degrees of freedom were automatically selected by the program. This method produced results which correlated well with whirligig data obtained from previous programs.

The computed mode shapes were then used to uncouple the equations of motion through the coordinate transformation:

$$\underline{x}(t) = \underline{\Phi} \underline{\eta}(t) \quad (6)$$

where $\underline{\Phi}$ = modal matrix, and

$\underline{\eta}(t)$ = displacement vector in terms of principal coordinates, rather than in physical space.

Substituting 6 into 2 and considering the forced response of the assumed viscously damped system, the equation of motion becomes, in transform space

$$\underline{M} \underline{\Phi} \underline{\ddot{\eta}} + \underline{c} \underline{\Phi} \underline{\dot{\eta}} + \underline{K} \underline{\Phi} \underline{\eta} = \underline{F} \quad (7)$$

where \underline{c} = damping matrix, and

\underline{F} = forcing function.

Premultiplying (7) by the transpose of the modal matrix gives the result

$$\underline{\Phi}^T \underline{M} \underline{\Phi} \dot{\underline{\eta}} + \underline{\Phi}^T \underline{C} \underline{\Phi} \dot{\underline{\eta}} + \underline{\Phi}^T \underline{K} \underline{\Phi} = \underline{\Phi}^T \underline{F} \quad (8)$$

Due to the adjoint property of the modal matrix, this simplifies significantly. The eigenvectors are normalized by the mass matrix; hence, all modal masses are equal to unity:

$$\underline{\Phi}^T \underline{M} \underline{\Phi} = \underline{I} \quad (9)$$

where \underline{I} is the identity matrix.

Rather than specify a discrete damping value associated with the friction damper installed between each blade, a gross modal damping value was assumed. This requires the assumption that the damping matrix is uncoupled by the transformation to principal coordinate space. The resultant modal damping matrix is then diagonal:

$$\underline{\Phi}^T \underline{C} \underline{\Phi} = \begin{bmatrix} 2 \zeta_n \omega_n \end{bmatrix} \quad (10)$$

where the matrix is diagonal and ζ_n is the damping ratio for the nth mode.

In addition, the stiffness matrix is transformed to a diagonal matrix whose terms are the squares of the undamped natural frequencies:

$$\underline{\Phi}^T \underline{K} \underline{\Phi} = \underline{\lambda} = \begin{bmatrix} \omega_n^2 \end{bmatrix} \quad (11)$$

Finally the physical force is transformed to a modal force:

$$\underline{\Phi}^T \underline{F} = \underline{P} \quad (12)$$

Substituting equations (9) through (12) into (8), the uncoupled equations of motion are obtained in terms of principal coordinate space:

$$\ddot{\underline{\eta}} + \left[2\zeta_n \omega_n \right] \dot{\underline{\eta}} + \underline{\Lambda} \underline{\eta} = \underline{P} \quad (13)$$

Due to the low damping, approximately 0.01 to 0.02, it is possible to use the undamped rather than the damped natural frequencies.

It should also be noted that although the eigenvectors extracted by the ANSYS code include components corresponding to each master degree of freedom, computational costs can be greatly reduced by considering only the degrees of freedom and modes of primary interest. Thus the number of physical coordinates, ie. the dimension of the vector $x(t)$, may be reduced to include only those required to describe the motion and applied loads at the blade tip, and consider only the eigenvector components corresponding to these degrees of freedom. In addition, review of the Campbell diagram shown as Figure 2.1-3 indicates that only the first six blade modes lie near the pump operating range; consequently, only these modes need to be considered, further simplifying the problem and reducing the solution time.

For each mode to be considered, there is an equation of motion in terms of its corresponding principal coordinates as derived from equation (13):

$$\ddot{\eta}_n + 2\zeta_n \omega_n \dot{\eta}_n + \omega_n^2 \eta_n = P_n \quad (14)$$

where

$n = 1, 2, \dots$, number of modes considered.

The n equations (ie eq 14) are then solved separately using the central difference method. In this method, the acceleration at time step "t" is given by:

$$\ddot{\eta}^t = \frac{1}{(\Delta t)^2} \left[\eta^{t-\Delta t} - 2\eta^t + \eta^{t+\Delta t} \right] \quad (15)$$

The velocity is given by:

$$\dot{\eta}^t = \frac{1}{2\Delta t} \left[\eta^{t+\Delta t} - \eta^{t-\Delta t} \right] \quad (16)$$

Substituting (15) and (16) into the equation of motion (14), and solving for $\eta^{t+\Delta t}$, the position at time step $t+\Delta t$,

$$\eta^{t+\Delta t} = \left\{ \frac{1}{(\Delta t)^2} + \frac{\zeta\omega}{\Delta t} \right\}^{-1} * \left[p^t - \left\{ \omega^2 - \frac{2}{(\Delta t)^2} \right\} \eta^t - \left\{ \frac{1}{(\Delta t)^2} - \frac{\zeta\omega}{\Delta t} \right\} \eta^{t-\Delta t} \right] \quad (17)$$

Substituting the result of (17) into (15) and (16), the acceleration and velocity from the preceding time step, i.e. at time t , may be calculated.

Note that the solution for the displacement after the first time step requires a special initial condition for $\eta^{-\Delta t}$. The initial condition used was:

$$\eta^{-\Delta t} = \eta^0 - \Delta t \dot{\eta}^0 + \frac{(\Delta t)^2}{2} \ddot{\eta}^0 \quad (18)$$

The initial displacement and velocity is to be specified, while the acceleration is determined by evaluating equation (14) at time $t = 0$.

Although the central difference method is conditionally stable, numerical difficulties can be easily avoided. The

requirement for stability is merely that the maximum time step be less than or equal to the minimum period among the modes used in the solution divided by pi:

$$\Delta t_{\max} \leq T_{\min} / \pi \quad (19)$$

Since only the first few modes are considered, the maximum time step is on the order of 10^{-6} seconds. It should be noted that this is not an unusually small time step, given the high-frequency blade oscillations. Consequently, the solution is not prohibitively expensive.

Once the modal response is known, equation (6) may be used to transform back from principal coordinates to physical coordinates. Similarly, the stress time history may be obtained from:

$$\underline{\sigma} = \begin{bmatrix} \sigma \end{bmatrix} \underline{\eta}(t) \quad (20)$$

where $\underline{\sigma}$ = stress vector, and

$$\begin{bmatrix} \sigma \end{bmatrix} = \text{modal stress matrix.}$$

Although the displacement and stress time histories provide useful information, comparison of analytical and experimental results are primarily based upon the frequency content and RMS time history of the response. Therefore, the program contains post-processing routines which calculate the necessary output.

The fast Fourier transform is used to determine the frequency content of the displacement and stress time histories. This is a discretization of the continuous Fourier transform:

$$X(f) = \int_0^T x(t) e^{-i2\pi ft} dt \quad (21)$$

where $X(f)$ = response in the frequency domain,
 $x(t)$ = response in the time domain for
 $0 \leq t \leq T$, and

The inverse transform is given by:

$$x(t) = \int_0^T A(f) e^{i2\pi ft} df \quad (22)$$

where the Fourier coefficients are functions of the frequency and are obtained from:

$$A(f) = \frac{1}{2\pi} \int_0^T x(t) e^{-i2\pi ft} dt \quad (23)$$

Subroutines taken from the International Mathematical and Statistical Library (IMSL) compute the integral on the right-hand side of equation (21). The coefficients are then plotted as harmonics of the fundamental frequency, which is determined from the frequency of the shaft rotation:

$$f_f = \frac{\text{shaft speed (RPM)}}{60 \text{ sec/min}} \quad (24)$$

Using a similar concept, the RMS time histories are also computed by discretization of an integral:

$$x_{\text{RMS}} = \left\{ \frac{1}{T} \int_0^T [x(t)]^2 dt \right\}^{\frac{1}{2}} \quad (25)$$

where

x_{RMS} = the RMS response for $0 \leq t \leq T$,
 $x(t)$ = response time history over $0 \leq t \leq T$, and
 T = time period over which RMS value is computed,
 and is equal to the time for one revolution.

Since the Fourier transform and the RMS time average apply only to stationary time histories, the program uses them only in the evaluation of the steady-state response.

2.1.2 Discussion of Results from Model

The most significant results obtained from the linear parametric analysis were the discoveries of critical speeds and contact arcs which maximized the response of the blade. In addition, it was found that regardless of whether the tangential friction force was applied to the blade tip near the center of the airfoil chord, or at the leading or trailing edge, the blade primarily responded in the lowest bending mode. Before discussing the causes for the occurrence of critical speeds and contact arcs, it will be instructive to consider the general aspects of the blade behavior in the time domain. Then the problem will be characterized in the frequency domain, yielding further insight into the response.

To begin, consider the behavior of a single blade as it moves through several revolutions of the turbine disk. This is shown in Figure 2.1-4 which illustrates a typical time history of stress in the root region of the blade. The time between peak stresses corresponds to one revolution of the disk. For a given revolution, the maximum stress occurs at the end of the contact arc, because the friction load causes the blade to deflect. At the end of the contact interval, the blade is released and it then experiences free, damped vibration for the remainder of the revolution. As can be seen from the figure, the blade response during the time of free vibration is a function of the damping ratio which was chosen as 0.01 throughout this analysis. An alternate method of showing the motion is with a state space plot presented in Figure 2.1-5. This graph, which is plotted for a single revolution of the turbine, clearly shows the disturbance from equilibrium due to rubbing and the subsequent damped response.

Since the blade is subjected to a periodic load, it is expected that certain frequencies might excite a resonant condition. The frequency content of the forcing function is dependent upon the shaft speed and length of the contact arc; hence, there should be certain critical speeds and contact at which the blade response is maximized. The existence of critical speeds is verified by the plots of steady-state rms blade tip displacement versus shaft speed presented in Figures 2.1-6 through 2.1-8. The friction coefficient and magnitude of the normal load are identical in all cases, however the contact arc varies from 10 degrees to 30 degrees. In each graph, it is evident that extreme displacements occur at 29500 RPM, 32500 RPM, and at 36000 RPM. Thus, for each contact arc, the blade response displays the same dependence on speed. Similarly, at a given speed, the amplitude of the

response is dependent upon the contact arc. This suggests the existence not only of critical speeds, but also of critical contact arcs, and provides motivation for further investigation into these observed patterns.

To explain the occurrence of the critical speeds, it is necessary to consider the frequency spectrum of the forcing function. Recall that the time history of the forcing function was shown in Figure 2.1-2 for one complete revolution of the shaft. Expressing the forcing function as a Fourier series and plotting the magnitude of the various Fourier coefficients as a function of harmonic number results in the plot of Figure 2.1-9. The harmonic numbers should be interpreted as multiples of the pump speed, thus the horizontal axis of Figure 2.1-9 is actually a frequency axis. This representation of the force reveals a broad band of frequency content. Consequently, when the speed is such that the frequency of one force harmonic is equal to the frequency of a blade mode then a resonant condition occurs. This is clearly presented in the Campbell diagram of Figure 2.1-10 which indicates the speeds at which interferences occur between various harmonics of the forcing function and the first mode of the blade. Clearly the ninth, tenth, and eleventh harmonics excite this mode at speeds of 36000, 32400, and 29455 RPM, respectively. Therefore, the critical speeds are simply those at which a resonant condition exists between one harmonic of the forcing function and the first bending mode of the blade.

Comparison of Figures 2.1-6 through 2.1-9 indicates that although the dependence of the response on speed is identical in all three cases, the amplitude of the displacement varies with the contact arc. To investigate this observation, it is instructive to use the Fourier series representation of the forcing function and vary the length of the contact arc. Thus the magnitude of each harmonic may be expressed as a function of the contact arc as shown in Figure 2.1-11. Here only the ninth, tenth, and eleventh harmonics are presented because they were identified as causing interferences within the operating range of the turbine. It is clear from the figure that there is a unique angle for which each harmonic attains its maximum value. This explains the difference in blade response for different contact arcs but identical speeds. Each harmonic of the forcing function is maximized by a certain contact arc, therefore there is a specific contact arc which yields the greatest response at each critical speed. These combinations, which can be retrieved from Figures 2.1-10 and 2.1-11, are listed in Table 2.1-2. It should be noted that the critical contact arcs are within the range of wear observed in the SSME first-stage tip seal.

In addition to considering different speeds and contact arcs, the sensitivity of the response to the location of the applied load was also investigated. Separate response analyses were completed with the friction force applied at the airfoil tip near the leading edge, midchord, and trailing edge locations. A summary of the results are presented in Table 2.1-3 which shows that the highest stresses were found when forcing the blade at the trailing edge.

The stresses presented in Table 2.1-3 have been normalized to show the blade response due to a peak friction force of 1 pound. Using the maximum stress given in this table of 220 psi it is easy to calculate the friction force necessary to create a given alternating stress. For example an alternating stress of 5000 psi rms would require a peak friction force of 22.7 lbs. Assuming a coefficient of friction of 0.2 would translate this into 114 pounds of normal force which is entirely within the expected range. Therefore, significant stresses can be generated by blade tip rubbing.

In summary, the turbine blade parametric analysis provided several interesting results. The significant dependence of the maximum steady-state response upon both speed and contact arc is summarized by the surface shown in Figure 2.1-12. This plot provides a qualitative representation of the effects of shaft speed and contact arc, and clearly illustrates the existence of critical conditions. The speed axis shows the frequency response of the blade while the contact arc axis tells how the magnitude of the driving force varies. Critical speeds and/or contact arcs occur when these variables produce a maximum response as shown in the figure.

2.1.3 Conclusions Drawn from Model

General conclusions which can be drawn from the analysis are that, for a turbine blade under tip rubbing excitation, there exist distinct critical speeds at which the dynamic response of the blade is maximized. Furthermore, at each speed, a critical contact arc exists which maximizes the response of the blade. The overall maximum response occurs at the point where the critical speed and critical contact arc occur simultaneously.

The parametric analysis also provided information for specific conclusions regarding the SSME turbine blade. From the results of the analysis, three critical operating points represent the speed at which resonance occurs between the applied friction load and the first bending mode of the blade. In addition, three critical contact arcs which

maximize the amplitudes of the resonant force harmonics were identified within the range of observed wear in the SSME first stage tip seal. Finally the rms alternating stresses at the blade root were found to be significant depending upon the value of the friction force. No measurements of friction force have been made, however the analysis shows that sizable stresses can be produced with reasonable values of friction force.

Parametric Analysis

Parameter	Minimum	Maximum	Increment
Normal Force	0	200 lb	50 lb
Friction Coefficient	0.1	0.3	0.1
Shaft Speed	28,000 rpm	38,000 rpm	1000 rpm
Contact Arc	10°	30°	10°

- 1 percent modal damping
- Single-point contact at blade tip
- Half sine wave forcing function during contact

2.1-14



Rockwell International
Rocketdyne Division

Table 2.1-1 Significant Parameters

87C-4-9227
2143m/3

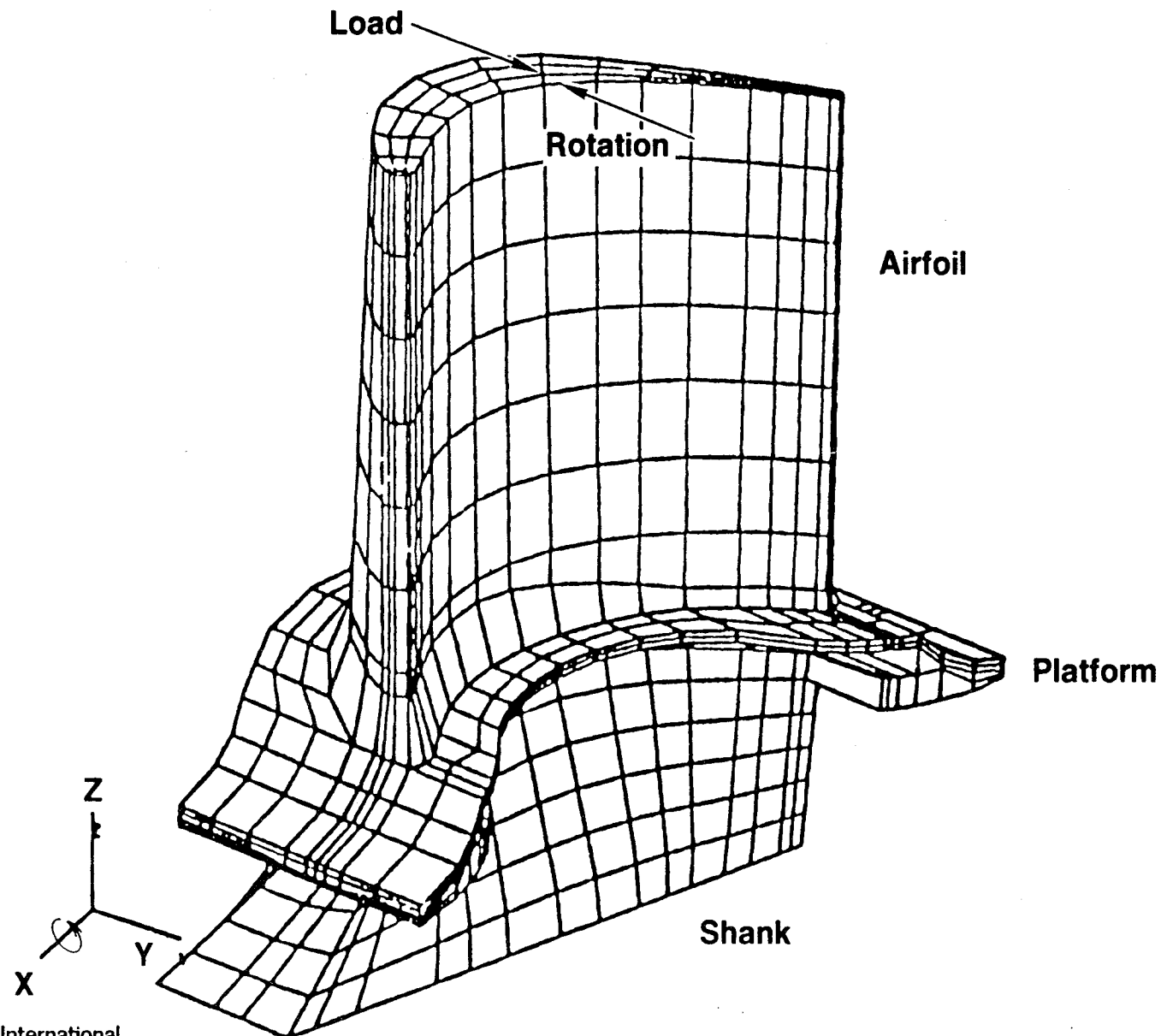
Table 2.1-2. Critical Speed and Contact Arc Combinations

Resonant Harmonic	Critical Speed (rpm)	Critical Contact Arc (deg)
9	36,000	27.3
10	32,400	24.6
11	29,455	22.4

Table 2.1-3. Normalized Radial Stress at Shank Root (1 lb peak friction force)

Arc (deg)	Force Applied	Steady State rms Stress (psi)		
		29,500 rpm	32,500 rpm	36,000 rpm
10	TE	128	129	125
10	MC	102	106	100
10	LE	97	101	94
20	TE	190	208	205
20	MC	148	170	167
20	LE	145	160	157
30	TE	170	206	220
30	MC	140	169	182
30	LE	130	158	170
TE = trailing edge; MC = midchord LE = leading edge				

HPFTP 1st Stage Turbine Blade Finite Element Model



2.1-16



Rockwell International
Rockeddyne Division

Figure 2.1-1 SSME HPFTP Turbine Blade Finite Element Model

87C-4-9328
2143m/18

Friction Force Time – History

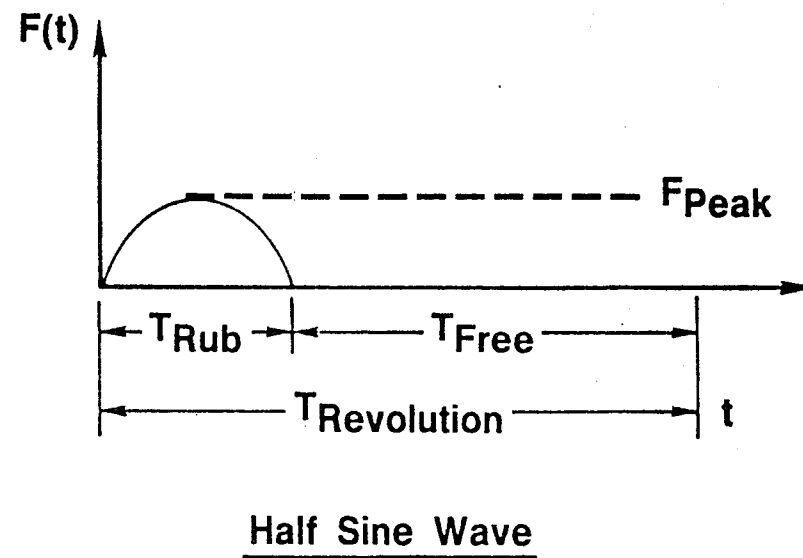


Figure 2.1-2 Half-sine Wave Forcing Function

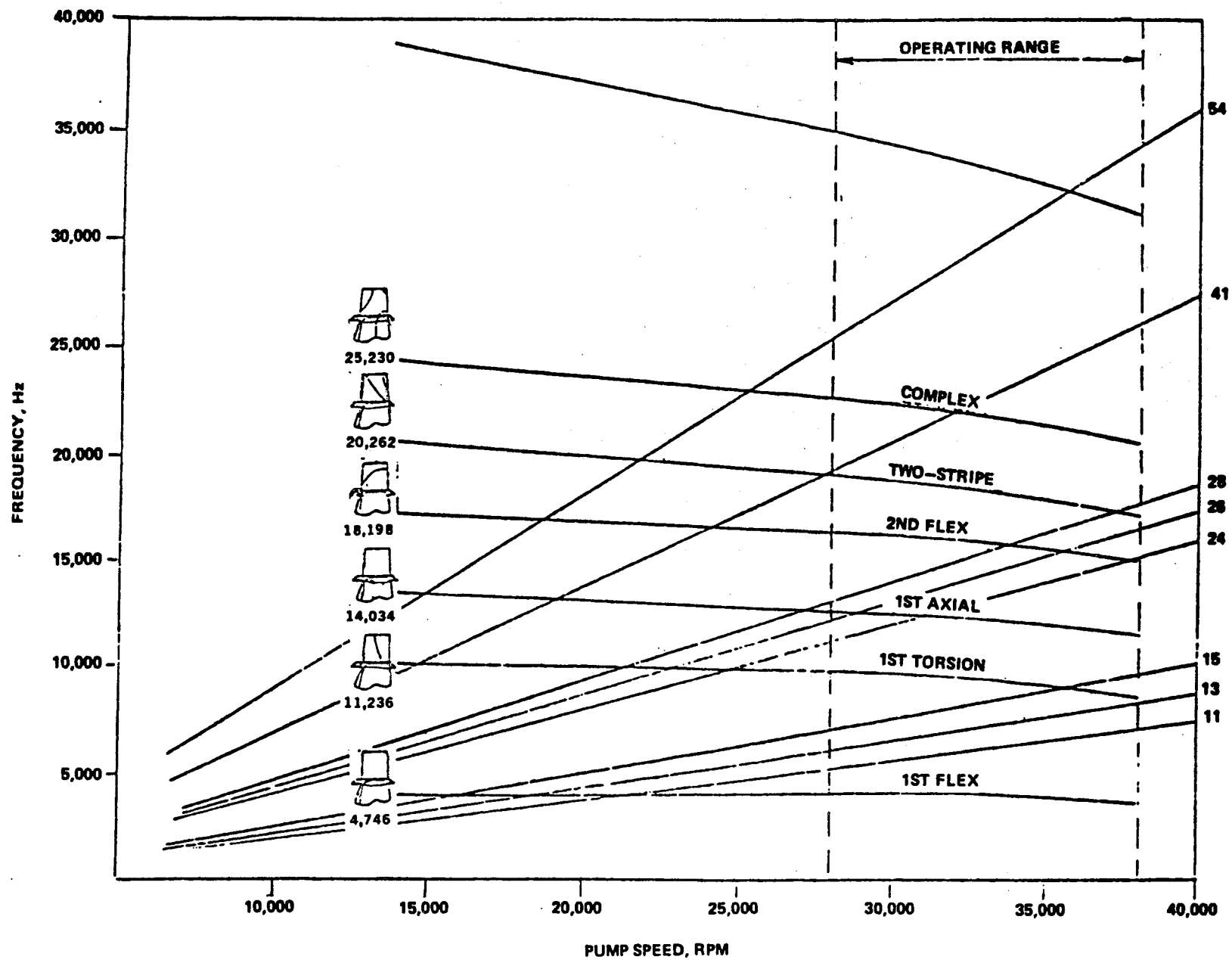


Figure 2.1-3 SSME HPFTP Turbine Blade Campbell Diagram

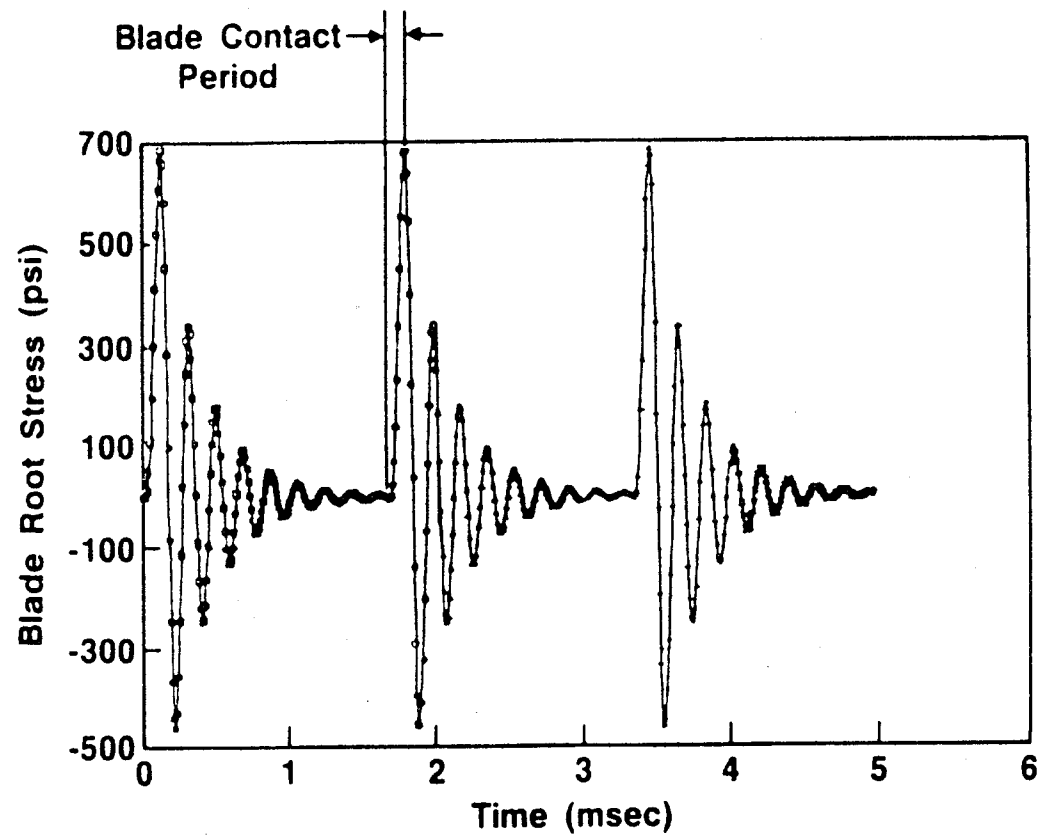
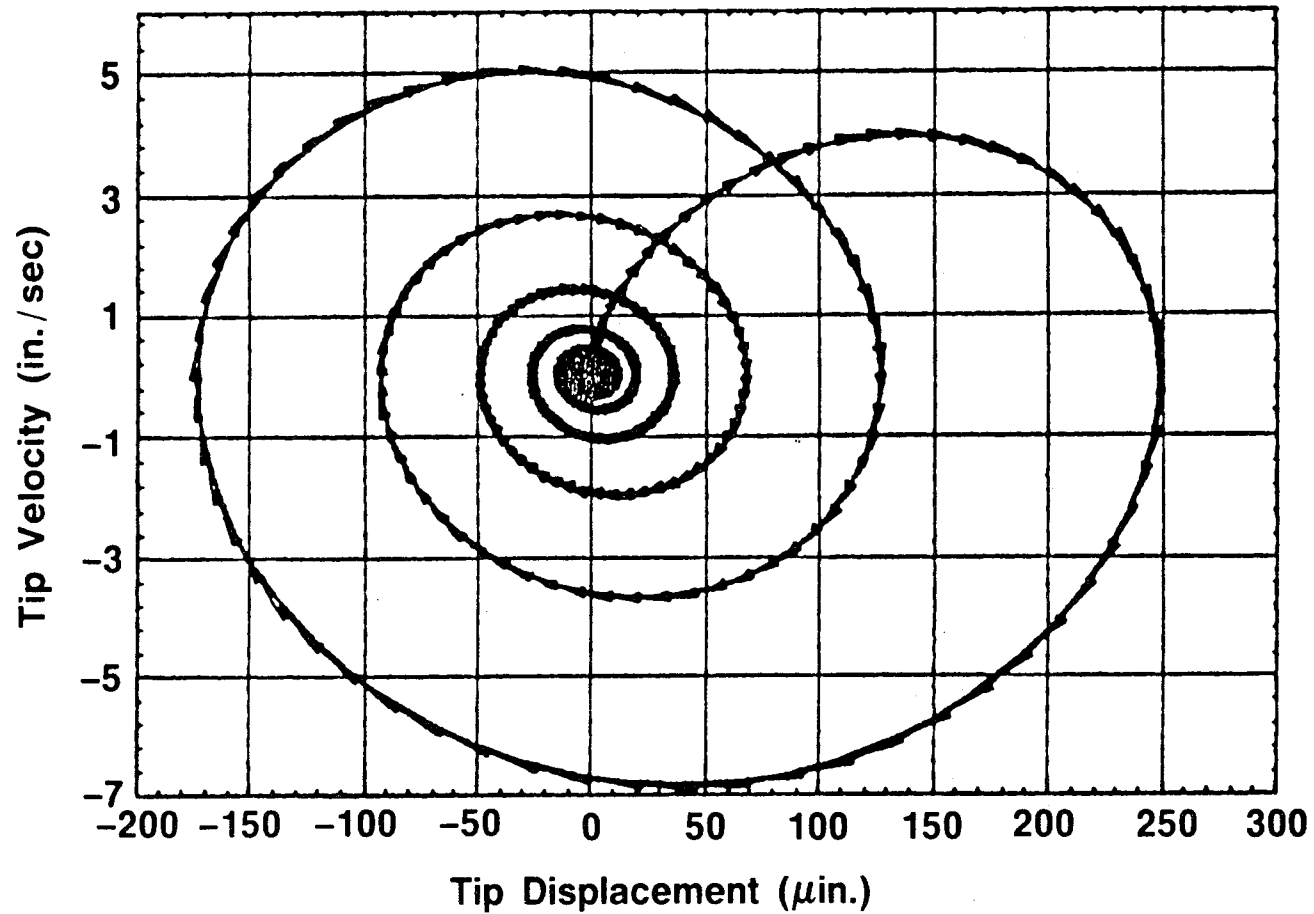


Figure 2.1-4 Stress Time History of Excited Blade

State Space Representation

Turbine Speed = 36,000 rpm



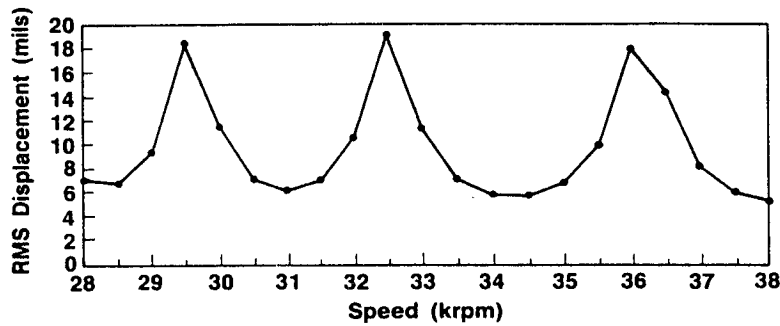
2.1-20



Rockwell International
Rocketdyne Division

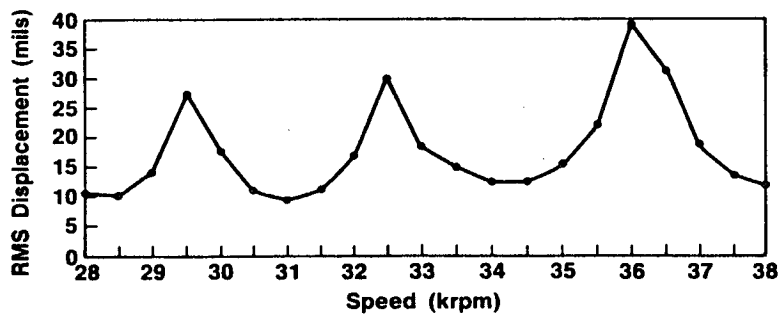
Figure 2.1-5 Space Plot, Blade Response

87C-4-9329
2143m/16



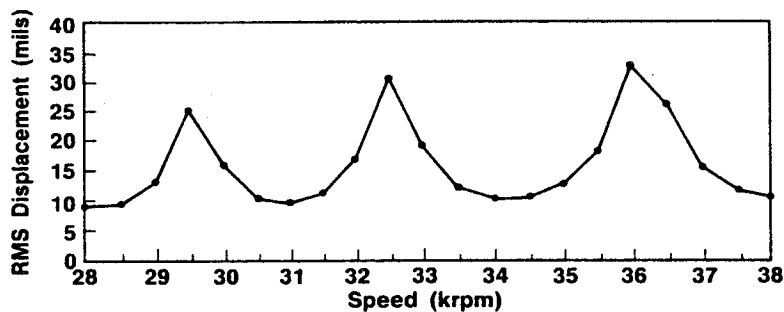
Degree of Freedom = 1: Node 681, DIR 1
 Contact Arc = 10 deg
 Friction Coefficient = 0.1

Figure 2.1-6 . Rms Blade Tip Displacement vs Speed
 (Contact Arc = 10 Deg)



Degree of Freedom = 1: Node 681, DIR 1
 Contact Arc = 20 deg
 Friction Coefficient = 0.1

Figure 2.1-7 . Rms Blade Tip Displacement vs Speed
 (Contact Arc = 20 Deg)

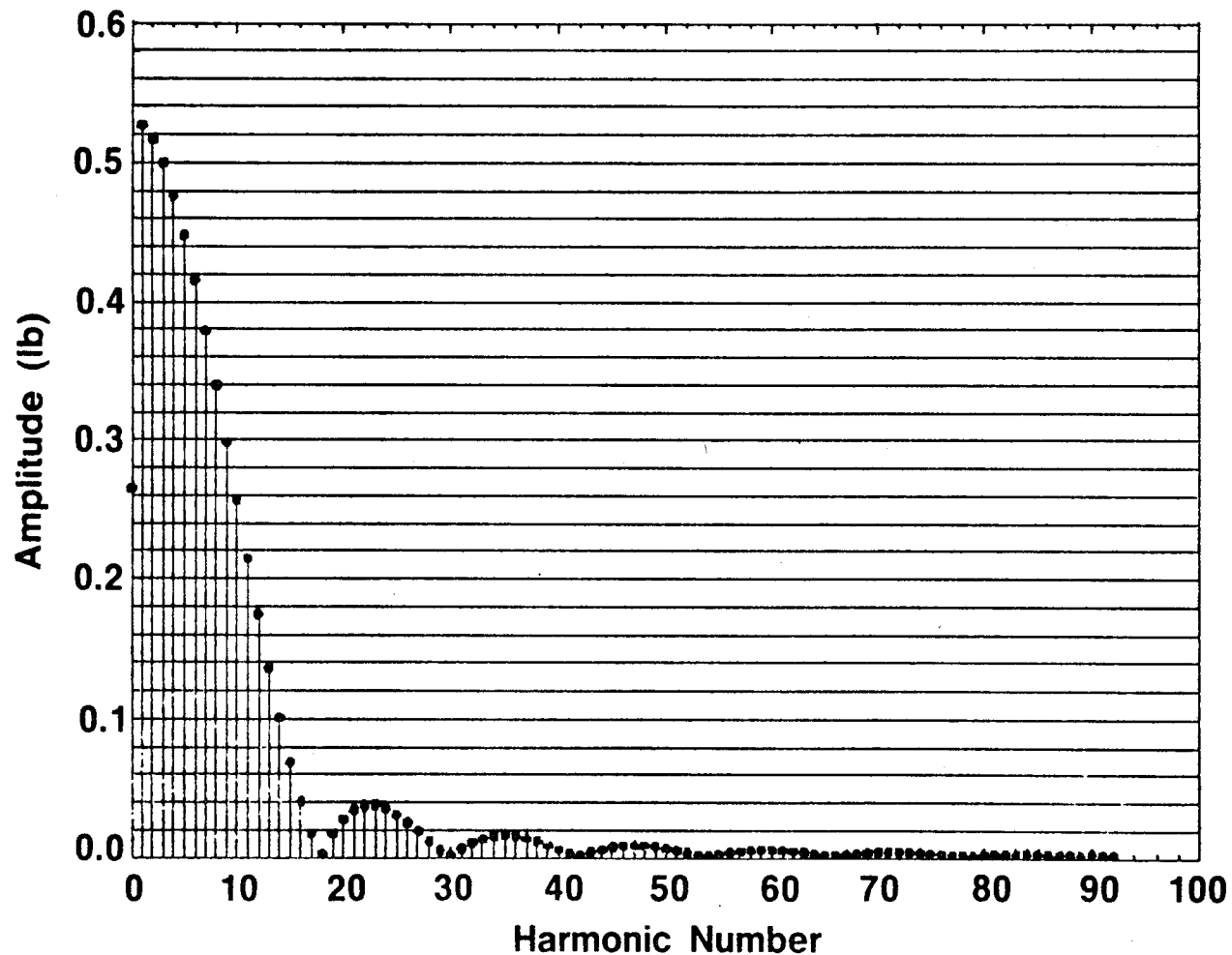


Degree of Freedom = 1: Node 681, DIR 1
 Contact Arc = 30 deg
 Friction Coefficient = 0.1

Figure 2.1-8 . Rms Blade Tip Displacement vs Speed
 (Contact Arc = 30 Deg)

Fourier Transform Of Force

Half Sine Wave Time History Over Contact Arc
Time Window = 1 Revolution



2.1-22



Rockwell International
Rocketdyne Division

Figure 2.1-9 Fourier Transform of Forcing Function

87C-4-9330
2143m/17



Rockwell International
Rockeltyne Division

HPFTP 1st Stage Blade Campbell Diagram

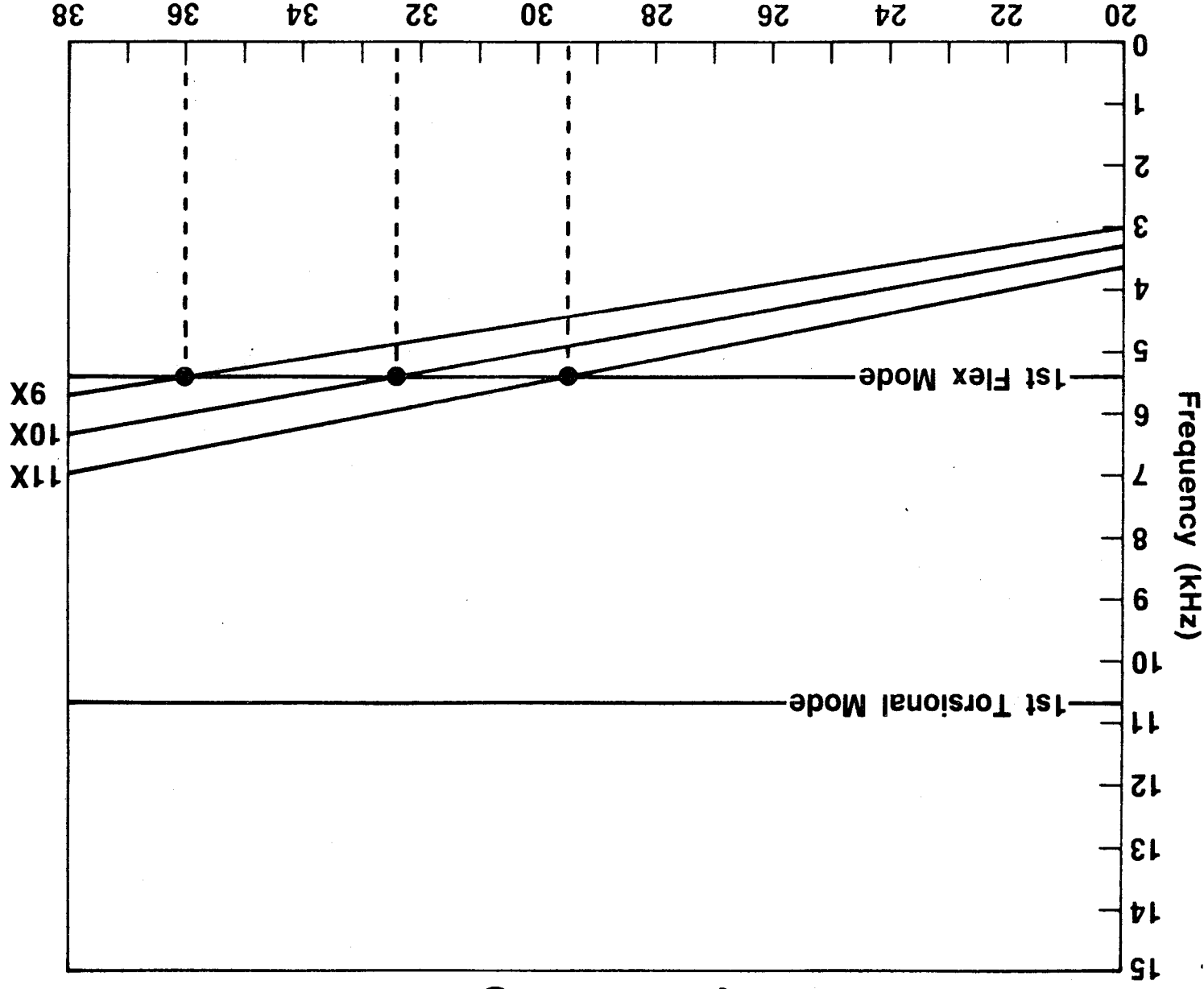
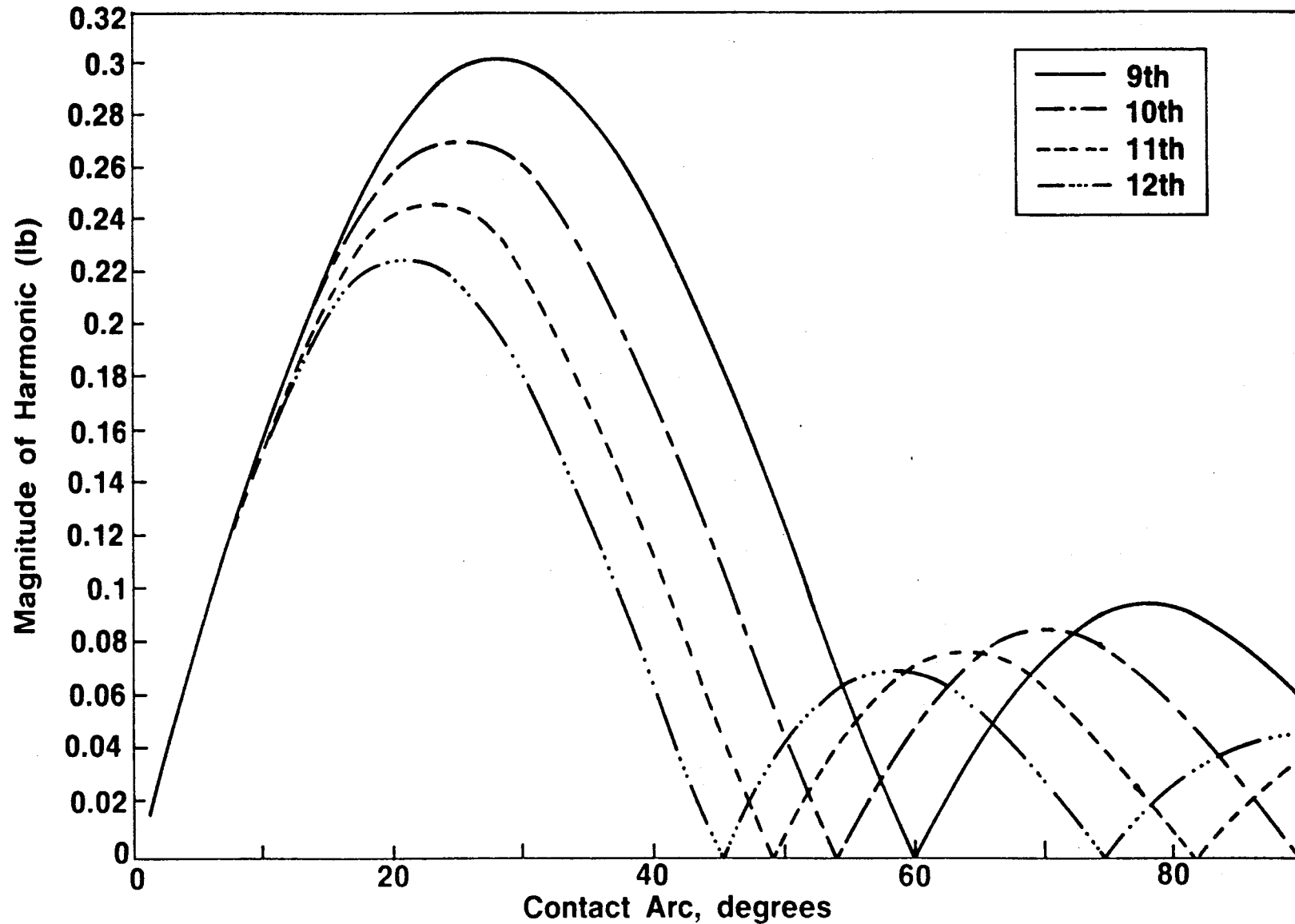


Fig 2.1-10. Campbell Diagram Showing Resonance with Forcing

87C-4-9327
2143m/19

Fourier Coefficients Of Forcing Function

Amplitudes Of Resonant Harmonics versus Contact Arc



2.1-24

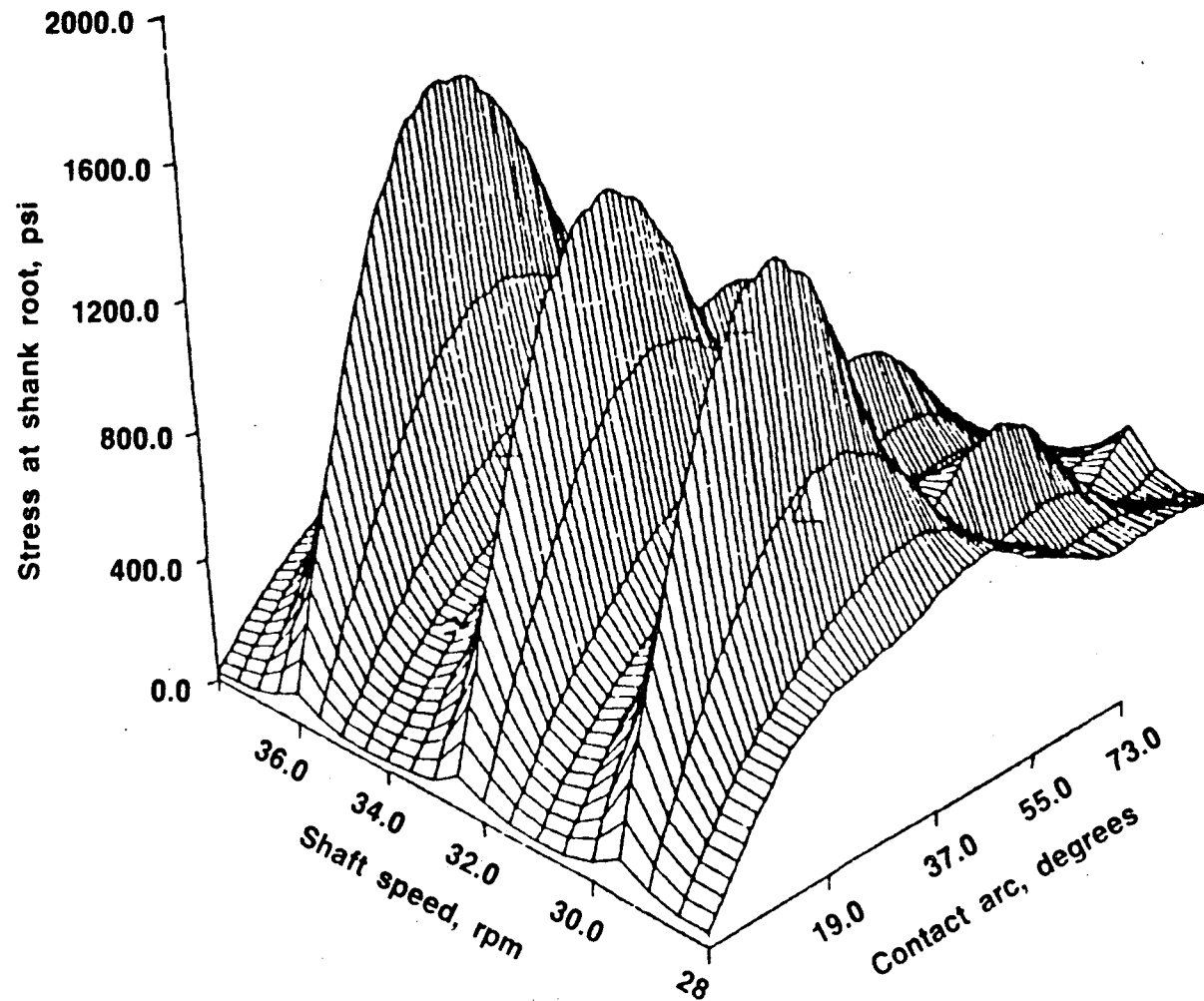


Rockwell International
Rocketdyne Division

87C-4-9332
2143m/23

Fig 2.1-11. Amplitudes of Resonant Harmonics vs Contact Arc

Critical Speed / Arc Summary



2.1-25



Rockwell International
Rocketdyne Division

Figure 2.1-12 Critical Speed/Arc Summary

87C-4-3217
2143m/27

2.2 EXPERIMENTAL VERIFICATION

2.2.1 Facility Description

The Rotary Dynamics Test Facility is located in Rocketdyne's Engineering Development Laboratory, and encompasses an area of approximately 1000 square feet with an enclosed control and instrumentation room, and an adjoining test cell 12 feet below the factory floor level.

The test chamber is cylindrical, 14 feet in diameter, and 11 feet tall, with a removable domed cover, and has a personnel access door. Evacuation of the chamber is accomplished by three vacuum pumps which can maintain chamber pressure at approximately 1 psia with the gaseous nitrogen purges turned on.

The prime mover for this facility is a 300 HP, 0 to 6000 RPM DC dynamometer which has its output shaft extended through the test chamber wall and is coupled to the input shaft of a 10:1 speed increasing gearbox. The gearbox output is coupled to the tester rotating assembly with a splined, double-ended quill-shaft approximately 6 inches long. Gearbox lubrication is accomplished with a recirculation system for vacuum levels above 100 torr and a single-pass blowdown system for vacuum levels below 100 torr.

The test control room, located on the factory floor level about 50 feet from the test chamber, contains the dynamometer control panel and the controls for regulating the test article operation. The test control room also contains the data recording equipment, which consists of a bank of FM. tape recorders used for high frequency data acquisition, and a digital computer used for low frequency data acquisition. Data transmission between the test chamber and the control room is via cables run in trenches below floor level.

2.2.2 Whirligig Tester

The whirligig tester, shown in cross-section in Figure 2.2-1, consists of a SSME HPFTP first stage turbine, a shaft supported on ball bearings with hydraulic squeeze film dampers, and a hydraulic bearing preload device. The whirligig is mounted on a two inch thick steel plate, which is attached to a Kurtsite base. Rotation is accomplished with a 300 horsepower electric motor and speed increasing gearbox through a quill shaft.

The Rocketdyne whirligig was originally designed in 1978, and has been used in a number of subsequent test programs. Various configurations, the basic whirligig hardware can be used to test either SSME HPFTP or HPOTP turbine hardware. Generally, some means of exciting the turbine blades is used, and the whirligig is instrumented to provide the relevant data.

In order to maximize the probability of successful collection of test data with minimum risk to the test hardware, the whirligig was designed with the following features:

2.2.2.1 Bearing Preload System. A hydraulic piston concept was utilized to provide the bearing axial preload during operation. The primary advantage of this design approach is that the bearing preload, and, hence bearing stiffness, can be modified as required during operation. This factor is important as it reduces testing downtime associated with changing preload values.

An additional design feature of the variable preload system is the emergency preload. In case of hydraulic pressure failure, a series of compression springs provide a minimum preload of 105 pounds. Normal operating preload is maintained from approximately 350 to 425 pounds, as set by hydraulic pressure prior to rotor rotation.

2.2.2.2 Squeeze Film Dampers. An oil film damper was incorporated at both the turbine wheel and drive ends of the assembly. This feature was incorporated to minimize any reactions on the unit as a result of critical speed modes, and to help reduce damage if the wheel should lose a blade during operation.

The damping configuration is basically an oil-filled annulus between the bearing carrier and the housing. The length of the annulus is approximately 0.800 inch, and the nominal radial clearance is 0.008 inches. The

hydraulic fluid inlet is 0.140 inch diameter and the bleed hole is 0.020 inches diameter. During operation, a constant pressure is applied to the hydraulic source which produces a gas-free film damper.

2.2.2.3 Bearing Coolant and Lubrication System. Similar bearing coolant systems were employed on both the drive and wheel end bearings. The whirligig uses 45 mm SSME HPFTP bearings. The lubrication system consists of an annular chamber with three equally spaced 0.050 inch diameter jets used to direct the coolant oil onto the bearings. The nominal flowrate is 1.2 gpm for each bearing. The impingement direction of the coolant jets with respect to the bearing centerline was designed specifically for the whirligig since one-of-a-kind ball bearing design was used to provide an increased flow-through effect to maximize the bearing cooling capacity.

2.2.2.4 Main Supports. The main supports at both ends of the whirligig are two-piece, split units. This was done to simplify the assembly of the whirligig and, consequently, to minimize downtime. The physical construction of the mounts is a steel weldment with reinforcements in critical areas to provide maximum strength.

2.2.2.5 Labyrinth Seal. A large labyrinth seal was designed to prevent the leakage of bearing oil onto the turbine disk and blades. The labyrinth seal fits onto the HPFTP first-to-second stage mating bolt circle. This labyrinth seal is purged with Nitrogen gas, and is equipped with a series of drains designed to carry oil away from the spinning turbine disk.

2.2.2.6 Slip Ring. A one-hundred channel slip ring is used to transmit the data from the rotating turbine disk. This slip ring was manufactured by Applied Sensors International, of Cincinnati, Ohio. The slip ring is lubricated and cooled by a freon-oil mixture. Previous testing revealed that a 95/5 percent mixture of Freon 113 with Brayco oil would allow the brushes to operate without experiencing hydrodynamic lift-off. The manufacturer recommends 0.2 gpm flow. The flow of the slip ring coolant was set by gaseous nitrogen pressure and flow-restricting orifice size. The orifice selected was 0.065 inches diameter, the inlet pressure was 40 psig, and the pressure drop across the slip ring was approximately 19 psig.

Figures 2.2-2 and 2.2-3 show the plumbing schematic

diagram. Figure 2.2-2 shows only the main features of the lubricant, coolant, and purge supply systems, while 2.2-3 shows the entire system in detail. The oil supply provides oil for bearing lubrication, for the squeeze film dampers at both ends of the whirligig, and for the hydraulic bearing preload system. These oil systems are all single-pass, blowdown systems. The bearing lubrication oil is collected in a catch tank for reuse. The preload and hydraulic damper use only small amounts of oil, which is not collected.

Figures 2.2-2 and 2.2-3 also show the schematic of the GN2 supply system. The GN2 is supplied by a high pressure source and is used to provide pressurization for the lubrication and hydraulic systems and to purge the labyrinth seals. As shown in Figure 2.2-3, all the pressures are controlled and adjusted with hand-operated pressure regulators and flow regulating orifices.

2.2.3 Turbine Disk and Blades

This program used a scrap SSME first stage HPFTP turbine disk, P/N RS007517, and scrapped blades. The blades used were rejected during manufacture for non-reworkable porosity indications or slight out-of tolerance conditions which would preclude their use for flight. Stress analysis of the blades showed that they would not fail due to the loads anticipated during this test program.

2.2.4 Tip Seal Test Module

In this program, the blades are excited with a device designed and constructed especially for this test program, which simulates the action of the tip seal rubbing against the rotating blades. This device, referred to as the "tip seal test module", is depicted schematically in figure 2.2-4, and is shown bolted to the whirligig base in Figures 2.2-5 and 2.2-6. This test module consists of a sturdy frame holding a hydraulically activated test article shaped like a brake shoe. This test article is hydraulically pressed against the tips of the rotating turbine blades. The test module was instrumented with piezoelectric load cells to give the components of the force exerted by the tip seal test article on the ends of the turbine blades and with a Linear Variable Displacement Transformer (LVDT) which gives a direct readout of the position of the test article. The test article contact with the rotating turbine blades was controlled from the test control room for contact duration, depth of contact beyond the point at which contact begins, and the ramp rate at which contact was initiated. The design and fabrication

of this test module was subcontracted by Rocketdyne to Shore Western Mfg., Inc., of Monrovia, California.

2.2.5 Test Article

The test article, shown in Figure 2.2-7, was manufactured from Inconel 718, and hardened to approximate the hardness of the RENE 41 tip seals used in the SSME HPFTP. The material substitution was necessitated by the difficulty of procuring RENE 41, but due to the similar composition and hardness of Inconel 718, the anticipated behavior of the materials close enough for purposes of this test. The HPFTP tip seals have an inner diameter of 11.030 inches. To simplify pre-test adjustment of the position of the test article with respect to the whirligig blades, this diameter was increased to 11.090 inches on the test article. This insured that the turbine blades would rub near the center of the arc instead of at the corner where the arc intersects the flat underside of the test article.

2.2.6 Instrumentation

Instrumentation is divided into two categories: 1) that necessary to assure safe and effective operation of the whirligig tester and tip seal test module, and 2) the test output data, which consisted primarily of strain gage data. The whirligig operational information was mostly low frequency digital data, and the test data was primarily high frequency, acquired by FM tape recorders. Table 2.2.6-1 lists the all of the instrumentation used in this test.

2.2.6.1 Whirligig Operations Monitoring Data. The whirligig operational data consisted of temperature, pressure, and lubricant flow rate measurements, which were acquired on a digital computer system, and shaft orbit and housing accelerometer information, which were acquired with high-speed FM. tape. the whirligig was equipped with bearing flow, pressure, temperature, vibration, and shaft speed and orbit instrumentation.

Pressure for the oil supplies and for the labyrinth seal purges is provided by a high-pressure GN2 system. Measured pressures for the oil supply system include: system supply pressure, bearing supply tank pressure, bearing preload pressure, and squeeze film damper pressure. Additionally, the test chamber pressure and the labyrinth seal supply pressure are measured. The slip ring coolant inlet pressure and pressure drop, and the slip ring purge pressures are also

measured.

Temperature monitoring was done on both bearings, the bearing lubrication outlet reservoir, both bearing housings, and the bearing preload housing. The dynamometer drive system and gear speed reducer were instrumented for gearbox temperatures and pressures.

The temperature, pressure, shaft orbit and acceleration data were important operation safety parameters, and so were also viewed in real time by the test monitors and operators. The low-frequency data, ie. pressures, temperatures, and lubricant flowrates, were viewed on a digital computer screen. The shaft orbit of each end of the whirligig was viewed as a Lissajous figure on an oscilloscope, and the whirligig housing acceleration was also viewed on an oscilloscope. Overlays on all the oscilloscope faces were marked with the redline limits, so that when the oscilloscope traces exceeded the marked outlines, the test monitor would call a redline test cut.

2.2.6.2 High-frequency Test Instrumentation. The high-frequency instrumentation, listed in Table 2.2.6-1, consisted of strain gage data, accelerometer and shaft displacement data, and test article displacement data from the Linear Variable Displacement Transformer (LVDT) attached to the hydraulic actuator piston. This data was acquired on a bank of 4 FM tape recorders. All these signals were also monitored in real time on oscilloscopes.

2.2.6.3 Turbine Blade Strain Gage Installation. This test was conducted to determine the stresses induced by the rubbing of the tip seal test article against the turbine blades. Therefore forty-eight blades had strain gages applied to their airfoil surfaces. The strain gaged blades were installed in the disk in four evenly-spaced sectors of twelve blades each. Figure 2.2-8 shows the location of the strain gages on the turbine blades, and Figure 2.2-9 maps the position of the instrumented blades on the wheel. The gage position was chosen after reviewing the results of tests conducted in 1978 on an SSME HPFTP turbine blade instrumented with 130 strain gages. The location chosen represents the highest strain response to induced vibration in the first mode of the blade.

It was anticipated before the test that some blades would be slightly higher than the others, and would therefore rub before the shorter blades. This could result in the possibility that some, or even most of the blades, would not rub at all. To make sure that the instrumented blades would rub, all uninstrumented were shortened several thousandths of

an inch with a grinder.

The turbine disk was wired in the Engineering Development Laboratory's Strain Gage Room. The wired turbine disk is shown in Figures 2.2-10 through 2.2-12. Figure 2.2-10 shows the entire wired disk. The small gage lead wires were epoxied to the disk, and led from small fir tree solder tabs, shown in Figure 2.2-11, through the curvic couplings as shown in Figures 2.2-11 and 2.2-12, to solder tabs on the inner diameter of the curvic coupling bosses, as shown in Figure 2.2-12. Due to the small gauge of the lead wires through the curvic coupling, it was not found to be necessary to increase the clearance of the curvic where it mated with the 2nd stage turbine disk, as shown in Figure 2.2-12. From the curvic solder tabs, larger gauge wires were epoxied to the disk and led out through the hole in the center of the disk. A 200-pin connector was used to connect these wires to the 100 channel slip ring.

Figures 2.2-13 and 2.2-14 show the application of a strain gage to the turbine blades. The strain gages were also installed in Rocketdyne's Engineering Development Laboratory's Strain Gage Room. The strain gages were applied to the turbine blades with epoxy, and the lead wires were routed over a small grind-out in the platform and down to the fir-trees. The passage of the lead wires through the platform grind-out is shown in Figure 2.2-14. At the fir trees, small solder tabs were attached to the shank of the blade, and also to the adjacent portion of the disk. Connection to the wired turbine disk was done with jumper wires, as shown in Figure 2.2-15. This was done to allow removal of the strain gaged blades without destroying either the strain gages or the turbine disk wiring.

The complete assembled wheel is shown in Figure 2.2-16.

Since this test program was conducted primarily to confirm the predictions of the analytical model, and since the analytical model doesn't explicitly include the effect of blade dampers, using instead a lumped damping parameter, the blades were installed without dampers. This also reduced strain gage installation time and expense, since the installation of dampers would necessitate EDM'ing the blades to allow passage of the strain gage lead wires under the dampers.

PARAMETER	UNITS	NOMINAL OR SETPOINT	BLUELINE	REDLINE	REDLINE CUT MANUAL/AUTO	BLUELINE ACTION	SYS 10	FM TAPE
WHIRLIGIG OPERATIONAL DATA								
TEMPERATURES:								
WHEEL END BEARING	F		200	300	MANUAL	ADJUST OIL FLOW	X	
DRIVE END BEARING	F		200	300	MANUAL	ADJUST OIL FLOW	X	
PRESSURES:								
PRELOAD	PSIG	40	35 - 45	65	MANUAL	OBSERVE TREND	X	
BEARING SUPPLY	PSIG	425	300	440	MANUAL	OBSERVE TREND	X	
DAMPER	PSIG	108	90 - 125	75 < P < 145	MANUAL	OBSERVE TREND	X	
LABY PURBE	PSIG	15	5 - 50	500	MANUAL	OBSERVE TREND	X	
CHAMBER PRESSURE	PSID	2 - 10	10	1	MANUAL	OBSERVE TREND	X	
							X	
SLIP RING:								
S/R SEAL TEMP	F		250	500	MANUAL	OBSERVE TREND	X	
S/R COOLANT INLET PRESS	PSIG	35	30 - 40			OBSERVE TREND	X	
S/R COOLANT PRESS DROP	PSID	15	10 - 20			OBSERVE TREND	X	
OTHER:								
WHEEL END BRG FLOW	GPM	1.2	1 - 1.5	0.75	MANUAL	OBSERVE TREND	X	
DRIVE END BRG FLOW	GPM	1.2	1 - 1.5	0.75	MANUAL	OBSERVE TREND	X	
WGIG ROTATIONAL SPEED	RPM	0 - 33000			AUTO/MANUAL		X	X
RAMP RATE	RPM/MIN	10000			AUTO DURING SPEEDUP & SHUTDOWN/ OFF DURING TEST			
WHEEL END ORBIT	IN		0.005	0.01	MANUAL	OBSERVE TREND		X
DRIVE END ORBIT	IN		0.005	0.01	MANUAL	OBSERVE TREND		X
HOUSING ACCELERATION	GRMS		4	15	AUTO W/ DELAY	OBSERVE TREND		X
TIME (IRIG)	MIN			TAPE LENGTH	MANUAL			X
LUBE DURATION (STOPWATCH)	MIN		40	35	MANUAL	OBSERVE TREND		
GEARBOX TEMPS	F		105	200	AUTO	OBSERVE TREND	X	
GEARBOX PRESS	PSIG		27	15	AUTO	OBSERVE TREND	X	
GEARBOX OUTPUT SHAFT SPEED	RPM	0 - 33000		33500	AUTO		X	X
TEST DATA:								
STRAIN GAUGES 1 - 48	MICROINCH							X
LOAD CELLS 1 - 3	LBF							X
TEST ARTICLE PLUNGE (LVDT)	GRMS	WITHIN 0.0005 OF TESTPLAN REQUIREMENT				NOTIFY TEST CONDUCTOR		X
TEST ARTICLE ACCELERATION	GRMS							

Table 2.2-1. Whirligig & Test Module Instrumentation List

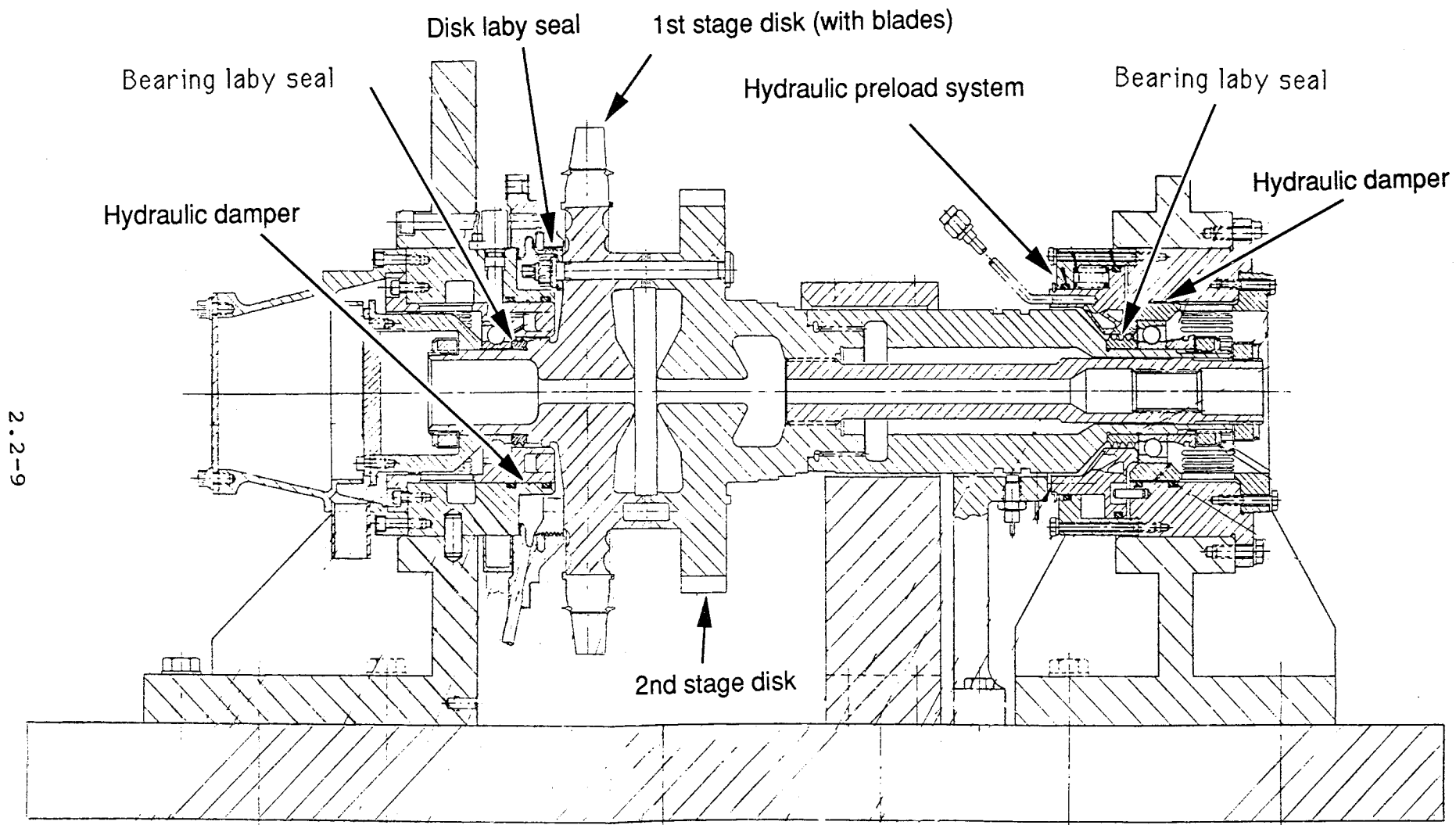


Figure 2.2-1 Cross-section of SSME HPFTP Whirligig

BLADE TIP RUBBING WHIRLIGIG

LUBURCANT, COOLANT, PURGE SUPPLY SCHEMATIC

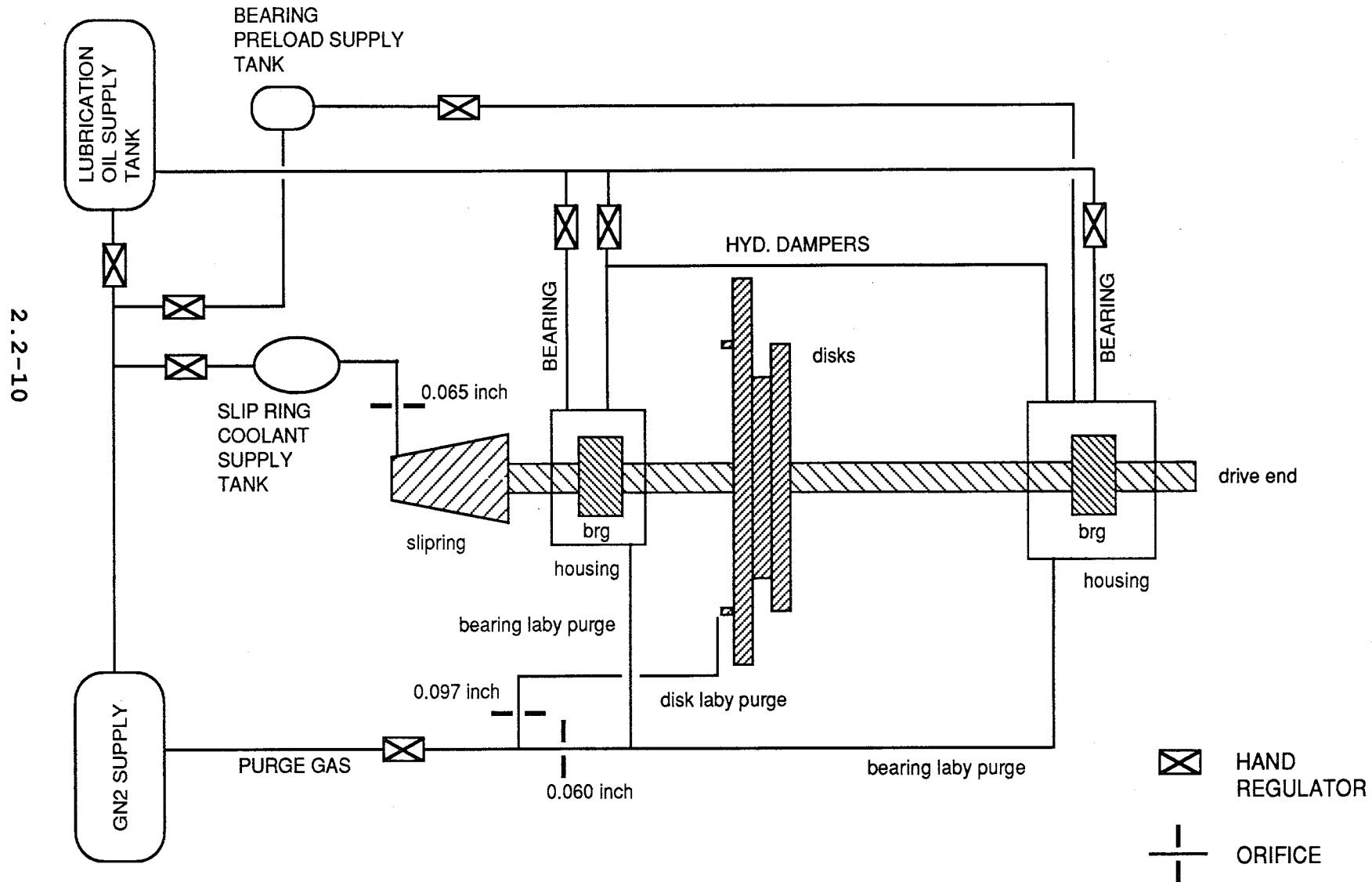


Figure 2.2-2. Overview of Whirligig Plumbing Supply System

WHIRLIGIG, BLADE TIP RUBBING FACILITY SCHEMATIC FIGURE 1

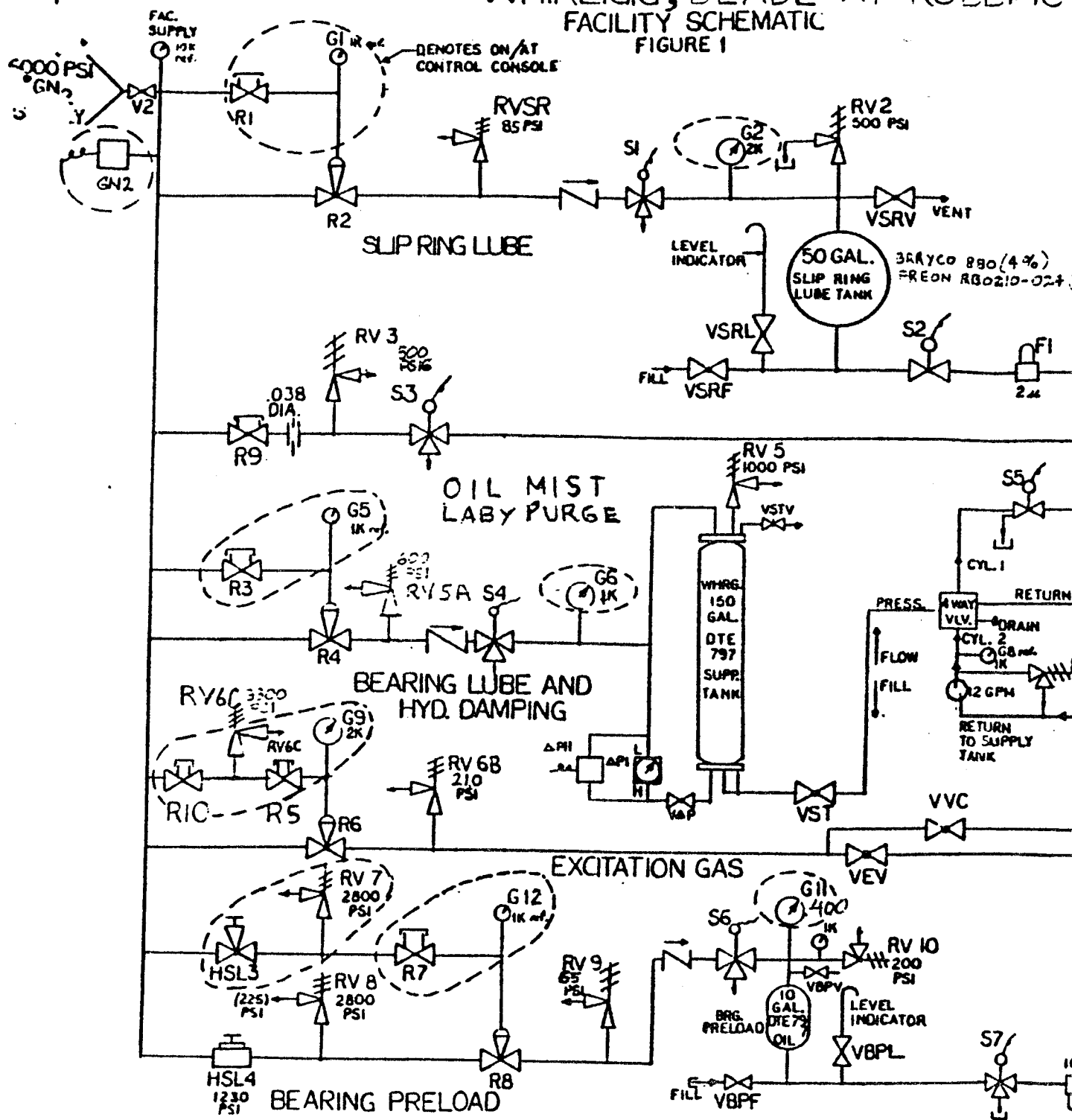


Figure 2.2-3 Detail of Whirligig Plumbing System

WHIRLIGIG, BLADE TIP RUBBING FACILITY SCHEMATIC FIGURE 1

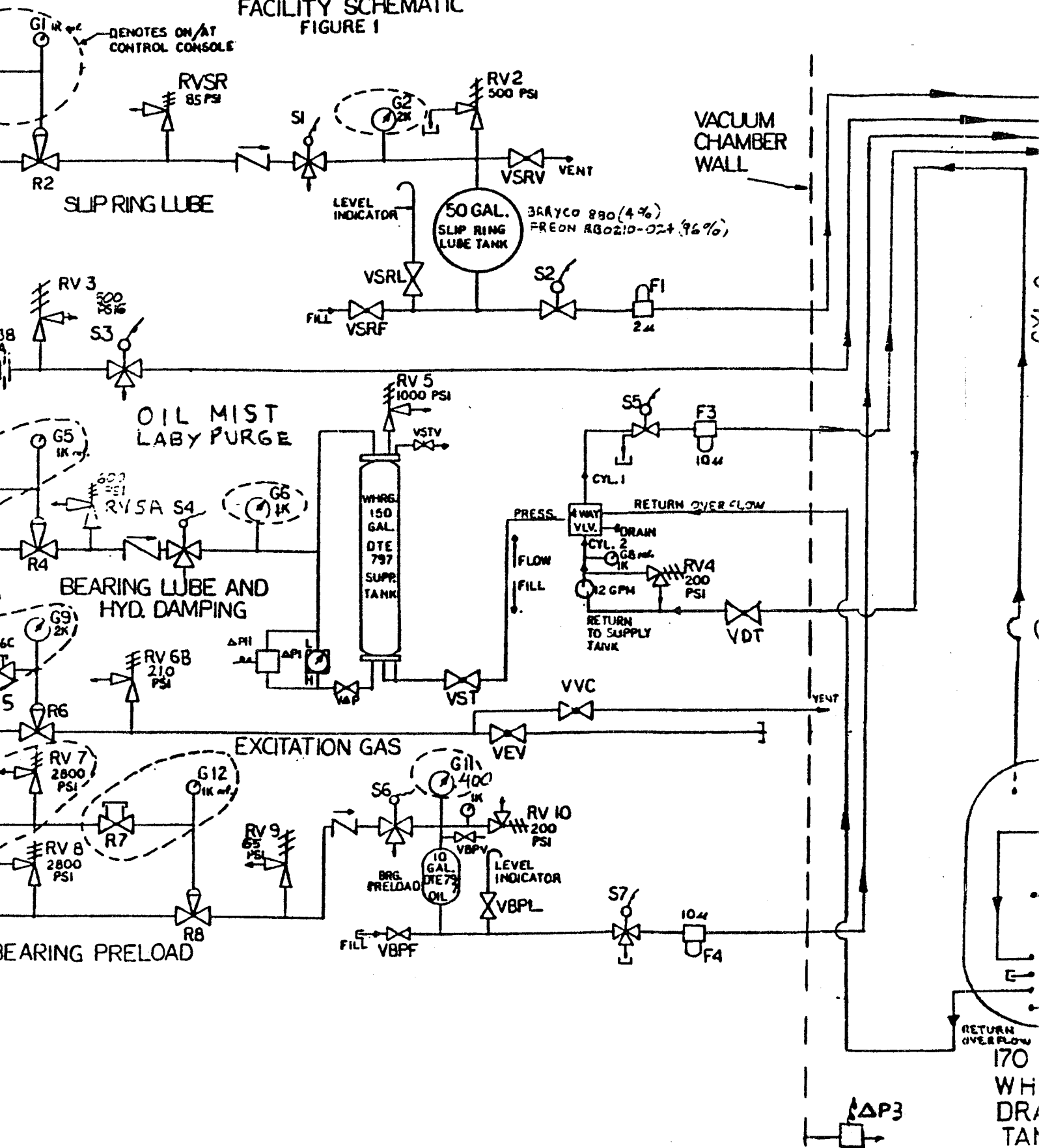
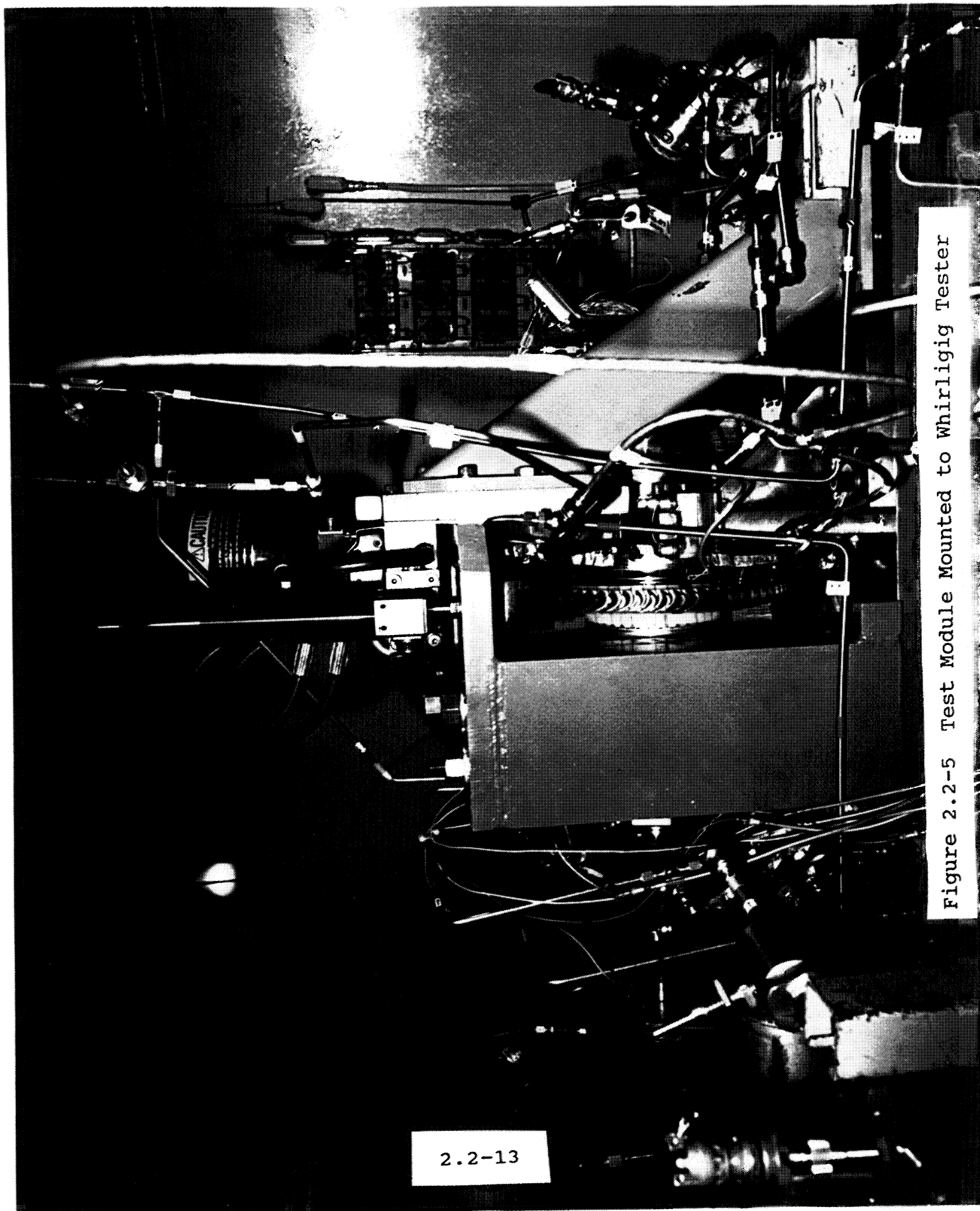


Figure 2.2-3 Detail of Whirligig Plumbing System



2.2-13

Figure 2.2-5 Test Module Mounted to Whirligig Tester

BLADE TIP RUBBING WHIRLIGIG

SCHEMATIC SHOWING TEST MODULE RELATIONSHIP TO WHIRLIGIG

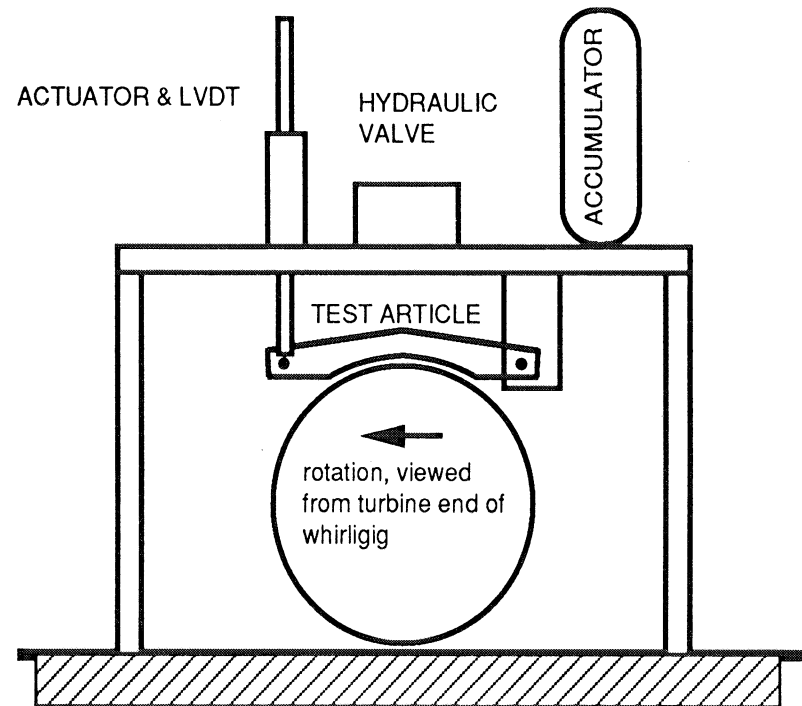


Fig 2.2-4. Schematic Diagram of Test Module Mounted to Whirligig Base

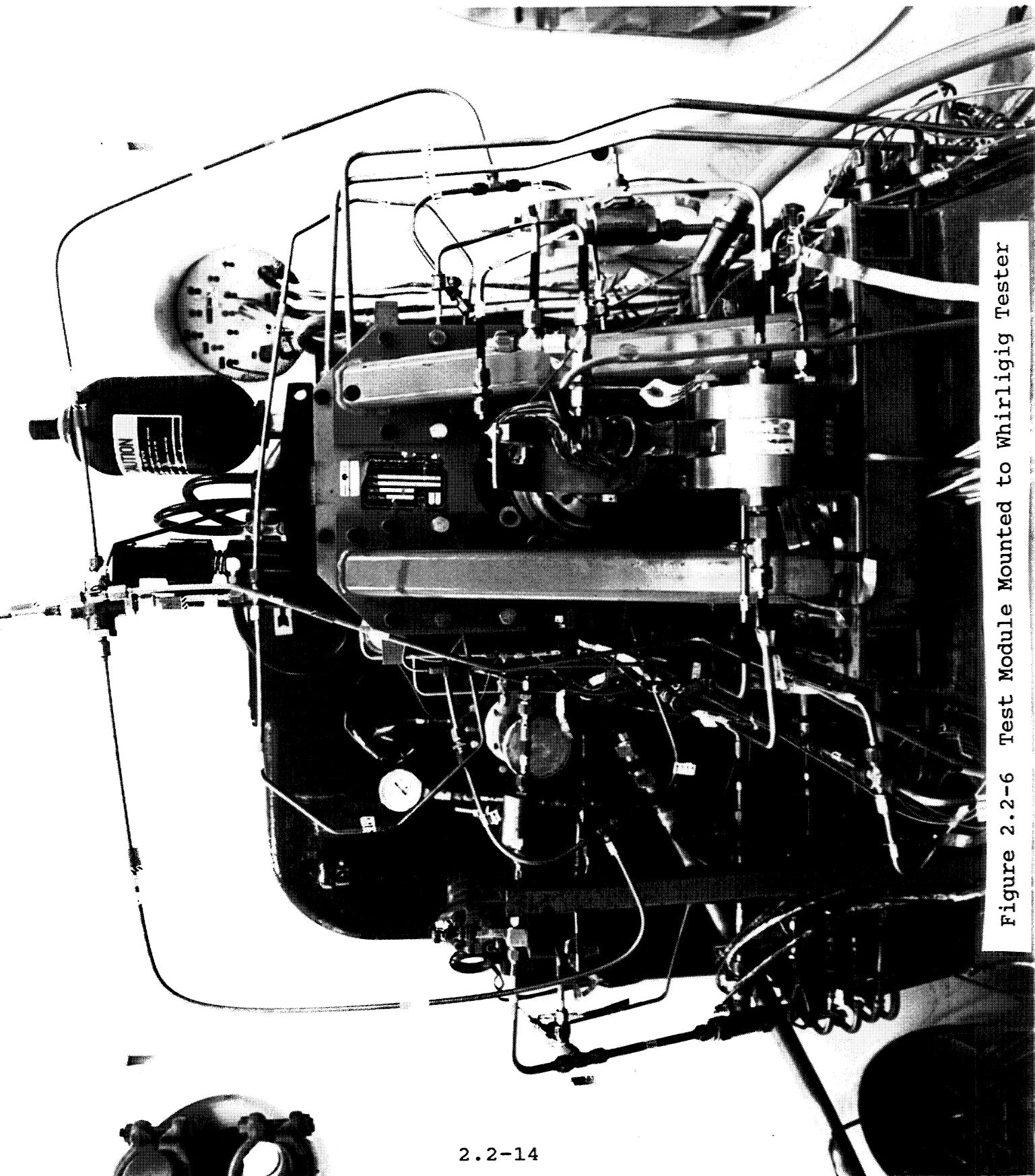


Figure 2.2-6 Test Module Mounted to Whirligig Tester


2.2-14

ORIGINAL PAGE
COLOR PHOTOGRAPH

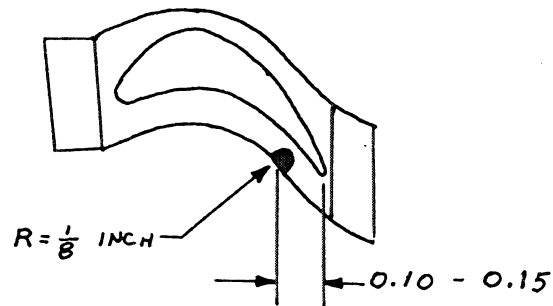
Figure 2.2-7 Tip Rubbing Test Article



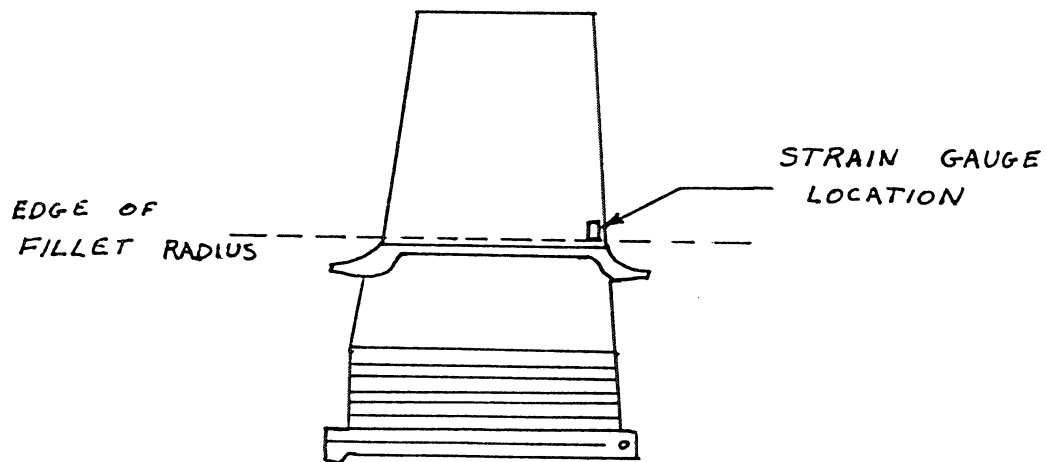
2.2-15

PREPARED BY:	 Rocketdyne Division Rockwell International	PAGE NO.
CHECKED BY:		REPORT NO.
DATE:		
BLADE TIP RUBBING STRESS PREDICTION WHIRLIGIG		

1ST STAGE SSME HPFTP TURBINE BLADE
STRAIN GAUGE APPLICATION



NOTCH THRU PLATFORM AS SHOWN.
MAY BE HAND GROUND. BREAK
EDGES AND CORNERS



CONCAVE SIDE VIEW

Figure 2.2-8 Strain Gage Position on Blade

BLADE TIP RUBBING WHIRLIGIG MAP OF STRAIN GAGED BLADES

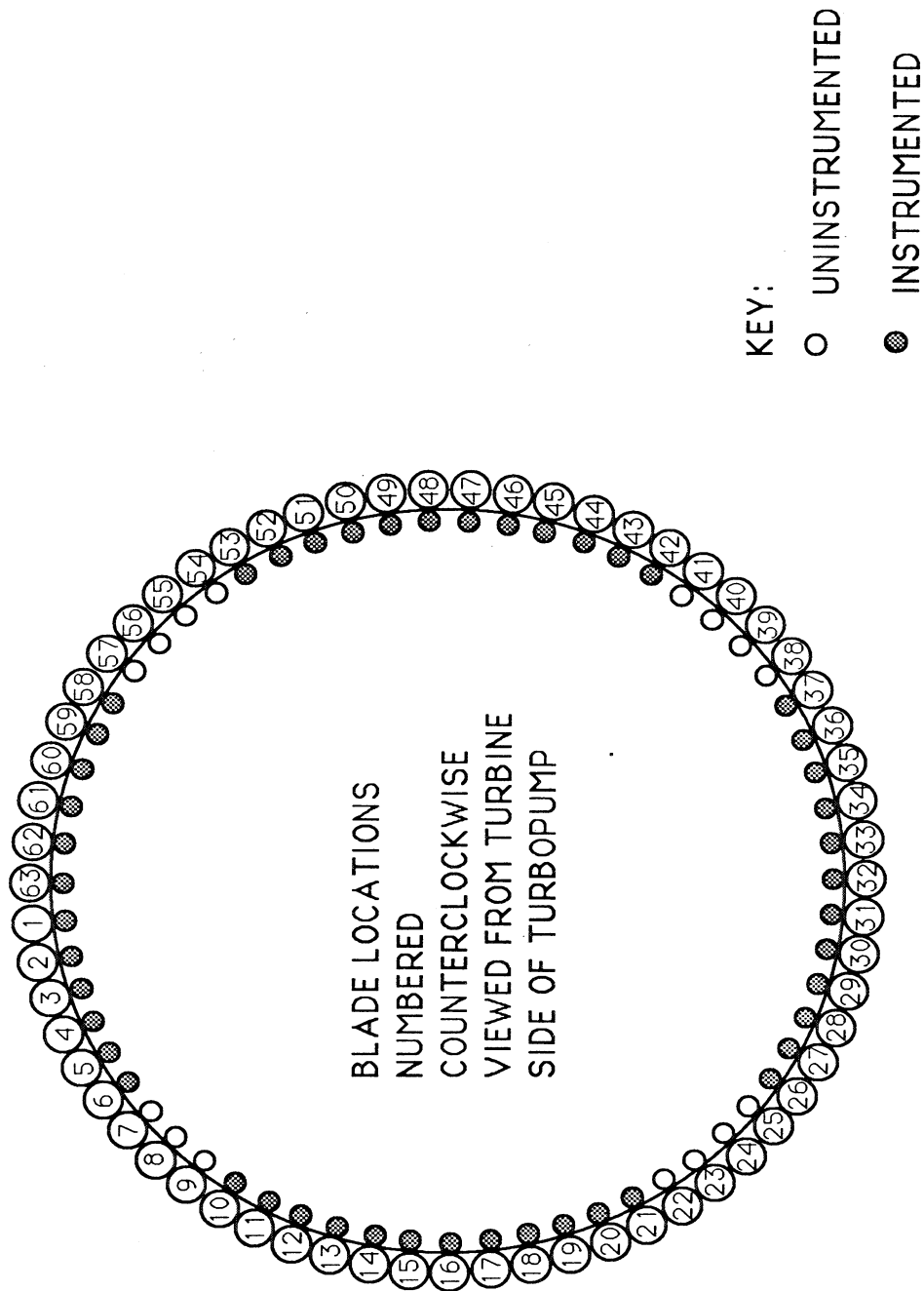


Figure 2.2-9 Positions of Strain Gaged Blades in Wheel

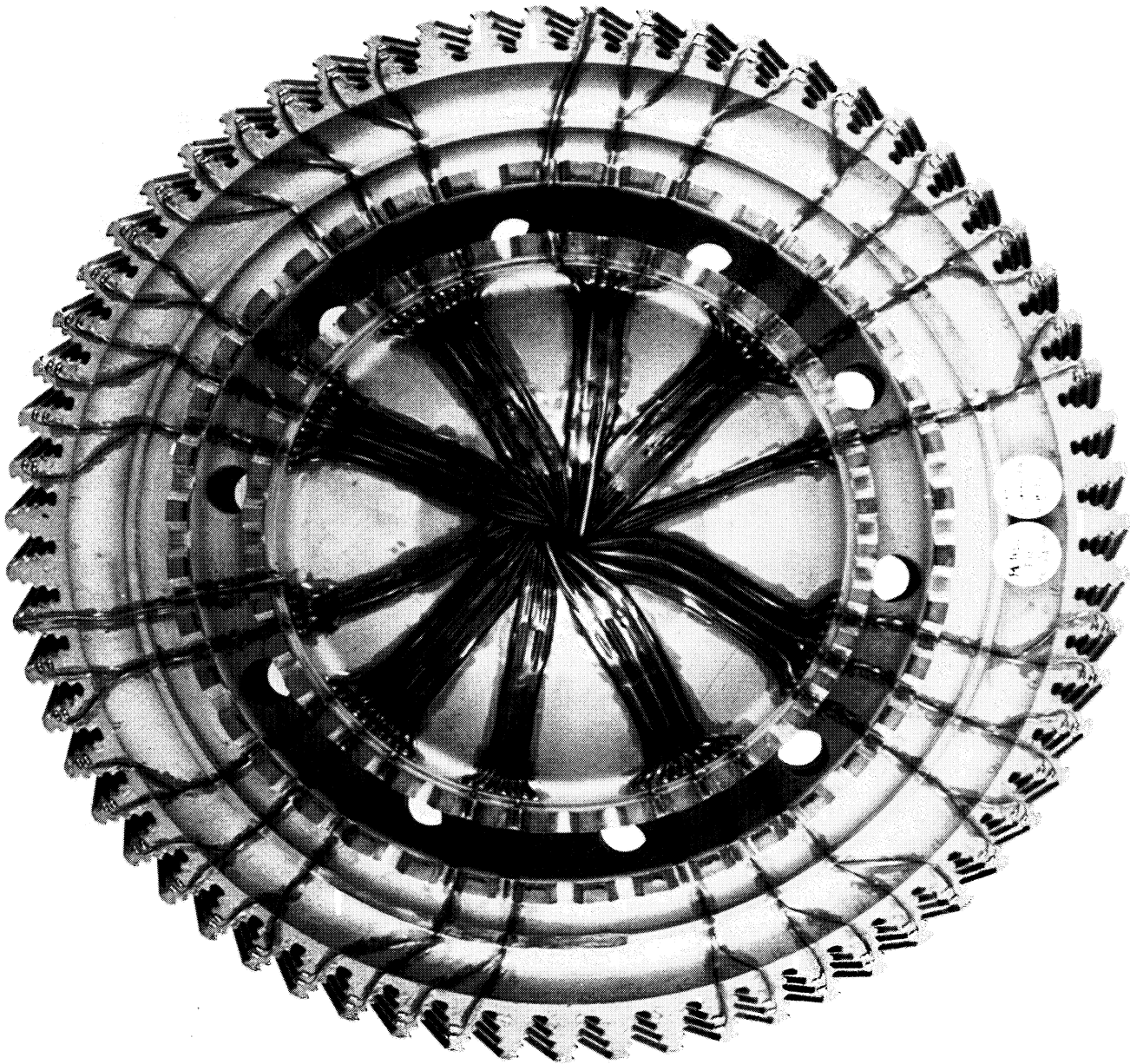


Figure 2.2-10 Wired Disk

2.2-18

ORIGINAL PAGE
COLOR PHOTOGRAPH

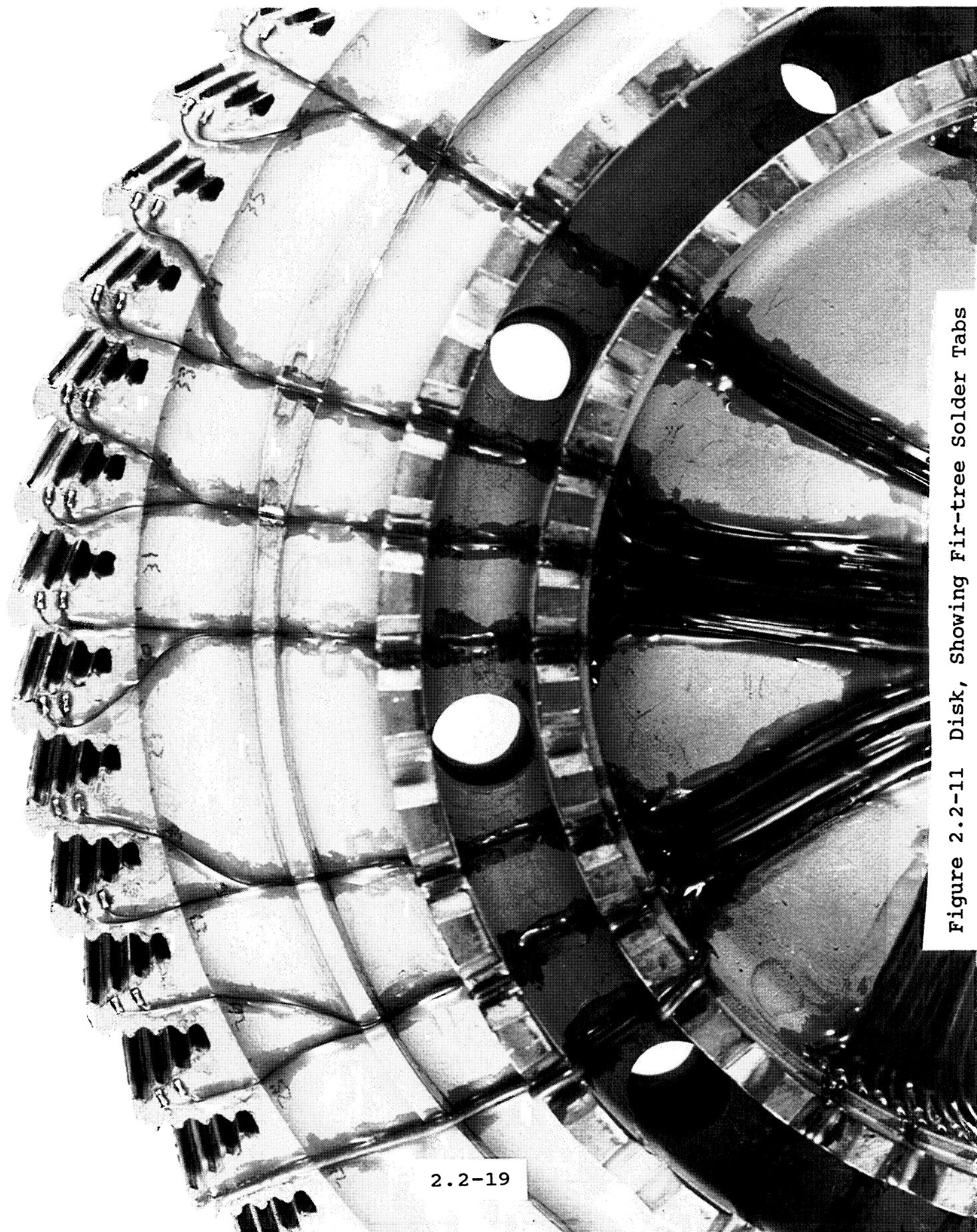


Figure 2.2-11 Disk, Showing Fir-tree Solder Tabs

2.2-19

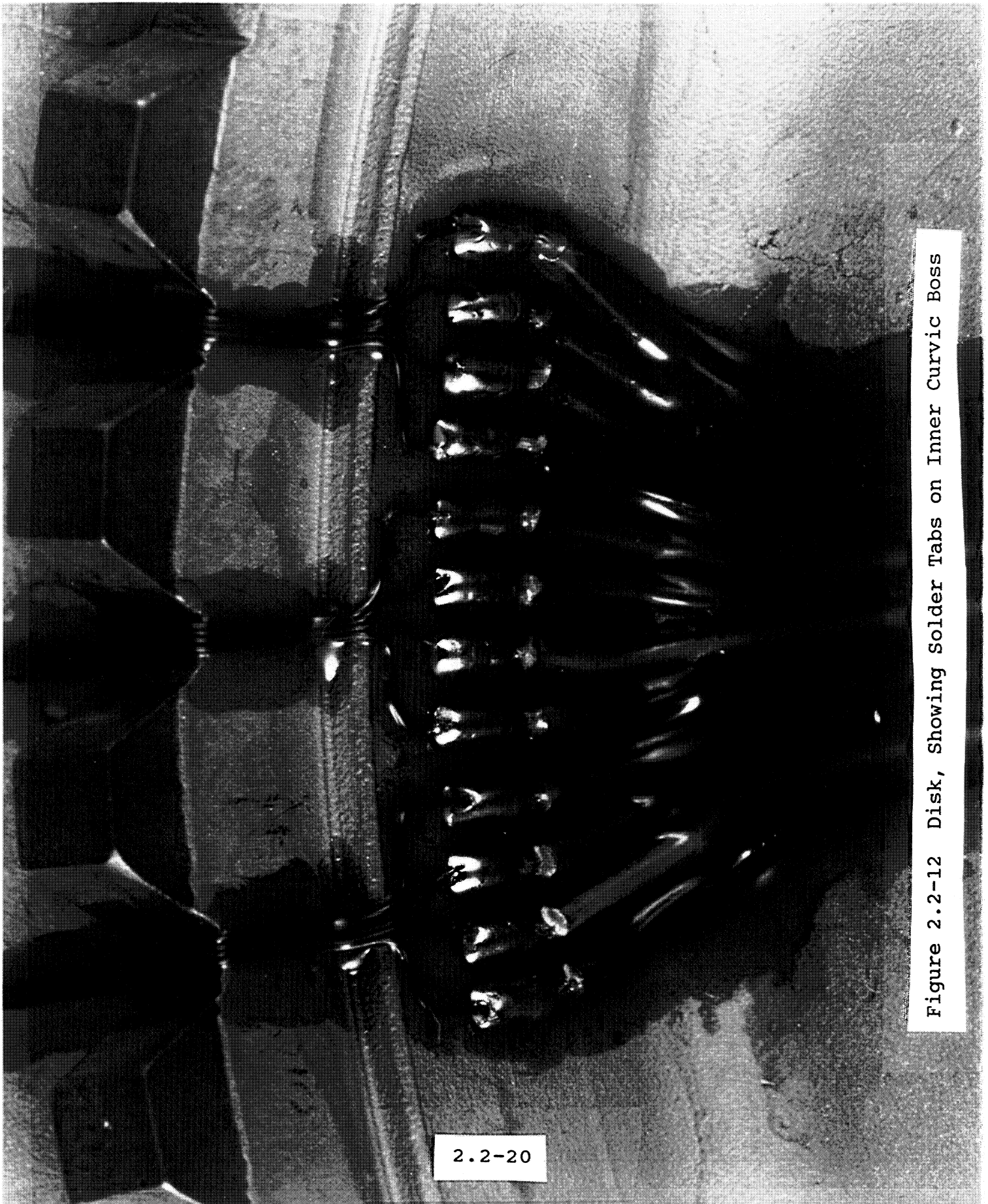


Figure 2.2-12 Disk, Showing Solder Tabs on Inner Curvic Boss

2.2-20



Figure 2.2-13 Strain Gage Applied to Turbine Blade

2.2-21

ORIGINAL PAGE
COLOR PHOTOGRAPH



Fig 2.2-14. Routing Lead Wire Through Grind-out in Platform

2.2-22

ORIGINAL PAGE
COLOR PHOTOGRAPH

2.2-23

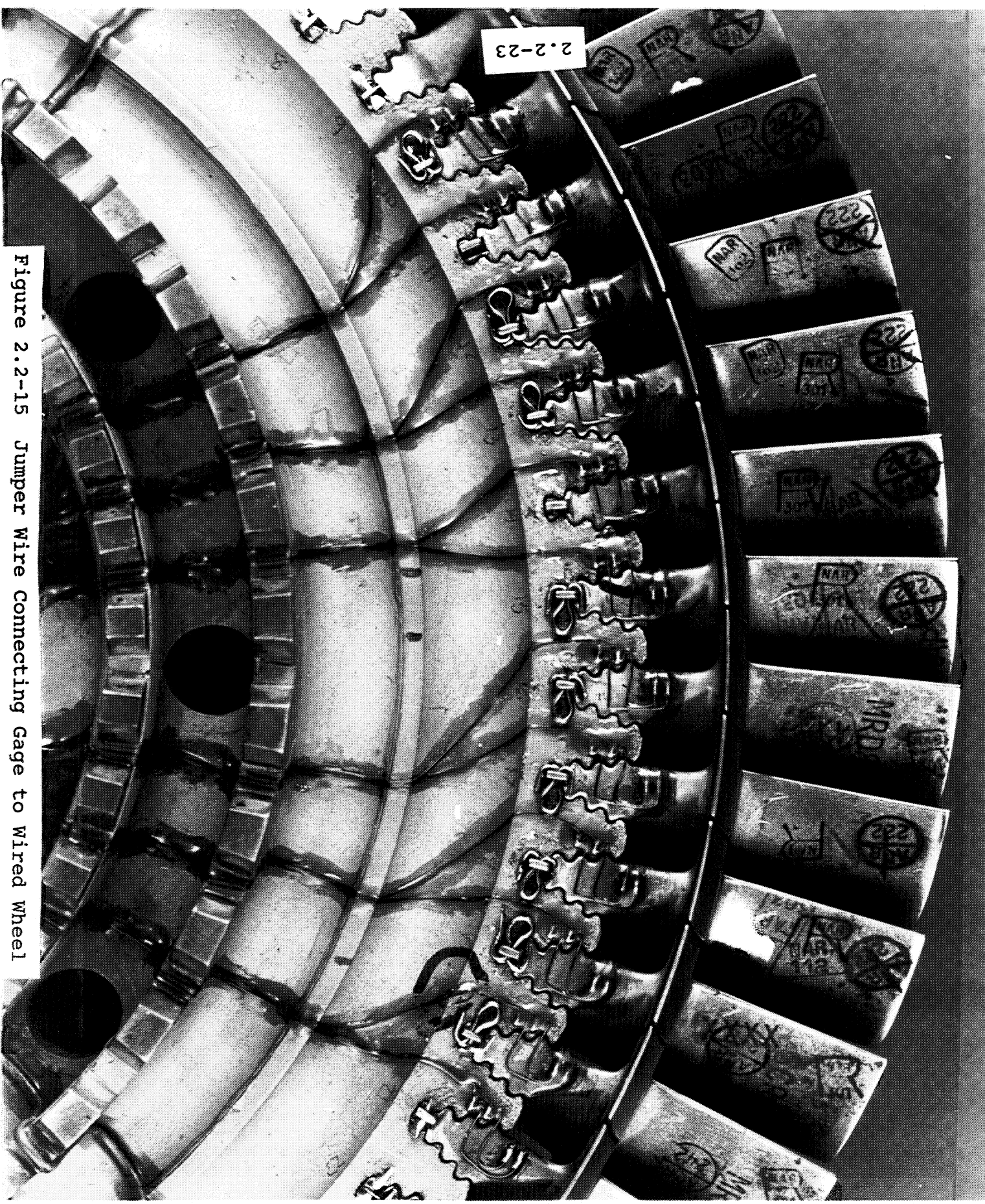
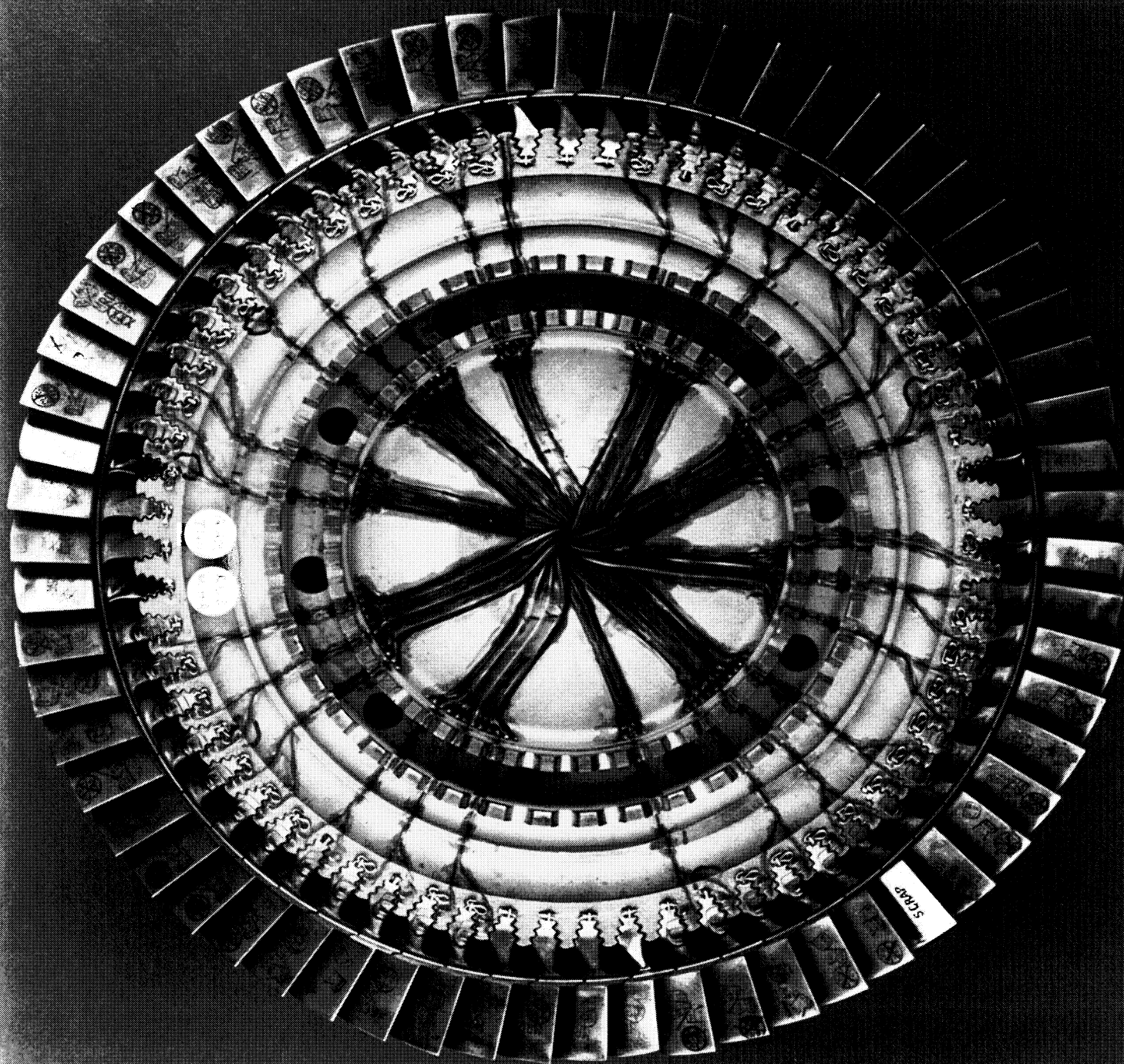


Figure 2.2-15 Jumper Wire Connecting Gage to Wired Wheel

2.2-24

Figure 2.2-16 Assembled HPFTP 1st Stage Disk



2.3 TEST PROGRAM

2.3.1 Goal of Test

The goals of the Blade Tip Rubbing Stress Prediction test program were to verify the predictions made during the analytical and parametric study phases of this program, to increase the level of understanding of the generation of stresses caused by turbine tip seal rubbing, and to simulate, as closely as possible, the rubbing behavior observed in SSME operation. This data can therefore be directly used to determine if rubbing-induced stresses are detrimental to SSME blades. To this purpose, testing was carried out using SSME HPFTP turbine hardware. The choice of the SSME HPFTP 1st stage turbine as a test vehicle was made for several reasons. First, a large body of analytical and experimental work has been performed on the HPFTP, and this led to the choice of the HPFTP for both the analytical and experimental phases of the program. Further, a pre-existing tester using HPFTP hardware was readily available. Finally, the SSME HPFTP turbine blades do rub on their tip seals, and this is one suspected cause of continued blade cracking.

The turbine blade tester, known as the "Whirligig" tester, is located in Rocketdyne's Engineering Development Laboratory, and since 1978, has been used in extensive test series aimed at improving SSME turbine performance and life.

For this test program a special test module was designed and fabricated to fit onto the baseline whirligig apparatus. This test module consists of a rigid frame holding a hydraulically activated device which simulates the turbine tip seal. The whirligig and tip rubbing test module are described elsewhere in this report. Rubbing of the blade tip on the tip seal is simulated by pressing the test article, which approximates the SSME HPFTP tip seal in radius and hardness, against the tips of the turbine blades as they spin past. The turbine blades were fitted with strain gages, and the test module was fitted with load cells which showed the force exerted on the turbine blades, and with accelerometers which show the vibratory environment of the test module.

2.3.2 Test Procedure

2.3.2.1 Whirligig Operation. To maintain consistency and safety in the operation of the whirligig tester, a set of procedures were developed during the 1978 HPFTP whirligig program, and have been modified as appropriate for all test series since. The following outline describes the operation of the whirligig tester.

1. Insure that all instrumentation and facility support functions are active and that all redline observers are ready. Turn on vacuum pumpdown system.
2. Apply slip ring coolant flow; verify flow rate and pressure.
3. Apply bearing lubrication oil flow to whirligig bearings. Start lubrication duration stopwatch. Verify lubrication supply pressure and flowrates to both bearings.
4. Pressurize the bearing damper system. Verify.
5. Pressurize the bearing preload system. Verify.
6. Turn on all data recorders and ensure that all instrumentation is active and recording.
7. Verify that test chamber pressure is within specified limits.
8. Begin whirligig rotation. Increase rotation speed to 5000 RPM. Verify proper operation before proceeding with test.
9. During test, continue to monitor whirligig operational parameters, and take appropriate blue line action as required. Stop test if any redlines are exceeded, and address situation before resuming test.
10. At end of test, reduce whirligig speed zero RPM. Turn off lubrication flow, bearing damper and preload pressure, and all purges. Secure systems.
11. Examine whirligig hardware condition when it is safe to enter test chamber.

2.3.2.2 Test Module Operation. The test module consists of a rigid frame supporting a hydraulic actuator mechanism which in turn moves the test article which approximates the SSME HPFTP 1st stage tip seals in hardness and radius of curvature. Before the test began, the gap between the test article, also known as the "brake shoe", and the turbine blades was set to 0.025 inches with feeler gauges, to account for the radial growth of the turbine disk at high rotational speed, plus adequate safety margin. The growth of the disk and blades due to rotational speed was calculated from a large Finite Element Model of the disk, and the predicted growth as a function of speed is shown in Table 2.3-1.

The test article position relative to the turbine disk was controlled with two ten-turn potentiometers, which can be seen in Figure 2.3-1, the test module control panel. The baseline position of the test article was controlled by a potentiometer labeled "setpoint", which was used to set the initial gap between the test article and the turbine blades. Once this point was established, the setpoint potentiometer was locked in position, and was not moved throughout the remainder of the test. The setpoint chosen was such that a 0.025 inch clearance existed between the stationary wheel and the test article.

By pressing an activation button, labeled "initiate contact" in Figure 2.3-1, the test article could be moved toward the turbine blades in a pulse of predetermined depth and duration. The depth was controlled by the second potentiometer, labeled "span" in Figure 2.3-1. The span potentiometer was set to produce a hydraulic piston displacement of 10 mils per revolution of the potentiometer dial, which was equivalent to 1 mil per numbered division on the dial, or 0.2 mils per small division. The pulse duration was set with three thumbwheels, and was variable from 0.001 to 0.999 seconds.

It should be noted that the above displacements are measured at the piston plunger. The actuator piston clevis was connected to one end of the test article, and the other end of the test article was supported by a pin. This meant that the distance between the center of the test article and the turbine blades moved only half as far as the piston; ie., the tester geometry gave a two-to-one increase in sensitivity. Thus the above described 0.2 mil piston movement, which corresponded to the minimum calibrated potentiometer adjustment, gave a displacement of the test article toward the turbine of only 0.1 mils.

2.3.2.3 Test Plan. Two tests were performed, a dynamic calibration test and the rubbing tests to gain strain gage data.

The test procedure consisted primarily of two processes: a) seeking the depth of movement which would result in the test article just touching the turbine blade tips, and b) "test rubs" where the depth of movement was set to 0.1 mil deeper (at the center of the test article) than the depth of rubbing initiation.

The process of seeking the depth of initiation of rubbing is shown graphically in Figure 2.3-2. The Y-axis represents the clearance between the test article "neutral position" and the blade tips, and the X-axis represents several attempts to establish the depth for the onset of rubbing. The depth of movement of the test article was adjusted incrementally, the activation button was pushed, and strain gage signal observers responded either "Rubbing Contact" or "No Rubbing", as appropriate. The incremental depth of plunge selected was 0.25 mils at the center of the brake shoe. The rub/no-rub verification was repeated as many times as necessary to satisfy the strain gage observers at each depth before the depth of plunge was increased. The duration of the plunge was set to 0.350 seconds while seeking the initiation of rubbing. This was considered long enough for the observers to clearly note contact. For the rubbing tests only (ie., not for the dynamic calibration test), when rubbing contact was confirmed at a particular depth, the depth was increased by 0.1 mils at the center of the brake shoe and the plunge duration was changed to 0.050 seconds. This duration was chosen to minimize frictional heating of the blade tips.

A preliminary dynamic calibration test was conducted to verify proper whirling operation and also to verify that the blade tips were making contact at the center of the test article arc. This was considered important for two reasons. First, contact with the "corner" of the arc, where the arc intersects the flat underside of the test article, would produce potentially destructive stress levels in the turbine blades. Second, the arc through which contact is made was shown in Phase I of this program to be an important parameter in the prediction of rubbing-induced stresses. In the HPFTP the rubbing arc is on the order of 15 to 30 degrees, and the examination of the test article shows that different blades experienced rubbing arcs of between 20 and 27 degrees. The Time-Speed profile for the Dynamic Calibration Test, from the test plan, is shown as Figure 2.3-3.

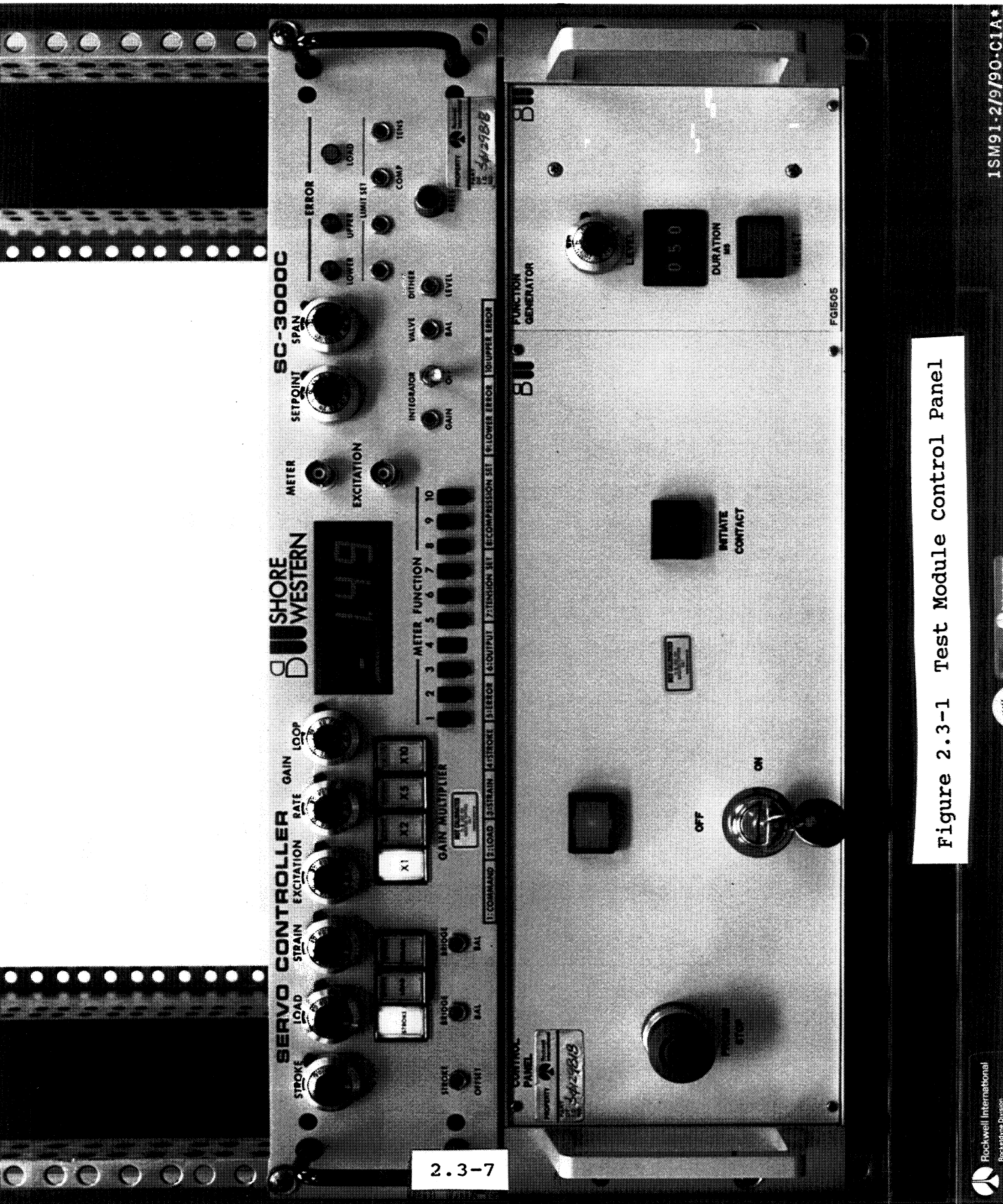
Although exact data on the depth of rubbing contact in the SSME HPFTP is unavailable, it was considered that 0.1 mil was a reasonable estimate, and so this was chosen as the depth of rubbing which would be produced in the test apparatus. The test plan for the rubbing test called for collection of data at turbine speeds of between 33,000 and 28,000 RPM, in 500 RPM increments. Two test rubs were performed at each speed, and the depth of rubbing contact beyond the depth of rubbing initiation was set to 0.1 mils for each rub.

Figure 2.3-4 shows the test plan Time-Speed and Event profile used for the rubbing test. The dynamic calibration and blade tip rubbing tests took approximately 15 minutes each, for a total test time of approximately 30 minutes. Rubbing data was collected on 12 channels, which is perfectly adequate for verifying the theoretical model. It was anticipated before the test began that some blades would be slightly higher than others, and that some blades might therefore not rub, and this was apparently the case. An additional 15 strain gages were lost due to failure of the epoxy bonding the wires to the disk.

WHIRLIGIG ROTOR GROWTH VS SPEED

ROTOR SPEED (RPM)	TIP GROWTH (INCHES)	DISK SHRINK PER 500 RPM (MILS)	EQUIV. DELTA (AT PLUNGER)	
			(MILS)	(SMALL INCR)
37,000	0.01499			
36,500	0.01458	-0.41	-0.82	4.1
36,000	0.01419	-0.39	-0.78	3.9
35,500	0.01380	-0.39	-0.78	3.9
35,000	0.01341	-0.39	-0.78	3.9
34,500	0.01303	-0.38	-0.76	3.8
34,000	0.01266	-0.37	-0.74	3.7
33,500	0.01229	-0.37	-0.74	3.7
33,000	0.01192	-0.37	-0.74	3.7
32,500	0.01156	-0.36	-0.72	3.6
32,000	0.01121	-0.35	-0.70	3.5
31,500	0.01086	-0.35	-0.70	3.5
31,000	0.01052	-0.34	-0.68	3.4
30,500	0.01018	-0.34	-0.68	3.4
30,000	0.00985	-0.33	-0.66	3.3
29,500	0.00953	-0.32	-0.64	3.2
29,000	0.00921	-0.32	-0.64	3.2
28,500	0.00889	-0.32	-0.64	3.2
28,000	0.00858	-0.31	-0.62	3.1
27,500	0.00828	-0.30	-0.60	3.0
27,000	0.00798	-0.30	-0.60	3.0
26,500	0.00769	-0.29	-0.58	2.9
26,000	0.00740	-0.29	-0.58	2.9
25,500	0.00712	-0.28	-0.56	2.8
25,000	0.00684	-0.28	-0.56	2.8
24,500	0.00657	-0.27	-0.54	2.7
24,000	0.00631	-0.26	-0.52	2.6
23,500	0.00605	-0.26	-0.52	2.6
23,000	0.00579	-0.26	-0.52	2.6
22,500	0.00554	-0.25	-0.50	2.5
22,000	0.00530	-0.24	-0.48	2.4
21,500	0.00506	-0.24	-0.48	2.4
21,000	0.00483	-0.23	-0.46	2.3
20,500	0.00460	-0.23	-0.46	2.3
20,000	0.00438	-0.22	-0.44	2.2

Table 2.3-1 Rotor Growth with Rotational Speed



ORIGINAL PAGE
COLOR PHOTOGRAPH

Figure 2.3-1 Test Module Control Panel

BLADE TIP RUBBING WHIRLIGIG TEST PLAN

SEARCH FOR INITIATION OF RUBBING CONTACT

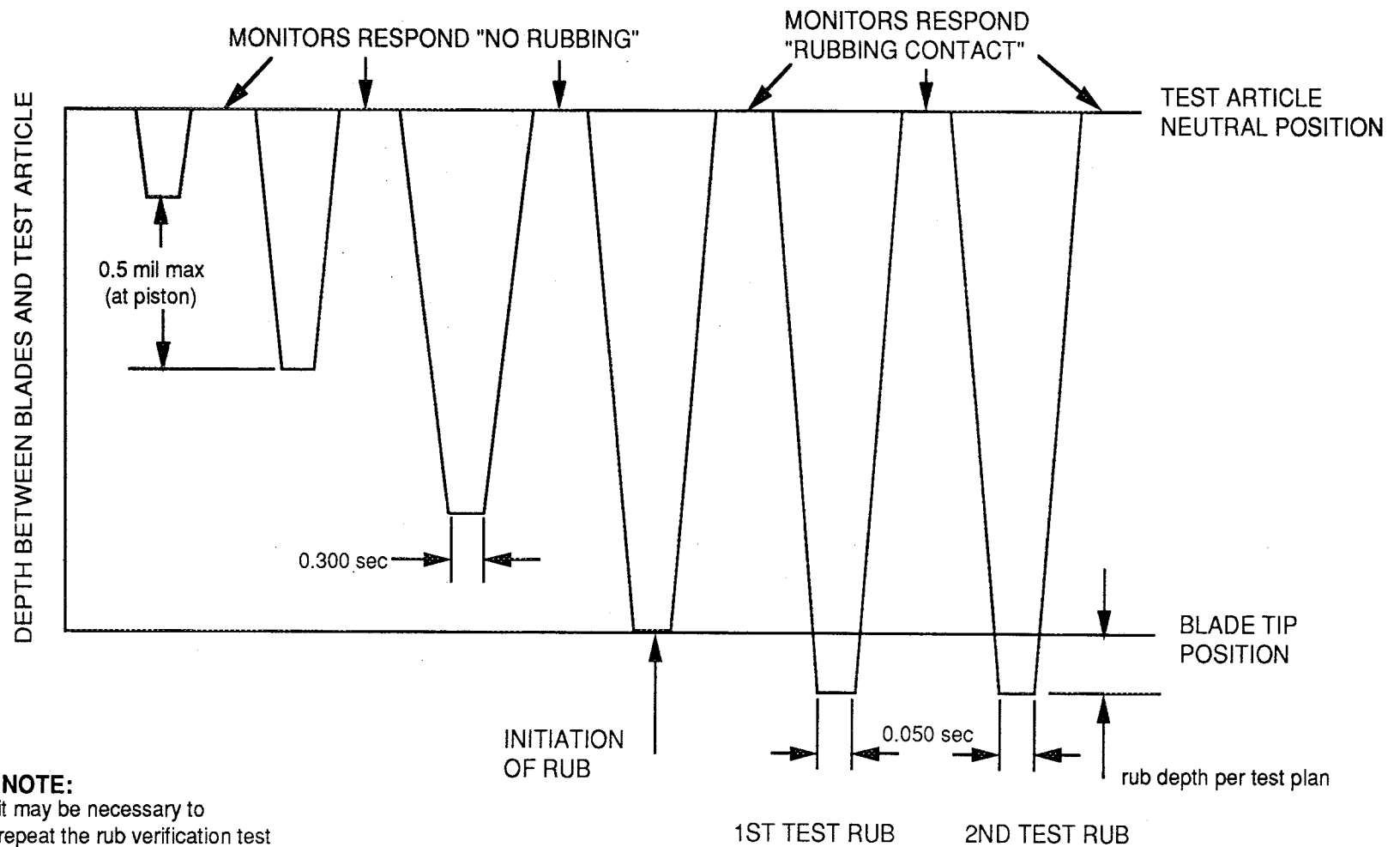


Figure 2.3-2 Seeking the Initiation of Rubbing Contact

BLADE TIP RUBBING WHIRLIGIG TEST PLAN **DYNAMIC CALIBRATION TEST TIME-SPEED PROFILE**

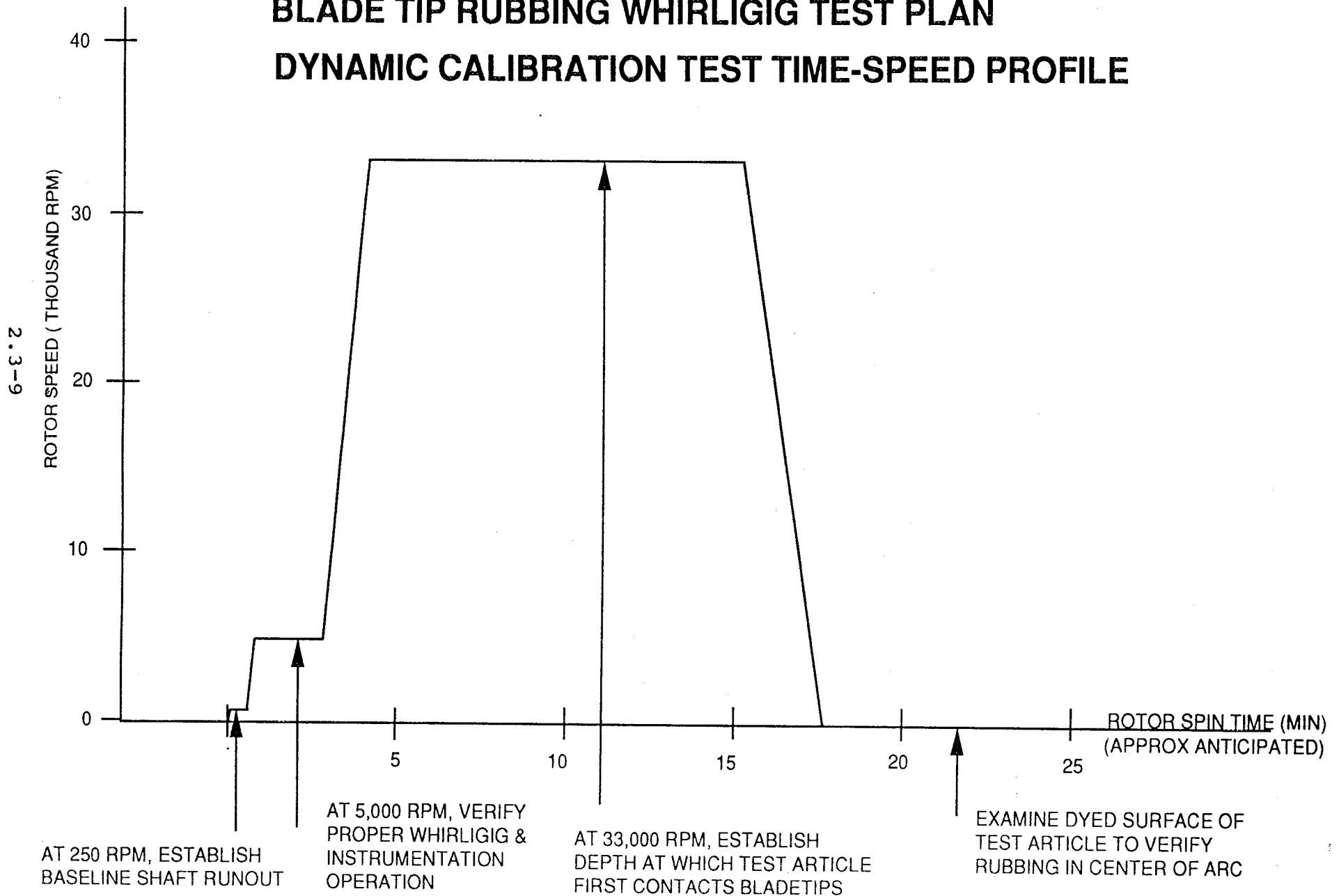


Figure 2.3-3, Dynamic Calibration Test Time-Speed Profile

2.3-10

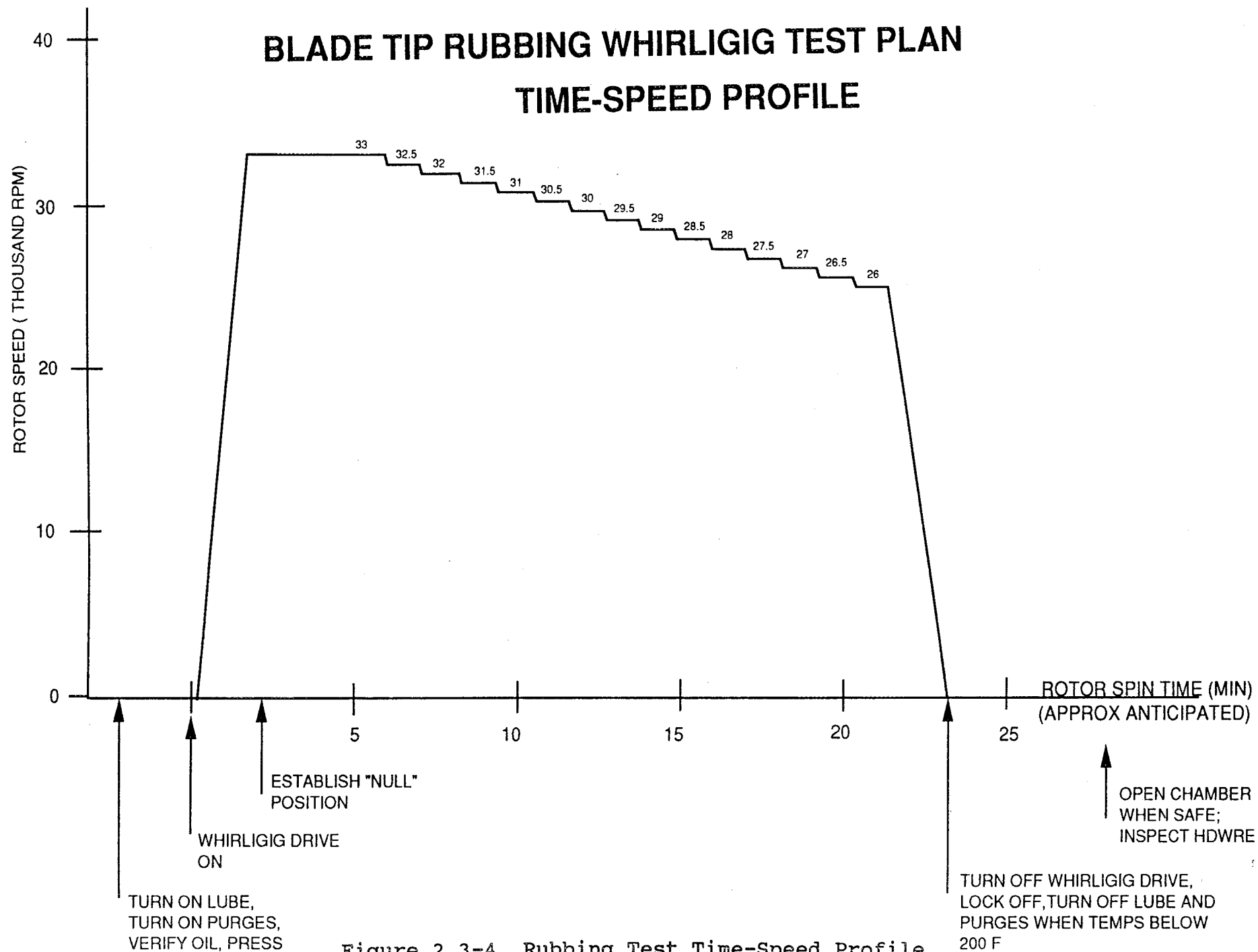


Figure 2.3-4 Rubbing Test Time-Speed Profile

2.4 TEST RESULTS

2.4.1 Summary

On November 19, 1990 the blade tip rubbing test was conducted in the Rocketdyne Engineering Development Laboratories. The test was run according to the previously described test plan which consisted of a speed ramp up to 32740 rpm followed by ten speed dwells at successively lower speeds during which rubbing was initiated. Of the 48 instrumented blades, 12 recorded measurable strains due to rubbing. Tabulation of the data shows peak-to-peak strain ranges as high as 920 $\mu\text{in/in}$. Strain levels were found to vary with shaft speed with the highest levels occurring at the higher speeds. The character of the strain signals was that of an initial rub-produced peak followed by several cycles of free vibration decay and then a repeat of the rub. The predominant frequencies of motion during free vibration were that of the first bending and first axial modes of the blade.

2.4.2 Shaft Speed versus Time

The test was run according to a test plan which called for an initial speed dwell at 33000 rpm followed by dwells at successively lower speeds in 500 rpm increments with the last data point scheduled to be 28000 rpm as shown in Figure 2.3-4. Because of limitations in the control of shaft speed, however, the test rubs did not occur at exactly the speeds called out in the plan. The actual speed profile followed during the test is shown in Figure 2.4-1 and consisted of ten dwells beginning at 32740 rpm and continuing downward at approximately 500 rpm increments. Table 2.4-1 gives the numerical values of speed at 5 second intervals throughout the test. Shaft speed was held constant at each level until satisfactory rub data was acquired and then the speed was adjusted for the next test point.

2.4.3 Strain Gage Data Processing

The data obtained during this test was highly transient in nature, consisting of short duration (150-350 milli-second) rub pulses. Processing of this type of data is usually restricted to filtered time-histories since most frequency domain methods require steady-state data to obtain good results. For the test data generated in this program, however, it was decided to use both time-history and frequency domain processing. The time-history processing consisted of low pass filtered plots at each of the rub points. Strain gage and accelerometer signals were expanded using time base expansion techniques on an ASTRO-MED data

processing machine which gave a frequency response of well over 20 KHz. The signals were processed at two different paper speeds to give compressed and expanded views of the response signal. Frequency domain data processing consisted of PSD plots taken during the time of the rub. It should be clearly understood that rub induced blade response is not a steady-state phenomenon and this method will give erroneous amplitude results due to the averaging inherent in the PSD process. It is believed, however, that an adequate picture of the frequency content of the data can be obtained from processing of this type and this is why PSD plots were used. The reader is cautioned that the amplitudes shown on the PSD charts could be significantly in error and it is best to consult the data tables which were based on strain time-histories.

2.4.4 Compressed Time-History Data

Compressed time-history data records were obtained for the entire test for each of the 45 strain gages which were recorded. Forty-eight gages were initially installed but three were lost pre-test and therefore were not recorded. Each strain record was carefully reviewed to determine if rubbing had occurred. Of the 45 blades with active strain gages installed, blade dynamic response during rubbing was noted on 12 blades, the data signal was lost on 6, and no rubbing indications were seen on 27 blades. For each of the signals the time duration and peak-to-peak strain range was noted during the period of the rub. Low pass filtering was not used during the processing of the compressed time-histories. The signals were AC coupled (2 Hz high pass filter) to remove any DC drift during the test. Typical compressed time-histories are shown in Figures 2.4-2 and 2.4-3 and clearly show the beginning and end of the rub as well as the overall character of the response. Of particular interest were the peaks observed near the beginning and end of the rub cycle. During the first few rubs the time-history signals were very erratic with numerous spikes during the rub. As the test progressed the signals changed to a smoother transition during the initiation and end of the rub. For example Figure 2.4-4 shows the rub response of blade number 2 at three different times during the testing. Notice that the first response plot, taken during the beginning of the test shows peaks at the beginning and end of the rub while those near the middle and end of the test do not have this behavior. Since the phenomenon occurred during rubbing near the beginning of the test and did not occur after the first two or three speed dwells it was hypothesized that it may be related to "wearing in" of the simulated tip seal. As will be discussed later the tip seal shows distinct wear patterns due to rubbing and this could

change the characteristics of the response. It is also possible that the phenomenon is speed related since only higher speeds show the peaking. Analysis results indicate that the compressed time-histories should be flat during the duration of the rub so the test results indicate a behavior that deviates from what was expected and is not completely understood.

2.4.5 Strain Levels versus Speed

The analysis results shown in Figure 2.1-12 show that, for a given contact arc, the maximum strain is dependent on shaft speed. To confirm this analytical result the data from the compressed time-history plots was tabulated and plotted as a function of speed. A typical compressed time-history plot which has been marked to show the strain range is presented in Figure 2.4-5. Strain range data from plots of this type was tabulated and plotted as a function of speed for each gage. Table 2.4-2 presents the tabulated data while Figures 2.4-6 thru 2.4-8 show the speed dependence in graphical form. It is clear from the plots that two families of behavior exist. The high speed points, which were taken first, are much larger in magnitude than those taken at lower speeds. This is a result of the peaking that occurred during rubbing on these tests and, as mentioned previously, may not be a function of speed but of changing tip seal characteristics due to wearing.

2.4.6 Expanded Time-History Data

Expanded time-histories of rub-induced blade response were obtained by first determining the exact time of the rub from the compressed records described above and then playing back the tape using 64:1 time base expansion and a very fast (200 mm/sec) paper speed. This yielded an actual time scale of 6400 mm/sec which gave excellent reproductions of the high frequency rub phenomenon. Samples of the data are shown in Figures 2.4-9 thru 2.4-17. In most cases the basic character of the signal consists of a peak due to the initial rub followed by free vibration decay until the next rub. The free vibration decay portion of the rub cycle varies to a great extent. It consists of first mode, third mode or a combination of first and third mode responses. In a few isolated instances a frequency near that of the fourth blade mode was also observed. The first blade mode consists of bending of the airfoil trailing edge in the easy direction (tangential to the disk rim), the third blade mode is bending in the stiff direction (axial), and the fourth mode is second flex in the easy direction. The blade second mode frequency (torsion) was not observed in the time-history data. An

example of a decay which is predominantly first mode response at about 4590 Hz can be seen in Figure 2.4-14. Similarly Figure 2.4-10 presents an example of third mode response during the decay at approximately 13075 Hz. On many occasions the character of the free vibration decay was observed to change abruptly from one mode to the other during the course of a few rubs as can be seen from strain gage 4 in Figure 2.4-10 and also by comparison of Figures 2.4-14 and 2.4-15 which were taken about 80 msec apart during the same rub. This was very puzzling as the analytical results show only first mode response during this period.

An interesting phenomenon was observed on several of the gages during rubbing. The rub character was similar to that previously described but the rub occurred every second shaft revolution instead of once per rev. Figures 2.4-11 and 2.4-14 show expanded traces of several strain gages during times when this phenomenon was observed. Initially it was believed that the rotor was responding in such a way as to orbit away from the tip seal in a 1/2 per rev manner but this proved to be untrue since the rotordynamic data from the test rig showed no subsynchronous behavior. The phenomenon does not occur on every blade either. Another, more plausible, explanation is that the tip seal segment is responding dynamically to the force of the rub and moves away from rotor during the period of the next blade pass. The data from an accelerometer mounted on the tip seal supports this hypothesis since it clearly responds during the rub and gives levels of up to 85 G's peak-peak. Samples of expanded time-history traces for the tip seal accelerometer are given in Figures 2.4-18 through 2.4-20 and clearly show rubbing which occurs every second revolution. In particular, Figure 2.4-19 shows blade tip rub on four successive shaft revolutions followed by four revolutions where blade tip rub is observed on every second pass. It is not known why the tip seal segment moves away after some of the rubs and stays in place after others.

2.4.7 Frequency Domain Data

Power Spectral Density (PSD) Plots of strain gage and accelerometer data are shown in Figures 2.4-21 thru 2.4-44 for the 0-5 KHz frequency range and Figures 2.4-45 thru 2.4-68 for the 0-20 KHz frequency range. As mentioned previously in this report, the information contained in these plots should be used to determine frequency information only, as the amplitudes can be erroneous due to averaging of non steady-state data. The 5 KHz PSD's use 9 frames of data for each plot while the 20 KHz PSD's use 30 frames. Each plot represents 300 msec of data during the time of a rub which is divided into frames and then amplitude averaged in the

frequency domain. Since the amplitude and frequency of the data can change dramatically during this period (see Figures 2.4-14 and 2.4-15 which were taken during the same rub) the averaging process will alter the amplitudes to incorrect values. Nevertheless the PSD plots give an excellent picture of the various frequencies which are present during the rub phenomenon.

Observations from the 5 KHz PSD plots herein are that the rub signal consists of the basic once per revolution frequency and integer multiples of this frequency up through 9N. In addition to the engine order frequencies the data shows the first blade mode very clearly. The first blade mode, which consists of airfoil bending in the flexible direction, can be easily seen on nearly all of the 5 KHz PSD plots at approximately 4500 Hz.

The 20 KHz PSD plots were not as informative as the 5 KHz plots and raised some unanswered questions concerning the response. A comparison of Figures 2.4-21 and 2.4-45 shows that the 20 KHz PSD does not resolve the engine order forcing functions as well and leads one to believe that only even multiples of shaft speed are present. This could be a result of the larger analysis bandwidth used or a greater number of data frame averages. The 20 KHz PSD uses an average of 30 data frames over the time slice while the 5 KHz PSD used 9 frames during the same time. The highest engine order observed in these plots was 36N which can easily be seen in Figure 2.4-46. In addition to the peaks at multiples of shaft speed the 20 KHz PSD's show what appears to be a mode at approximately 9100 Hz. This frequency, which remains nearly stationary as shaft speed is changed, does not correlate with any known blade frequency. The torsion mode is the nearest neighbor at 10300 Hz and it was never observed on any of the time-history data. At this time it is not known what caused the peak at 9100 Hz.

A few Power Spectral Density plots were also taken at times when the blades were rubbing on every second revolution as discussed previously. An example is presented in Figure 2.4-31 which shows not only integer multiples of shaft speed but also half integer multiples. This is an expected result in the data when the rubbing occurs every other revolution.

2.4.8 Post Test Hardware Inspection

After the test a visual inspection of the blade tips was completed with the goal of determining which blades actually contacted the tip seal and which did not. Table 2.4-3 presents the results of the inspection which shows rubbing on 29 of the 48 instrumented blades. The remaining 15

uninstrumented blades were machined with shortened tips so that rubbing could not occur. The location of rubbing was predominately at the trailing edge of the blade tip on the suction side of the blade, but sometimes extended to as much as 90 percent of the cross sectional area. Figure 2.4-69 shows typical rub marks on several blades.

In addition to the blade tips the seal segment was inspected after the rubbing test. Figures 2.4-70 and 2.4-71 present photographs of the simulated tip seal which clearly shows the rub marks.

The whirligig assembly was also inspected for signs of debonding which normally occurs on a small percentage of the strain gage leadwires. A photograph showing debonding of leadwires in the area between the first and second stage turbine disks is shown in Figure 2.4-72. This debonding is responsible for the loss of signal observed on some of the gages during the test.

2.4.9 Correlation of Rub Inspection with Strain Data

As mentioned above, Table 2.4-3 presents the results of the inspection of the blade tips for signs of rubbing. Twenty-nine of the 48 instrumented blades rubbed on the tip seal and, of these, 10 produced response time-histories which were visible in the data. Twelve of the remaining 19 gages failed and the data from the other seven gages showed no indications of rubbing. Prior to the test these seven data channels were operative and the signal does not show any obvious breakup during the test. No instrumentation checks other than visual examinations were made post test to determine if the channels had failed. Further investigation was not done to determine why these seven gages did not produce signals during rubbing.

In addition to data from the 10 blades that rubbed, blades 32 and 37 recorded strains during the time of rubbing yet rub marks were not seen on the blade tips in the post-test inspection. Figure 2.4-73 schematically shows the positions of the blades which rubbed as compared to those which produced rubbing data. Typical time-histories for these blades are shown in Figures 2.4-16 and 2.4-17. Of particular interest is blade 37 of Figure 2.4-17 which produced a time-history that looks very similar to the rubbing signals of other blades that had definite rub marks. A thorough re-examination of this blade under magnification did not show any rub marks whatsoever. The response may be due to dynamic coupling through the disk, although the character of the signal is expected to be more like that of blade 32. Each of the two unrubbed blades were positioned

next to blades which had easily identifiable rub marks so coupling is a distinct possibility. Time-histories for blades 31 and 36 are presented alongside those of blades 32 and 37 for comparison purposes. As can be seen from the figures, the magnitude of response of these two blades is comparable.

2.4.10 Rub Angle

The rub angle as measured from the simulated tip seal during post test inspections was found to be approximately 27 degrees. Since approximately 30 test rubs were completed with this hardware it is impossible to tell if all the test rubs contacted the seal over the same arc. Ideally the test should consist of a single rub and then an inspection of the tip seal, however the schedule and budget constraints did not allow for replacement of the tip seal after every rub. For the purposes of this study it will be assumed that the contact arc remained constant throughout the test.

2.4.11 Comparison to SSME Hardware

One of the major goals of the test program was to determine if rub induced stresses are of sufficient magnitude to degrade SSME blade life. To this affect the testing was designed to create rub patterns similar to what is observed in typical post-test hardware inspections. Although there are a wide range of rub marks found during inspection, the consensus of the Rocketdyne Turbomachinery Group is that the rub patterns found on the simulated tip seal are very similar to those found in actual hardware. Figures 2.4-70 and 2.4-71 show photographs of the test seal alongside a recently hot-fired seal segment from HPFTP 4405 showing the similarity between the two. From this comparison it is safe to conclude that the test adequately simulated SSME rubbing conditions.

2.4.12 Blade Damping

As explained previously, after the initial rub pulse, the motion consists of free vibration which is predominately either the first blade bending mode or the first axial mode. Since friction dampers were not installed for this test it was an easy matter to determine the blade damping from the decay of the strain signal during the free vibration portion of the cycle. Using the log decrement method the damping of the blade was found to range from approximately $\zeta = .010$ to $\zeta = .012$ and represents a combination of material and fir tree root damping. It is interesting to note that damping of other blades with brazed fir trees has been measured as low as $\zeta = .0025$. This indicates that the blade/disk interface provides a significant amount of damping which will not be

realized in integrally bladed disks (Blisks). Blisk configurations have been proposed in several upcoming programs and should be studied carefully from the standpoint of damping before being committed to production.

2.4.13 Blade Natural Frequencies

The frequency of the first blade mode which consists primarily of airfoil bending (first flex mode) was found from the free vibration portion of the rubbing cycle to range from 4350 Hz to 4900 Hz. Similarly the first axial mode was found to range from 12900 Hz to 13550 Hz. In a few cases the blades were seen to vibrate at a frequency near the second flex mode as well, which was measured at 17500 to 18350 Hz. These frequencies compare to an values of 4750 Hz, 14030 Hz, and 18200 Hz for the three modes, respectively, which were obtained from past whirligig testing. The torsion mode, measured previously at 11240 Hz was not observed in any of the blade tip rubbing testing.

Table 2.4-1
Shaft Speed Time-History

TIME	DELTA TIME (SEC)	ELAPSED TIME (MIN)	GBOX SPEED 1 (RPM)	TIME	DELTA TIME (SEC)	ELAPSED TIME (MIN)	GBOX SPEED 1 (RPM)
153555	0	0.000	0	154050	5	4.917	32720
153600	5	0.083	250	154055	5	5.000	32740
153605	5	0.167	1300	154100	5	5.083	32740
153610	5	0.250	2110	154105	5	5.167	32740
153615	5	0.333	2950	154110	5	5.250	32600
153620	5	0.417	3770	154115	5	5.333	32260
153625	5	0.500	4610	154120	5	5.417	32220
153630	5	0.583	5470	154125	5	5.500	32160
153635	5	0.667	6340	154130	5	5.583	32030
153640	5	0.750	7170	154135	5	5.667	32020
153645	5	0.833	8020	154140	5	5.750	32020
153650	5	0.917	8900	154145	5	5.833	32030
153655	5	1.000	9750	154150	5	5.917	32020
153700	5	1.083	10630	154155	5	6.000	32040
153705	5	1.167	11490	154200	5	6.083	32040
153710	5	1.250	12360	154205	5	6.167	32040
153715	5	1.333	13230	154210	5	6.250	32040
153720	5	1.417	14110	154215	5	6.333	32040
153725	5	1.500	14970	154220	5	6.417	31830
153730	5	1.583	15840	154225	5	6.500	31540
153735	5	1.667	16690	154230	5	6.583	31540
153740	5	1.750	17580	154235	5	6.667	31540
153745	5	1.833	18470	154240	5	6.750	31560
153750	5	1.917	19340	154245	5	6.833	31540
153755	5	2.000	20200	154250	5	6.917	31550
153800	5	2.083	21080	154255	5	7.000	31540
153805	5	2.167	21940	154300	5	7.083	31550
153810	5	2.250	22840	154305	5	7.167	31550
153815	5	2.333	23730	154310	5	7.250	31560
153820	5	2.417	24590	154315	5	7.333	31540
153825	5	2.500	25470	154320	5	7.417	31560
153830	5	2.583	26350	154325	5	7.500	31510
153835	5	2.667	27220	154330	5	7.583	31050
153840	5	2.750	28090	154335	5	7.667	31030
153845	5	2.833	28960	154340	5	7.750	31030
153850	5	2.917	29840	154345	5	7.833	31030
153855	5	3.000	30720	154350	5	7.917	31040
153900	5	3.083	31600	154355	5	8.000	31020
153905	5	3.167	32490	154400	5	8.083	31040
153910	5	3.250	32660	154405	5	8.167	31020
153915	5	3.333	32650	154410	5	8.250	31030
153920	5	3.417	32660	154415	5	8.333	31030
153925	5	3.500	32660	154420	5	8.417	31040
153930	5	3.583	32680	154425	5	8.500	31030
153935	5	3.667	32670	154430	5	8.583	30930
153940	5	3.750	32670	154435	5	8.667	30550
153945	5	3.833	32680	154440	5	8.750	30560
153950	5	3.917	32680	154445	5	8.833	30560
153955	5	4.000	32690	154450	5	8.917	30560
154000	5	4.083	32690	154455	5	9.000	30560
154005	5	4.167	32690	154500	5	9.083	30560
154010	5	4.250	32690	154505	5	9.167	30560
154015	5	4.333	32700	154510	5	9.250	30560
154020	5	4.417	32700	154515	5	9.333	30550
154025	5	4.500	32710	154520	5	9.417	30180
154030	5	4.583	32710	154525	5	9.500	30050
154035	5	4.667	32720	154530	5	9.583	30070
154040	5	4.750	32730	154535	5	9.667	30070
154045	5	4.833	32740	154540	5	9.750	30070

Table 2.4-1 (Continued)
Shaft Speed Time-History

TIME	DELTA TIME (SEC)	ELAPSED TIME (MIN)	GBOX SPEED 1 (RPM)	TIME	DELTA TIME (SEC)	ELAPSED TIME (MIN)	GBOX SPEED 1 (RPM)
154545	5	9.833	30070	155035	5	14.667	28030
154550	5	9.917	30070	155040	5	14.750	27480
154555	5	10.000	30050	155045	5	14.833	26530
154600	5	10.083	30060	155050	5	14.917	25610
154605	5	10.167	30060	155055	5	15.000	24720
154610	5	10.250	30050	155100	5	15.083	23790
154615	5	10.333	29550	155105	5	15.167	22870
154620	5	10.417	29540	155110	5	15.250	21960
154625	5	10.500	29550	155115	5	15.333	21010
154630	5	10.583	29550	155120	5	15.417	20110
154635	5	10.667	29560	155125	5	15.500	19200
154640	5	10.750	29550	155130	5	15.583	18270
154645	5	10.833	29540	155135	5	15.667	17370
154650	5	10.917	29540	155140	5	15.750	16440
154655	5	11.000	29540	155145	5	15.833	15520
154700	5	11.083	29530	155150	5	15.917	14600
154705	5	11.167	29530	155155	5	16.000	13690
154710	5	11.250	29430	155200	5	16.083	12770
154715	5	11.333	29090	155205	5	16.167	11870
154720	5	11.417	29070	155210	5	16.250	10950
154725	5	11.500	29050	155215	5	16.333	10030
154730	5	11.583	29050	155220	5	16.417	9120
154735	5	11.667	29050	155225	5	16.500	8190
154740	5	11.750	29040	155230	5	16.583	7290
154745	5	11.833	29060	155235	5	16.667	6400
154750	5	11.917	29060	155240	5	16.750	5520
154755	5	12.000	29050	155245	5	16.833	4640
154800	5	12.083	29060	155250	5	16.917	3740
154805	5	12.167	29060	155255	5	17.000	2890
154810	5	12.250	28870	155300	5	17.083	2040
154815	5	12.333	28530	155305	5	17.167	1260
154820	5	12.417	28540	155310	5	17.250	170
154825	5	12.500	28540	155315	5	17.333	0
154830	5	12.583	28540	155320	5	17.417	0
154835	5	12.667	28550	155325	5	17.500	190
154840	5	12.750	28540	155330	5	17.583	0
154845	5	12.833	28540				
154850	5	12.917	28530				
154855	5	13.000	28530				
154900	5	13.083	28550				
154905	5	13.167	28540				
154910	5	13.250	28550				
154915	5	13.333	28540				
154920	5	13.417	28540				
154925	5	13.500	28280				
154930	5	13.583	28030				
154935	5	13.667	28040				
154940	5	13.750	28040				
154945	5	13.833	28050				
154950	5	13.917	28030				
154955	5	14.000	28030				
155000	5	14.083	28020				
155005	5	14.167	28040				
155010	5	14.250	28050				
155015	5	14.333	28040				
155020	5	14.417	28040				
155025	5	14.500	28030				
155030	5	14.583	28030				

Table 2.4-2
Strain Ranges During Rubbing

Speed (rpm)	Strain Gages											
	2	4	5	6	31	32	35	36	37	45	53	60
28040	160	-	260	200	-	-	-	-	-	-	-	140
28540	260	240	224	-	-	-	-	-	-	-	-	-
28540	220	-	160	-	-	-	-	-	-	-	-	280
29060	200	-	160	-	-	-	-	-	-	-	-	-
30060	200	-	-	-	-	-	-	-	-	-	-	-
30550	200	-	-	-	-	-	-	-	-	-	-	-
31040	200	-	-	-	-	-	-	-	-	-	-	-
31540	180	-	-	-	-	-	-	-	-	-	-	-
31560	200	-	-	-	-	-	-	-	-	-	-	180
32040	520	500	536	464	192	-	-	-	-	-	-	196
32040	520	750	736	920	288	352	208	176	272	280	192	252
32740	320	900	656	768	272	272	208	304	400	208	272	376

All strain range units are $\mu\text{in/in}$

" - " symbol indicates no rubbing was detected

Table 2.4-3
Results of Blade Tip Inspection

Blade No.	Blade Instr	Visual % Rub	Strain Data
1	S/G	10%	-
2	S/G	10%	Rub
3	S/G	25%	-
4	S/G	75%	Rub
5	S/G	25%	Rub
6	S/G	25%	Rub
7	-	NONE	-
8	-	NONE	-
9	-	NONE	-
10	S/G	25%	-
11	S/G	10%	-
12	S/G	90%	-
13	S/G	90%	-
14	S/G	10%	-
15	S/G	15%	-
16	S/G	70%	-
17	S/G	15%	-
18	S/G	25%	-
19	S/G	85%	-
20	S/G	75%	-
21	S/G	60%	-
22	-	NONE	-
23	-	NONE	-
24	-	NONE	-
25	-	NONE	-
26	S/G	0%	-
27	S/G	0%	-
28	S/G	15%	-
29	S/G	0%	-
30	S/G	0%	-
31	S/G	10%	Rub
32	S/G	0%	Rub
33	S/G	0%	-
34	S/G	0%	-
35	S/G	2%	Rub
36	S/G	5%	Rub
37	S/G	0%	Rub

Blade No.	Blade Instr	Visual % Rub	Strain Data
38	-	NONE	-
39	-	NONE	-
40	-	NONE	-
41	-	NONE	-
42	S/G	0%	-
43	S/G	0%	-
44	S/G	0%	-
45	S/G	10%	Rub
46	S/G	0%	-
47	S/G	0%	-
48	S/G	0%	-
49	S/G	0%	-
50	S/G	0%	-
51	S/G	0%	-
52	S/G	15%	-
53	S/G	5%	Rub
54	-	NONE	-
55	-	NONE	-
56	-	NONE	-
57	-	NONE	-
58	S/G	0%	-
59	S/G	80%	-
60	S/G	20%	Rub
61	S/G	0%	-
62	S/G	10%	-
63	S/G	75%	-

BLADE TIP RUBBING WHIRLIGIG

WHIRLIGIG TIME-SPEED PROFILE

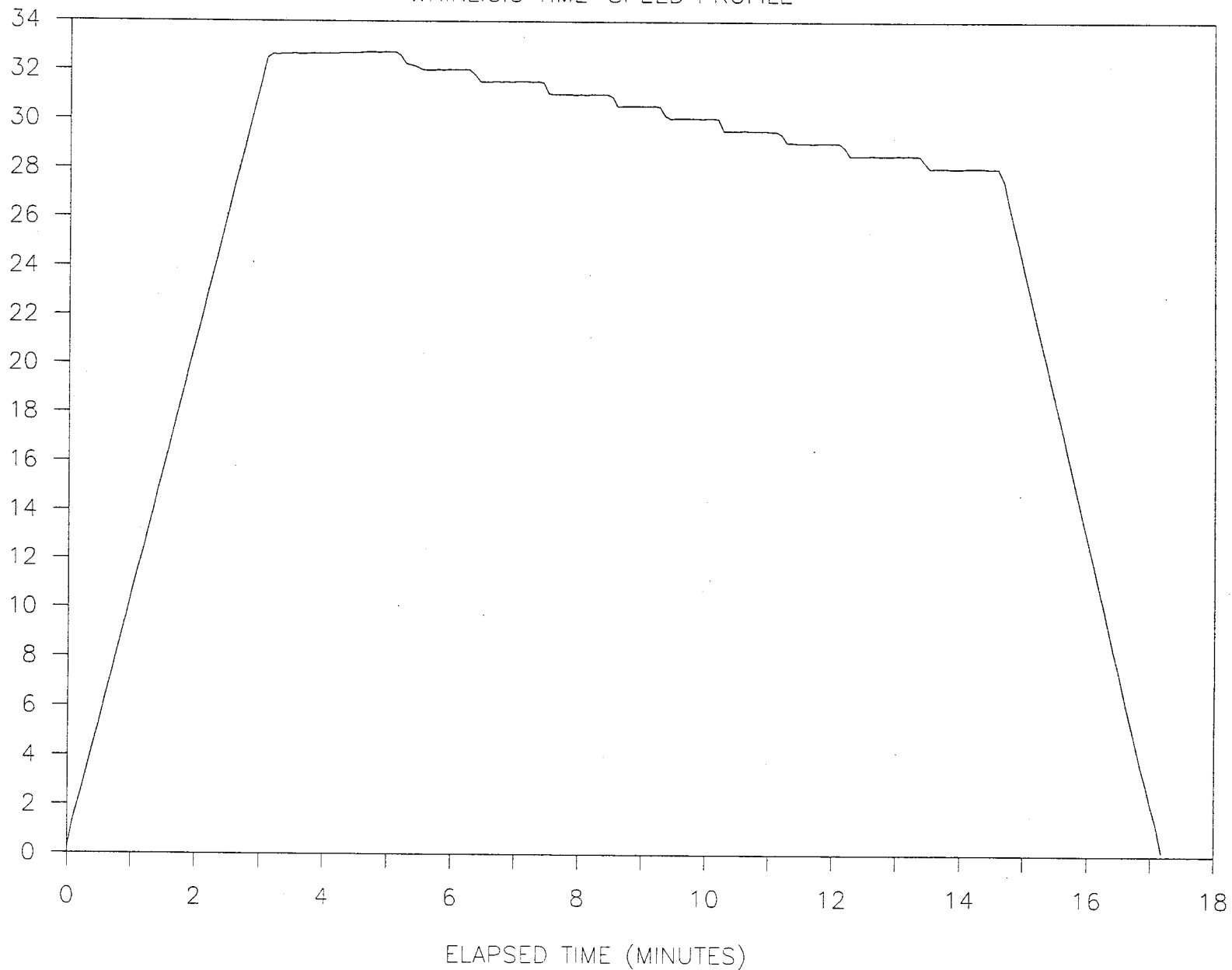
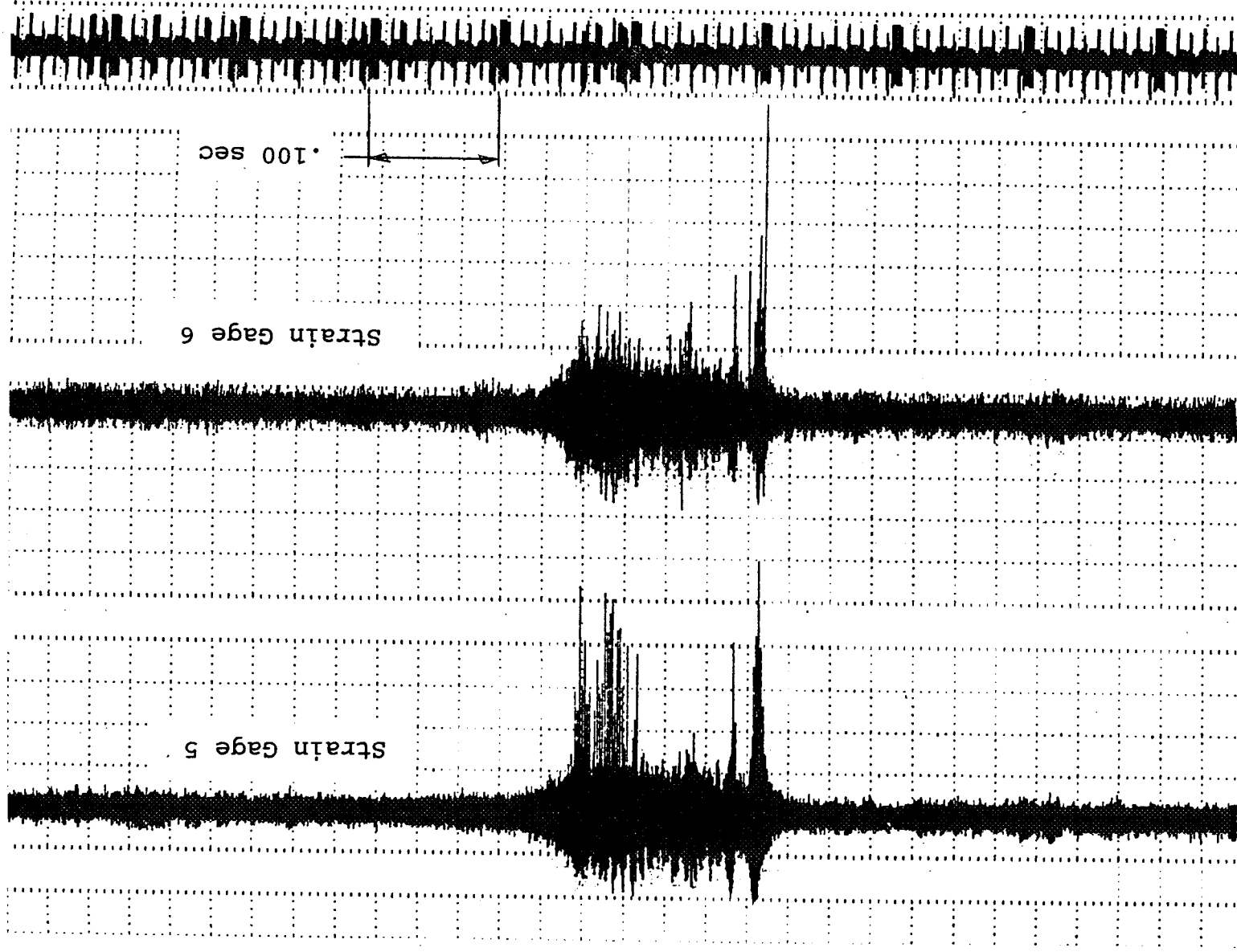


Figure 2.4-1
Speed Time-History

Figure 2.4-2
Compressed Time-History
32740 Rpm



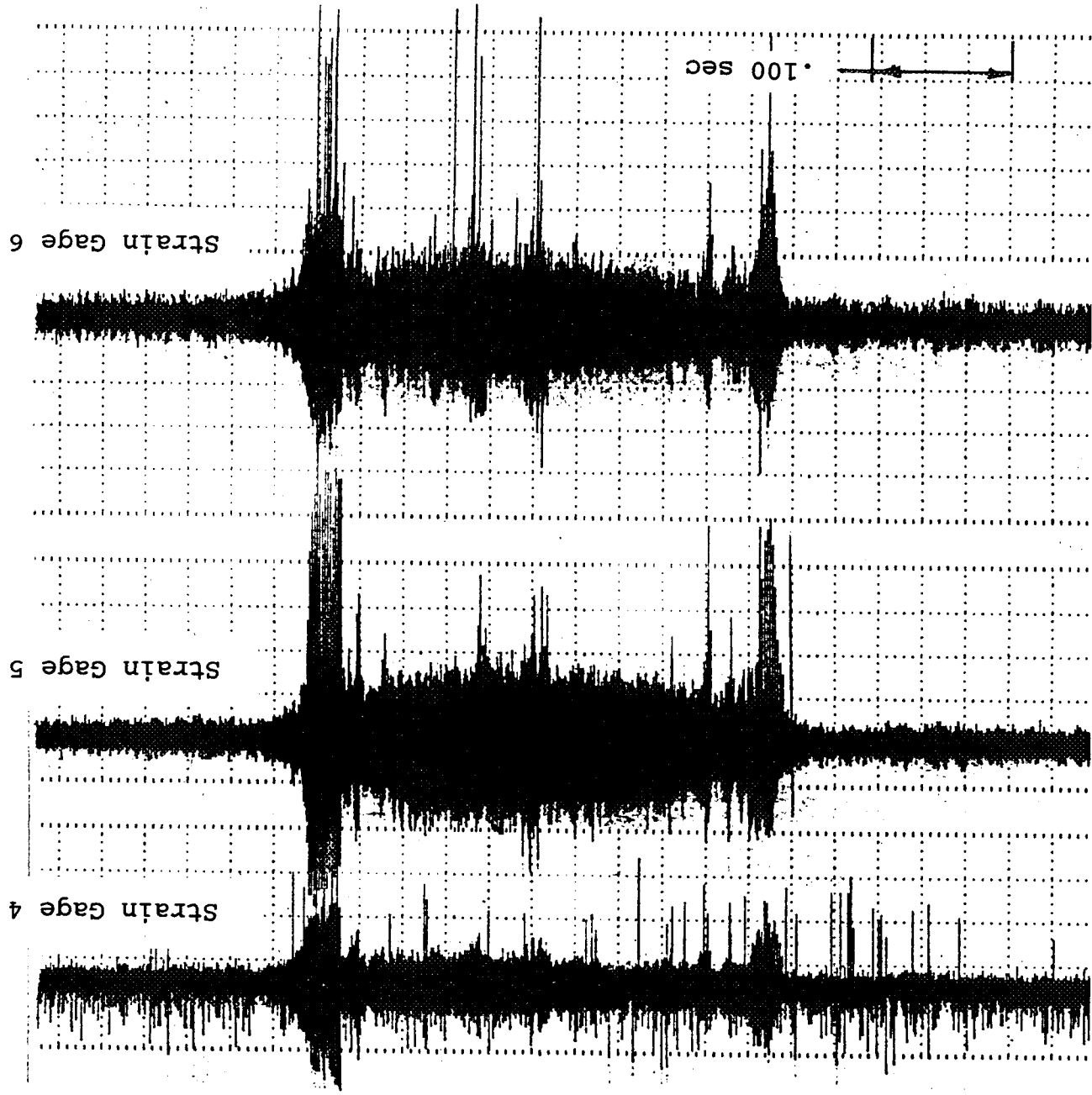
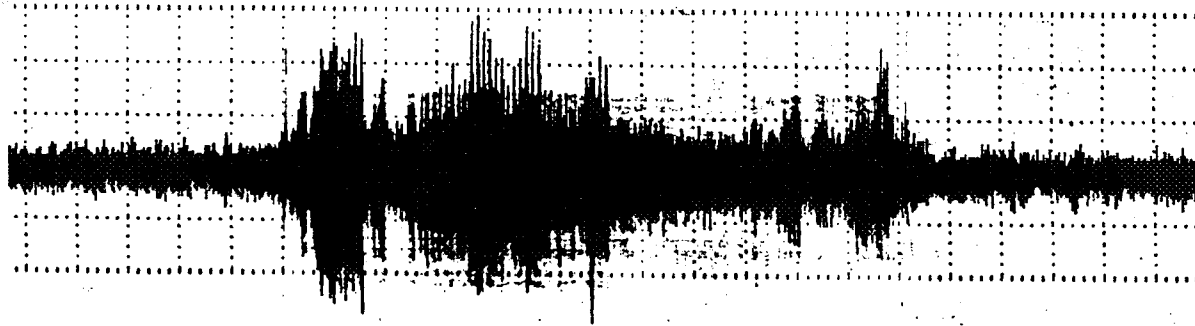


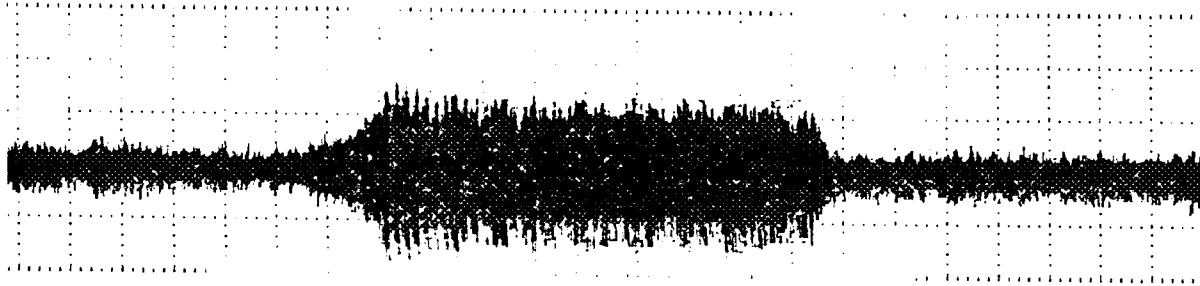
Figure 2.4-3
Compressed Time-History
32740 Rpm

Rub Response Near
Beginning of Test



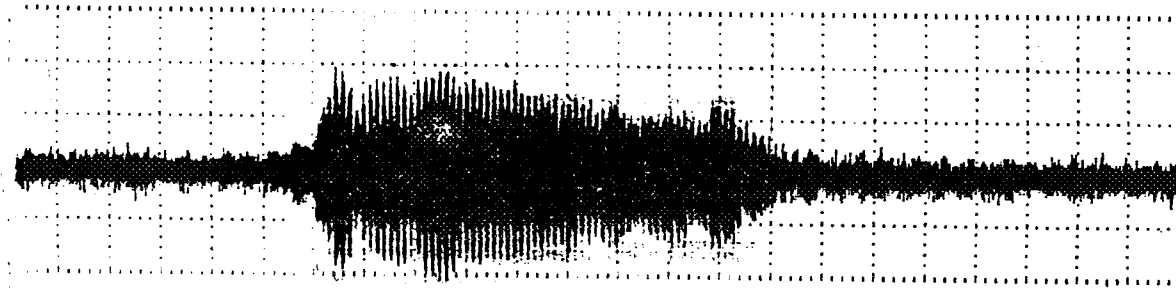
32740 rpm

Rub Response Near
Middle of Test



31030 rpm

Rub Response Near
End of Test



28870 rpm

Figure 2.4-4
Strain Gage 2 Time-History vs. Speed

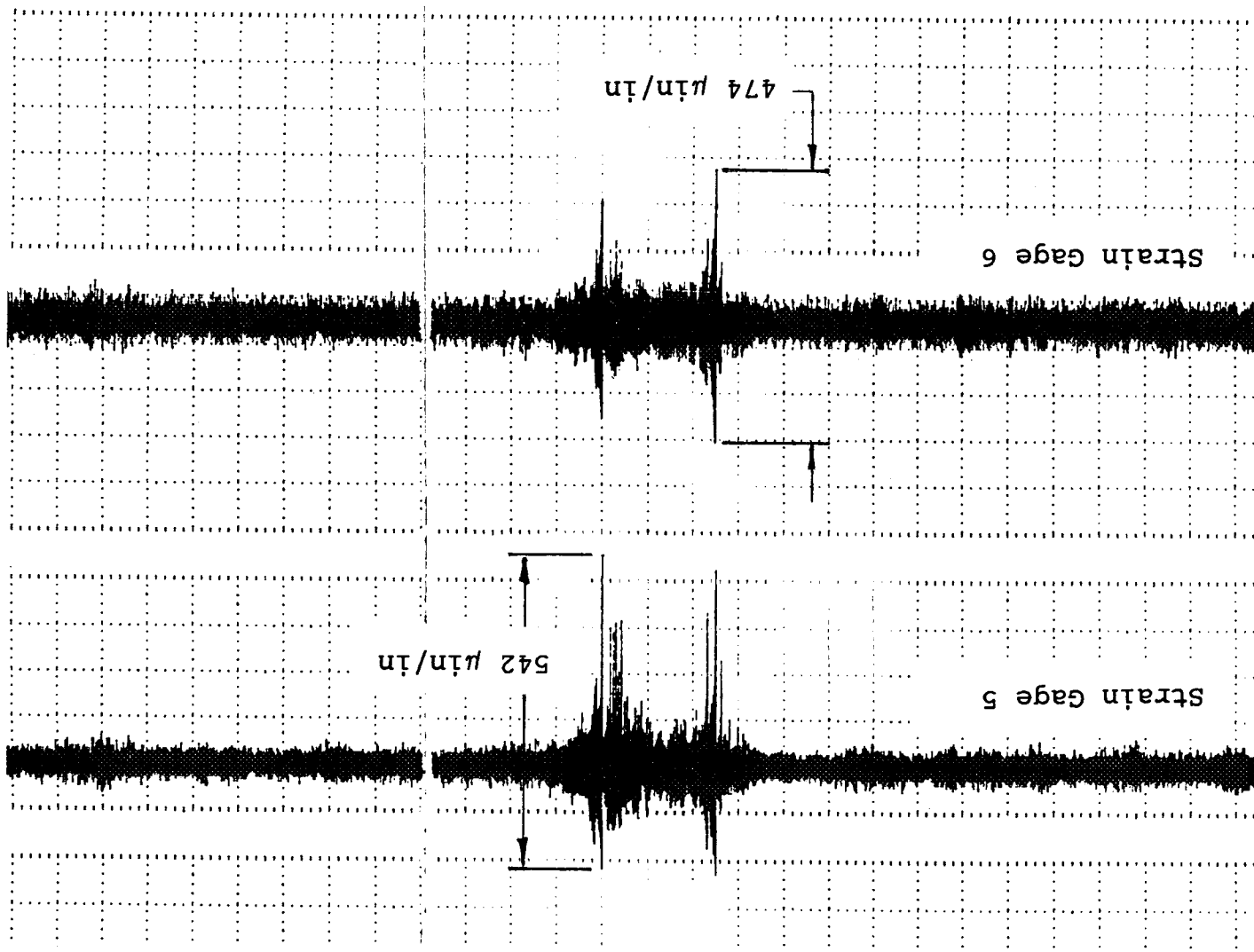
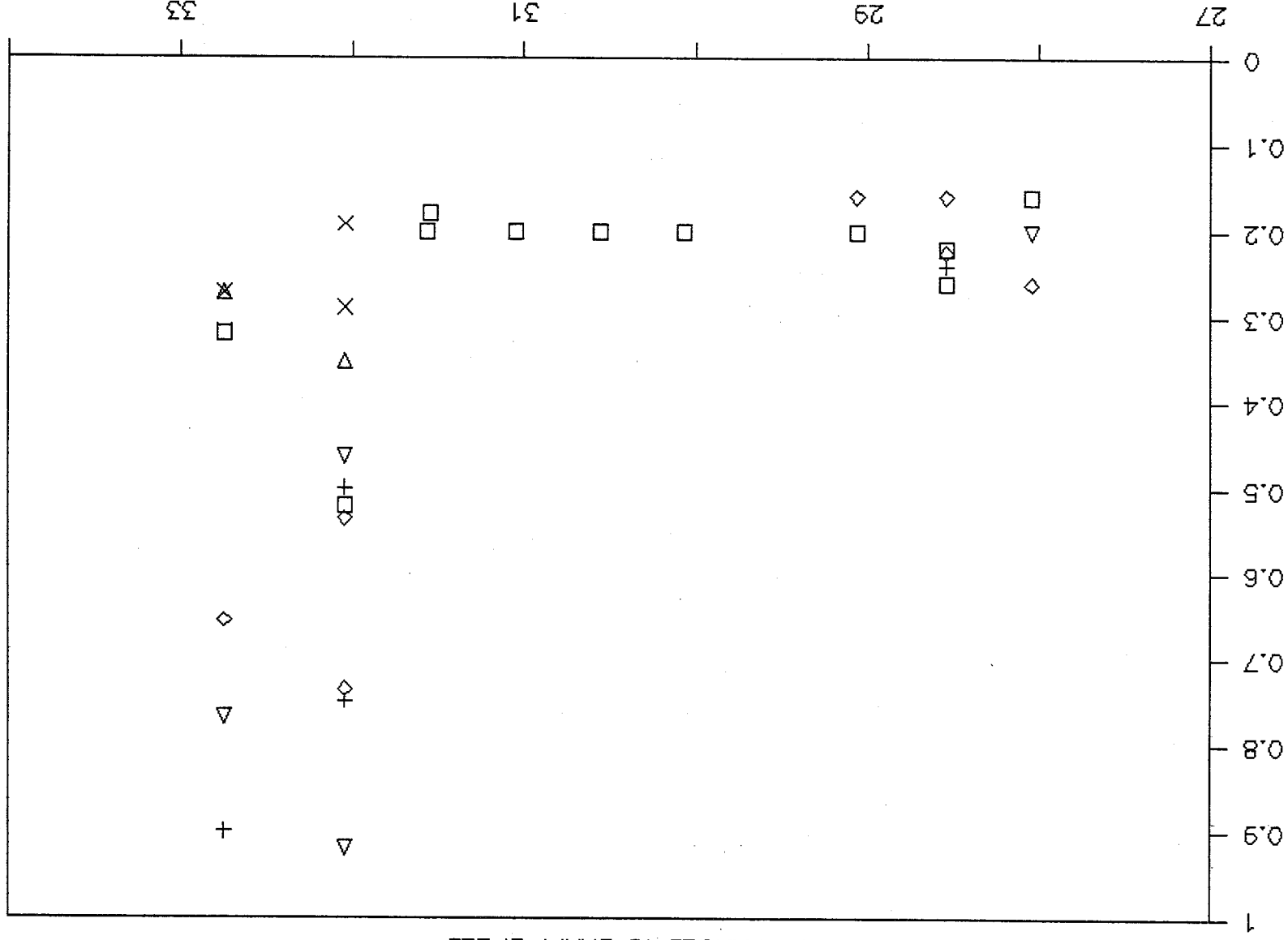


Figure 2.4-5
Strain Range During Rubbing
32040 Rpm

STRAIN RANGE (μ IN/IN)
(Thousands)



BLADE TIP RUBBING TEST

STRAIN RANGES vs SHAFT SPEED

SHAFT SPEED (RPM)
(Thousands)

SG 6

SG 31

SG 32

SG 32

SG 2

SG 4

SG 5

SG 6

SG 31

SG 32

Strain Range vs. Speed

Figure 2.4-6

STRAIN RANGE (μ IN/IN)
(Thousands)

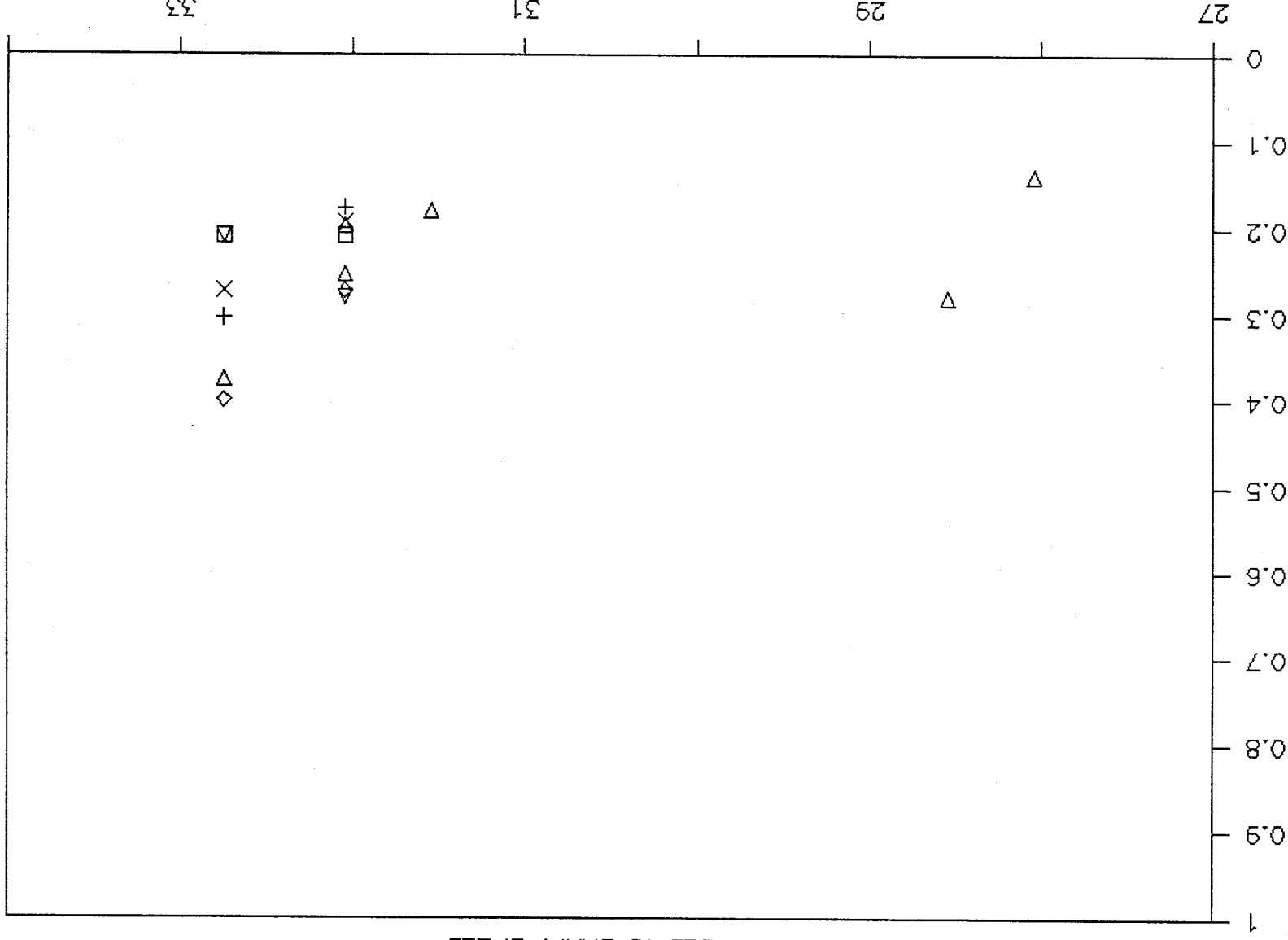


Figure 2.4-7
Strain Range vs. Speed

BLADE TIP RUBBING TEST

STRAIN RANGES vs SHAFT SPEED

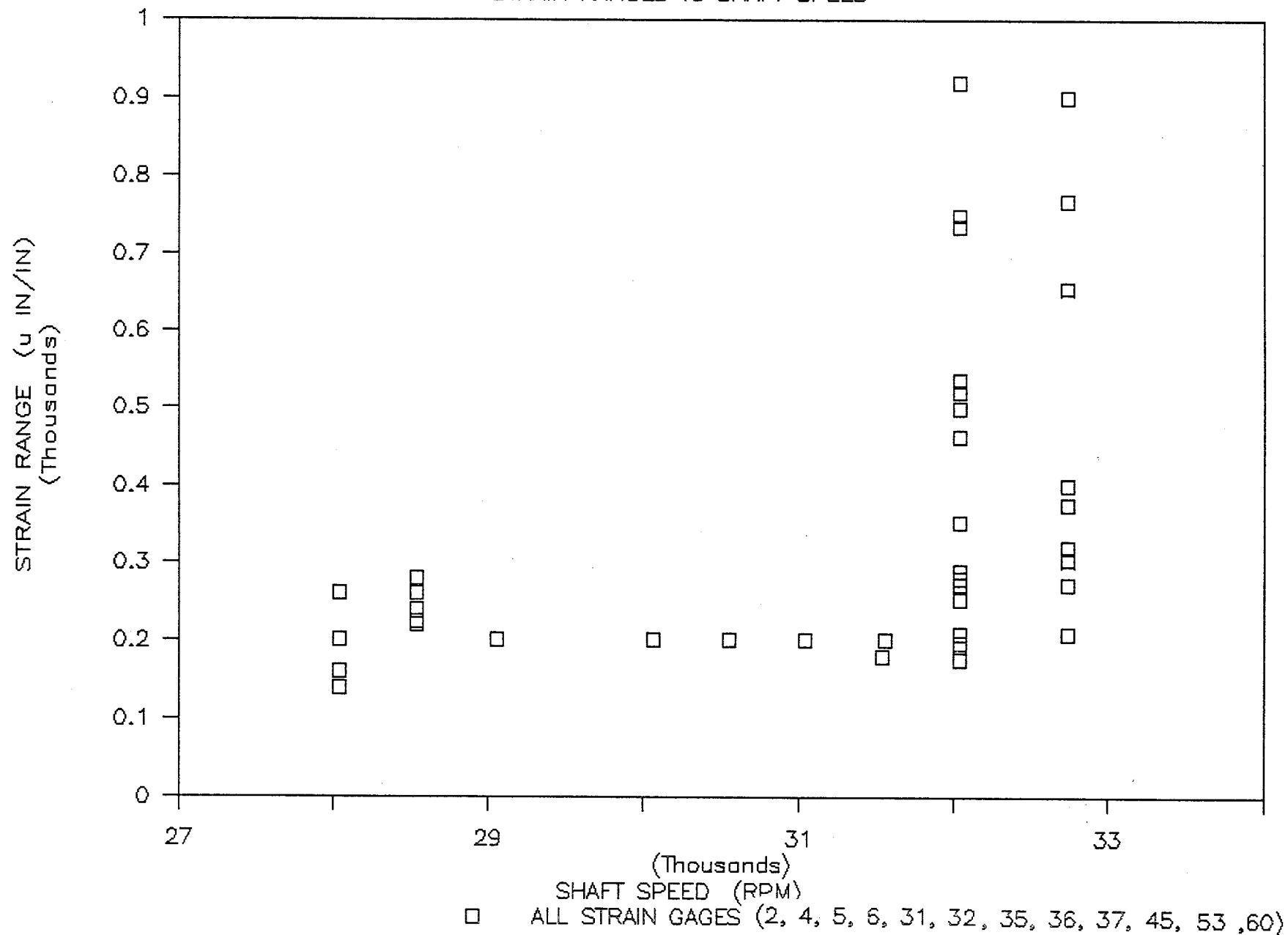
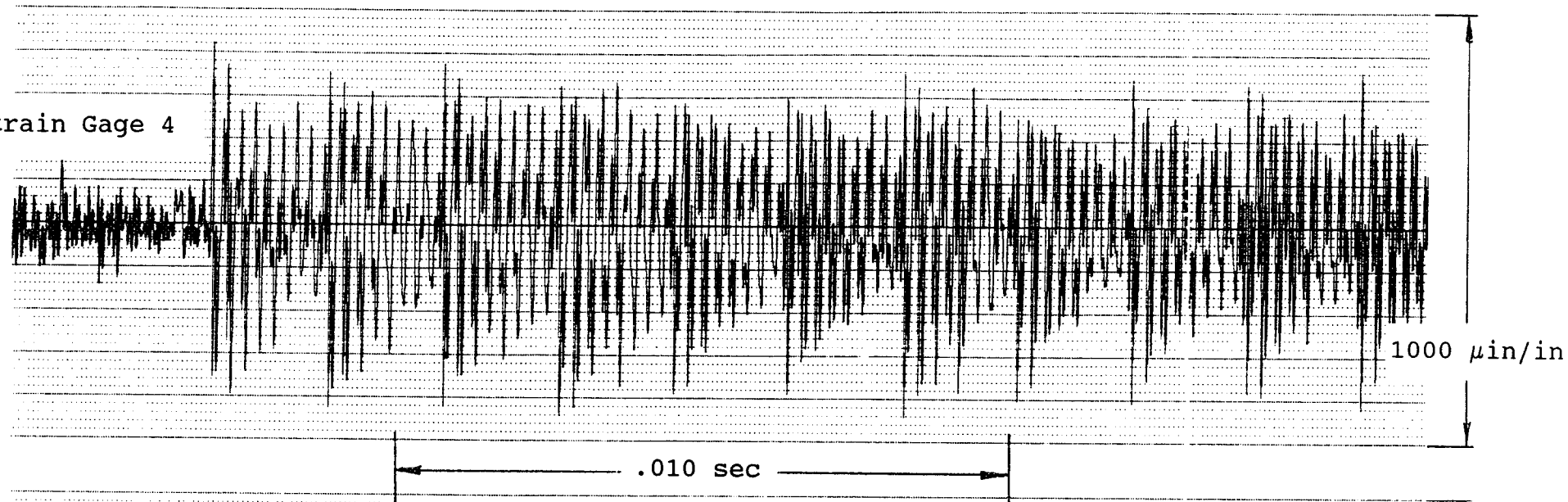


Figure 2.4-8
Strain Range vs. Speed

Strain Gage 4



Strain Gage 5

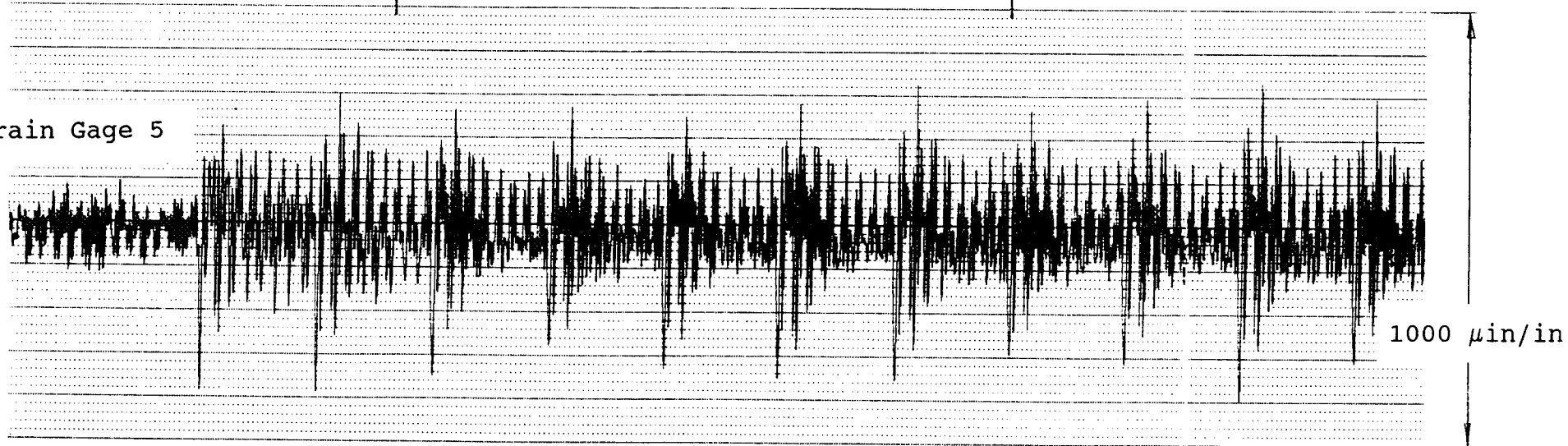
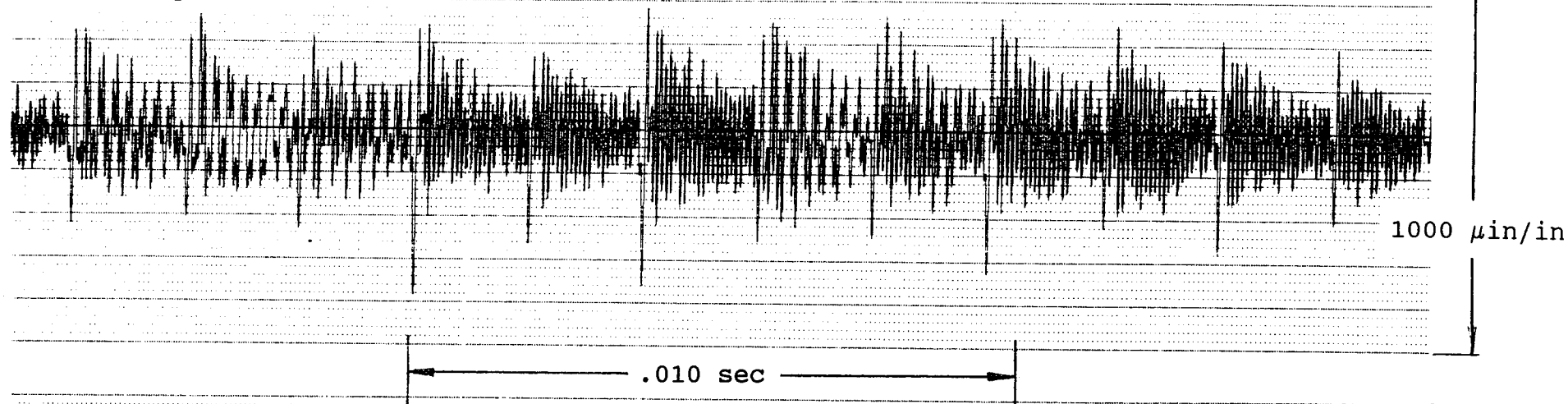


Figure 2.4-9
Strain Time-History
100-20000 Hz Band Pass Filtered
32740 rpm

Strain Gage 4



Strain Gage 5

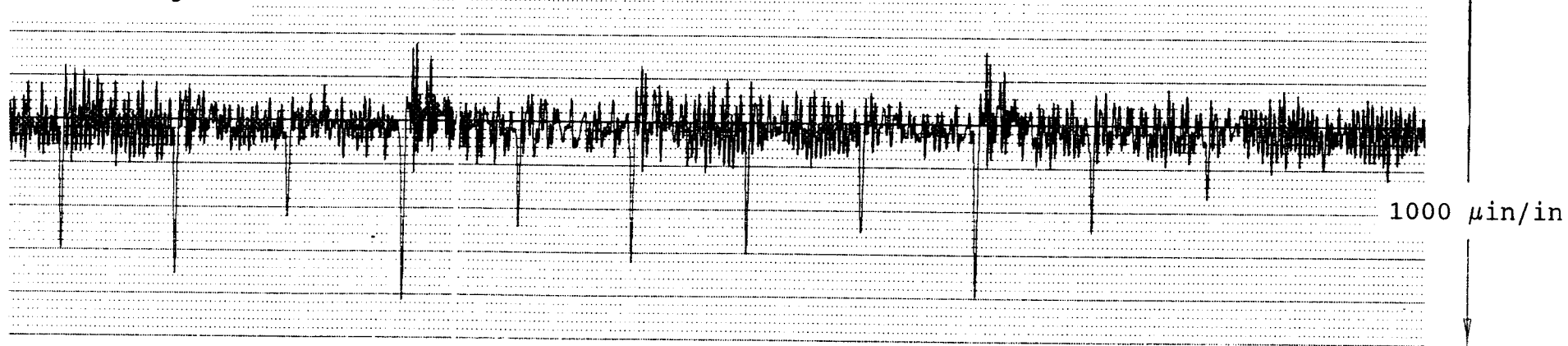
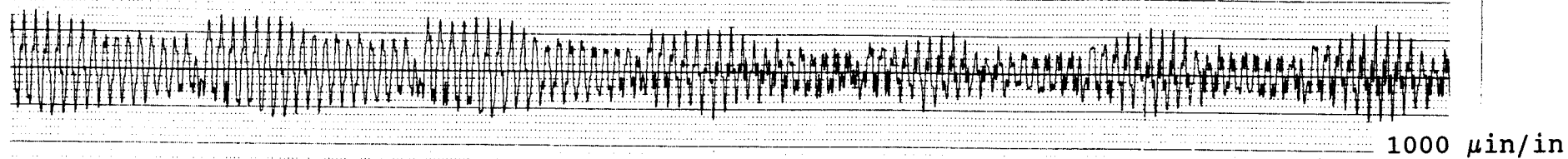


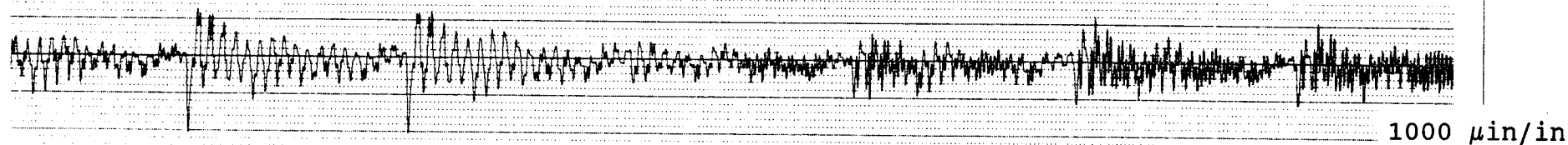
Figure 2.4-10
Strain Time-History
100-20000 Hz Band Pass Filtered
32160 rpm

Strain Gage 2



.010 sec

Strain Gage 4



Strain Gage 5

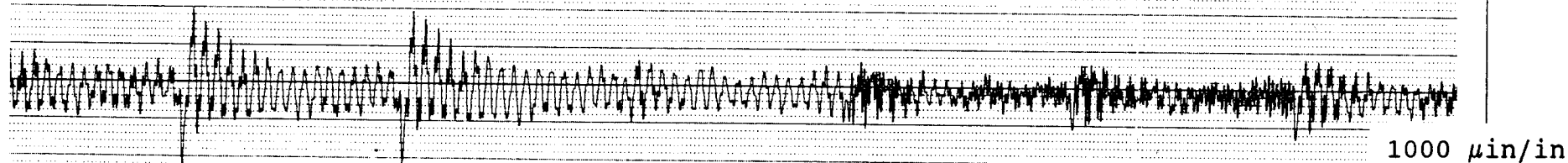


Figure 2.4-11
Strain Time-History
100-20000 Hz Band Pass Filtered
28530 rpm

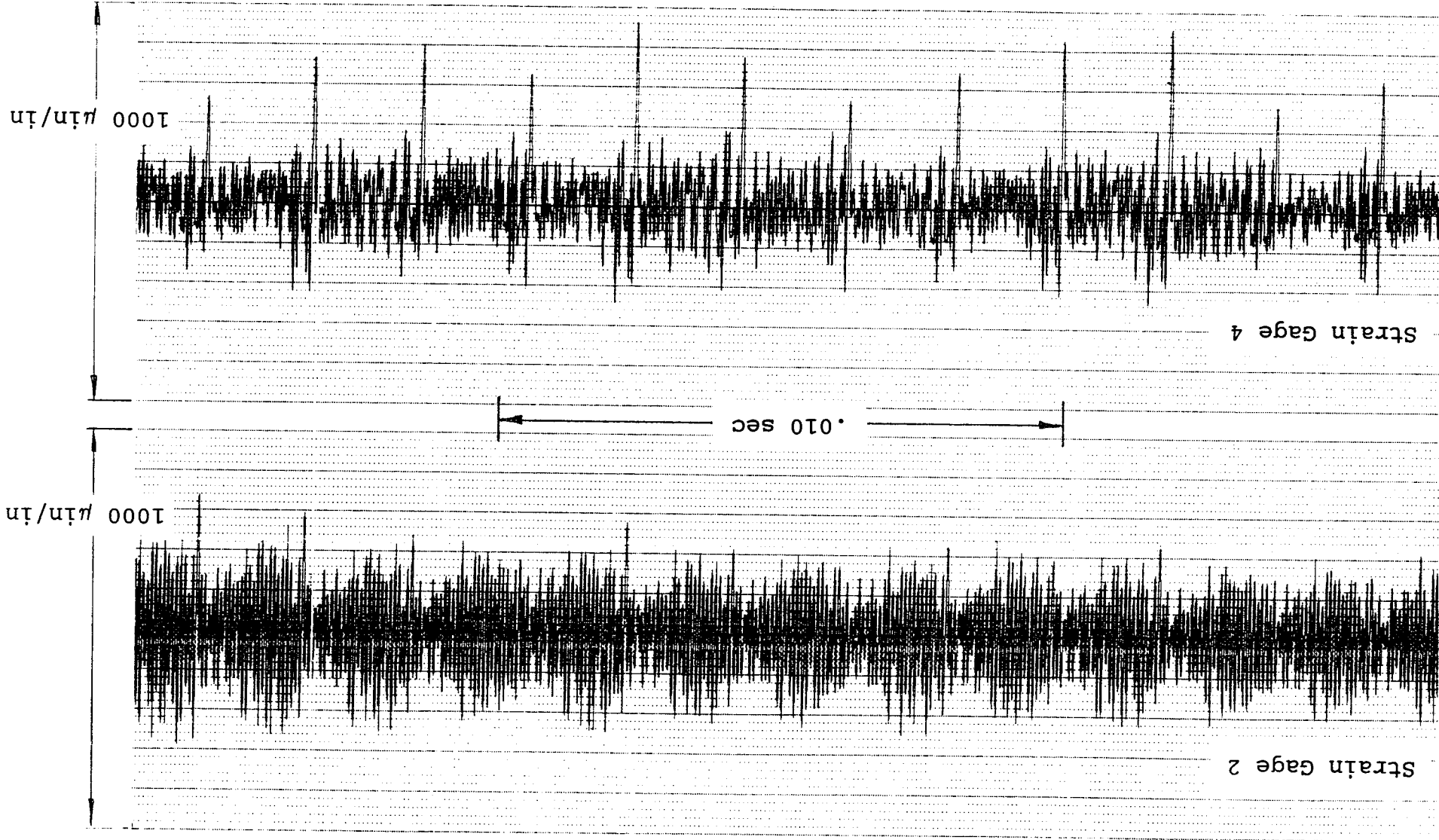
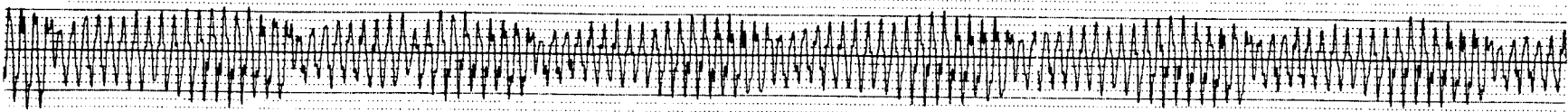


Figure 2.4-12
Strain Time-History
100-20000 Hz Band Pass Filtered
31630 rpm

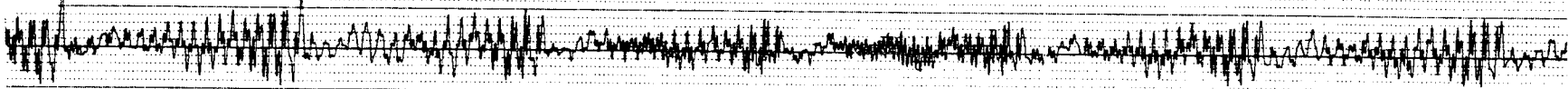
Strain Gage 2

1000 $\mu\text{in/in}$

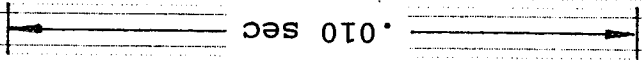


Strain Gage 4

1000 $\mu\text{in/in}$



.010 sec



Strain Gage 5

1000 $\mu\text{in/in}$

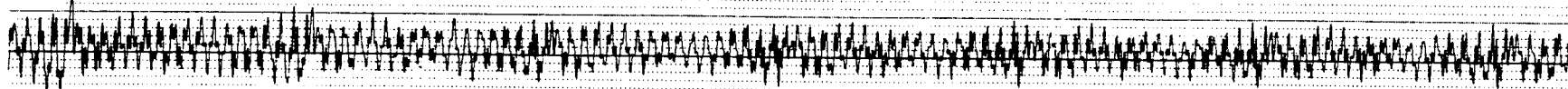


Figure 2.4-13
Strain Time-History
100-20000 Hz Band Pass Filtered
32040 rpm

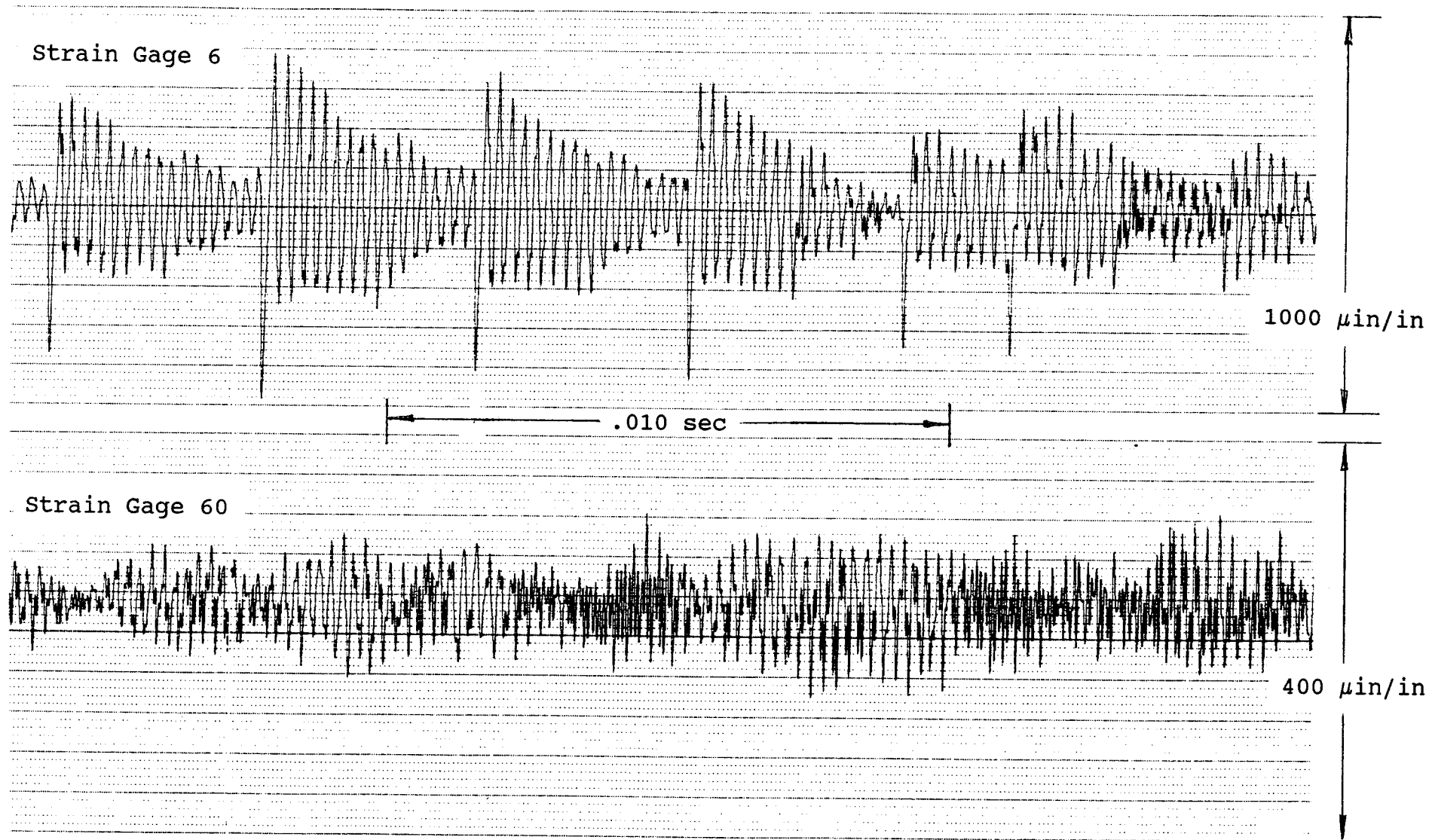


Figure 2.4-14
Strain Time-History
100-20000 Hz Band Pass Filtered
31540 rpm

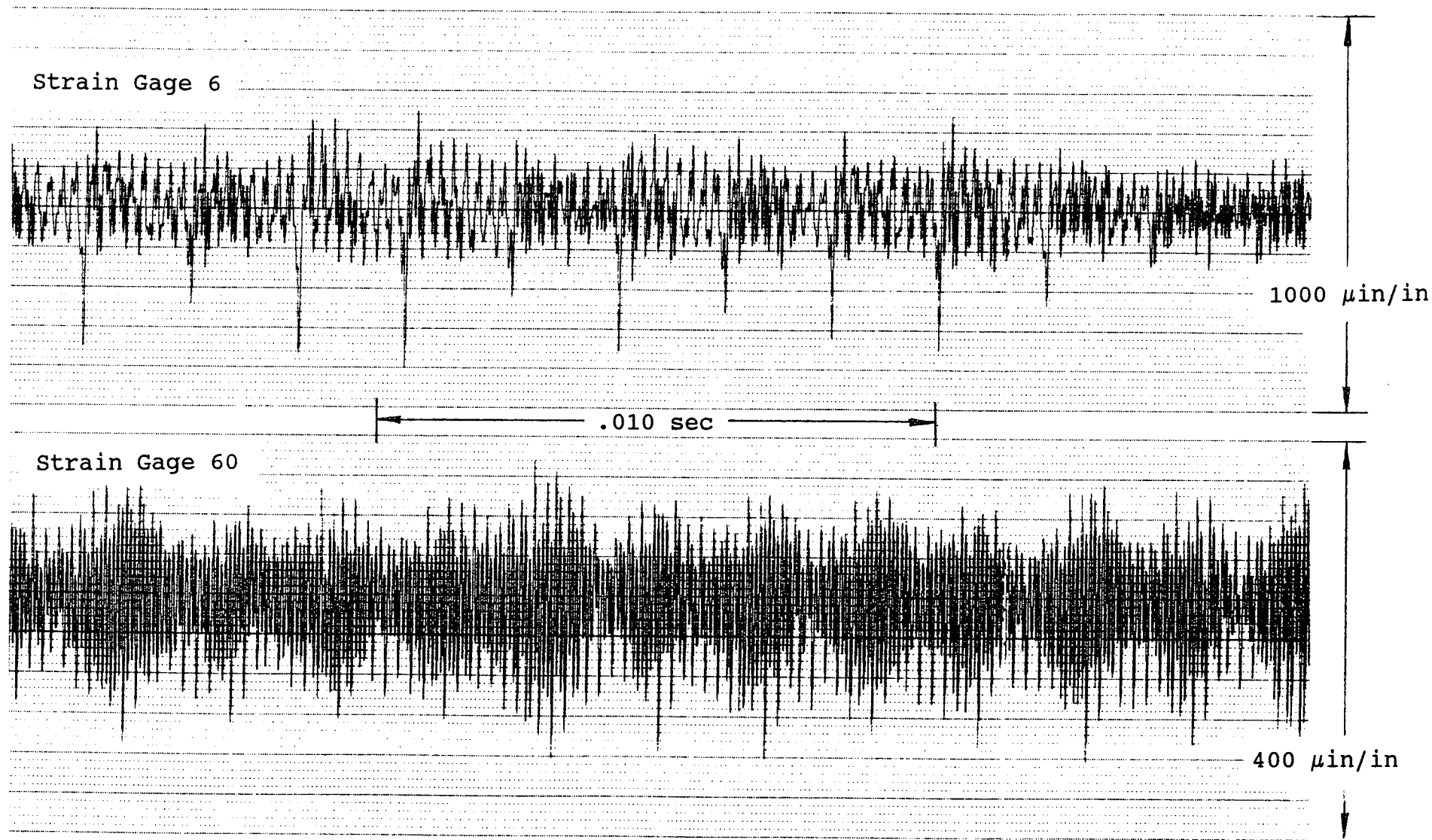


Figure 2.4-15
Strain Time-History
100-20000 Hz Band Pass Filtered
31540 rpm

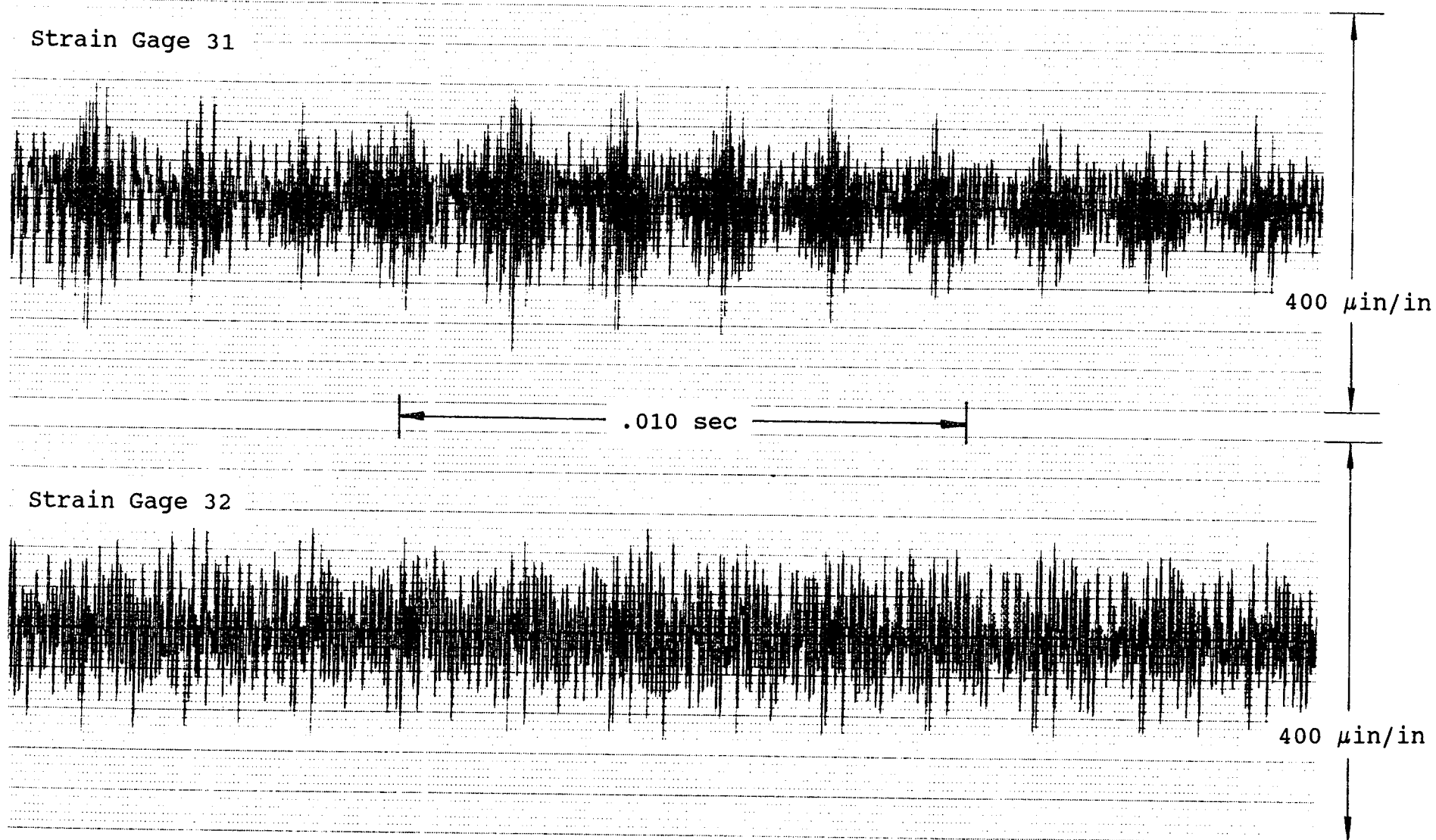
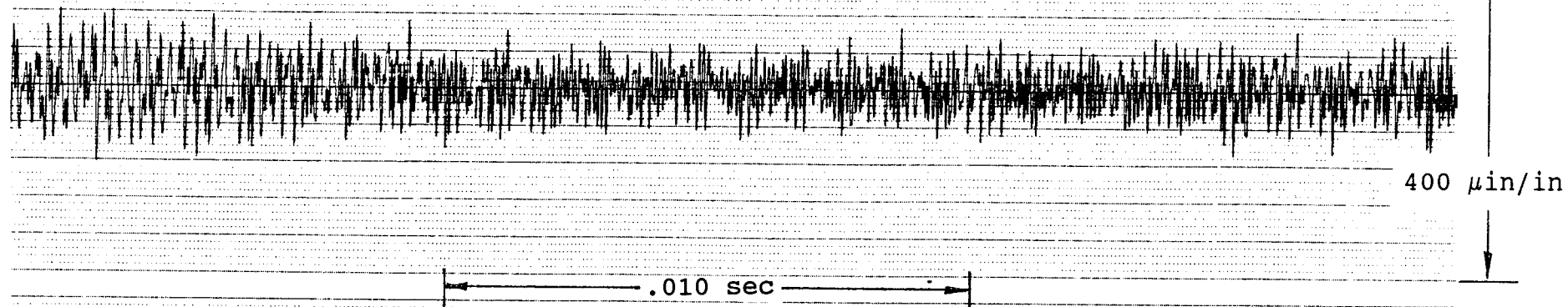
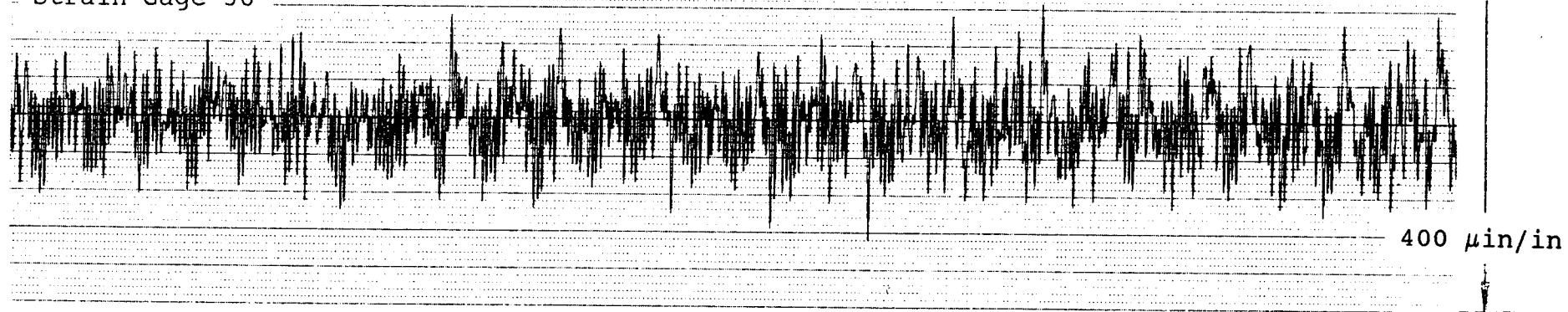


Figure 2.4-16
Strain Time-History
100-20000 Hz Band Pass Filtered
32740 rpm

Strain Gage 35



Strain Gage 36



Strain Gage 37

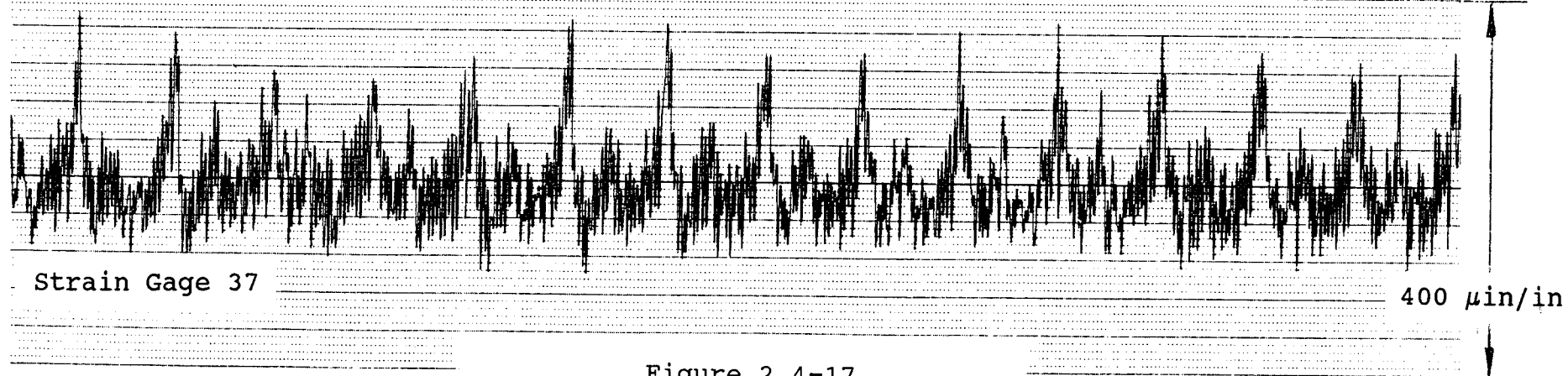


Figure 2.4-17
Strain Time-History
100-20000 Hz Band Pass Filtered
32740 rpm

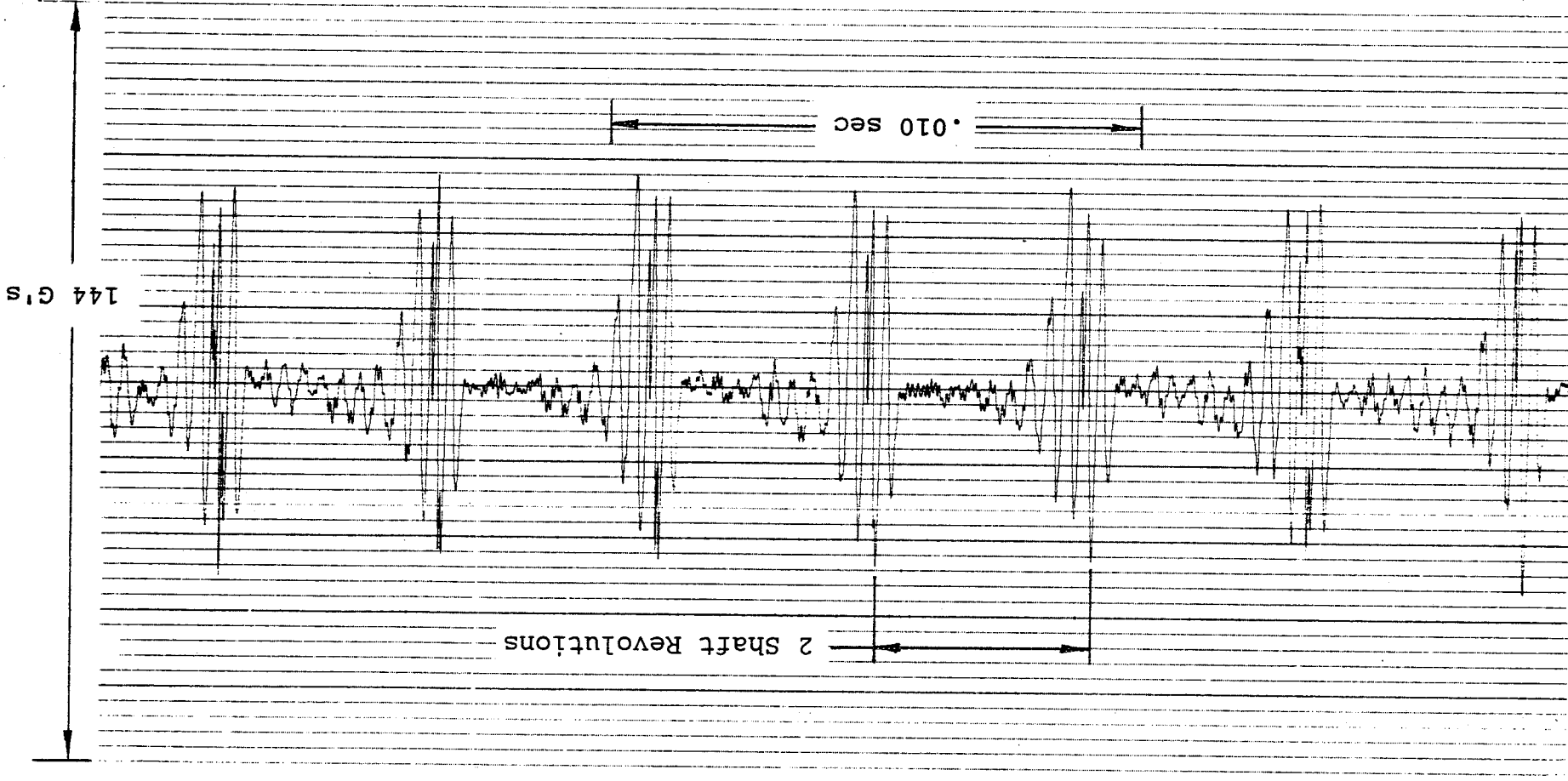


Figure 2.4-18
Tip Seal Accelerometer Time-History
30060 rpm

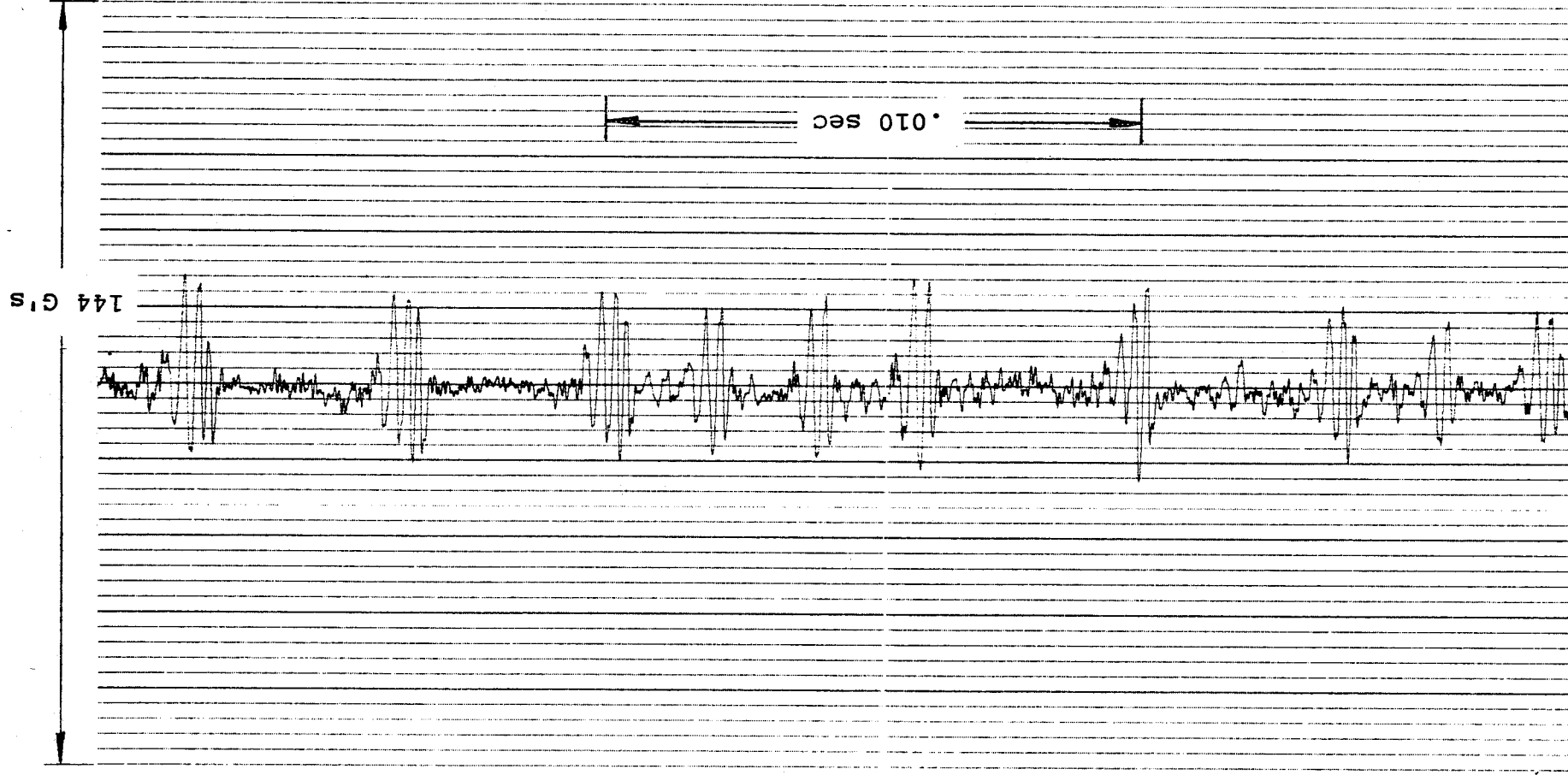


Figure 2.4-19
Tip Seal Accelerometer Time-History
31540 rpm

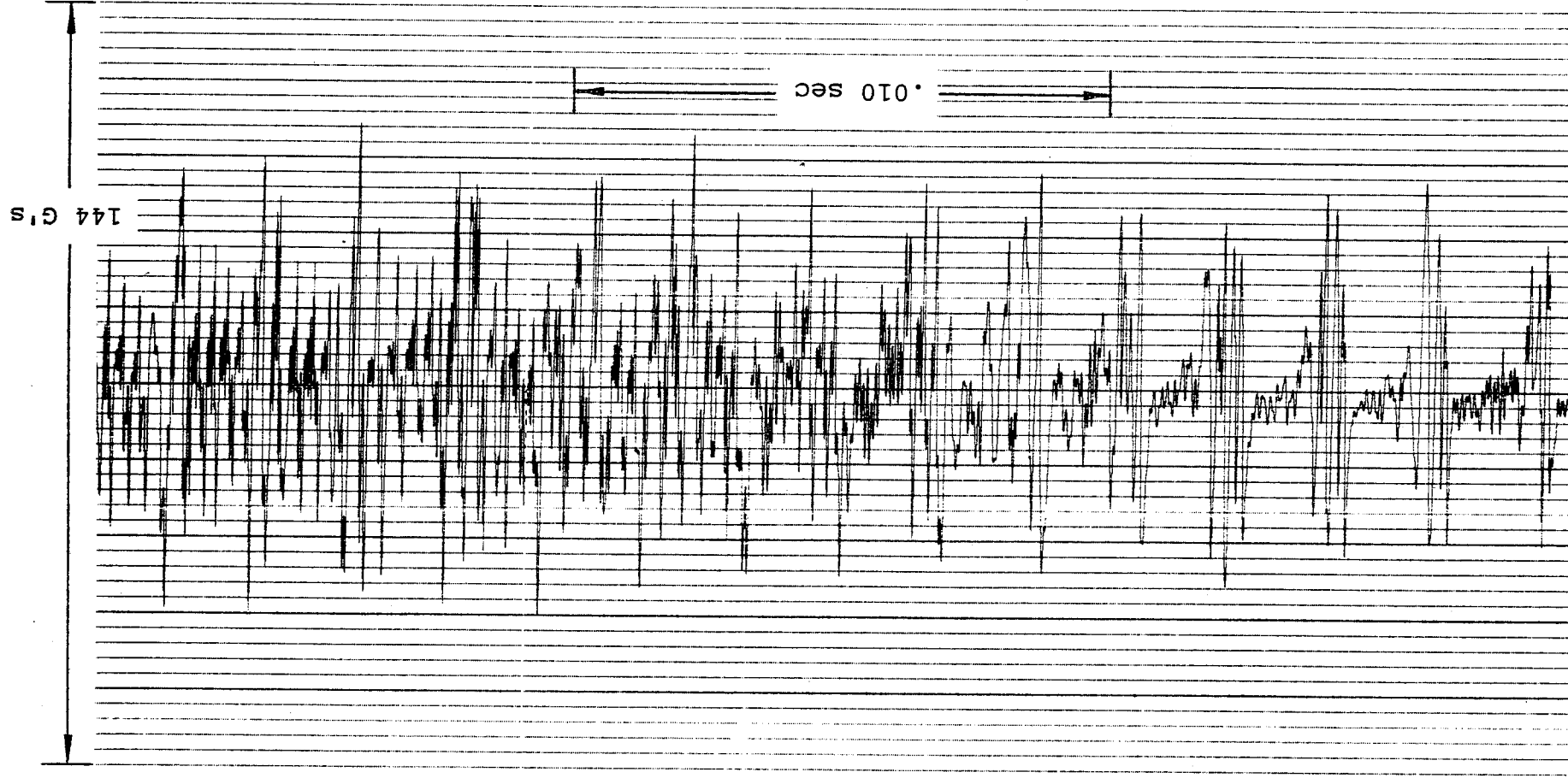
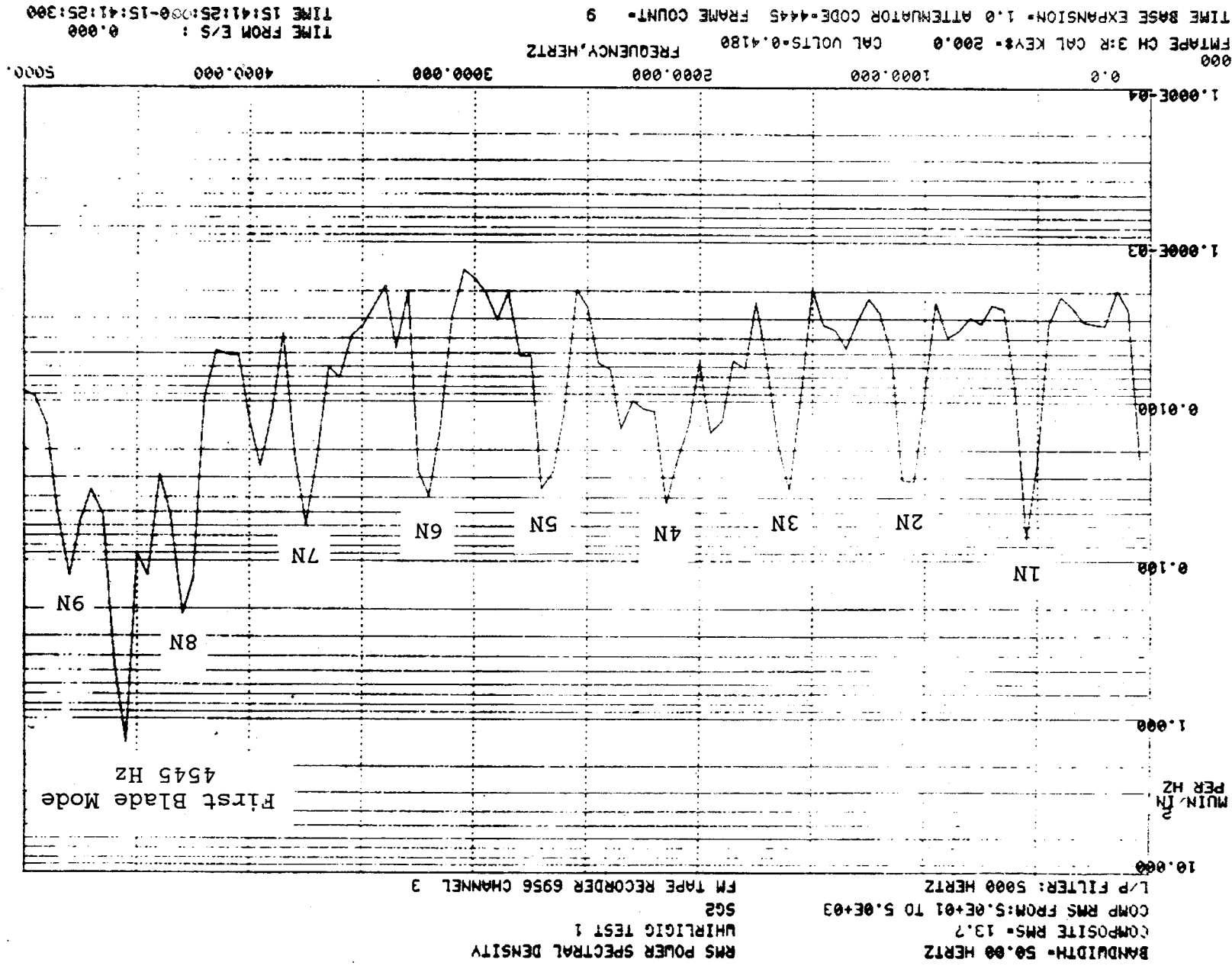


Figure 2.4-20
Tip Seal Accelerometer Time-History
32030 rpm

QUALITY
CONTROL
UNIT



BANDWIDTH= 50.00 HERTZ
 COMPOSITE RMS= 34.0
 COMP RMS FROM: 5.0E+01 TO 5.0E+03
 L/P FILTER: 5000 HERTZ

RMS POWER SPECTRAL DENSITY
 WHIRLIGIG TEST 1
 SG 4
 FM TAPE RECORDER 6956 CHANNEL 5

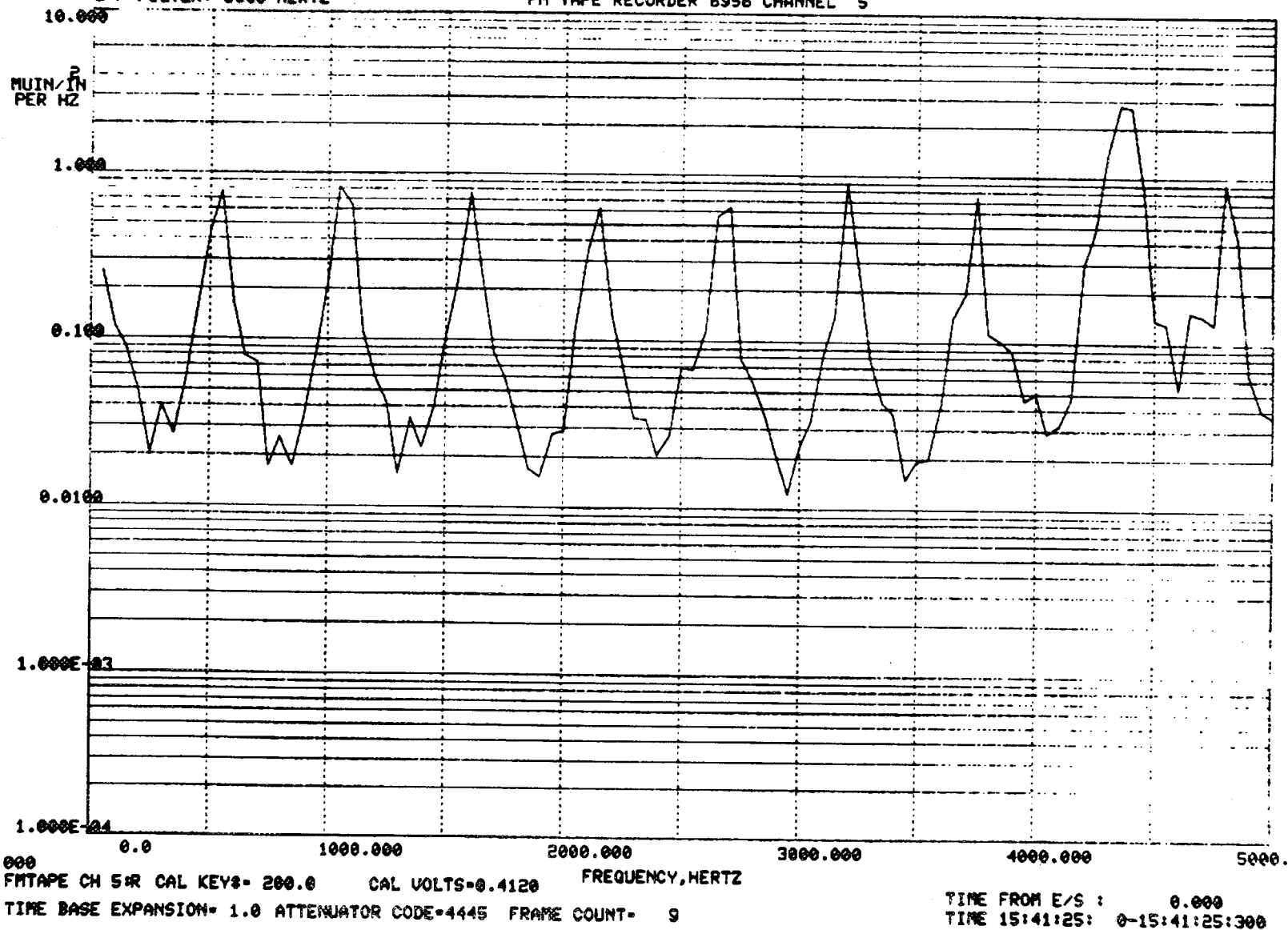


Figure 2.4-22 Strain PSD During Rubbing - SG #4 - 0 to 5 Khz - 32160 Rpm

BANDWIDTH= 50.00 HERTZ
 COMPOSITE RMS= 23.4
 COMP RMS FROM: 5.0E+01 TO 5.0E+03
 L/P FILTER: 5000 HERTZ

RMS POWER SPECTRAL DENSITY
 WHIRLIGIG TEST 1
 SG 5
 FM TAPE RECORDER 6956 CHANNEL 6

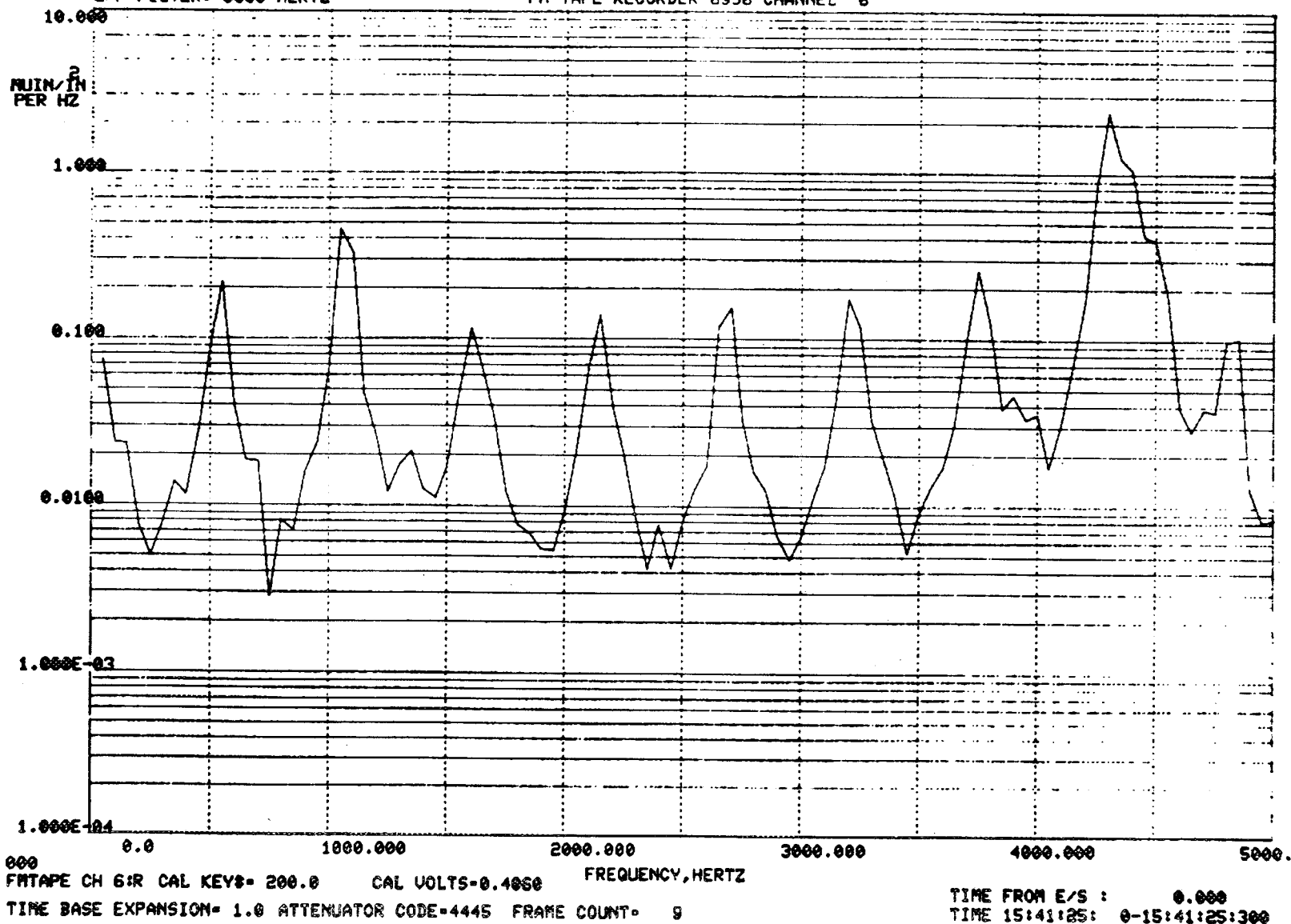


Figure 2.4-23 Strain PSD During Rubbing - SG #5 - 0 to 5 Khz - 32160 Rpm

2.4-35

ORIGINAL PAGE IS
 OF POOR QUALITY

BANDWIDTH= 50.00 HERTZ
 COMPOSITE RMS=7.850E-02
 COMP RMS FROM:5.0E+01 TO 5.0E+03
 L/P FILTER: 5000 HERTZ

RMS POWER SPECTRAL DENSITY
 WHIRLIGIG TEST 1
 SG 6
 FM TAPE RECORDER 6956 CHANNEL 7

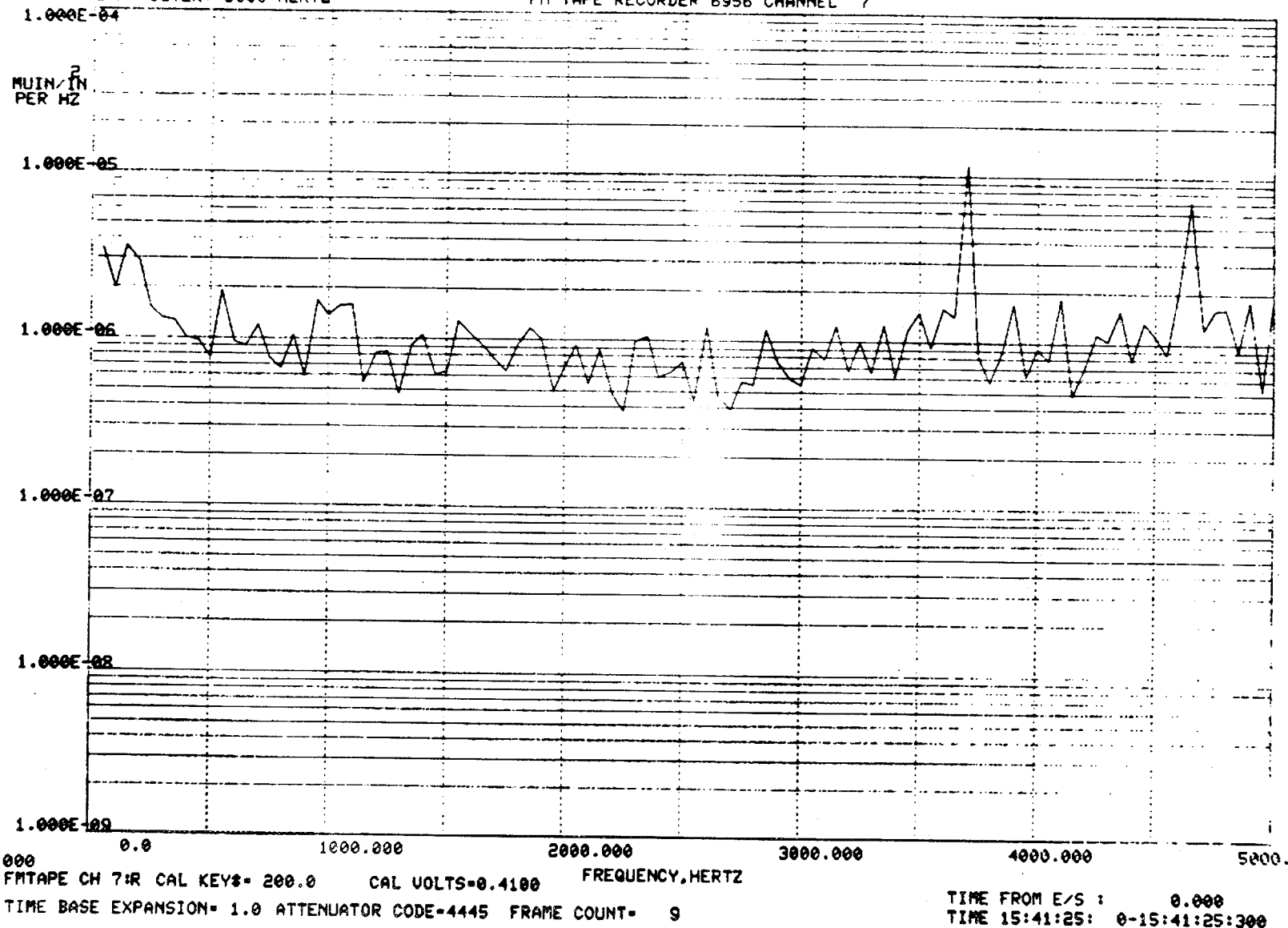


Figure 2.4-24 Strain PSD During Rubbing - SG #6 - 0 to 5 Khz - 32160 Rpm

BANDWIDTH= 50.00 HERTZ
 COMPOSITE RMS= 13.4
 COMP RMS FROM: 5.0E+01 TO 5.0E+03
 L/P FILTER: 5000 HERTZ

RMS POWER SPECTRAL DENSITY
 WHIRLIGIG TEST 1
 SG 60
 FM TAPE RECORDER 6956 CHANNEL 10

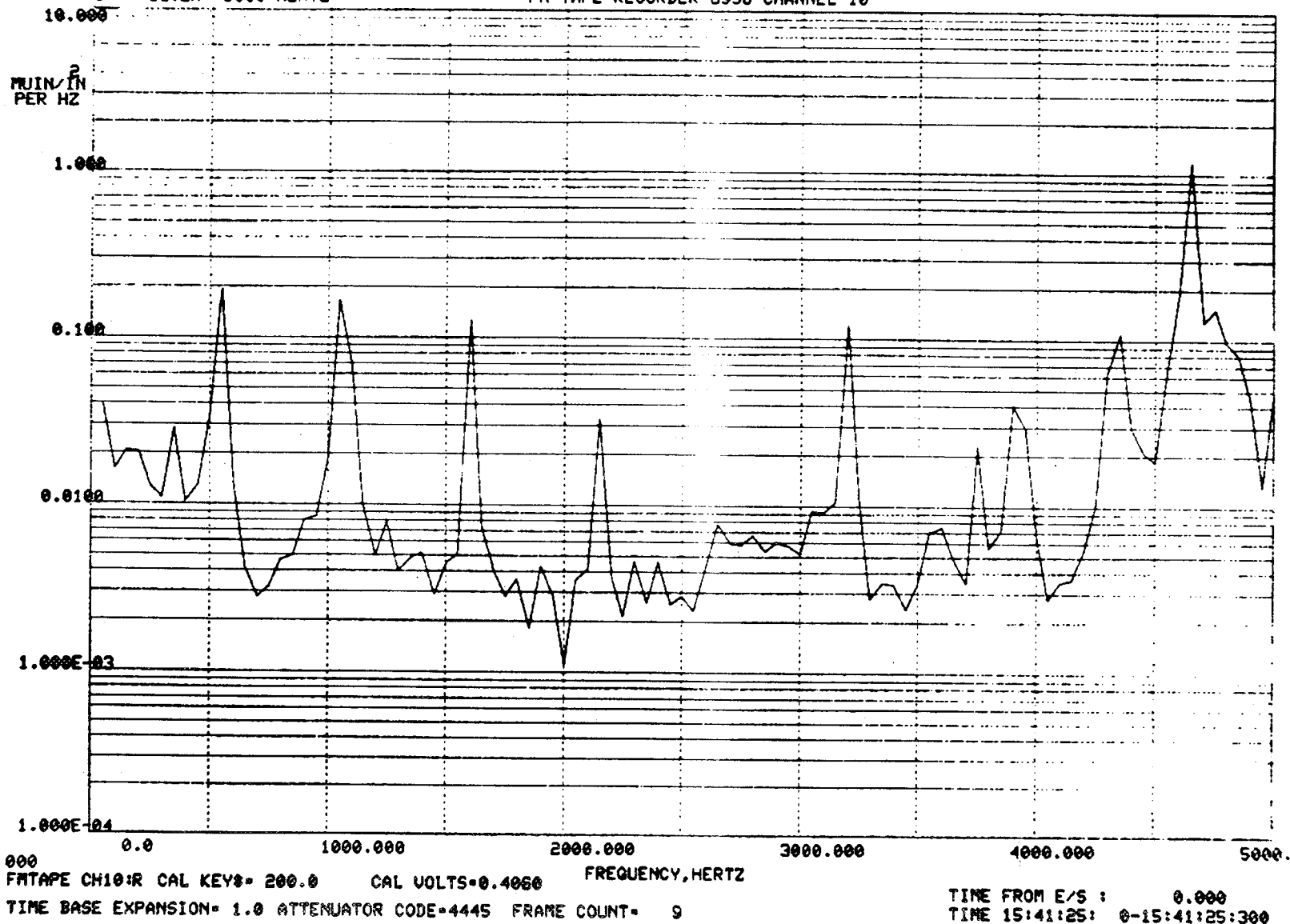


Figure 2.4-25 Strain PSD During Rubbing - SG #60 - 0 to 5 Khz - 32160 Rpm

BANDWIDTH= 50.00 HERTZ
 COMPOSITE RMS= 18.0
 COMP RMS FROM: 5.0E+01 TO 5.0E+03
 L/P FILTER: 5000 HERTZ

RMS POWER SPECTRAL DENSITY
 WHIRLIGIG TEST 1
 SG2
 FM TAPE RECORDER 6956 CHANNEL 3

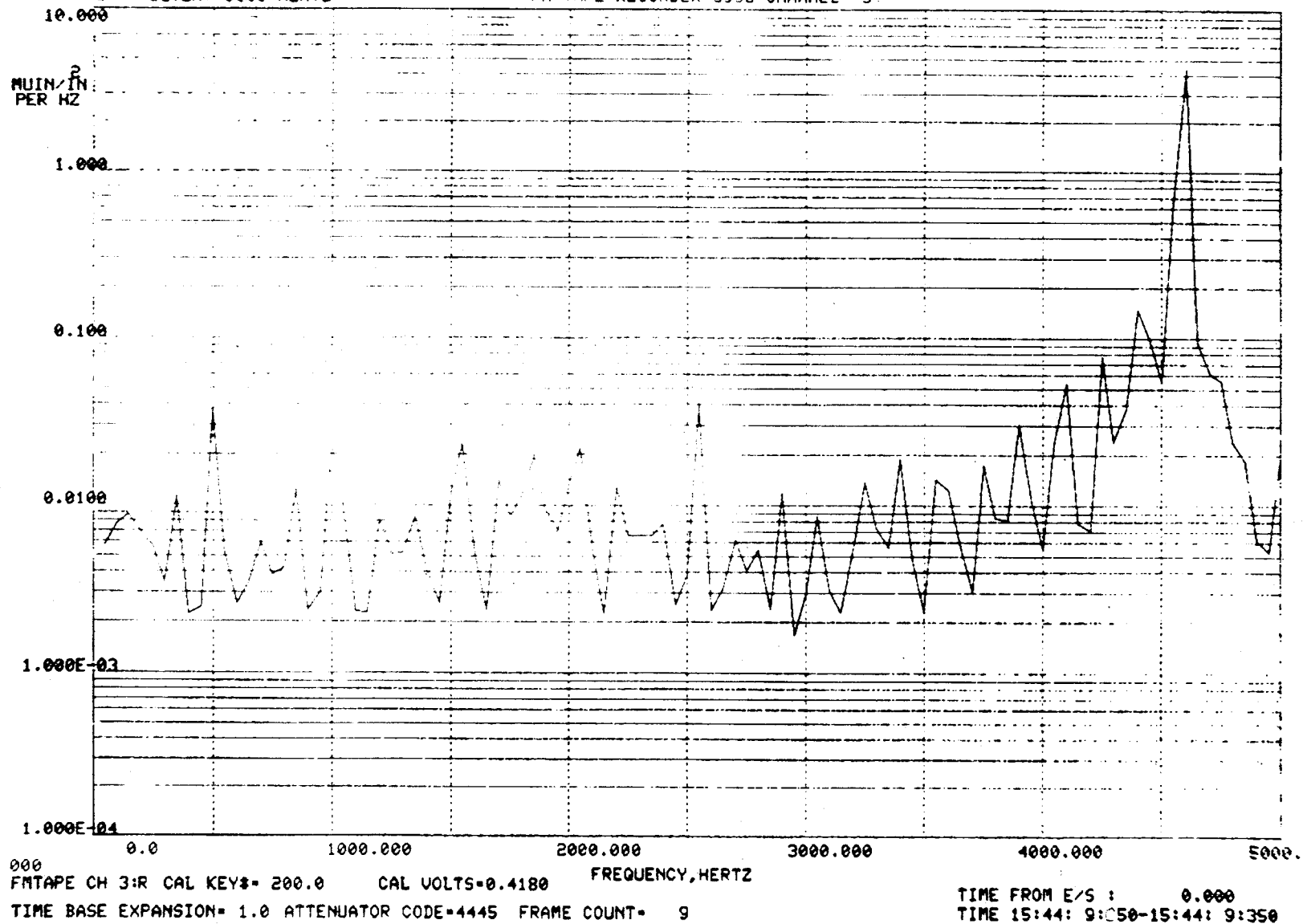


Figure 2.4-26 Strain PSD During Rubbing - SG #2 - 0 to 5 Khz - 31030 Rpm

2.4-38

ORIGINAL PAGE IS
 OF POOR QUALITY

BANDWIDTH= 50.00 HERTZ
 COMPOSITE RMS= 17.3
 COMP RMS FROM: 5.0E+01 TO 5.0E+03
 L/P FILTER: 5000 HERTZ

RMS POWER SPECTRAL DENSITY
 WHIRLIGIG TEST 1
 SG 4
 FM TAPE RECORDER 6956 CHANNEL 5

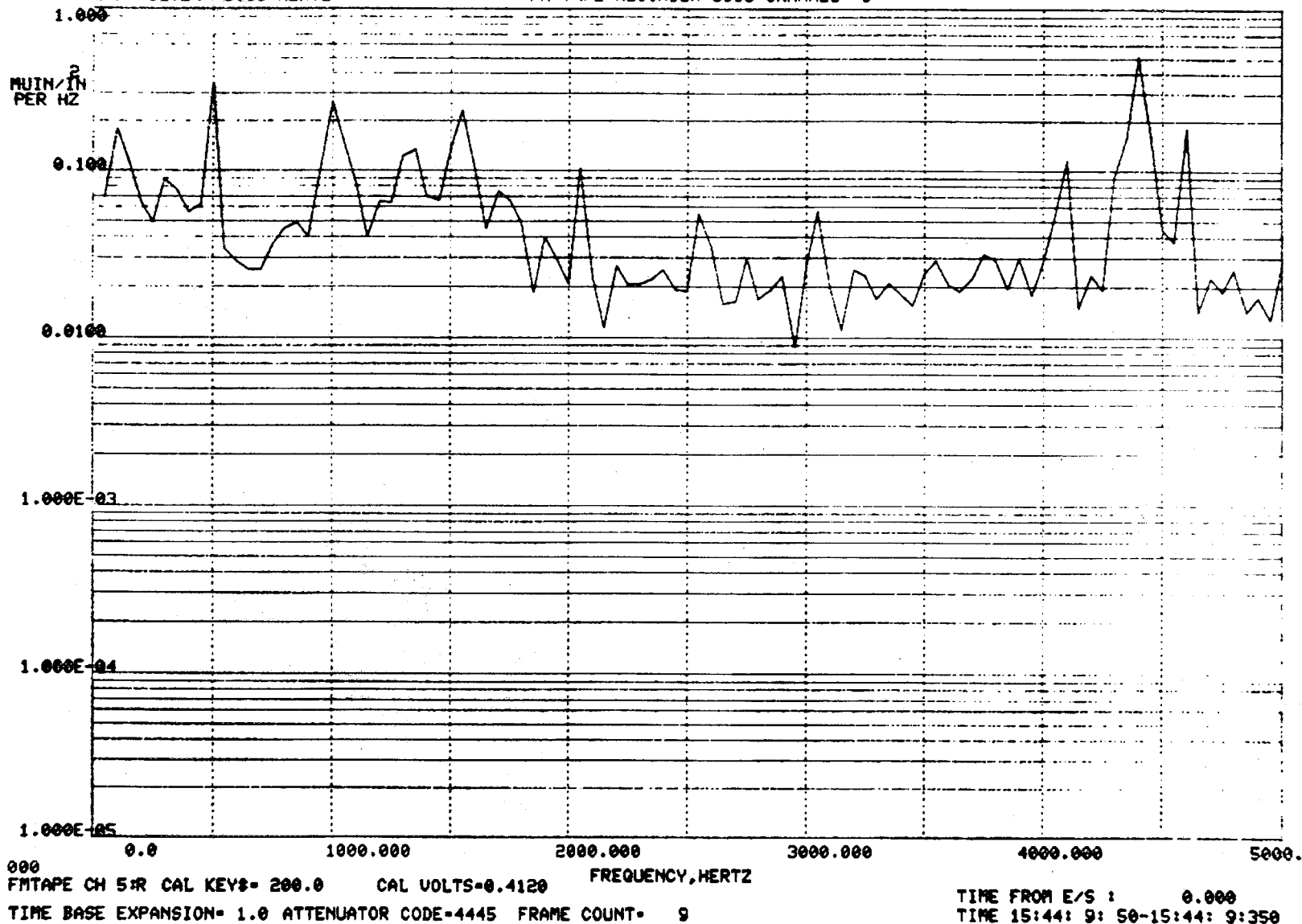


Figure 2.4-27 Strain PSD During Rubbing - SG #4 - 0 to 5 Khz - 31030 Rpm

BANDWIDTH= 50.00 HERTZ
 COMPOSITE RMS= 9.96
 COMP RMS FROM: 5.0E+01 TO 5.0E+03
 L/P FILTER: 5000 HERTZ

RMS POWER SPECTRAL DENSITY
 WHIRLIGIG TEST 1
 SG 5
 FM TAPE RECORDER 6956 CHANNEL 6

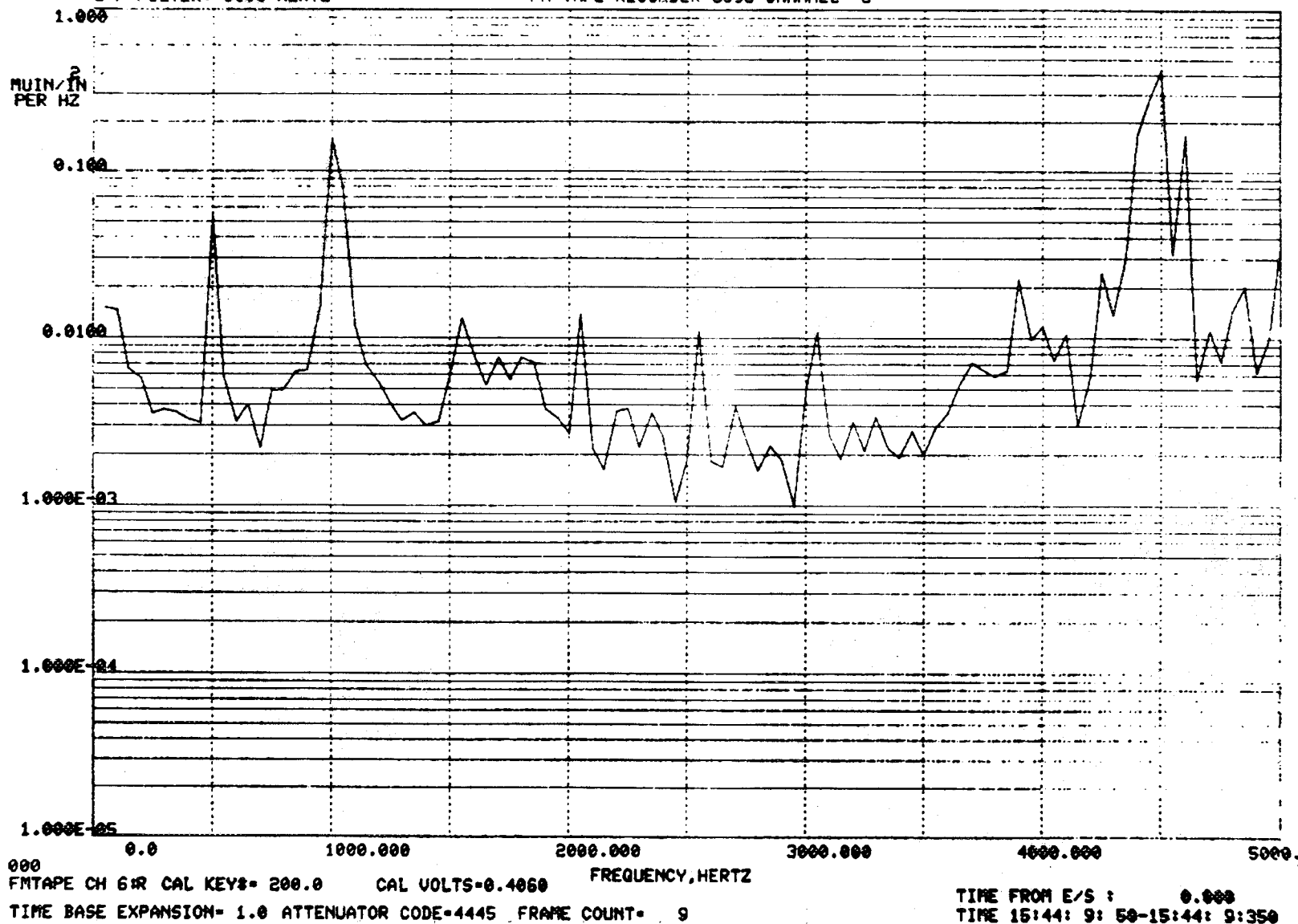


Figure 2.4-28 Strain PSD During Rubbing - SG #5 - 0 to 5 Khz - 31030 Rpm

BANDWIDTH= 50.00 HERTZ
 COMPOSITE RMS=5.895E-02
 COMP RMS FROM:5.0E+01 TO 5.0E+03
 L/P FILTER: 5000 HERTZ

RMS POWER SPECTRAL DENSITY
 WHIRLIGIG TEST 1
 SG 6
 FM TAPE RECORDER 6956 CHANNEL 7

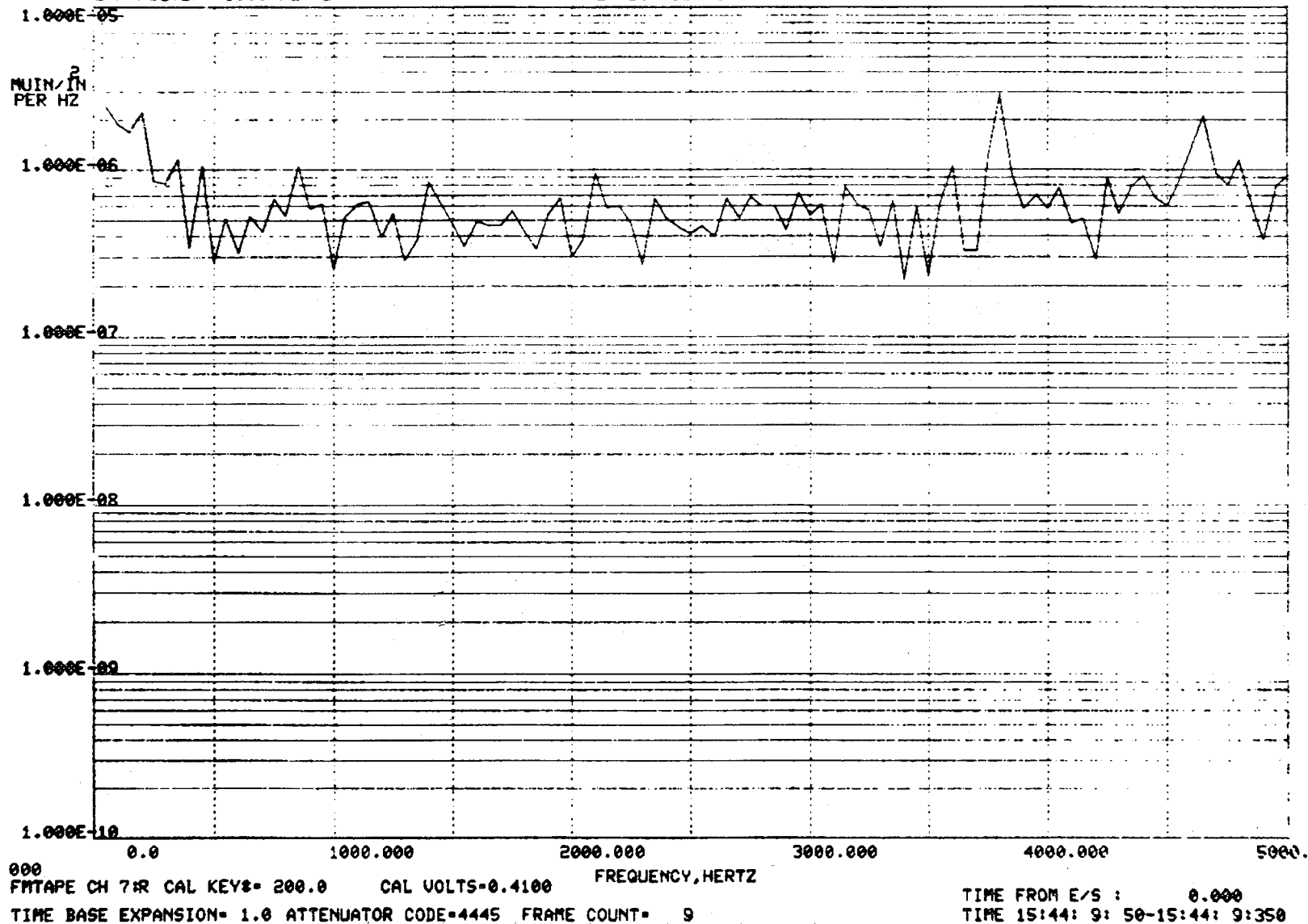


Figure 2.4-29 Strain PSD During Rubbing - SG #6 - 0 to 5 Khz - 31030 Rpm

BANDWIDTH= 50.00 HERTZ
 COMPOSITE RMS= 10.7
 COMP RMS FROM: 5.0E+01 TO 5.0E+03
 L/P FILTER: 5000 HERTZ

RMS POWER SPECTRAL DENSITY
 WHIRLIGIG TEST 1
 SG 60
 FM TAPE RECORDER 6956 CHANNEL 10

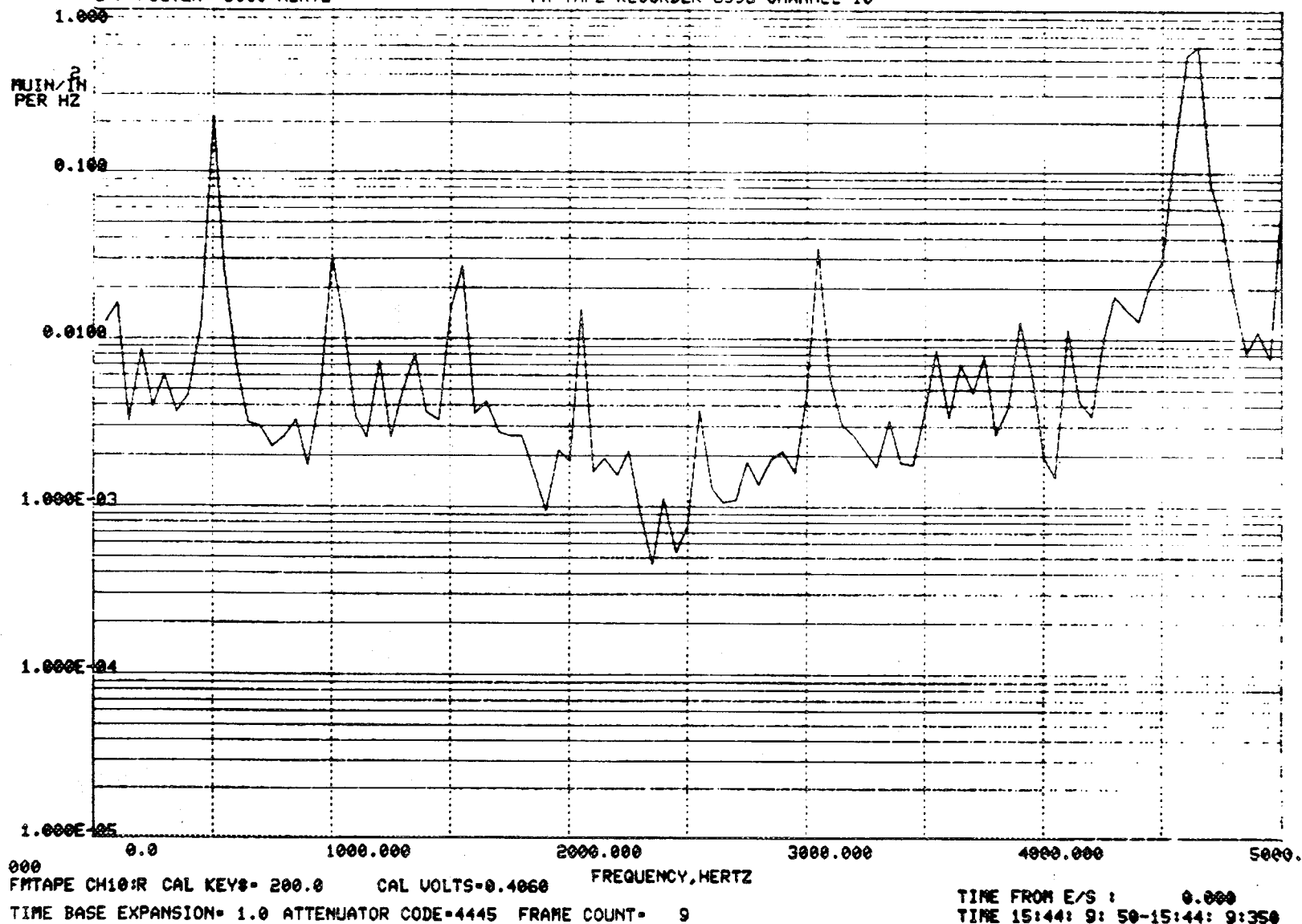


Figure 2.4-30 Strain PSD During Rubbing - SG #60 - 0 to 5 Khz - 31030 Rpm

2.4-42

ORIGINAL PAGE IS
 OF POOR QUALITY

BANDWIDTH= 50.00 HERTZ
 COMPOSITE RMS= 26.9
 COMP RMS FROM: 5.0E+01 TO 5.0E+03
 L/P FILTER: 5000 HERTZ

RMS POWER SPECTRAL DENSITY
 WHIRLIGIG TEST :
 SG2
 FM TAPE RECORDER 6956 CHANNEL 3

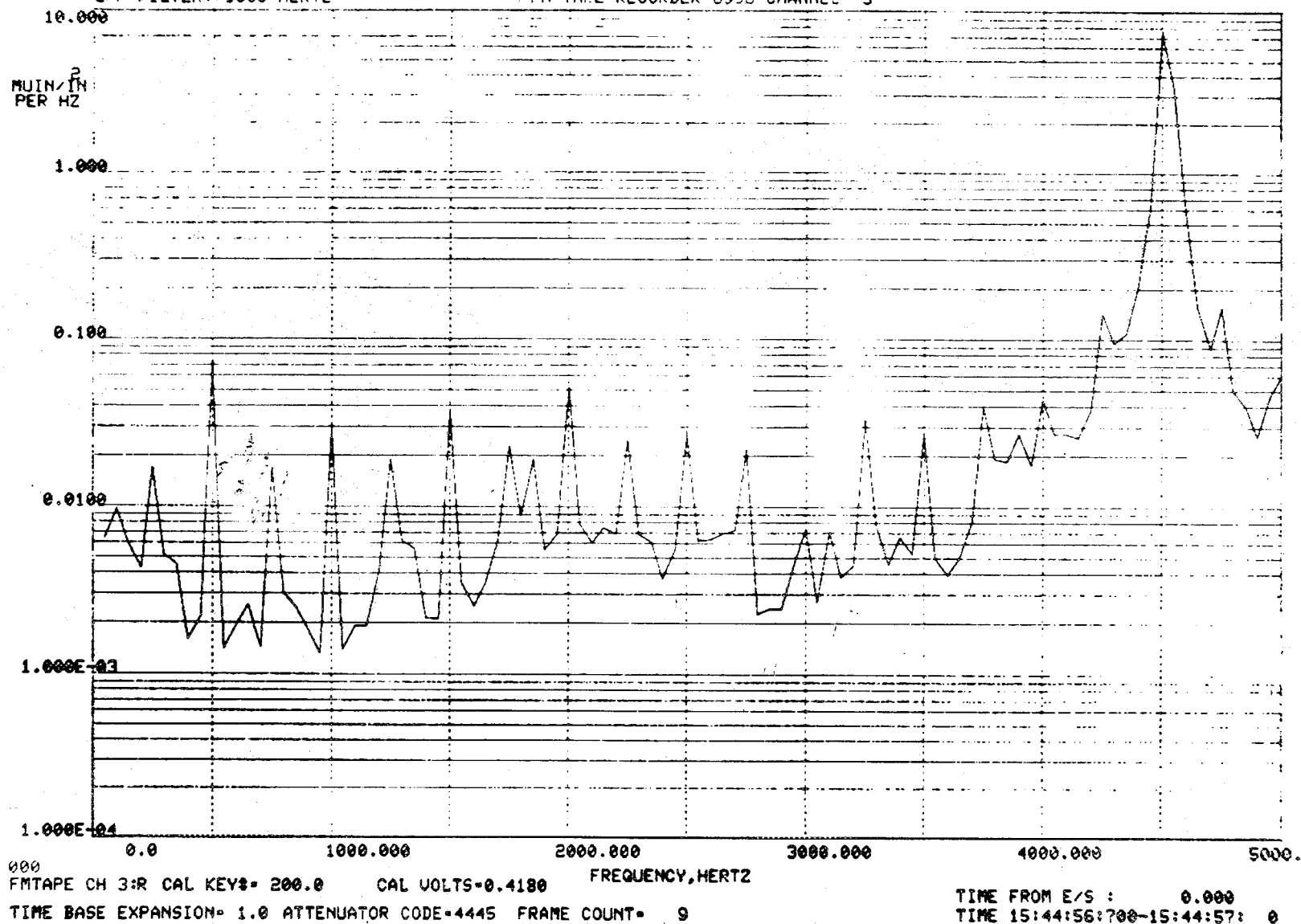
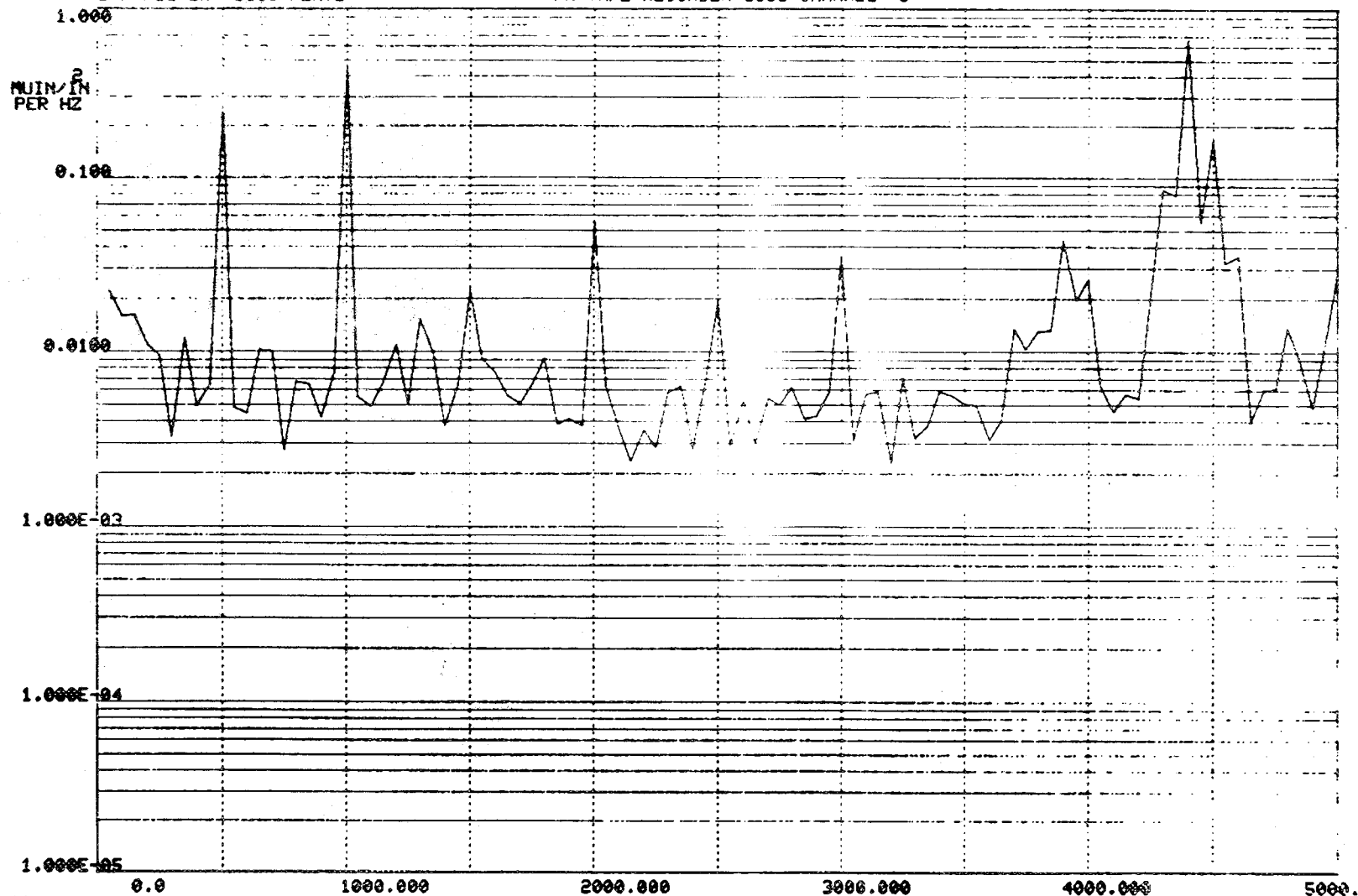


Figure 2.4-31 Strain PSD During Rubbing - SG #2 - 0 to 5 Khz 30560 rpm

BANDWIDTH= 50.00 HERTZ
 COMPOSITE RMS= 11.5
 COMP RMS FROM: 5.0E+01 TO 5.0E+03
 L/P FILTER: 5000 HERTZ

RMS POWER SPECTRAL DENSITY
 WHIRLIGIG TEST 1
 SG 4
 FM TAPE RECORDER 6956 CHANNEL 5



000
 FM TAPE CH 5:R CAL KEY= 200.0 CAL VOLTS=0.4120 FREQUENCY,HERTZ
 TIME BASE EXPANSION= 1.0 ATTENUATOR CODE=4445 FRAME COUNT= 9

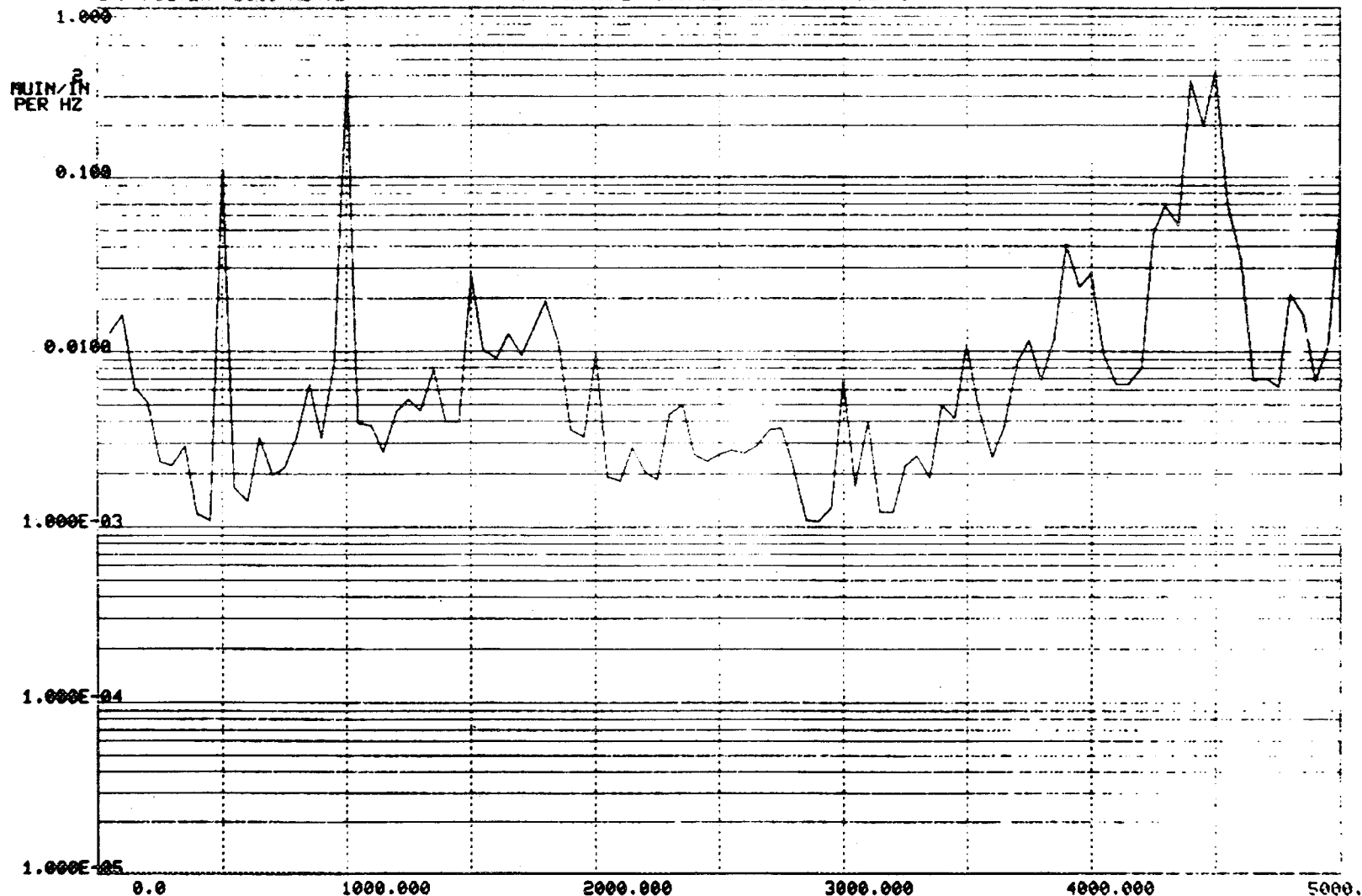
TIME FROM E/S : 0.000
 TIME 15:44:56:700-15:44:57: 0

Figure 2.4-32 Strain PSD During Rubbing - SG #4 - 0 to 5 Khz - 30560 Rpm

2.4-44

BANDWIDTH= 50.00 HERTZ
 COMPOSITE RMS= 11.1
 COMP RMS FROM: 5.0E+01 TO 5.0E+03
 L/P FILTER: 5000 HERTZ

RMS POWER SPECTRAL DENSITY
 WHIRLIGIG TEST 1
 SG 5
 FM TAPE RECORDER 6956 CHANNEL 6



000
 FM TAPE CH 6:R CAL KEYS= 200.0 CAL VOLTS=0.4060
 TIME BASE EXPANSION= 1.0 ATTENUATOR CODE=4445 FRAME COUNT= 9

TIME FROM E/S : 0.000
 TIME 15:44:56:700-15:44:57: 0

Figure 2.4-33 Strain PSD During Rubbing - SG #5 - 0 to 5 KHz - 30560 Rpm

2.4-45

ORIGINAL PAGE IS
 OF POOR QUALITY

BANDWIDTH= 50.00 HERTZ
 COMPOSITE RMS=6.126E-02
 COMP RMS FROM:5.0E+01 TO 5.0E+03
 L/P FILTER: 5000 HERTZ

RMS POWER SPECTRAL DENSITY
 WHIRLIGIG TEST 1
 SG 6
 FM TAPE RECORDER 6956 CHANNEL 7

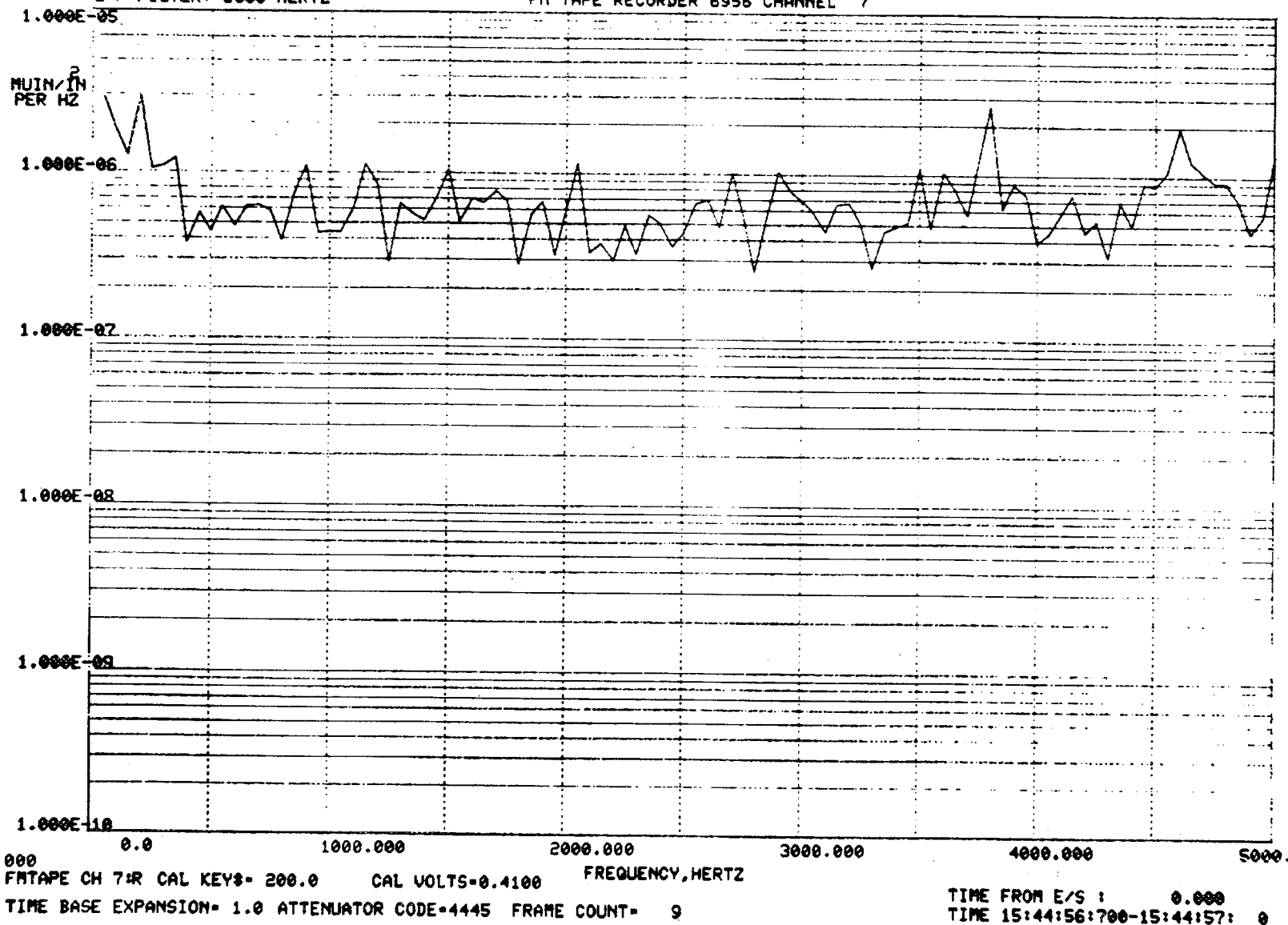
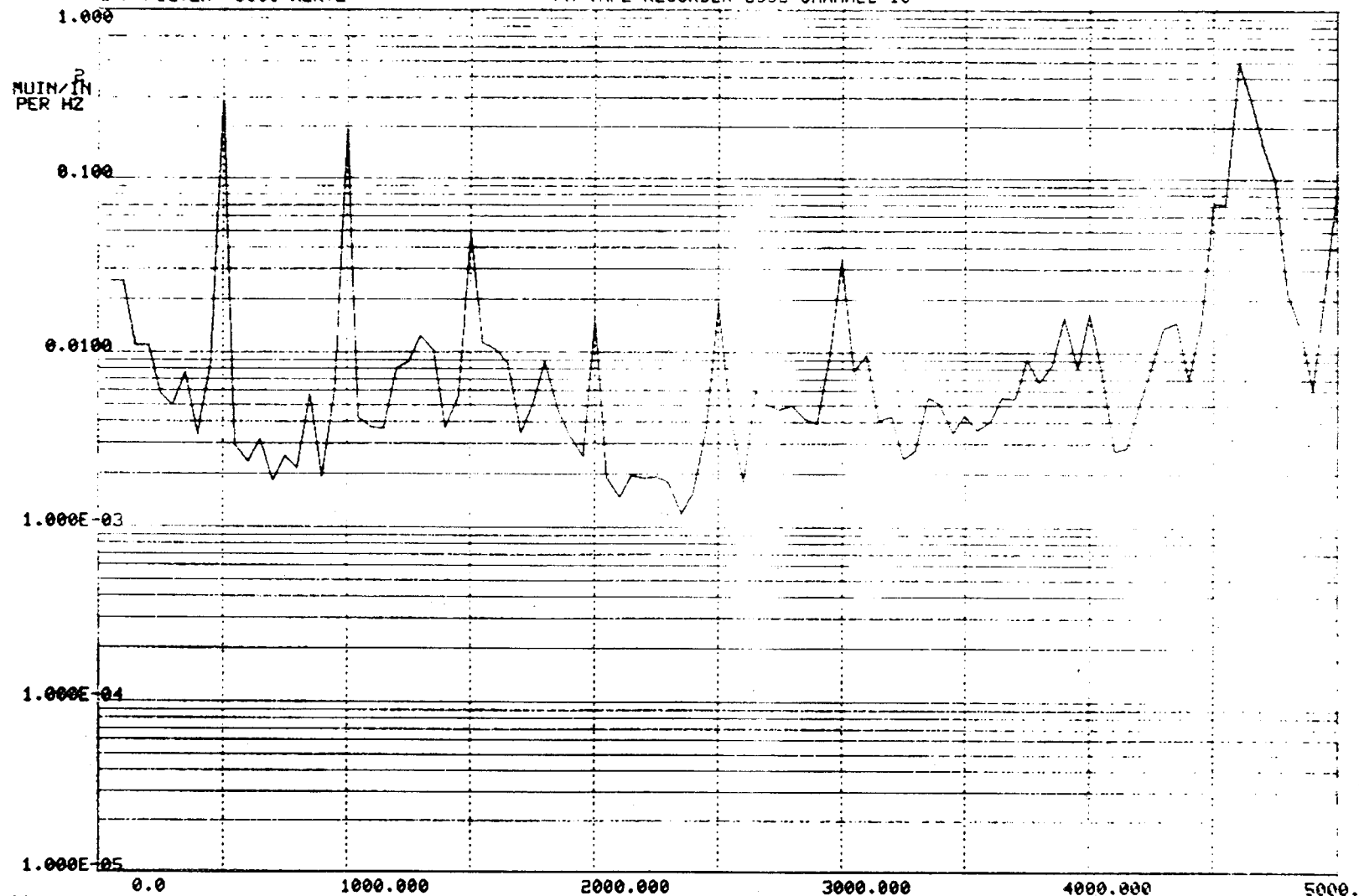


Figure 2.4-34 Strain PSD During Rubbing - SG #6 - 0 to 5 Khz - 30560 Rpm

BANDWIDTH= 50.00 HERTZ
 COMPOSITE RMS= 11.1
 COMP RMS FROM: 5.0E+01 TO 5.0E+03
 L/P FILTER: 5000 HERTZ

RMS POWER SPECTRAL DENSITY
 WHIRLIGIG TEST 1
 SG 60
 FM TAPE RECORDER 6955 CHANNEL 10



000
 FMTAPE CH10:R CAL KEYS= 200.0 CAL VOLTS=0.4060 FREQUENCY,HERTZ
 TIME BASE EXPANSION= 1.0 ATTENUATOR CODE=4445 FRAME COUNT= 9

TIME FROM E/S : 0.000
 TIME 15:44:56:700-15:44:57: 0

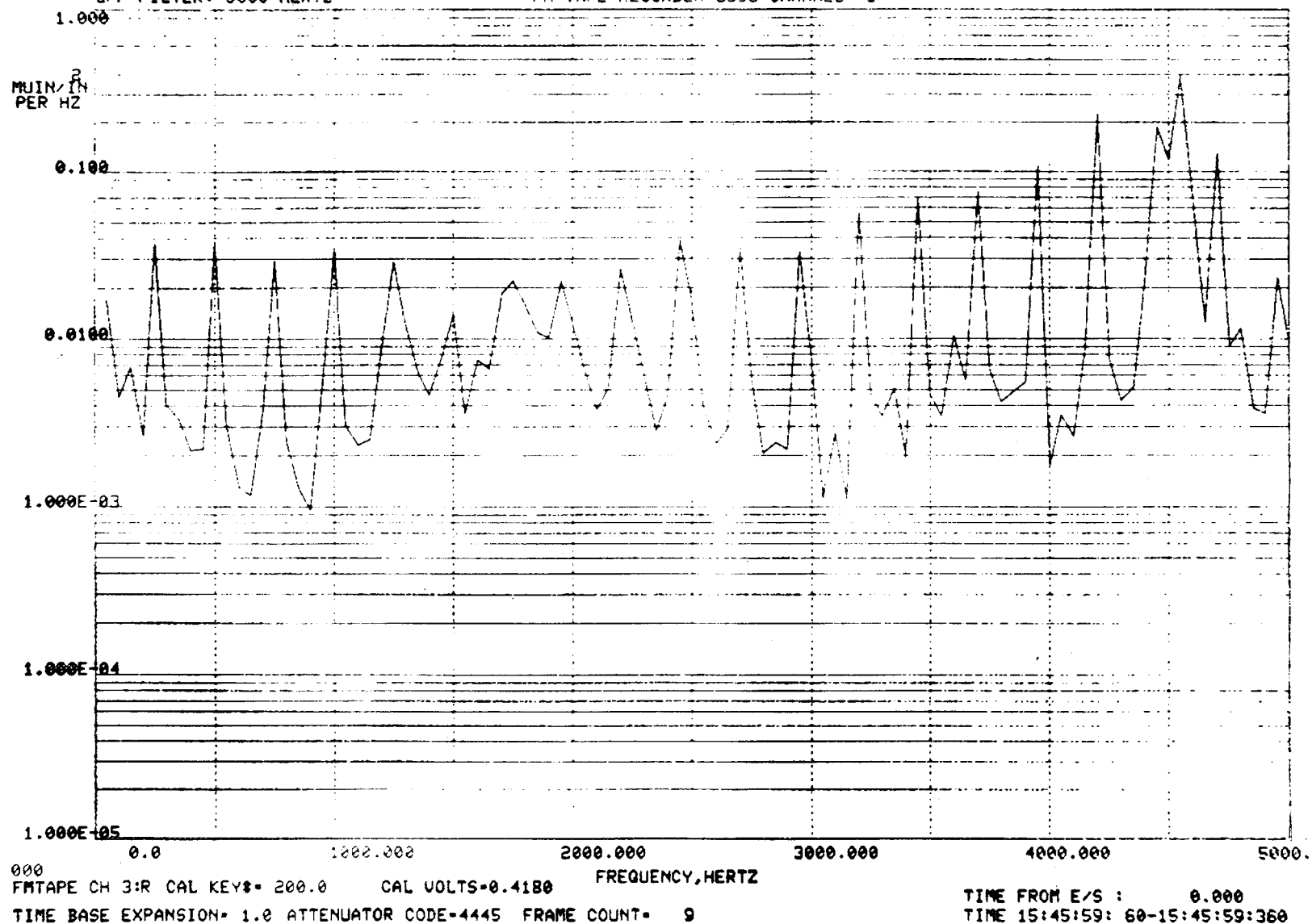
Figure 2.4-35 Strain PSD During Rubbing - SG #60 - 0 to 5 Khz - 30560 Rpm

2.4-47

ORIGINAL PAGE IS
 OF POOR QUALITY

BANDWIDTH= 50.00 HERTZ
 COMPOSITE RMS= 10.6
 COMP RMS FROM: 5.0E+01 TO 5.0E+03
 L/P FILTER: 5000 HERTZ

RMS POWER SPECTRAL DENSITY
 WHIRLIGIG TEST 1
 SG2
 FM TAPE RECORDER 6956 CHANNEL 3



2.4-48

Figure 2.4-36 Strain PSD During Rubbing - SG #2 - 0 to 5 Khz - 30060 Rpm

BANDWIDTH= 50.00 HERTZ
 COMPOSITE RMS= 19.1
 COMP RMS FROM: 5.0E+01 TO 5.0E+03
 L/P FILTER: 5000 HERTZ

RMS POWER SPECTRAL DENSITY
 WHIRLIGIG TEST 1
 SG 4
 FM TAPE RECORDER 6956 CHANNEL 5

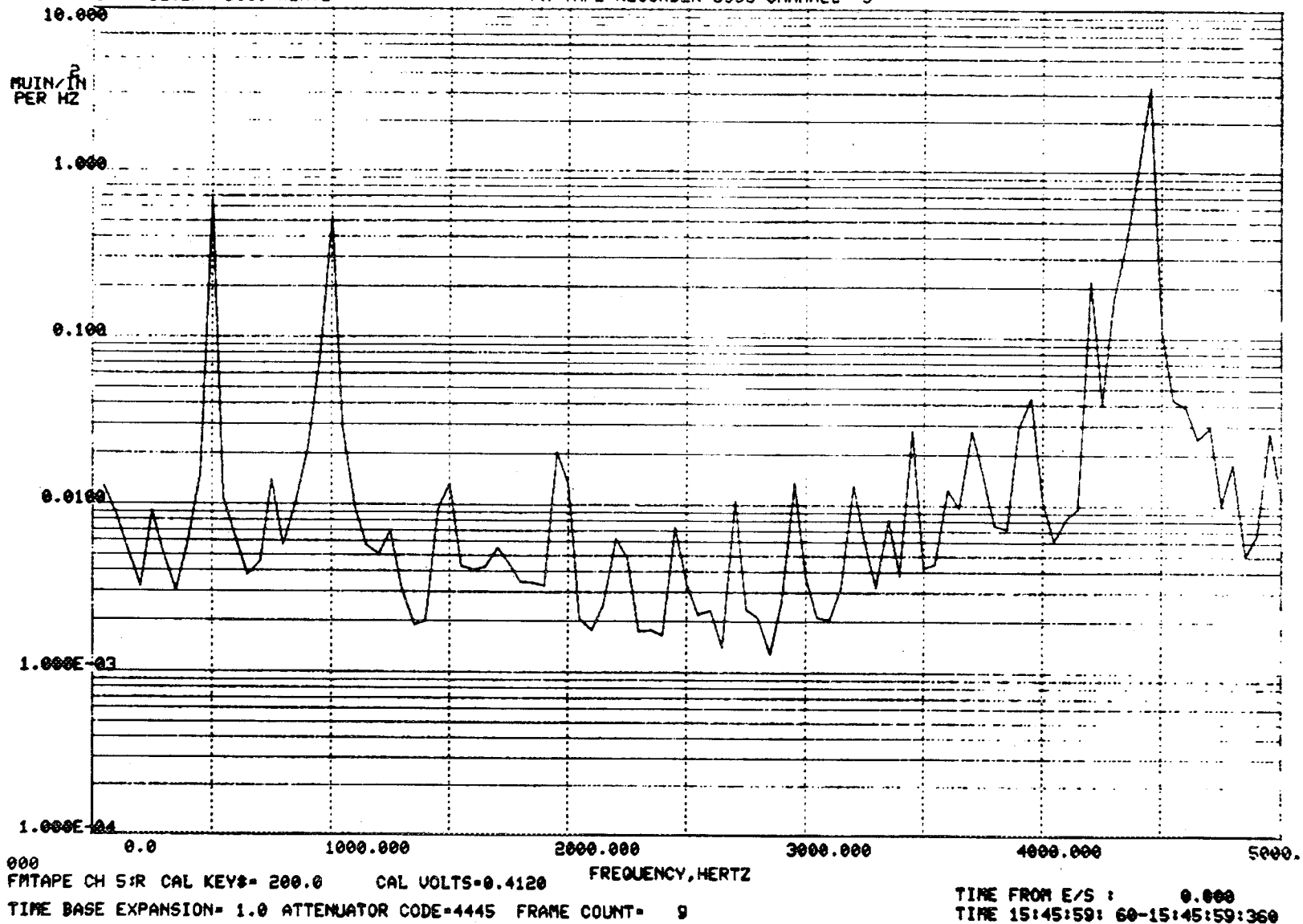


Figure 2.4-37 Strain PSD During Rubbing - SG #4 - 0 to 5 Khz - 30060 Rpm

2.4-49

ORIGINAL PAGE IS
 OF POOR QUALITY

BANDWIDTH= 50.00 HERTZ
 COMPOSITE RMS= 15.8
 COMP RMS FROM: 5.0E+01 TO 5.0E+03
 L/P FILTER: 5000 HERTZ

RMS POWER SPECTRAL DENSITY
 WHIRLIGIG TEST 1
 SG 5
 FM TAPE RECORDER 6956 CHANNEL 6

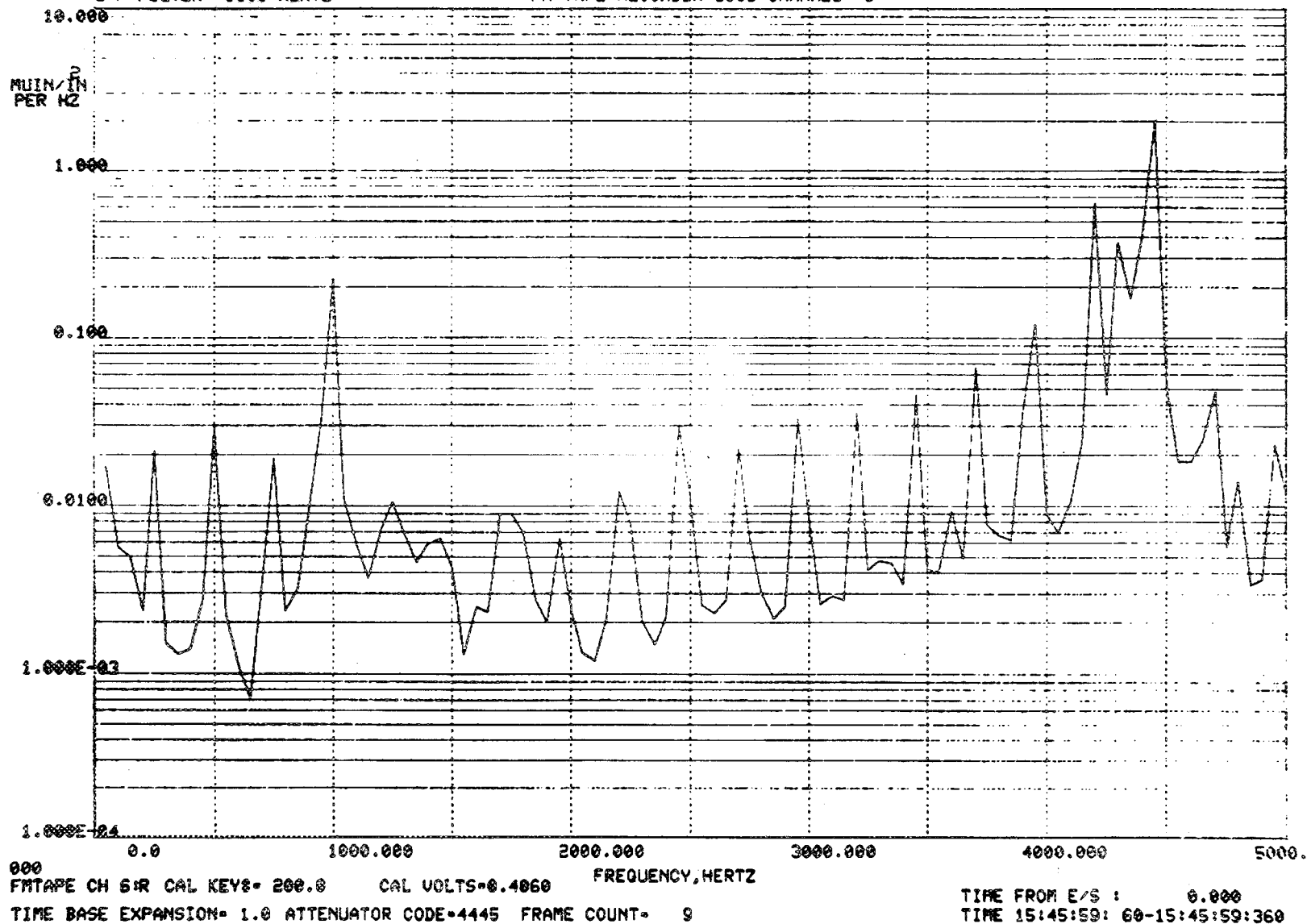


Figure 2.4-38 Strain PSD During Rubbing - SG #5 - 0 to 5 Khz - 30060 Rpm

BANDWIDTH= 50.00 HERTZ
 COMPOSITE RMS=5.806E-02
 COMP RMS FROM:5.0E+01 TO 5.0E+03
 L/P FILTER: 5000 HERTZ

RMS POWER SPECTRAL DENSITY
 WHIRLIGIG TEST 1
 SG 6
 FM TAPE RECORDER 6956 CHANNEL 7

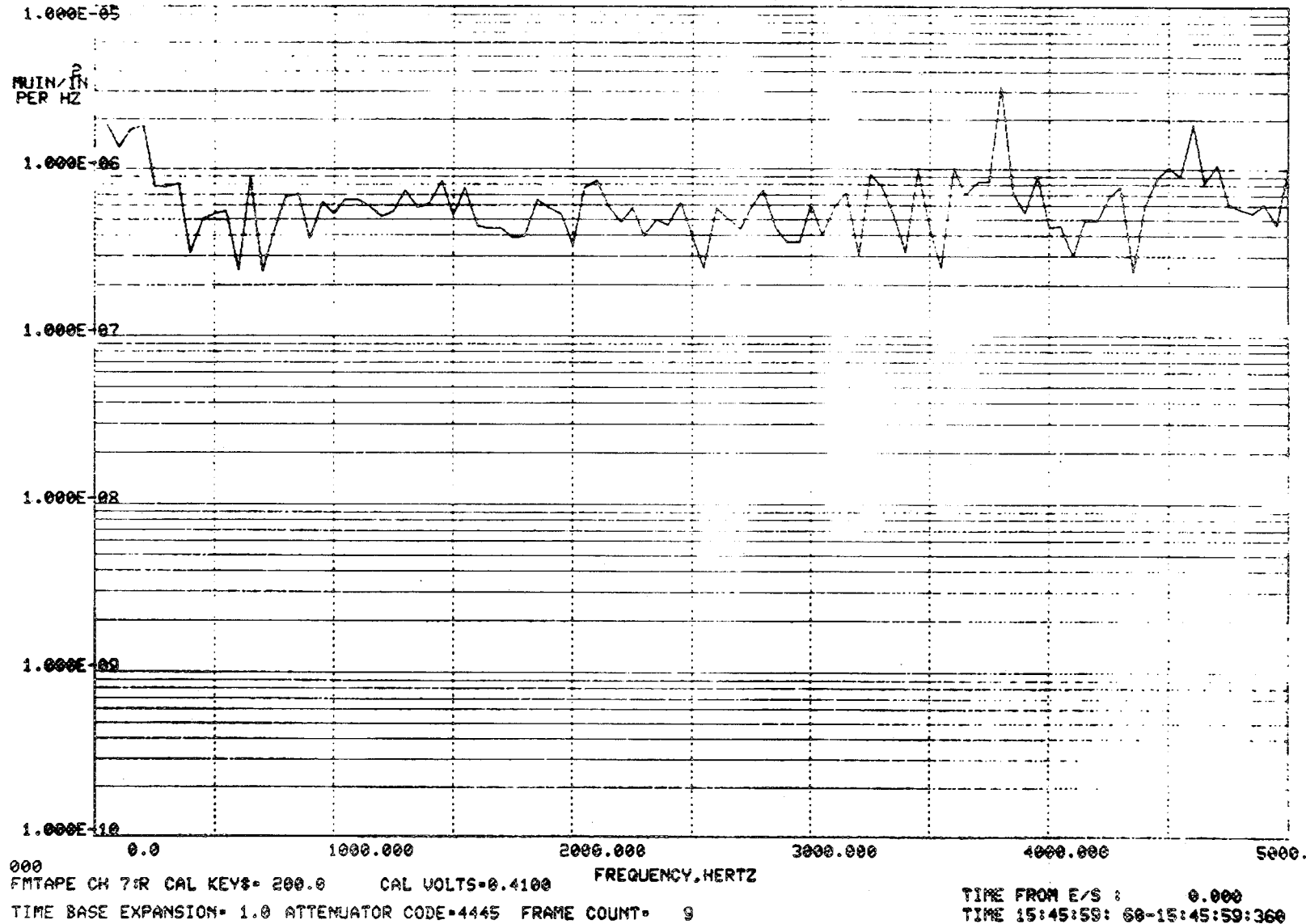


Figure 2.4-39 Strain PSD During Rubbing - SG #6 - 0 to 5 Khz - 30060 Rpm

2.4-51

ORIGINAL PAGE IS
 OF POOR QUALITY

BANDWIDTH= 50.00 HERTZ
 COMPOSITE RMS= 10.3
 COMP RMS FROM: 5.0E+01 TO 5.0E+03
 L/P FILTER: 5000 HERTZ

RMS POWER SPECTRAL DENSITY
 WHIRLIGIG TEST 1
 SG 60
 FM TAPE RECORDER 6956 CHANNEL 10

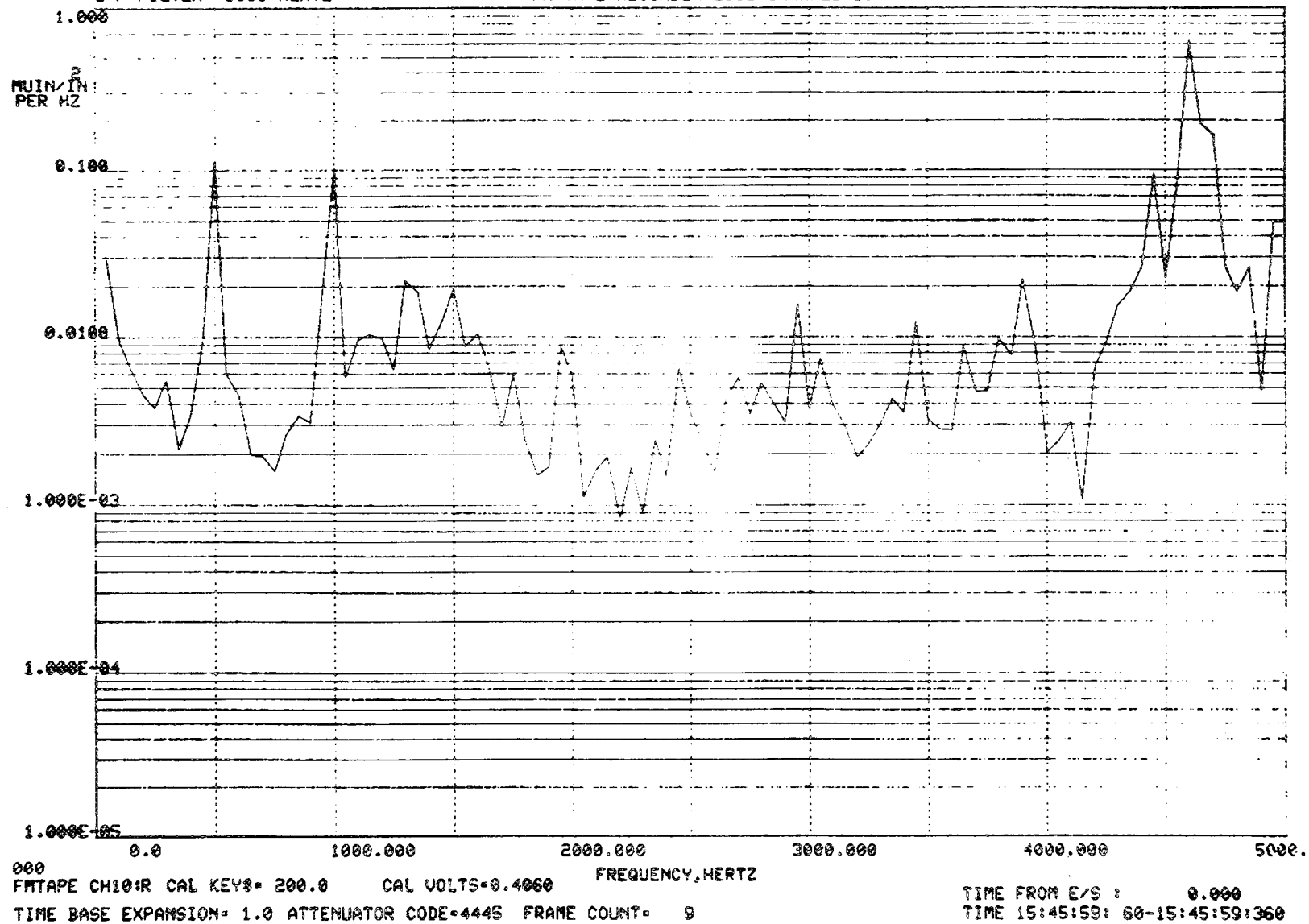


Figure 2.4-40 Strain PSD During Rubbing - SG #60 - 0 to 5 Khz - 30060 Rpm

2.4-52

ORIGINAL PAGE IS
 OF POOR QUALITY

BANDWIDTH= 50.00 HERTZ
 COMPOSITE RMS= 10.1
 COMP RMS FROM: 5.0E+01 TO 5.0E+03
 L/P FILTER: 5200 HERTZ

RMS POWER SPECTRAL DENSITY
 WHIRLIGIG TEST 1
 TEST ARTICLE ACCEL
 FM TAPE RECORDER 6959 CHANNEL 16

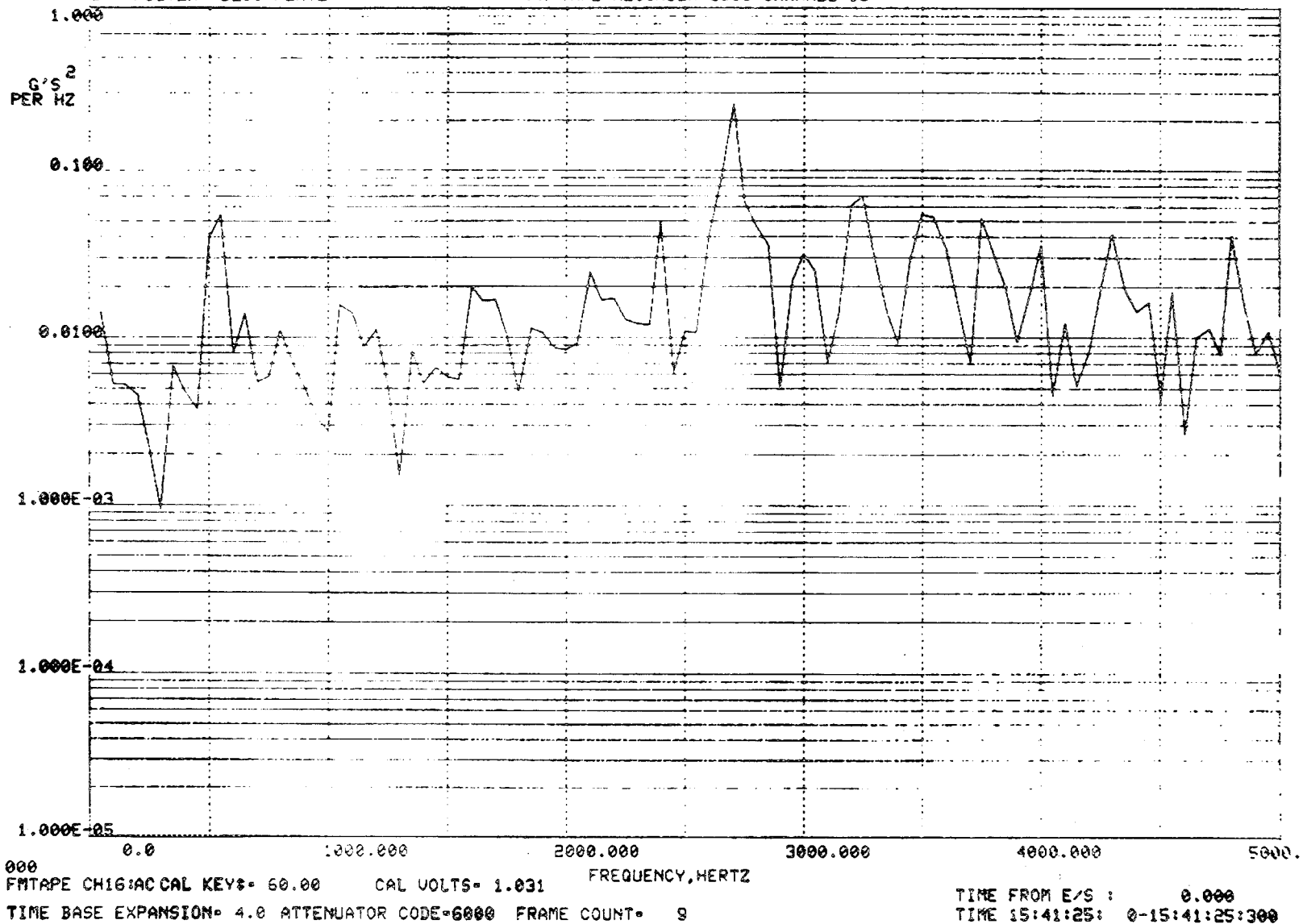


Figure 2.4-41 Test Article Accelerometer PSD During Rubbing - 0 to 5 Khz - 32160 Rpm

2.4-53

ORIGINAL PAGE IS
 OF POOR QUALITY

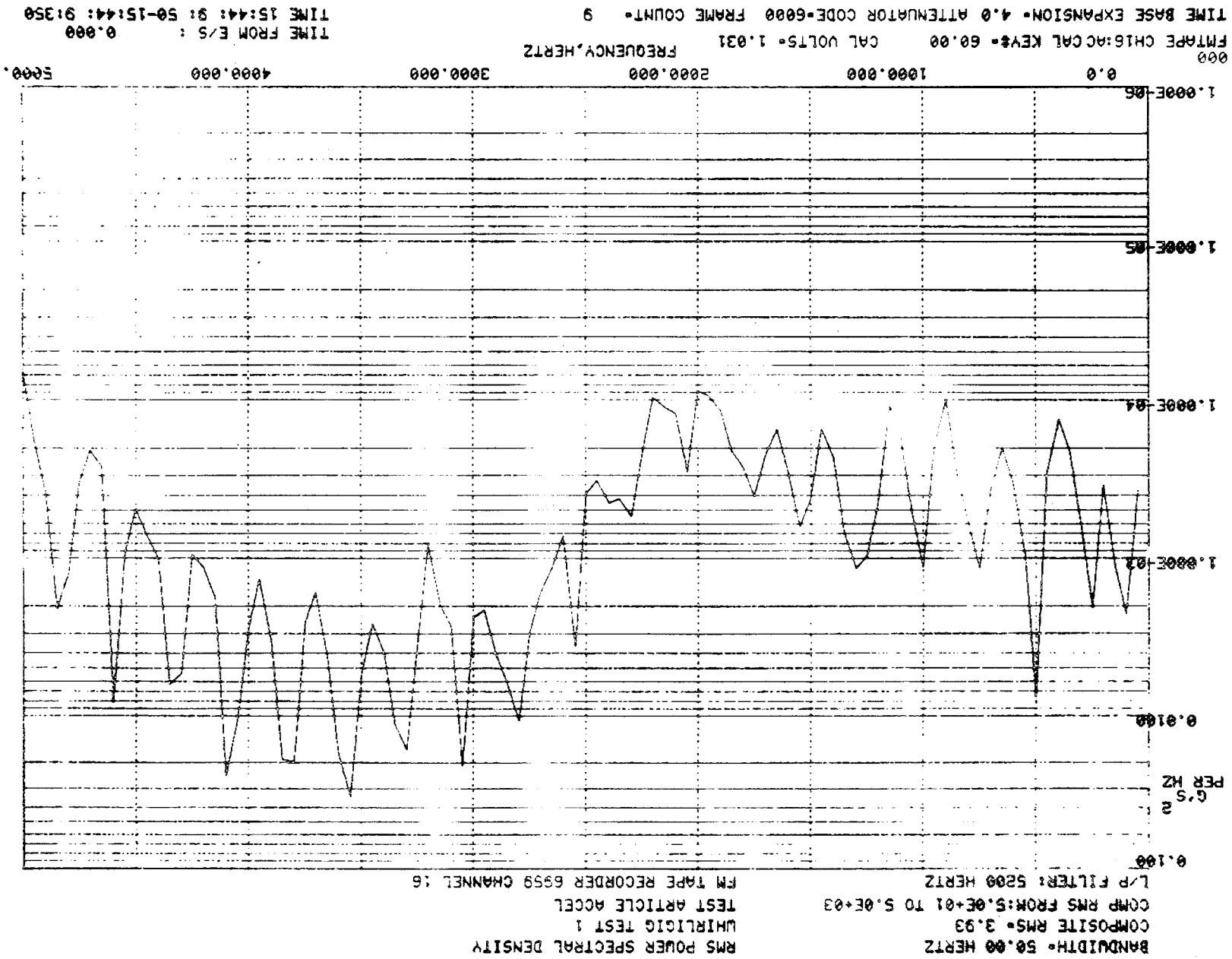


Figure 2.4-42 Test Article Accelerometer PSD During Rubbing - 0 to 5 Khz - 31030 Rpm

BANDWIDTH= 50.00 HERTZ
 COMPOSITE RMS= 7.08
 COMP RMS FROM: 5.0E+01 TO 5.0E+03
 L/P FILTER: 5200 HERTZ

RMS POWER SPECTRAL DENSITY
 WHIRLIGIG TEST 1
 TEST ARTICLE ACCEL
 FM TAPE RECORDER 6959 CHANNEL 16

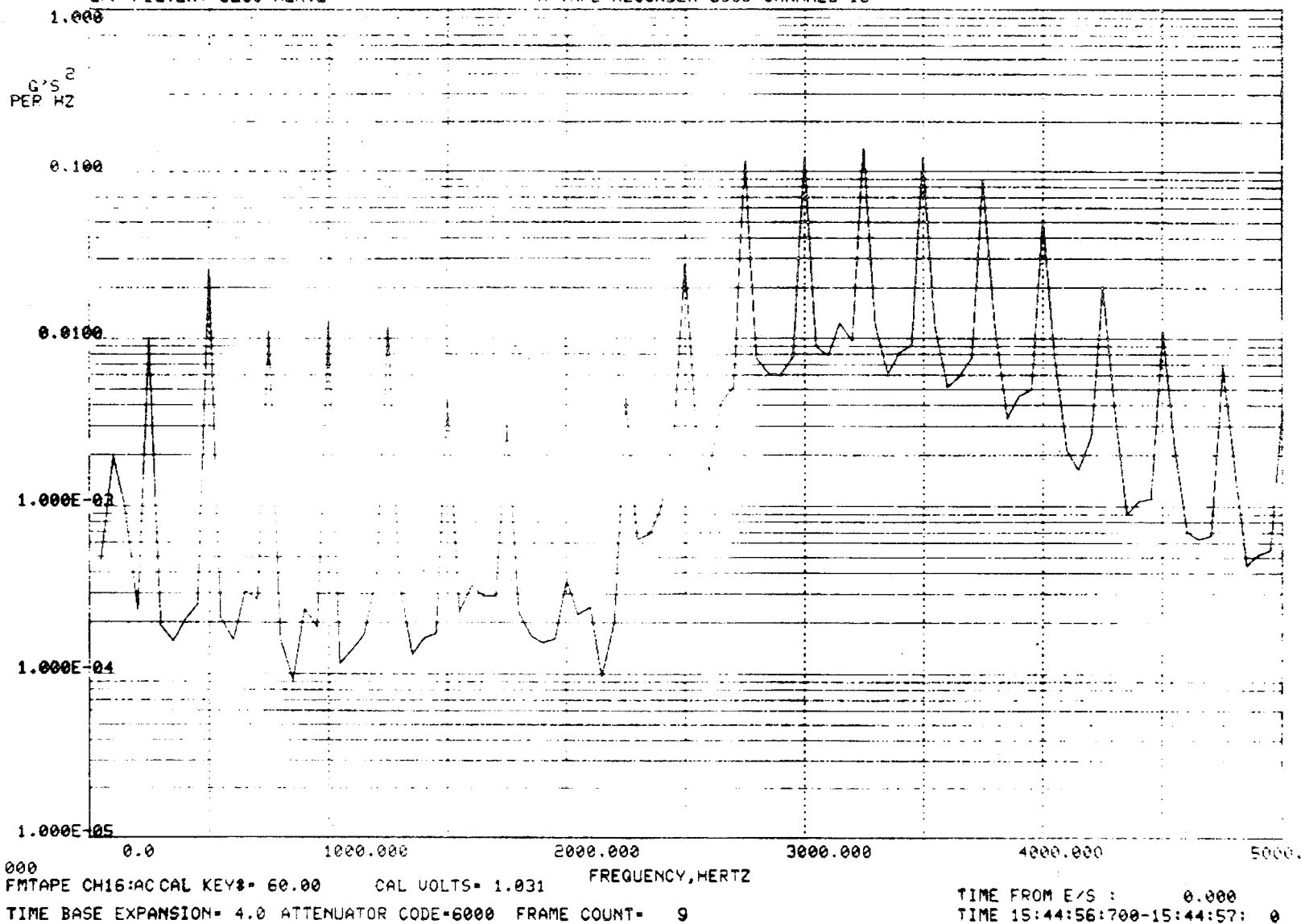
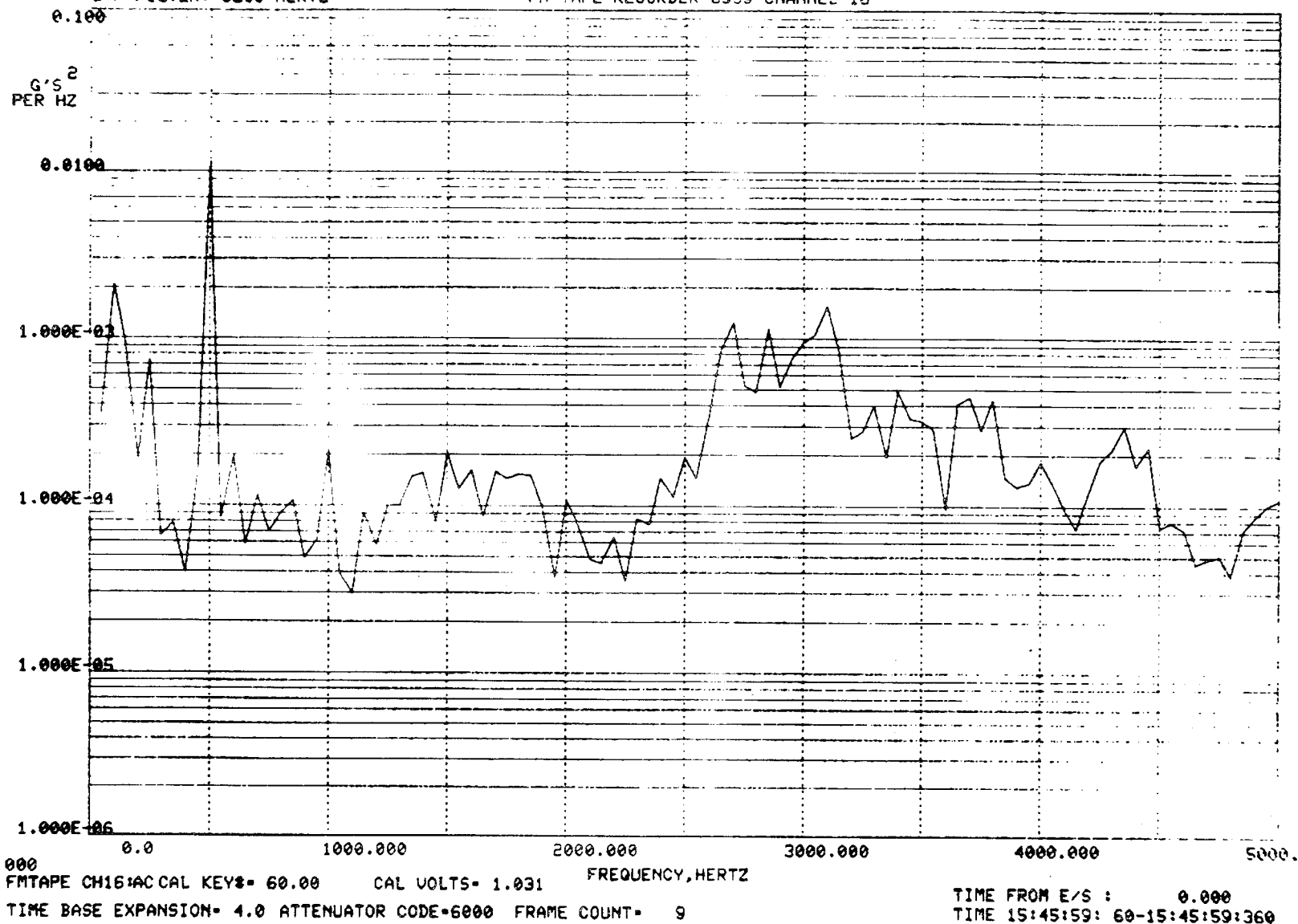


Figure 2.4-43 Test Article Accelerometer PSD During Rubbing - 0 to 5 Khz - 30560 Rpm

BANDWIDTH= 50.00 HERTZ
 COMPOSITE RMS= 1.37
 COMP RMS FROM: 5.0E+01 TO 5.0E+03
 L/P FILTER: 5200 HERTZ

RMS POWER SPECTRAL DENSITY
 WHIRLIGIG TEST 1
 TEST ARTICLE ACCEL
 FM TAPE RECORDER 6959 CHANNEL 16



2.4-56

Figure 2.4-44 Test Article Accelerometer PSD During Rubbing - 0 to 5 Khz - 30060 Rpm

ORIGINAL PAGE IS
 OF POOR
 QUALITY

BANDWIDTH=125.00 HERTZ
 COMPOSITE RMS= 9.19
 COMP RMS FROM:1.2E+02 TO 2.0E+04
 L/P FILTER: 20K HERTZ

RMS POWER SPECTRAL DENSITY
 WHIRLIGIG TEST 1
 SG 2
 FM TAPE RECORDER 6956 CHANNEL 3

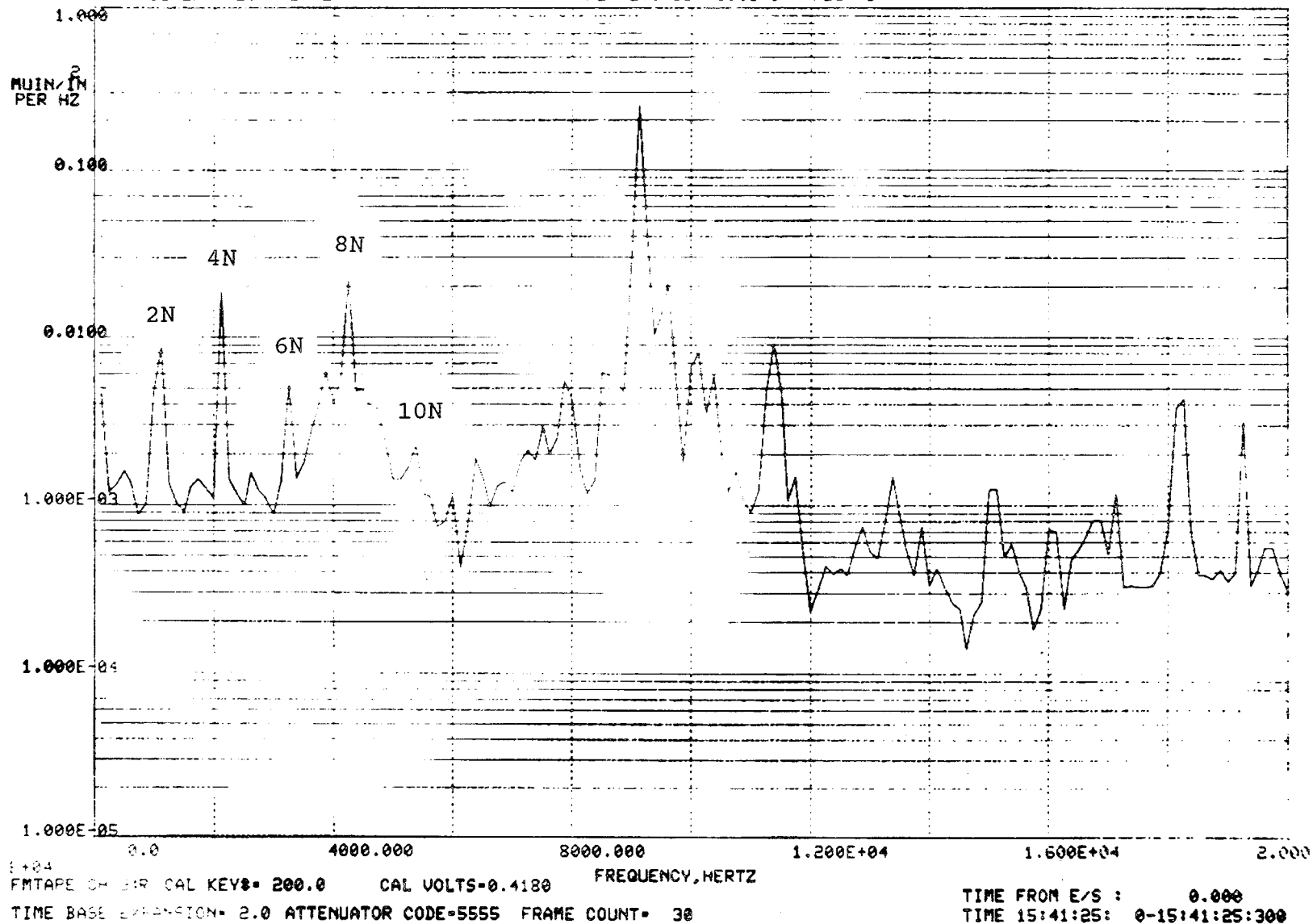
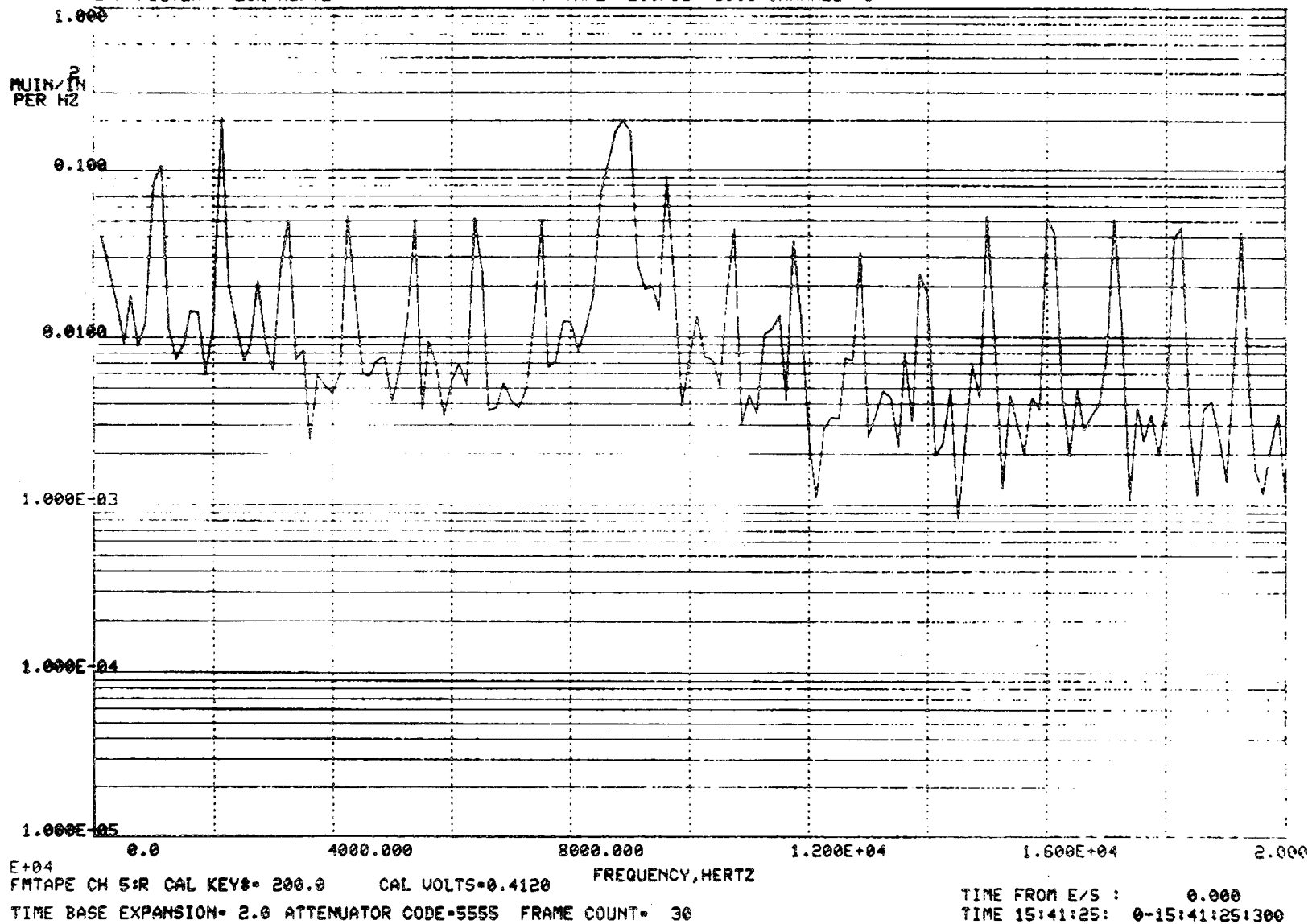


Figure 2.4-45 Strain PSD During Rubbing - SG #2 - 0 to 20 Khz 32160 rpm

BANDWIDTH=125.00 HERTZ
 COMPOSITE RMS= 19.3
 COMP RMS FROM:1.2E+02 TO 2.0E+04
 L/P FILTER: 20K HERTZ

RMS POWER SPECTRAL DENSITY
 WHIRLIGIG TEST 1
 SG 4
 FM TAPE RECORDER 6956 CHANNEL 5



BANDWIDTH=125.00 HERTZ
 COMPOSITE RMS= 11.5
 COMP RMS FROM:1.2E+02 TO 2.0E+04
 L/P FILTER: 20K HERTZ

RMS POWER SPECTRAL DENSITY
 WHIRLIGIG TEST 1
 SG 5
 FM TAPE RECORDER 6956 CHANNEL 6

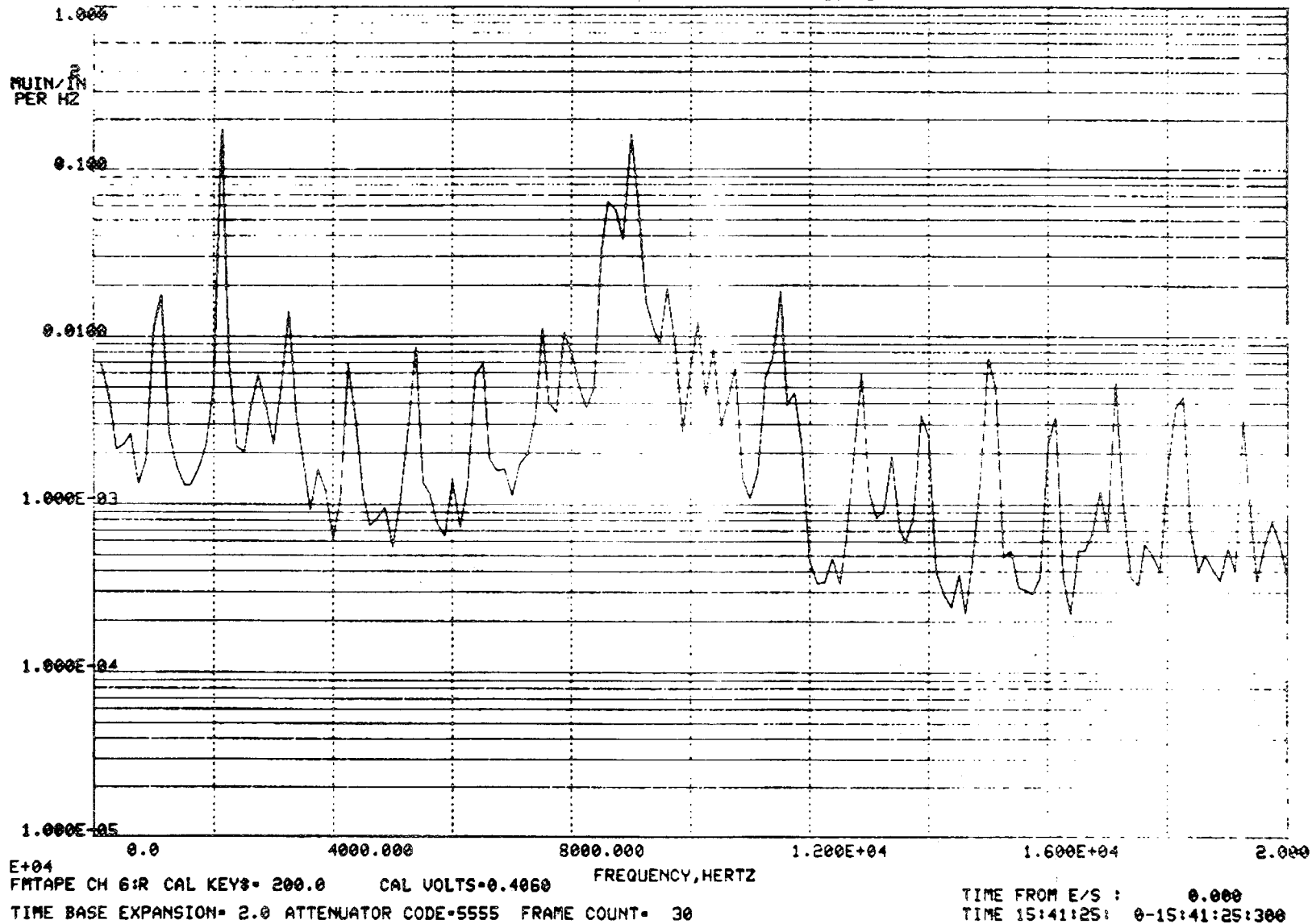


Figure 2.4-47 Strain PSD During Rubbing - SG #5 - 0 to 20 Khz - 32160 Rpm

BANDWIDTH=125.00 HERTZ
 COMPOSITE RMS=8.331E-02
 COMP RMS FROM:1.2E+02 TO 2.0E+04
 L/P FILTER: 20K HERTZ

RMS POWER SPECTRAL DENSITY
 WHIRLIGIG TEST 1
 SG 6
 FM TAPE RECORDER 6956 CHANNEL 7

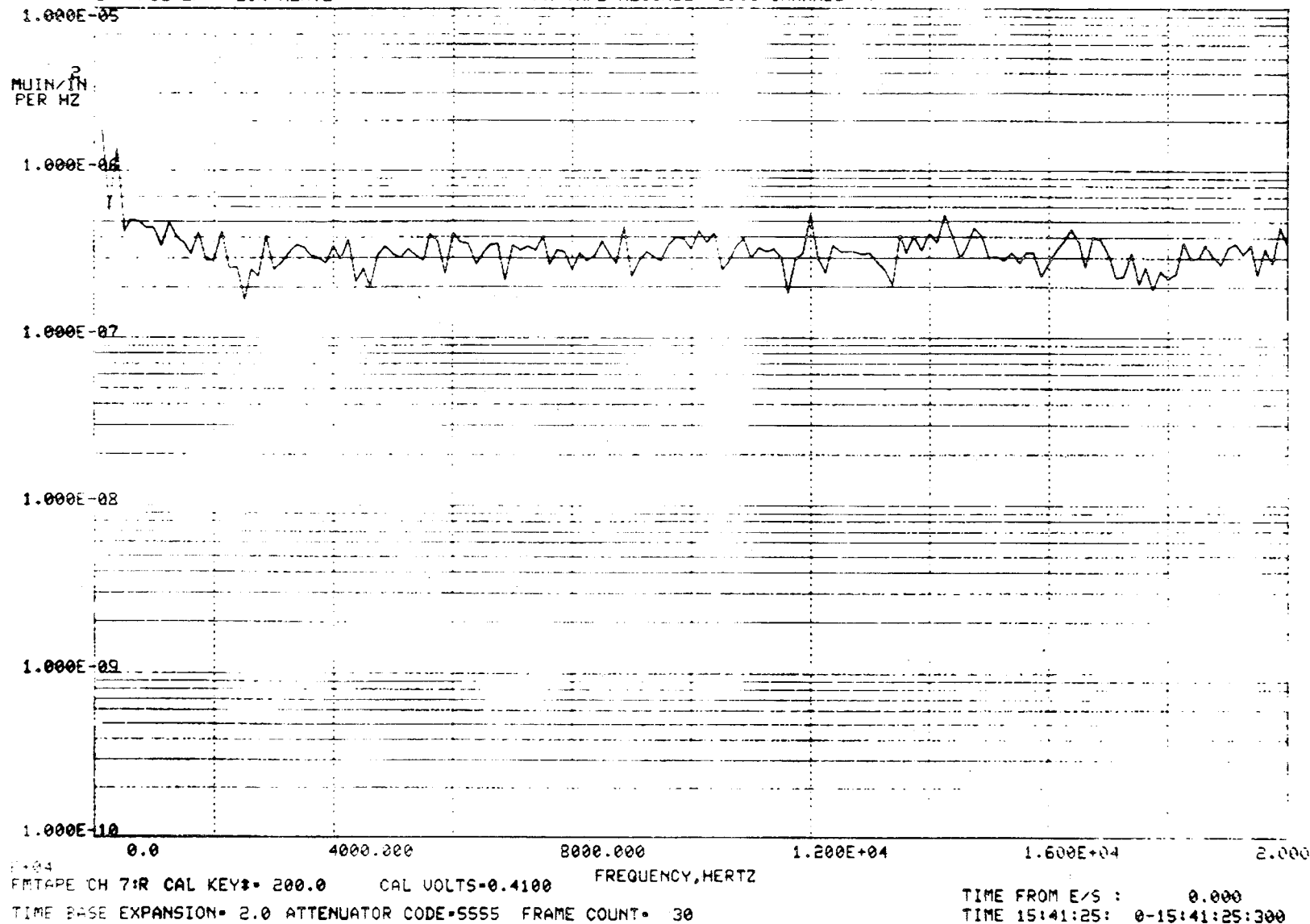


Figure 2.4-48 Strain PSD During Rubbing - SG #6 - 0 to 20 Khz - 32160 Rpm

2.4-60

ORIGINAL PAGE IS
 OF POOR QUALITY

BANDWIDTH=125.00 HERTZ
 COMPOSITE RMS= 12.0
 COMP RMS FROM:1.2E+02 TO 2.0E+04
 L/P FILTER: 20K HERTZ

RMS POWER SPECTRAL DENSITY
 WHIRLIGIG TEST 1
 SG 60
 FM TAPE RECORDER 6956 CHANNEL 10

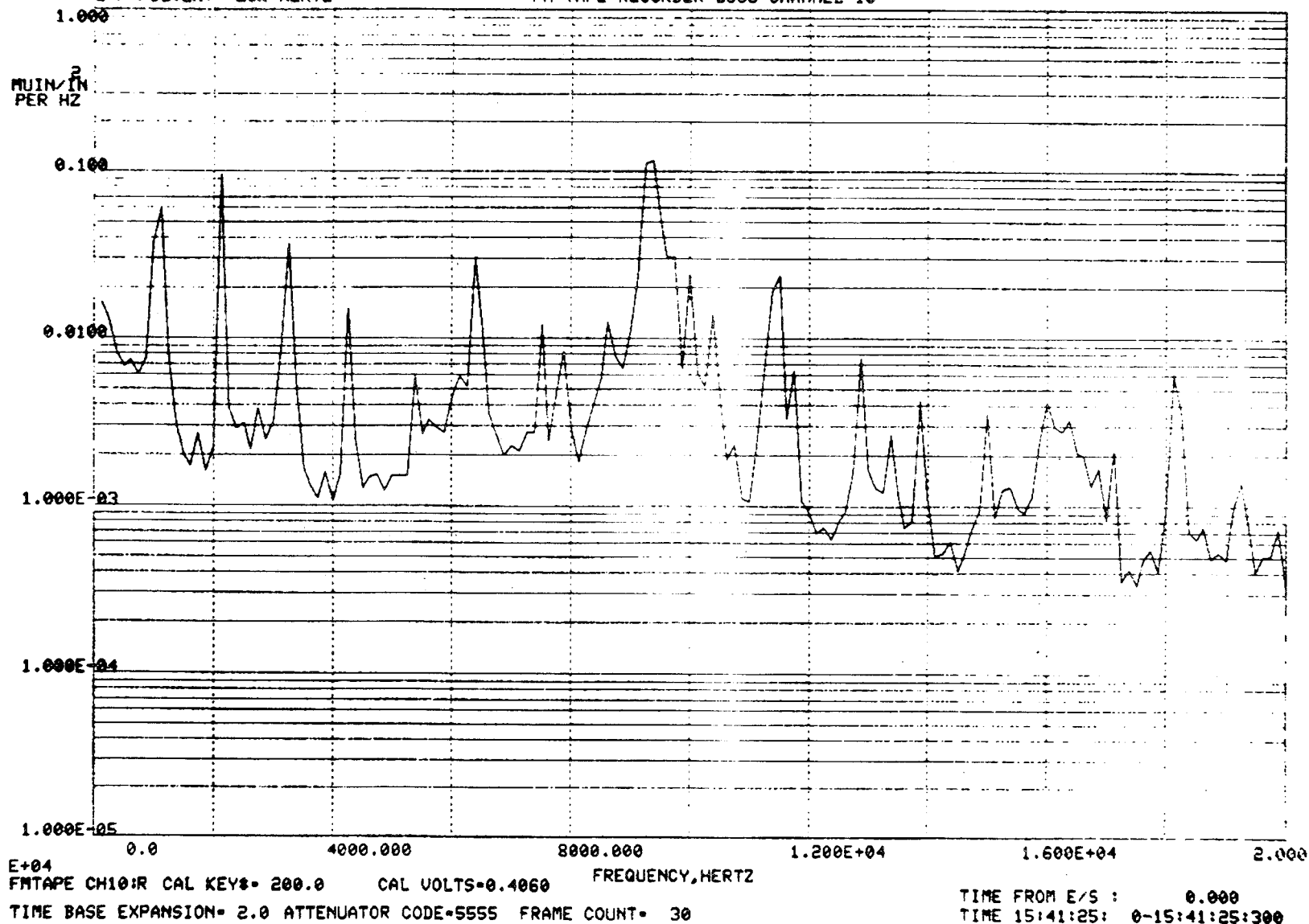


Figure 2.4-49 Strain PSD During Rubbing - SG #60 - 0 to 20 Khz - 32160 Rpm

BANDWIDTH=125.00 HERTZ
 COMPOSITE RMS= 9.03
 COMP RMS FROM:1.2E+02 TO 2.0E+04
 L/P FILTER: 20K HERTZ

RMS POWER SPECTRAL DENSITY
 WHIRLIGIG TEST 1
 SG 2
 FM TAPE RECORDER 6956 CHANNEL 3

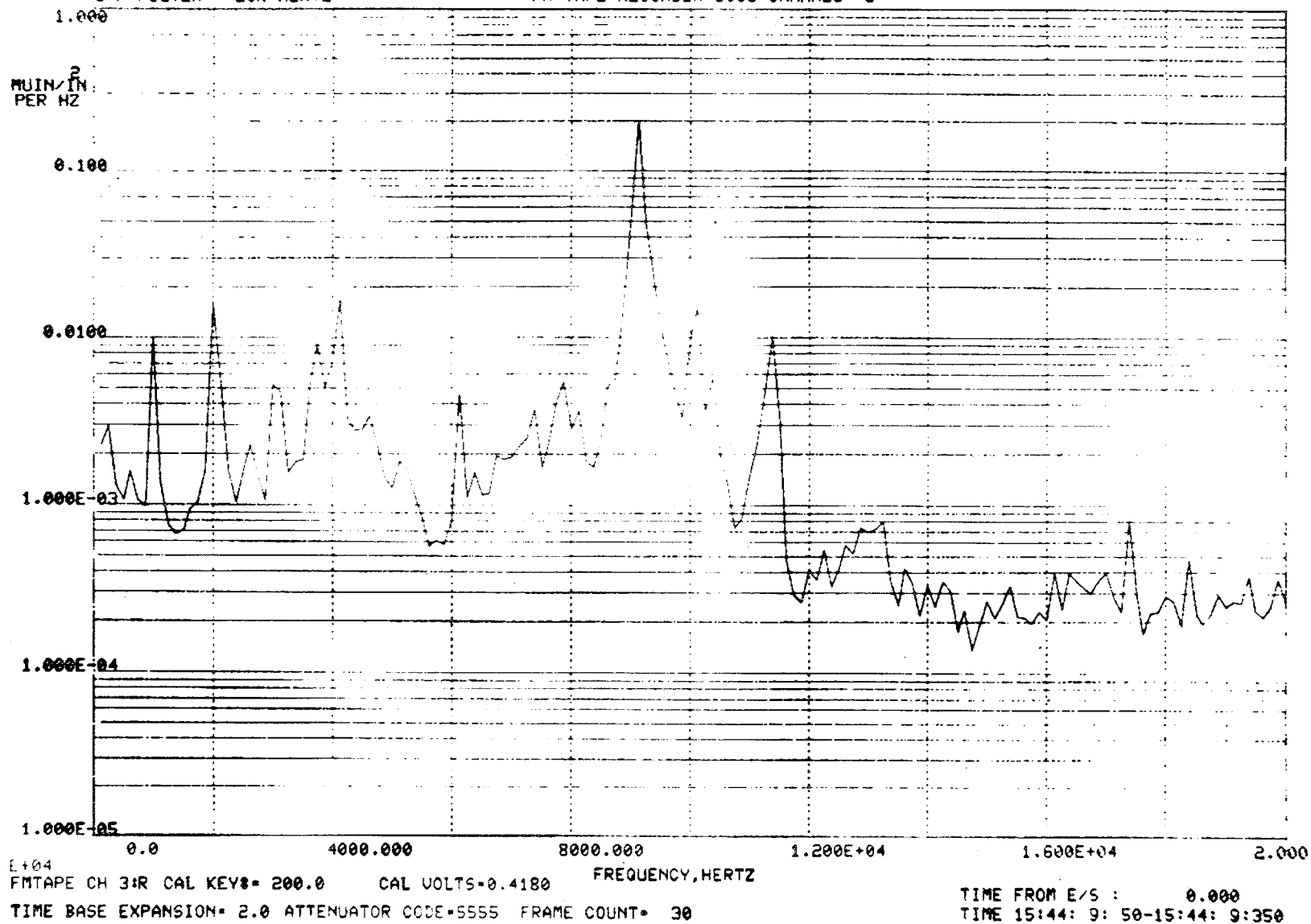
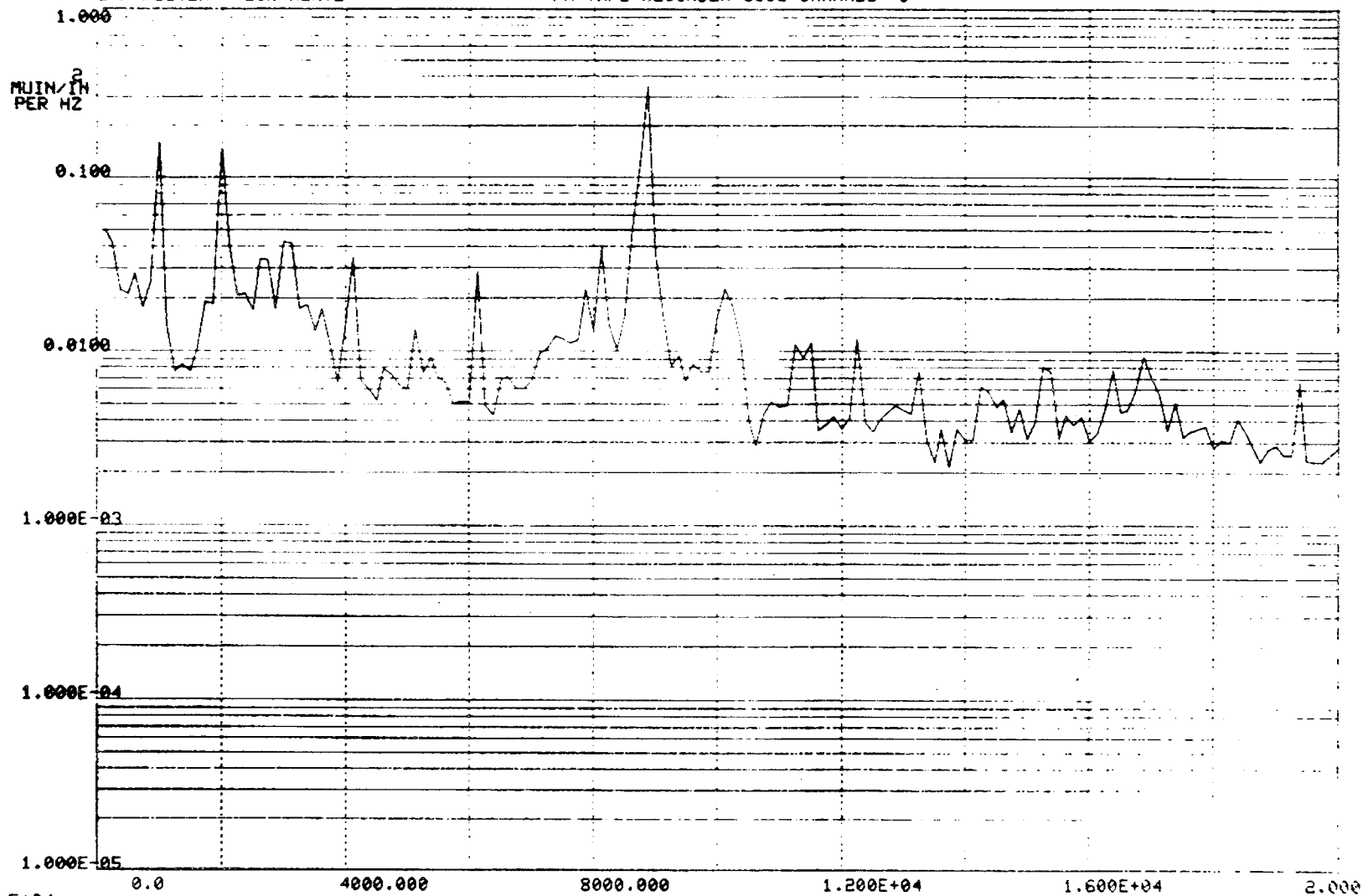


Figure 2.4-50 Strain PSD During Rubbing - SG #2 - 0 to 20 Khz - 31030 Rpm

BANDWIDTH=125.00 HERTZ
 COMPOSITE RMS= 17.2
 COMP RMS FROM:1.2E+02 TO 2.0E+04
 L/P FILTER: 20K HERTZ

RMS POWER SPECTRAL DENSITY
 WHIRLIGIG TEST 1
 SG 4
 FM TAPE RECORDER 6956 CHANNEL 5



E+04
 FMTAPE CH 5:R CAL KEY#= 200.0 CAL VOLTS=0.4120
 TIME BASE EXPANSION= 2.0 ATTENUATOR CODE=5555 FRAME COUNT= 30

TIME FROM E/S : 0.000
 TIME 15:44: 9: 50-15:44: 9:350

Figure 2.4-51 Strain PSD During Rubbing - SG #4 - 0 to 20 Khz - 31030 Rpm

2.4-63

ORIGINAL PAGE IS
 OF POOR QUALITY

BANDWIDTH=125.00 HERTZ
 COMPOSITE RMS= 10.7
 COMP RMS FROM:1.2E+02 TO 2.0E+04
 L/P FILTER: 20K HERTZ

RMS POWER SPECTRAL DENSITY
 WHIRLIGIG TEST 1
 SG 5
 FM TAPE RECORDER 6956 CHANNEL 6

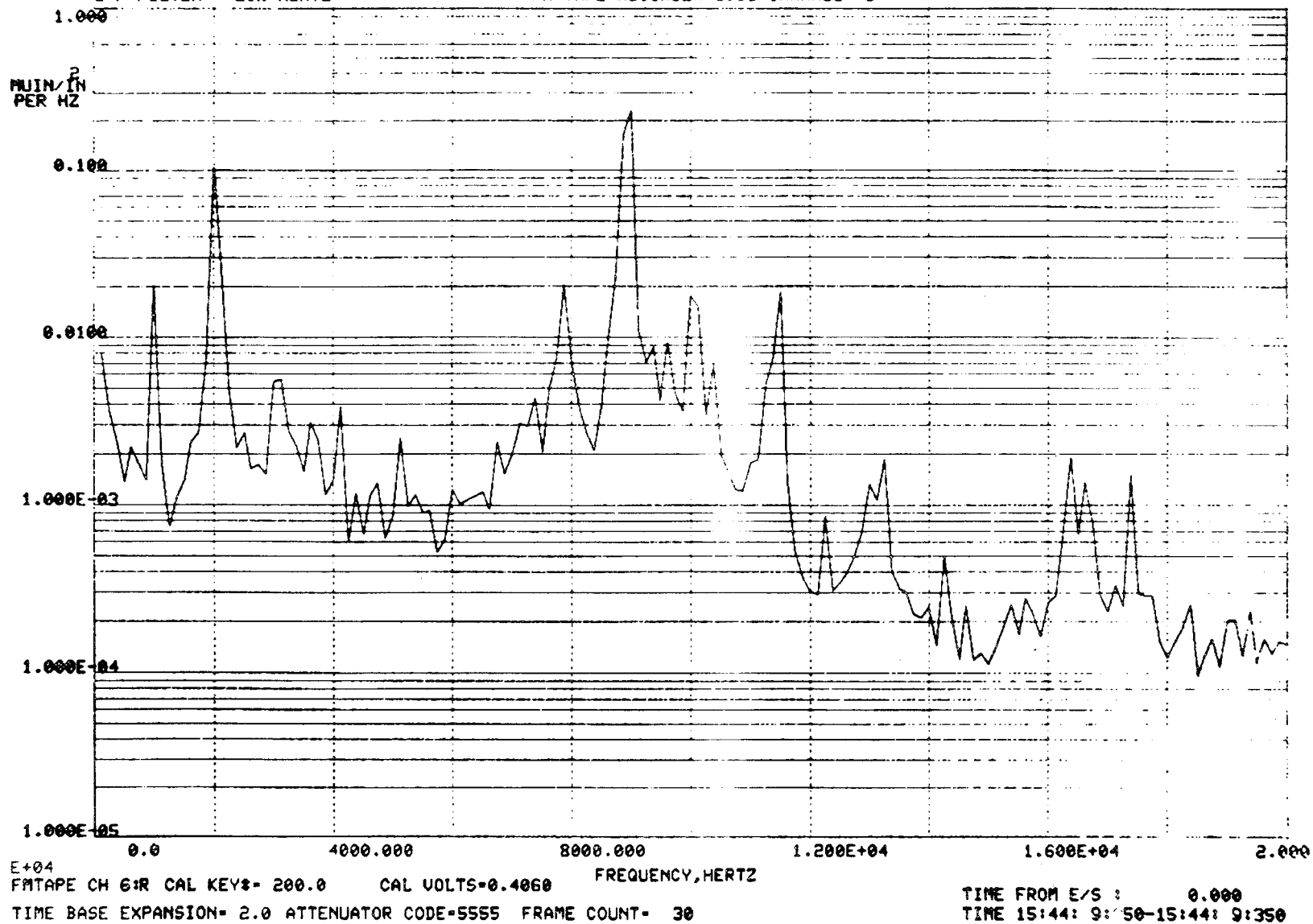


Figure 2.4-52 Strain PSD During Rubbing - SG #5 - 0 to 20 Khz - 31030 Rpm

BANDWIDTH=125.00 HERTZ
 COMPOSITE RMS=0.339
 COMP RMS FROM:1.2E+02 TO 2.0E+04
 L/P FILTER: 20K HERTZ

RMS POWER SPECTRAL DENSITY
 WHIRLIGIG TEST 1
 SG 6
 FM TAPE RECORDER 6956 CHANNEL 7

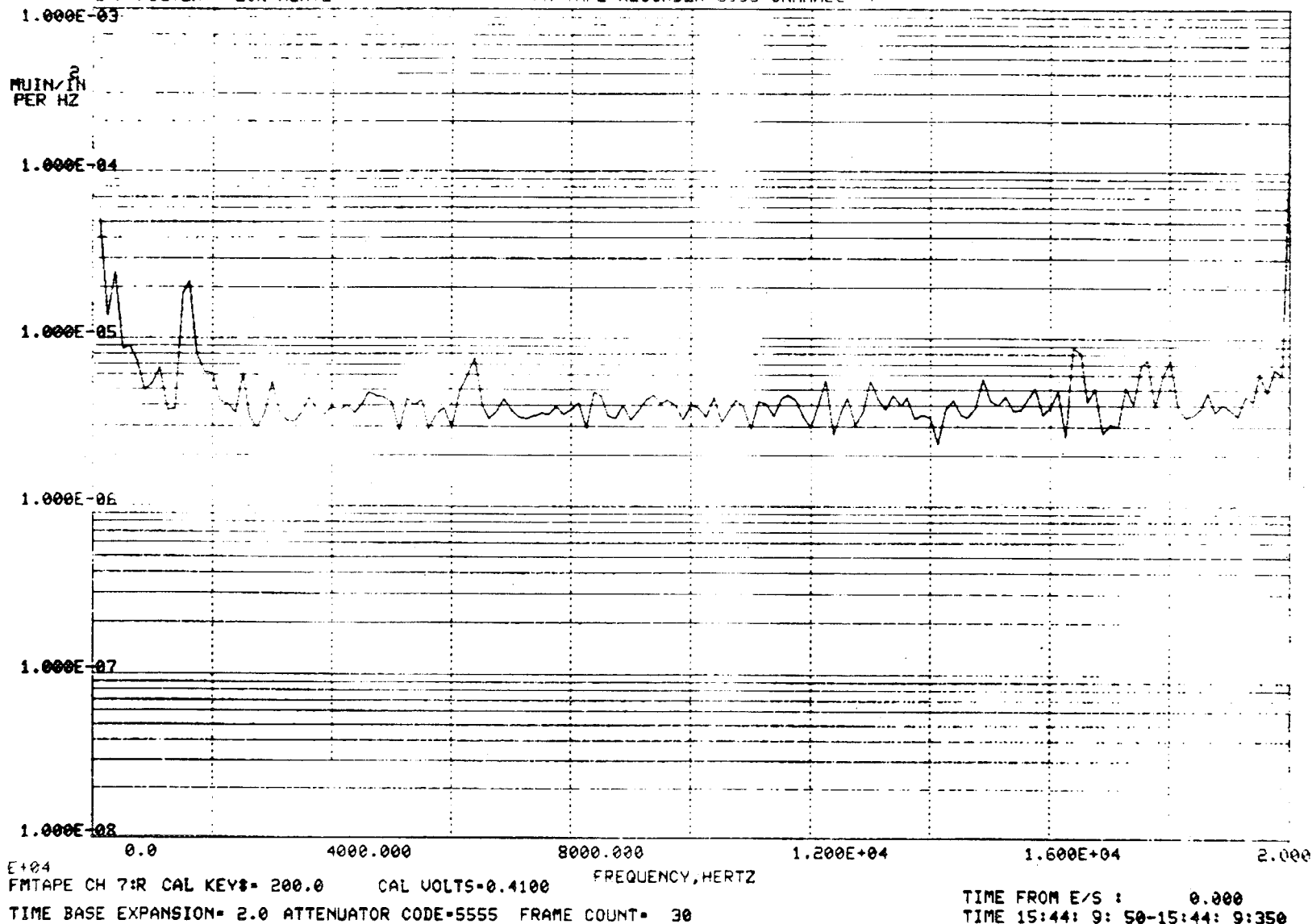


Figure 2.4-53 Strain PSD During Rubbing - SG #6 - 0 to 20 Khz - 31030 Rpm

BANDWIDTH=125.00 HERTZ
 COMPOSITE RMS= 11.1
 COMP RMS FROM:1.2E+02 TO 2.0E+04
 L/P FILTER: 20K HERTZ

RMS POWER SPECTRAL DENSITY
 WHIPLIG TEST 1
 SG 60
 FM TAPE RECORDER 6956 CHANNEL 10

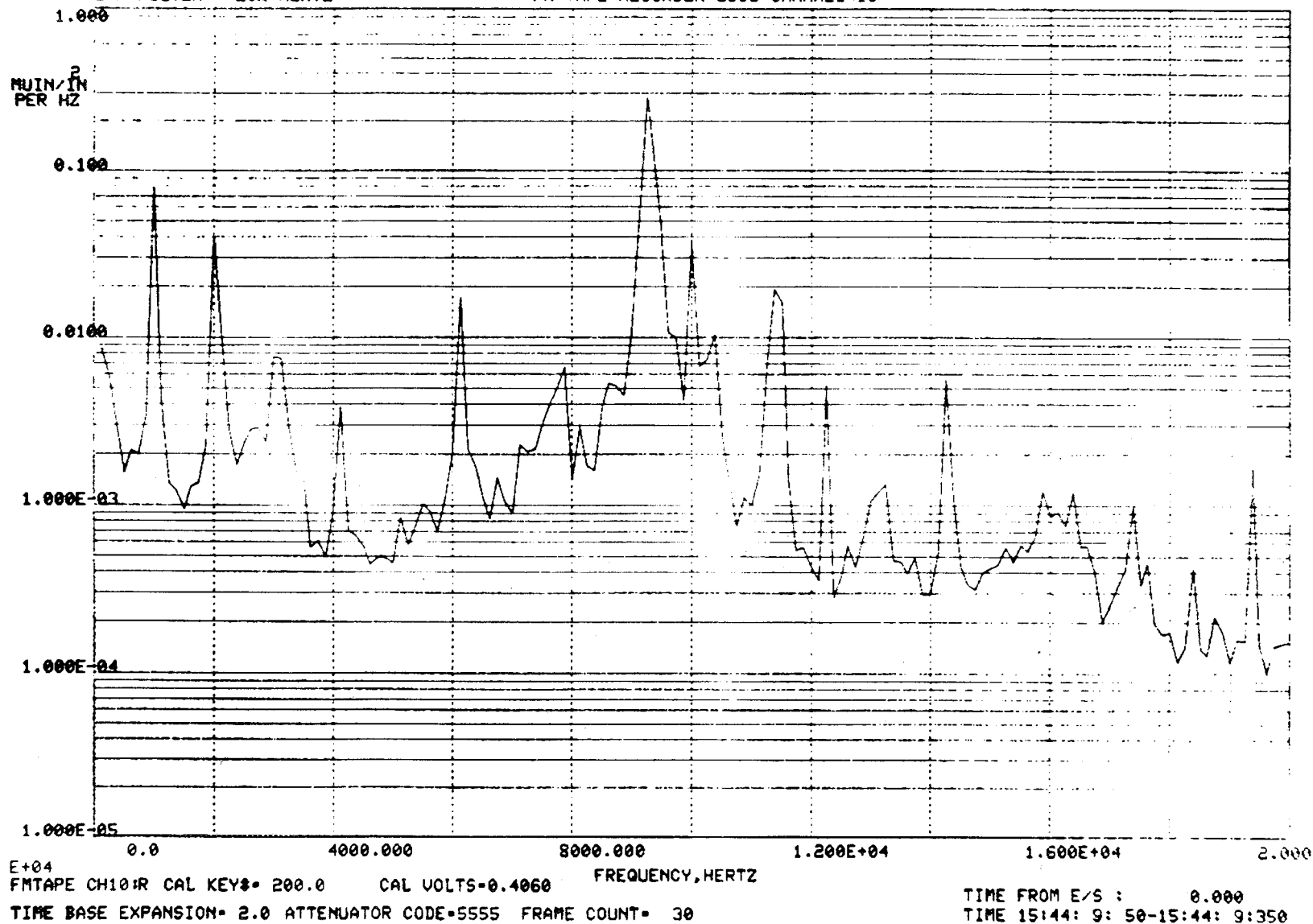
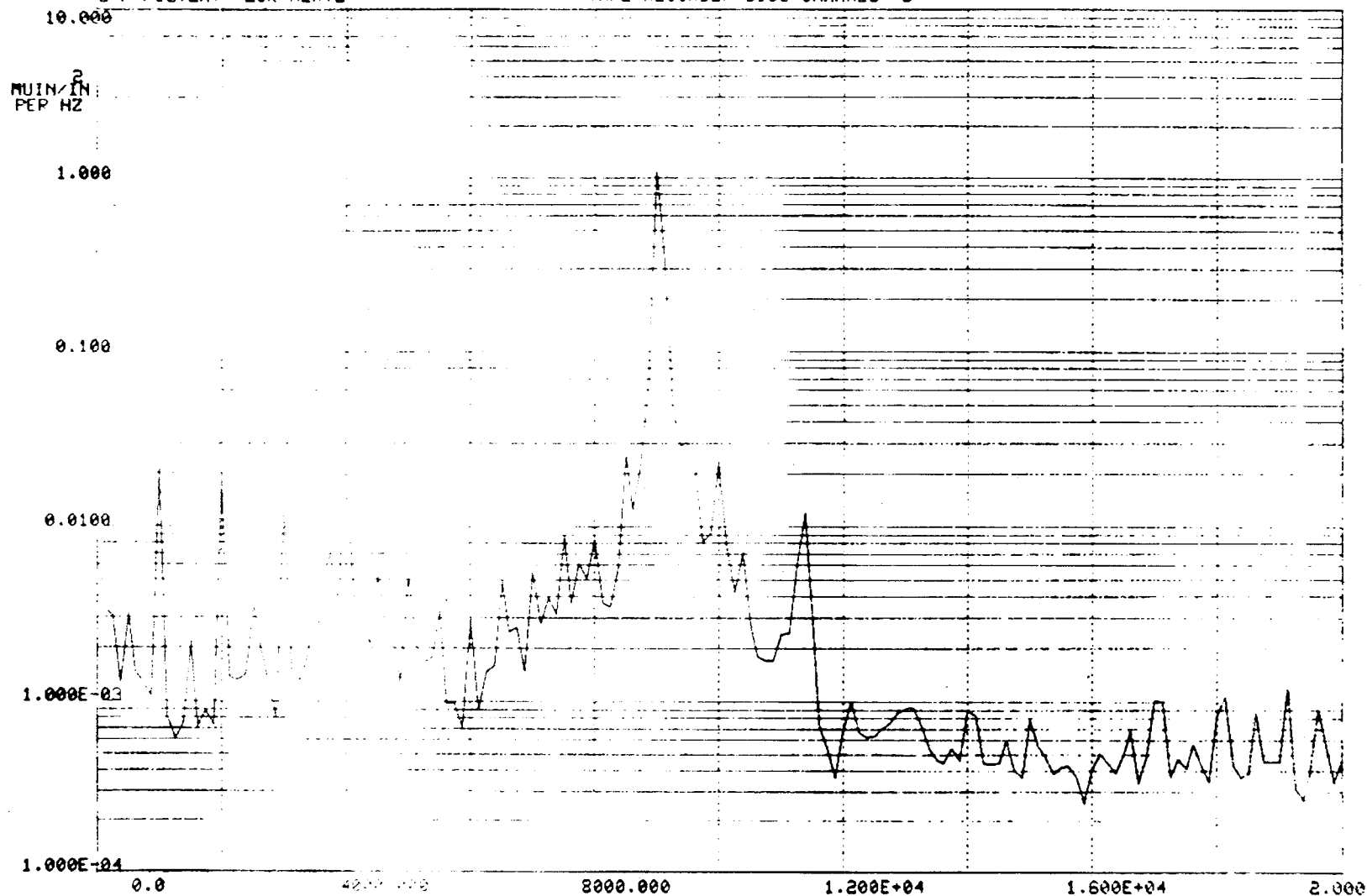


Figure 2.4-54 Strain PSD During Rubbing - SG #60 - 0 to 20 Khz - 31030 Rpm

BANDWIDTH=125.00 HERTZ
 COMPOSITE RMS= 16.1
 COMP RMS FROM:1.2E+02 TO 2.0E+04
 L/P FILTER: 20K HERTZ

RMS POWER SPECTRAL DENSITY
 WHIRLIGIG TEST 1
 SG 2
 FM TAPE RECORDER 6956 CHANNEL 3



E+04
 FM TAPE CH 3:R CAL KEY= 200.0 AC VOLTS=0.4180
 TIME BASE EXPANSION= 2.0 ATTENUATOR CODE=5555 FRAME COUNT= 30

TIME FROM E/S : 0.000
 TIME 15:44:56:700-15:44:57: 0

Figure 2.4-55 Strain PSD During Rubbing - SG #2 - 0 to 20 Khz 30560 rpm

BANDWIDTH=125.00 HERTZ
 COMPOSITE RMS= 13.0
 COMP RMS FROM:1.2E+02 TO 2.0E+04
 L/P FILTER: 20K HERTZ

RMS POWER SPECTRAL DENSITY
 WHIRLIGIG TEST :
 SG 4
 FM TAPE RECORDER 6956 CHANNEL 5

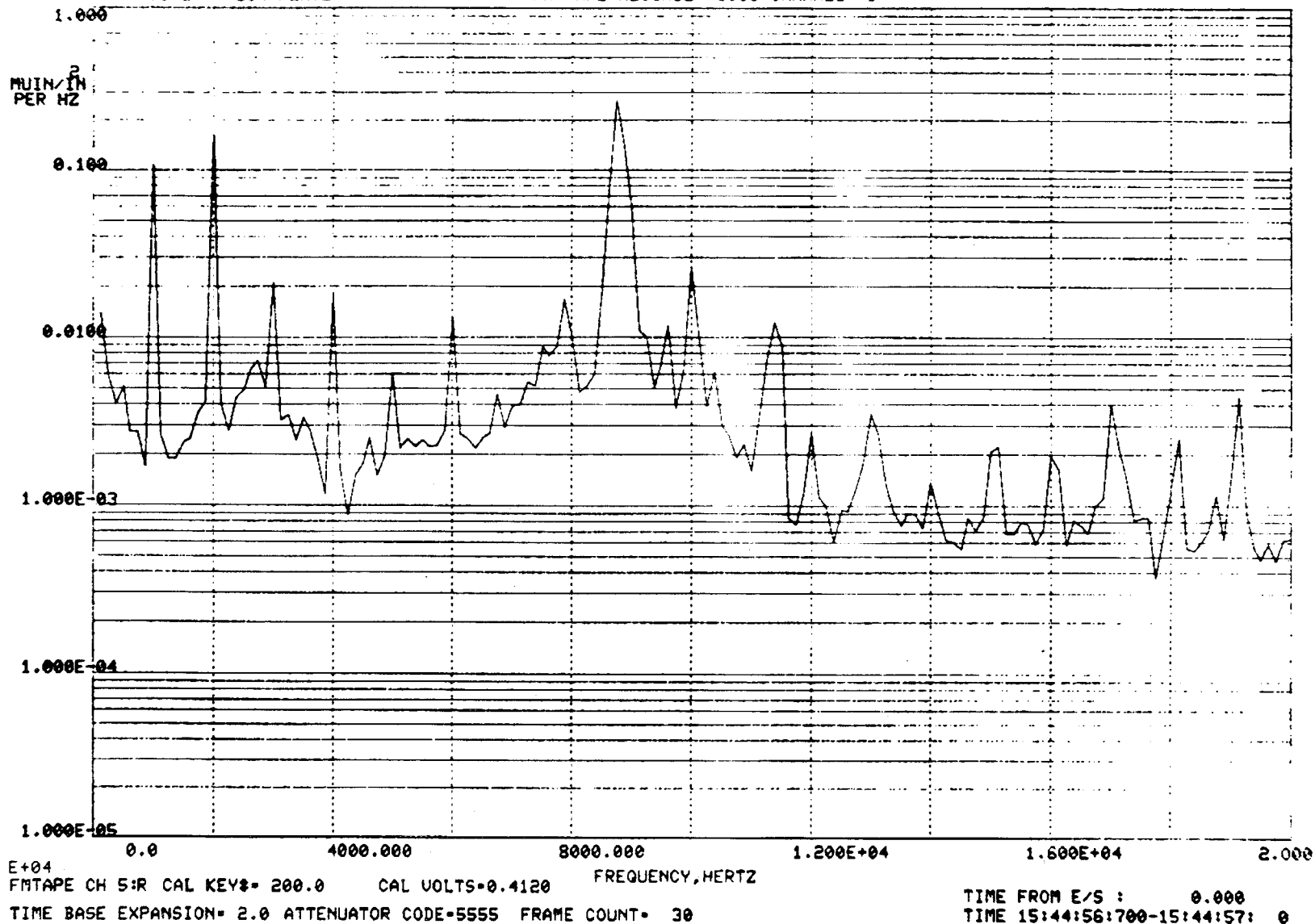


Figure 2.4-56 Strain PSD During Rubbing - SG #4 - 0 to 20 Khz - 30560 Rpm

BANDWIDTH=125.00 HERTZ
 COMPOSITE RMS= 11.9
 COMP RMS FROM:1.2E+02 TO 2.0E+04
 L/P FILTER: 20K HERTZ

RMS POWER SPECTRAL DENSITY
 WHIRLIGIG TEST 1
 SG 5
 FM TAPE RECORDER 6956 CHANNEL 6

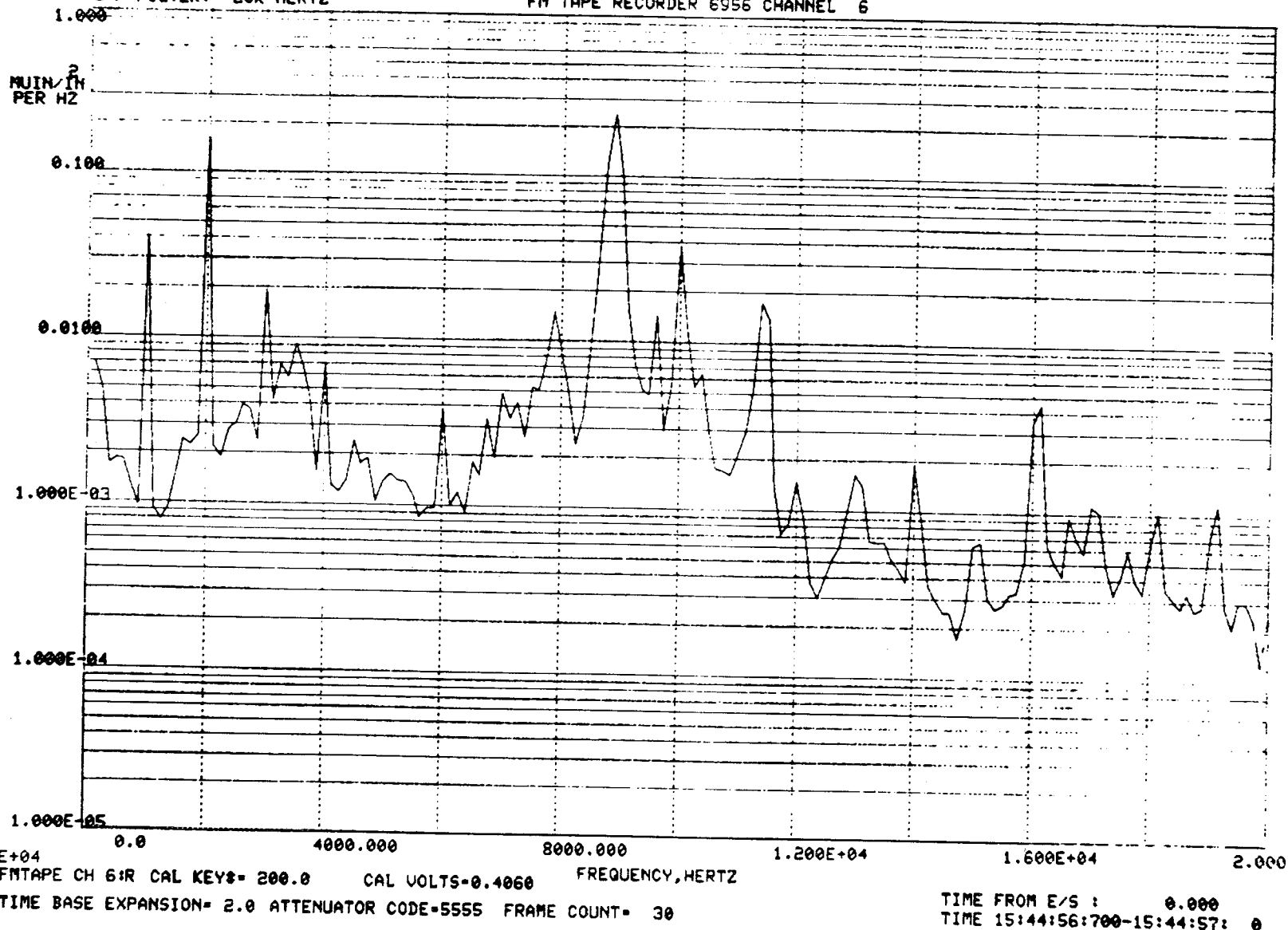
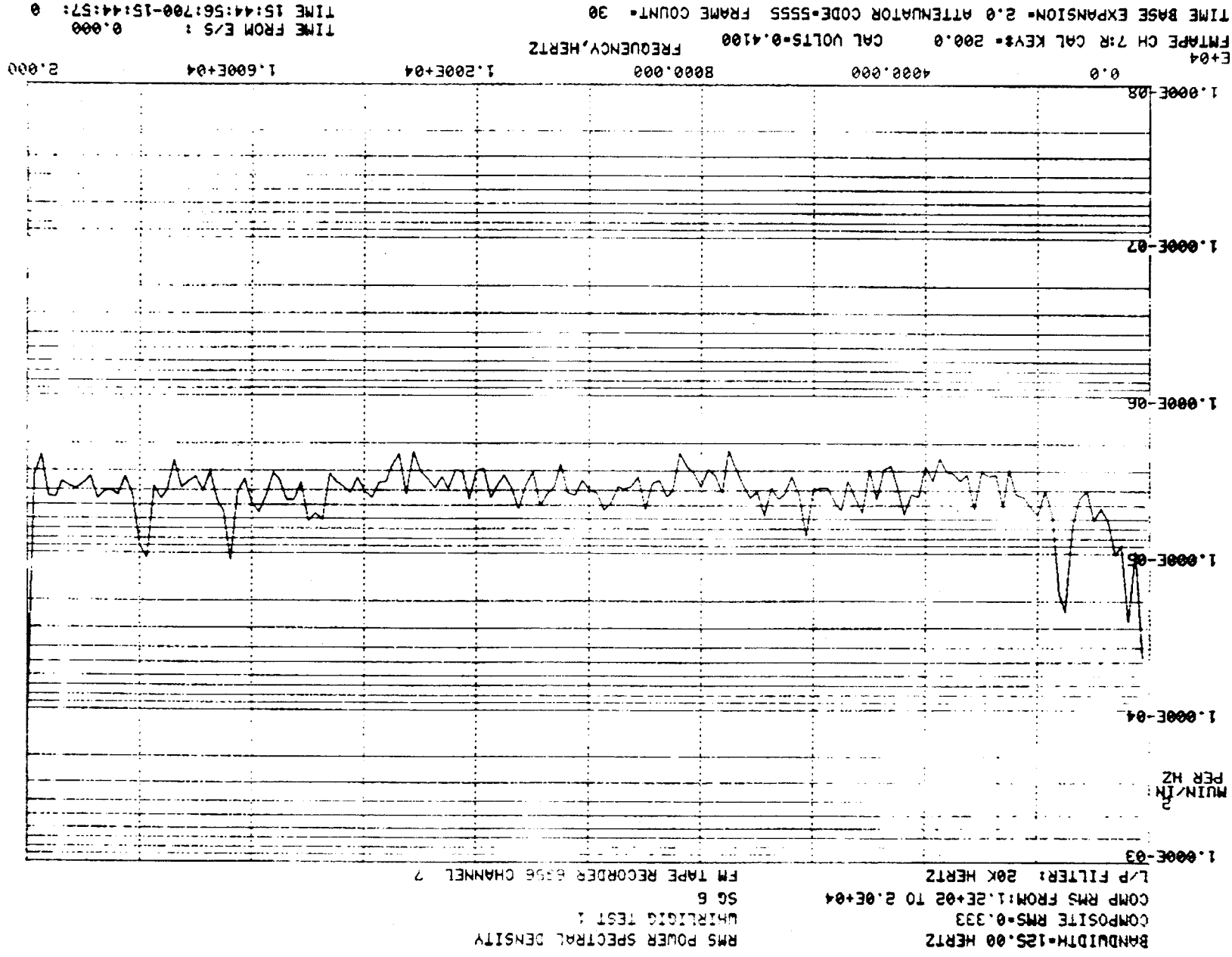
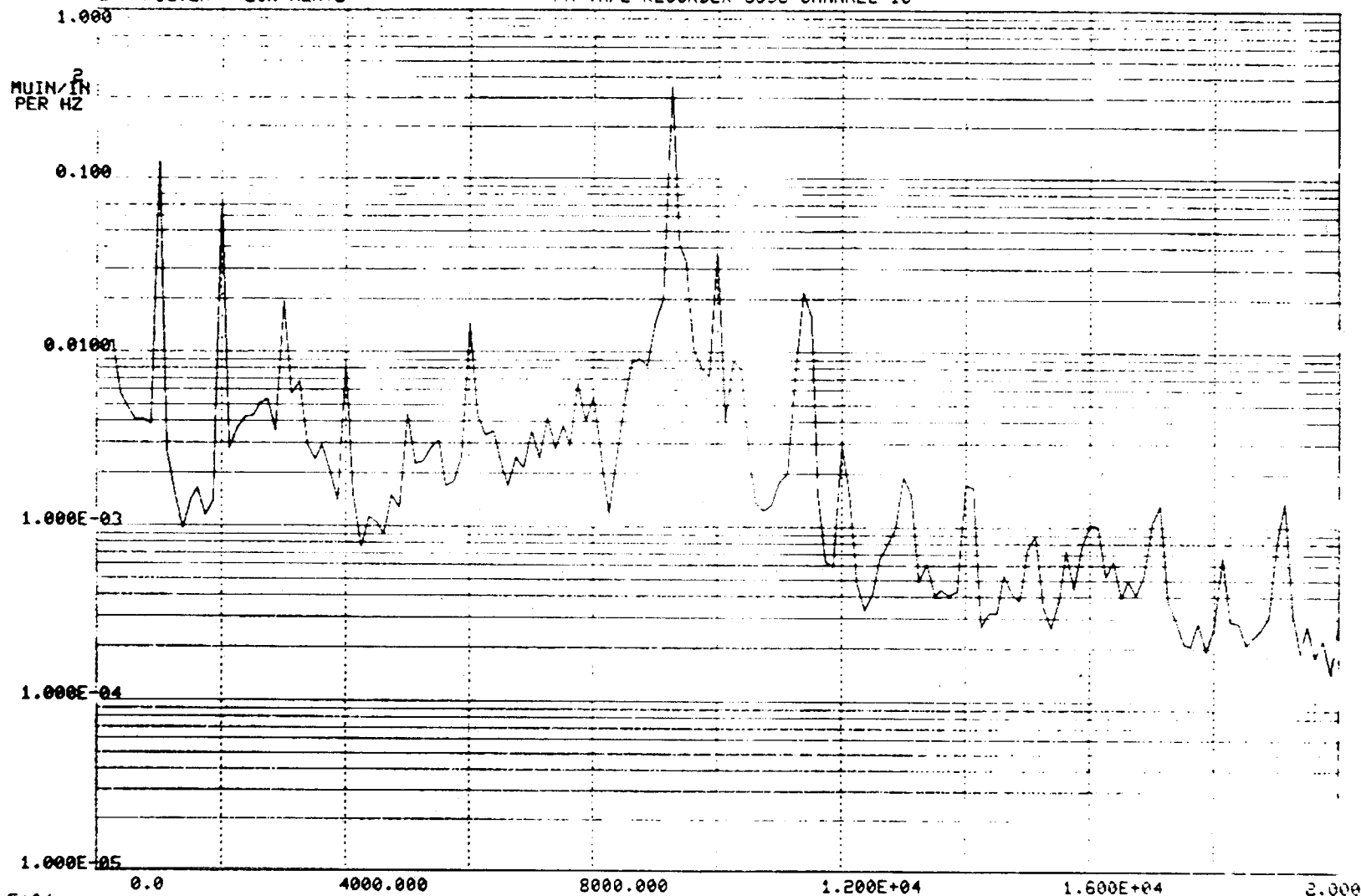


Figure 2.4-57 Strain PSD During Rubbing - SG #5 - 0 to 20 Khz - 30560 Rpm



BANDWIDTH=125.00 HERTZ
 COMPOSITE RMS= 11.8
 COMP RMS FROM:1.2E+02 TO 2.0E+04
 L/P FILTER: 20K HERTZ

RMS POWER SPECTRAL DENSITY
 WHIRLIGIG TEST 1
 SG 60
 FM TAPE RECORDER 6956 CHANNEL 10



E+04
 FMTAPE CH101R CAL KEYS= 200.0 CAL VOLTS=0.4060
 TIME BASE EXPANSION= 2.0 ATTENUATOR CODE=5555 FRAME COUNT= 30

TIME FROM E/S : 0.000
 TIME 15:44:56:700-15:44:57: 0

Figure 2.4-59 Strain PSD During Rubbing - SG #60 - 0 to 20 Khz - 30560 Rpm

2.4-71

ORIGINAL FROM 75
 OF POWER QUALITY

BANDWIDTH=125.00 HERTZ
 COMPOSITE RMS= 8.55
 COMP RMS FROM:1.2E+02 TO 2.0E+04
 L/P FILTER: 20K HERTZ

RMS POWER SPECTRAL DENSITY
 WHIRLIGIG TEST 1
 SG 2
 FM TAPE RECORDER 6956 CHANNEL 3

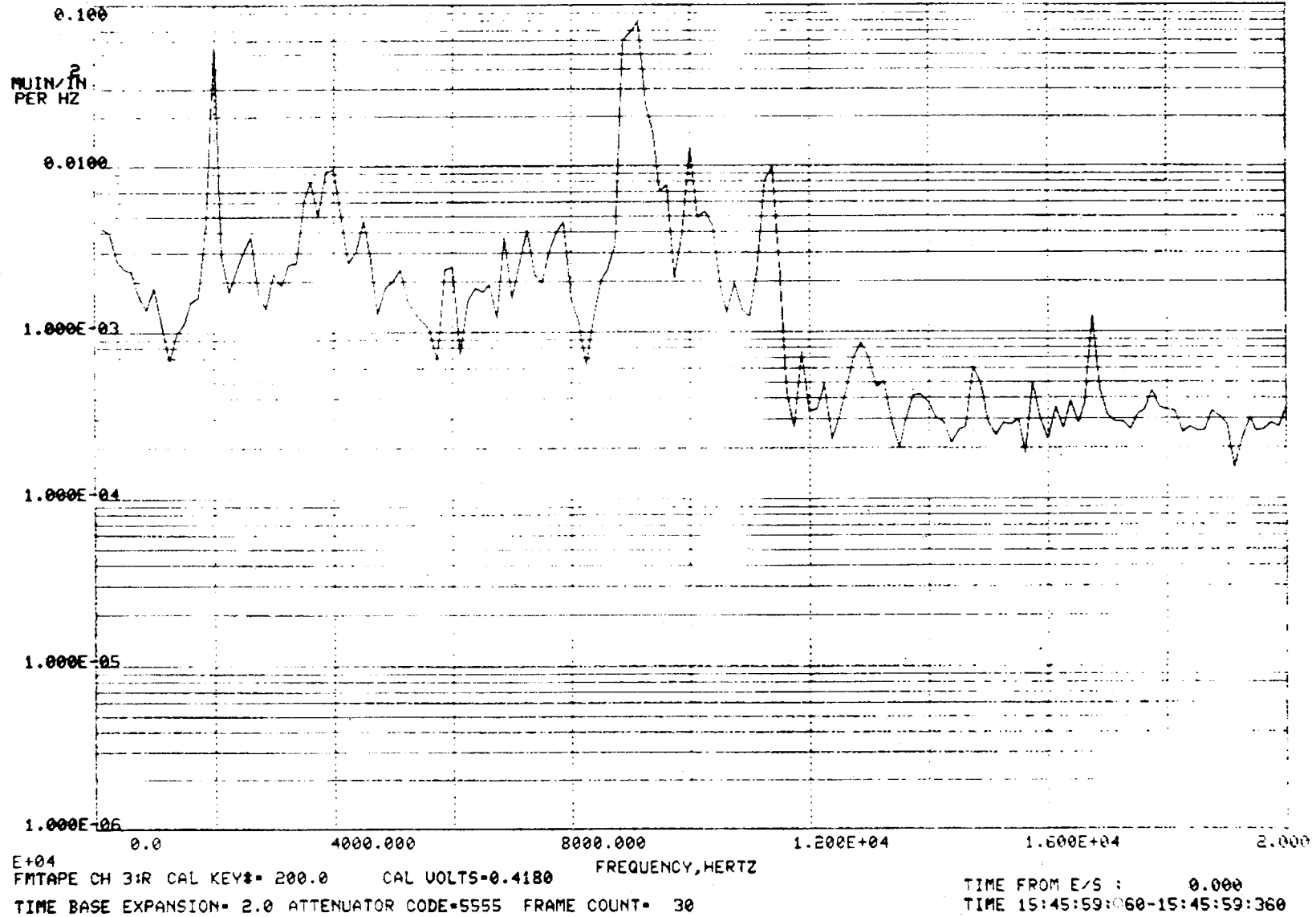


Figure 2.4-60 Strain PSD During Rubbing - SG #2 - 0 to 20 Khz - 30060 Rpm

BANDWIDTH=125.00 HERTZ
 COMPOSITE RMS= 13.3
 COMP RMS FROM:1.2E+02 TO 2.0E+04
 L/P FILTER: 20K HERTZ

RMS POWER SPECTRAL DENSITY
 WHIRLIGIG TEST 1
 SG 4
 FM TAPE RECORDER 6956 CHANNEL 5

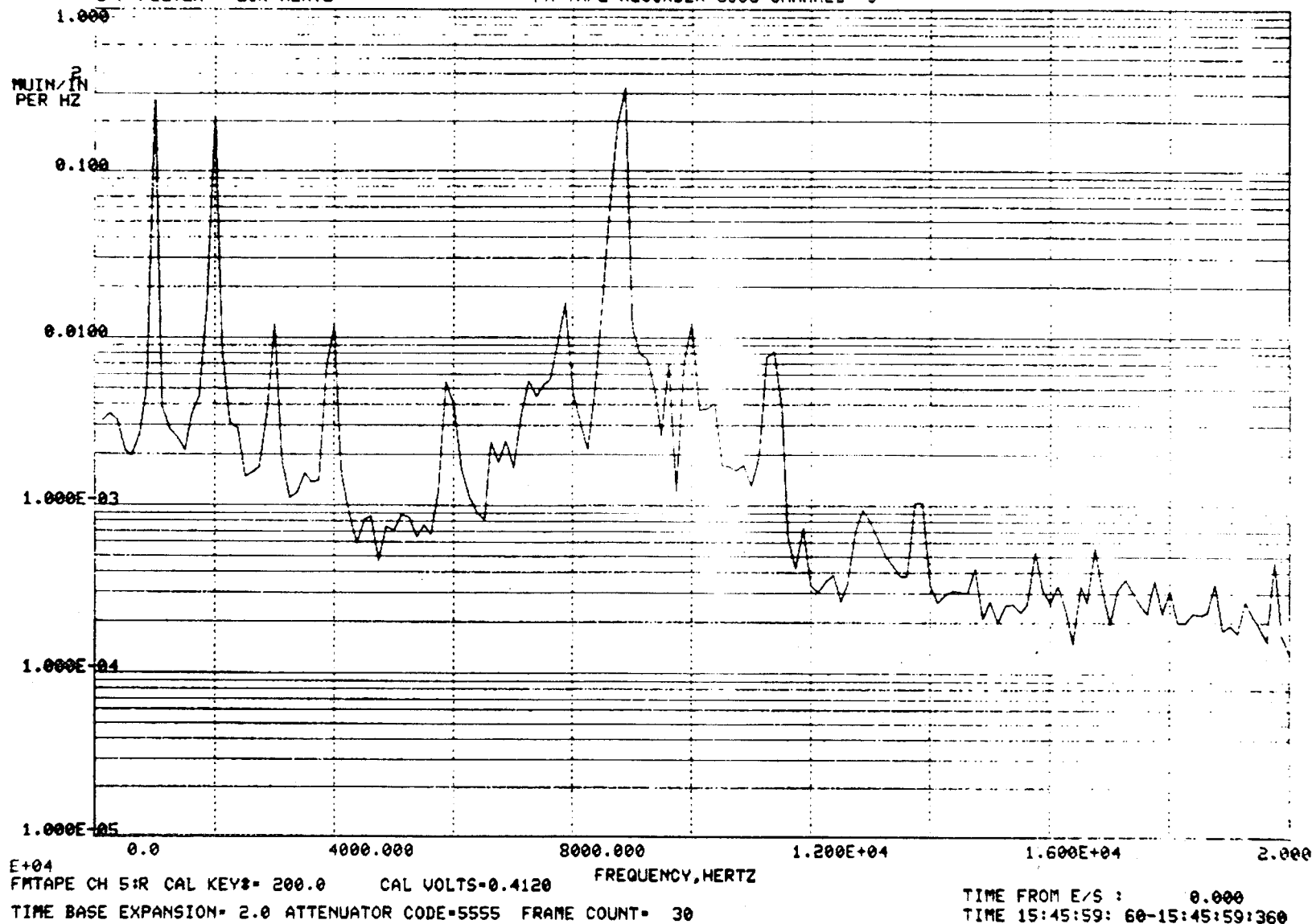


Figure 2.4-61 Strain PSD During Rubbing - SG #4 - 0 to 20 Khz - 30060 Rpm

BANDWIDTH=125.00 HERTZ
 COMPOSITE RMS= 8.96
 COMP RMS FROM:1.2E+02 TO 2.0E+04
 L/P FILTER: 20K HERTZ

RMS POWER SPECTRAL DENSITY
 WHIRLIGIG TEST 1
 SG 5
 FM TAPE RECORDER 6956 CHANNEL 6

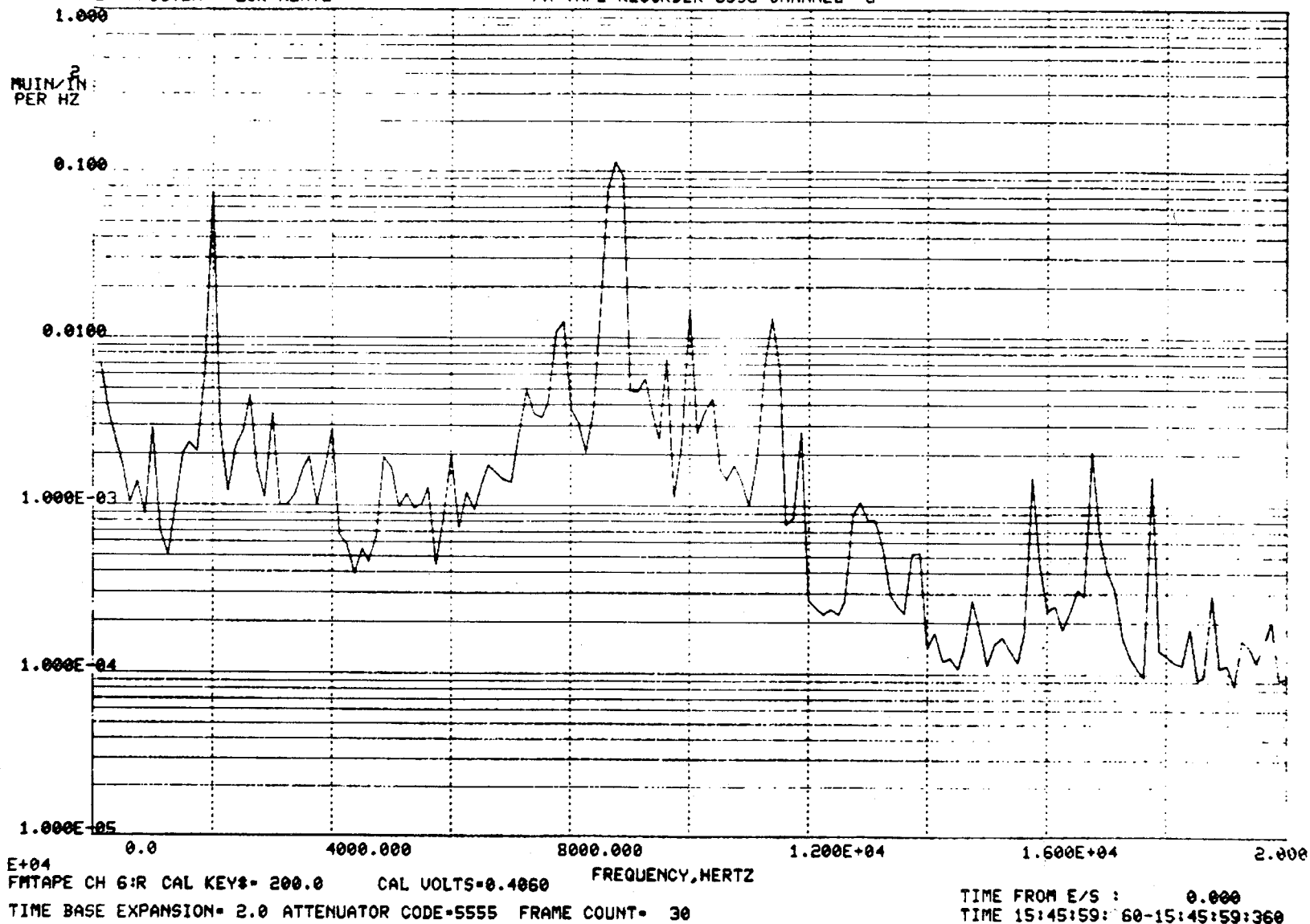


Figure 2.4-62 Strain PSD During Rubbing - SG #5 - 0 to 20 Khz - 30060 Rpm

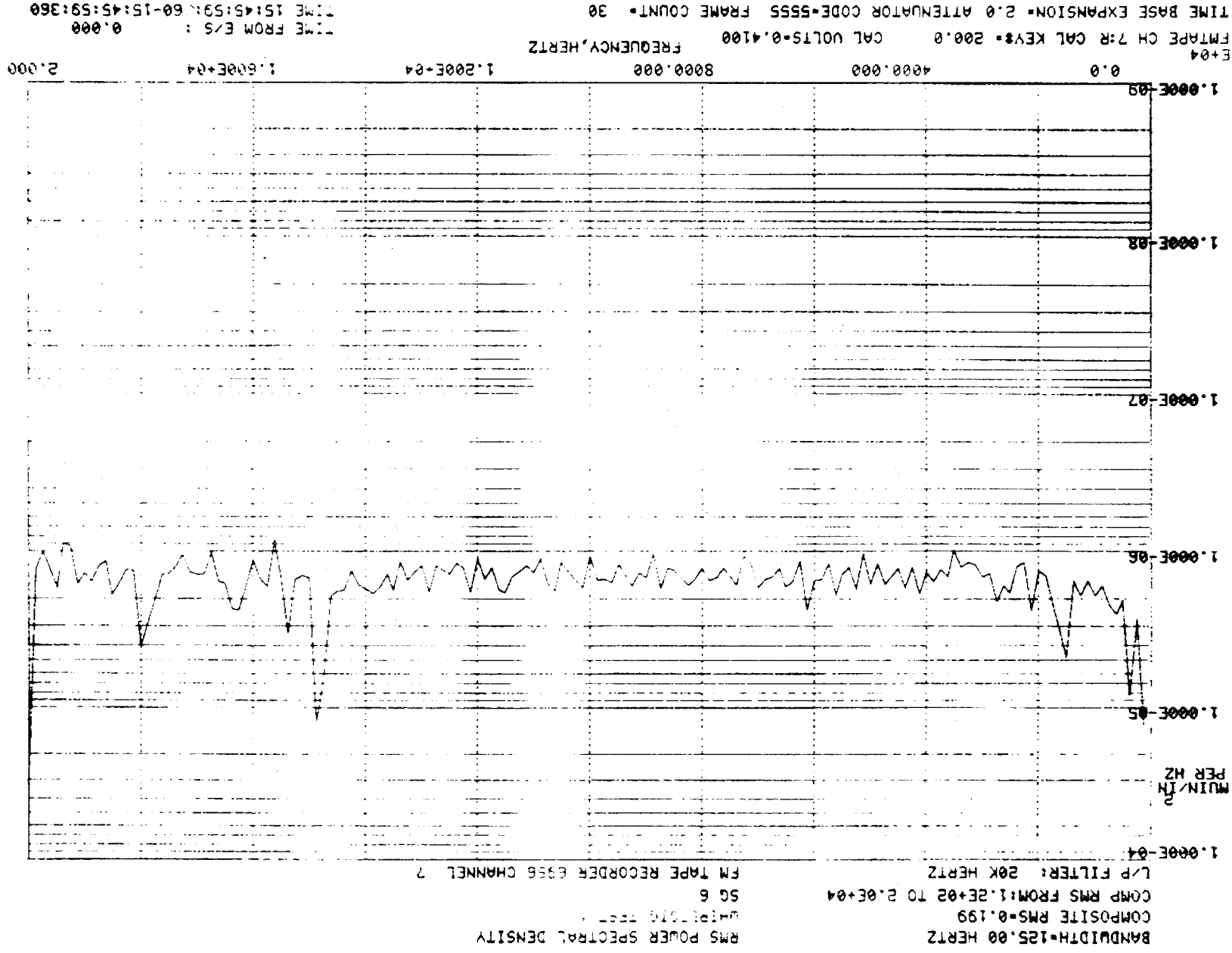


Figure 2.4-63 Strain PSD During Rubbing - SG #6 - 0 to 20 Khz - 30060 Rpm

BANDWIDTH=125.00 HERTZ
 COMPOSITE RMS= 11.1
 COMP RMS FROM:1.2E+02 TO 2.0E+04
 L/P FILTER: 20K HERTZ

RMS POWER SPECTRAL DENSITY
 WHIRLIGIG TEST 1
 SG 60
 FM TAPE RECORDER 6956 CHANNEL 10

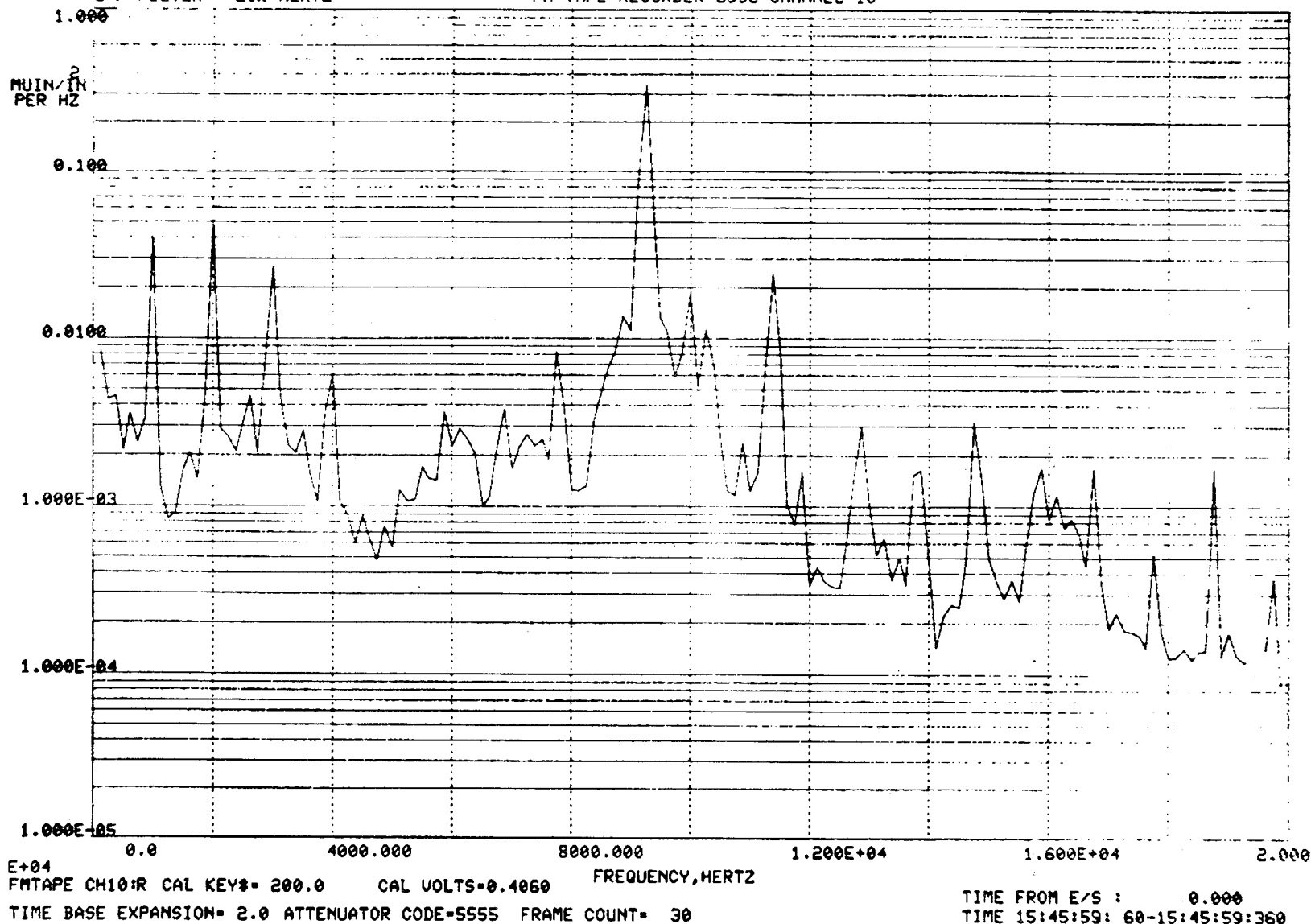


Figure 2.4-64 Strain PSD During Rubbing - SG #60 - 0 to 20 Khz - 30060 Rpm

2.4-76

ORIGINAL PAGE IS
 OF POOR QUALITY

BANDWIDTH=125.00 HERTZ
 COMPOSITE RMS= 15.3
 COMP RMS FROM:1.2E+02 TO 2.0E+04
 L/P FILTER: 20K HERTZ

RMS POWER SPECTRAL DENSITY
 WHIRLIGIG TEST 1
 TEST ARTICLE ACCEL
 FM TAPE RECORDER 6959 CHANNEL 16

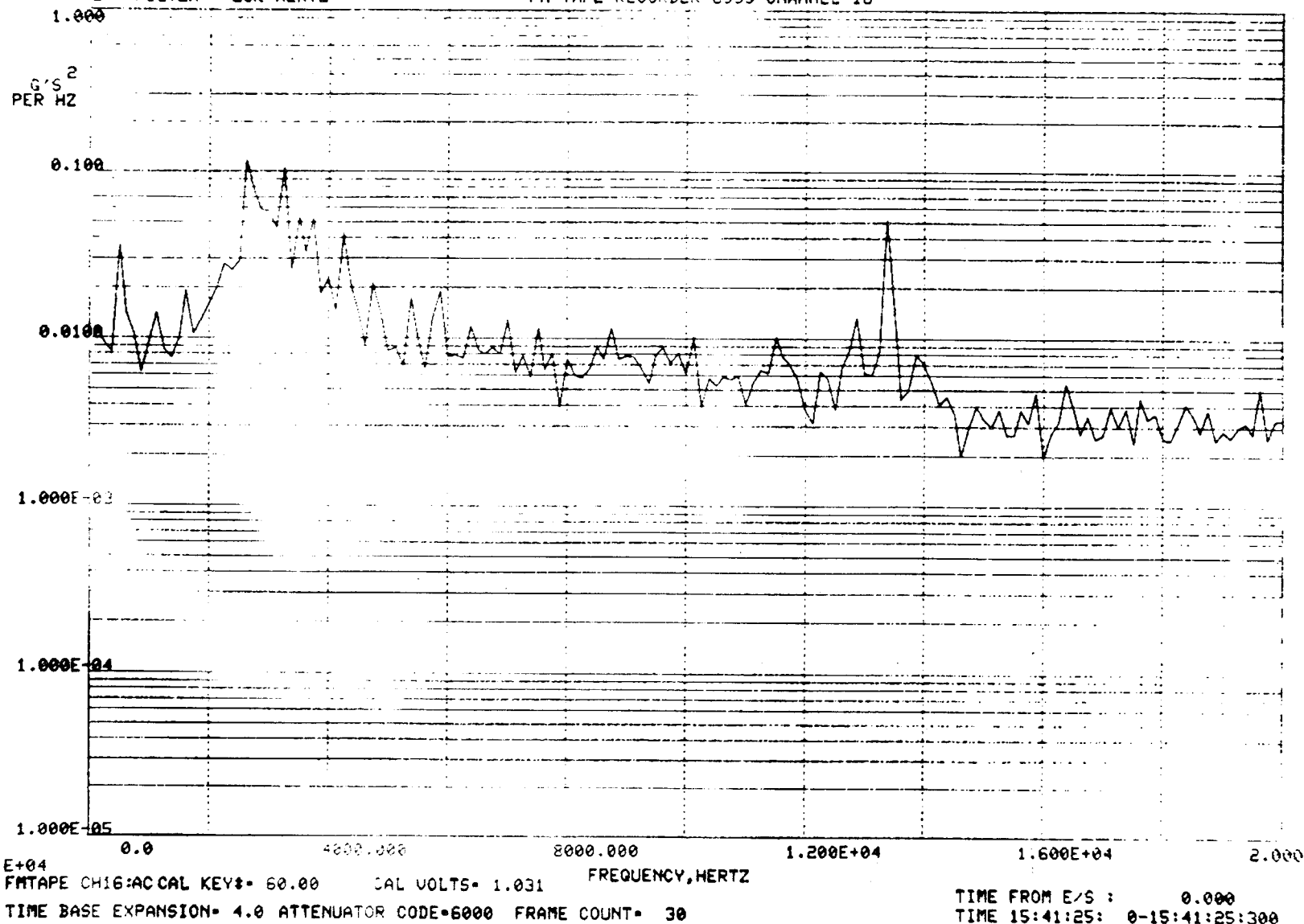


Figure 2.4-65 Test Article Accelerometer PSD During Rubbing - 0 to 20 Khz - 32160 Rpm

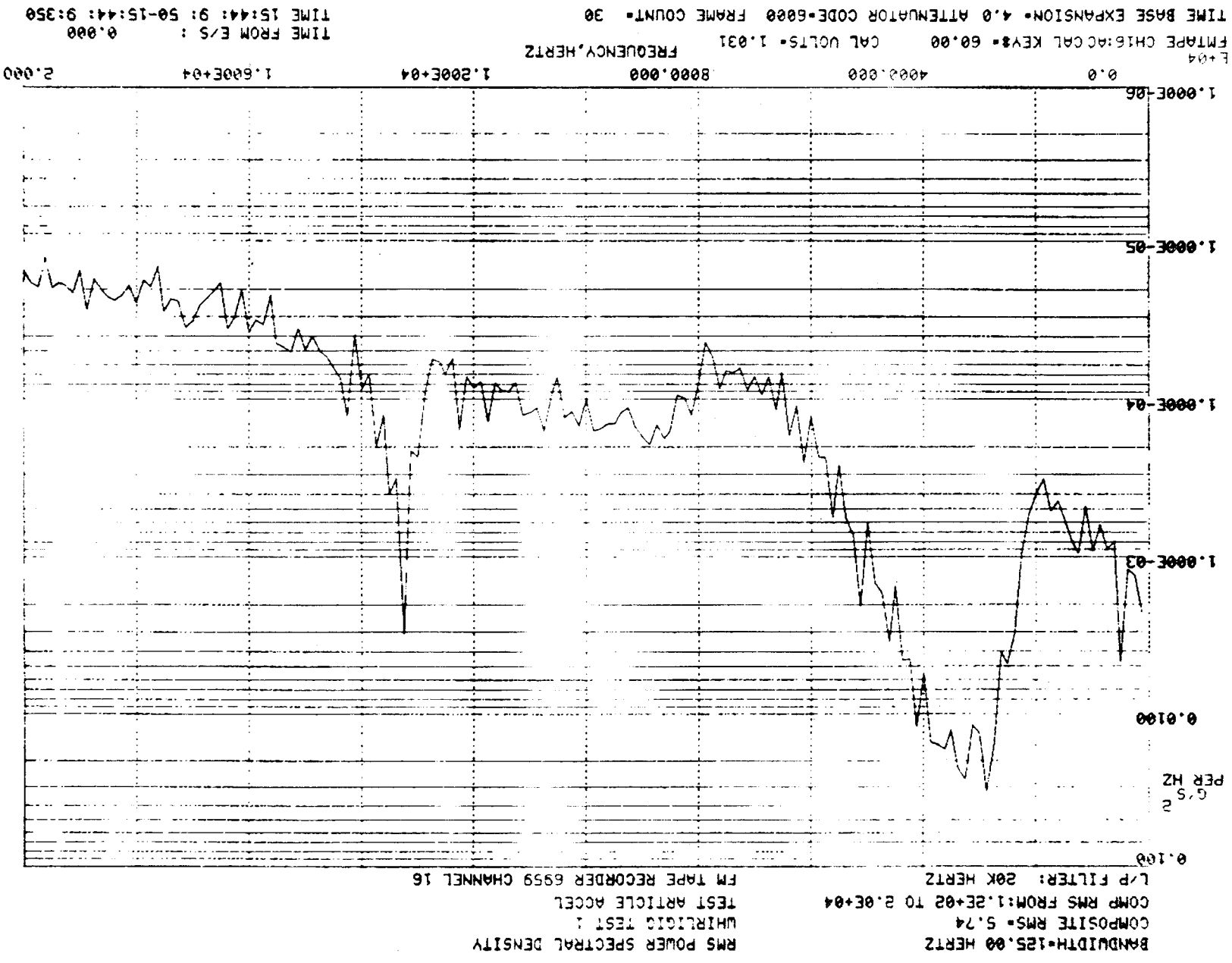


Figure 2.4-66 Test Article Accelerometer PSD During Rubbing - 0 to 20 Khz - 31030 Rpm

BANDWIDTH=125.00 HERTZ
 COMPOSITE RMS= 7.46
 COMP RMS FROM:1.2E+02 TO 2.0E+04
 L/P FILTER: 20K HERTZ

RMS POWER SPECTRAL DENSITY
 WHIRLIGIG TEST :
 TEST ARTICLE ACCEL
 FM TAPE RECORDER 6959 CHANNEL 16

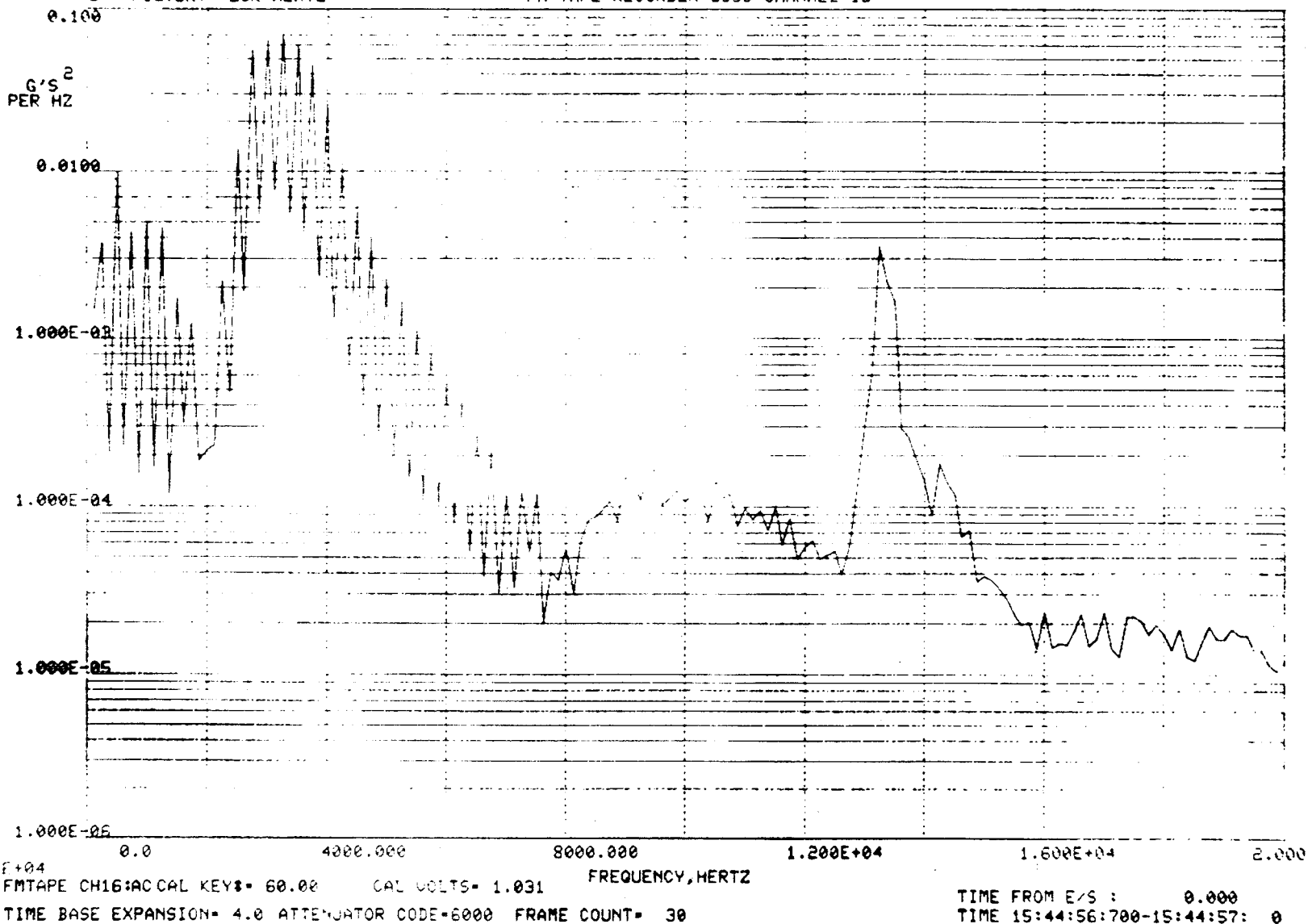


Figure 2.4-67 Test Article Accelerometer PSD During Rubbing - 0 to 20 Khz - 30560 Rpm

2.4-79

ORIGINAL PAGE IS
 OF POOR QUALITY

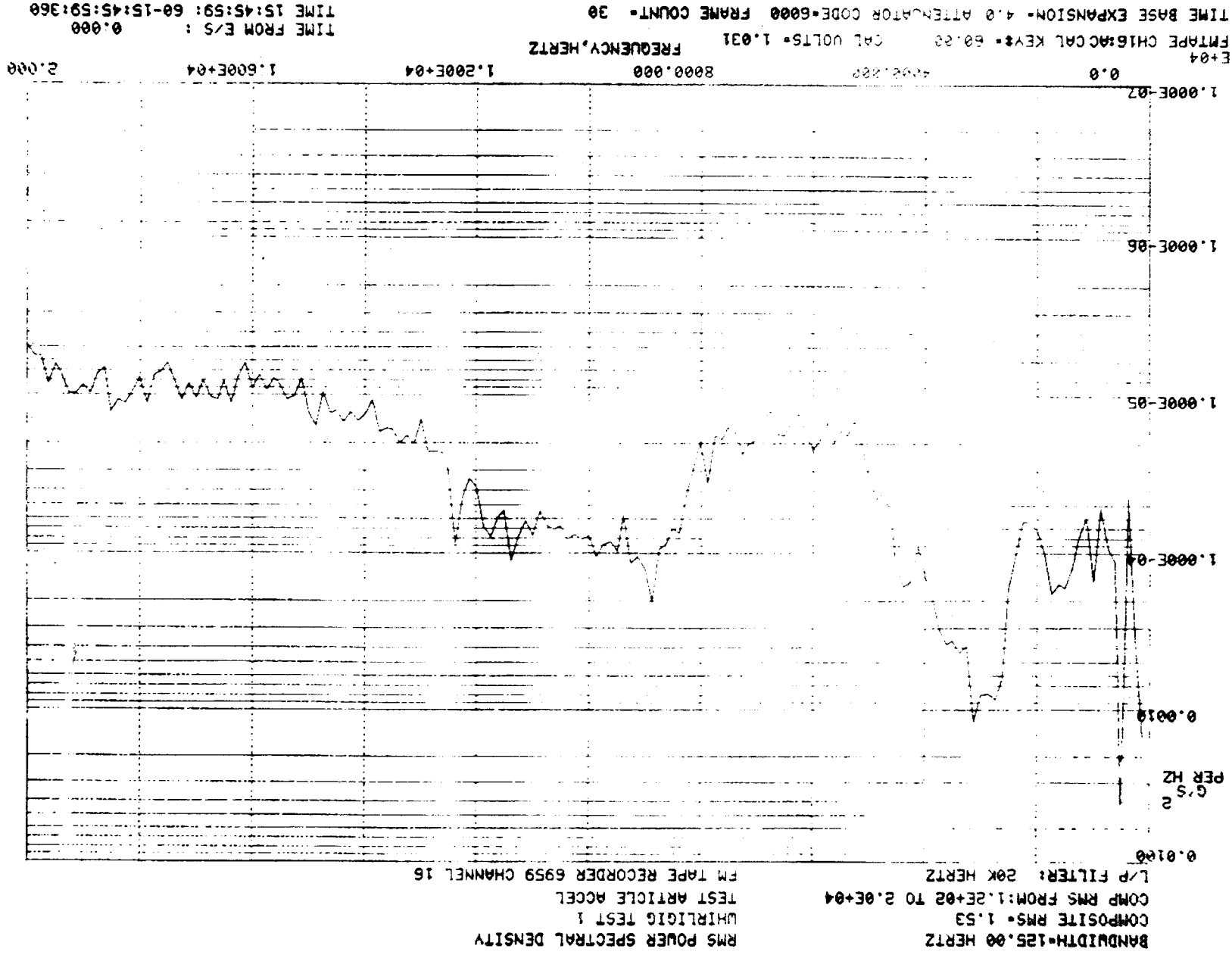


Figure 2.4-68 Test Article Accelerometer PSD During Rubbing - 0 to 20 Khz - 30060 Rpm

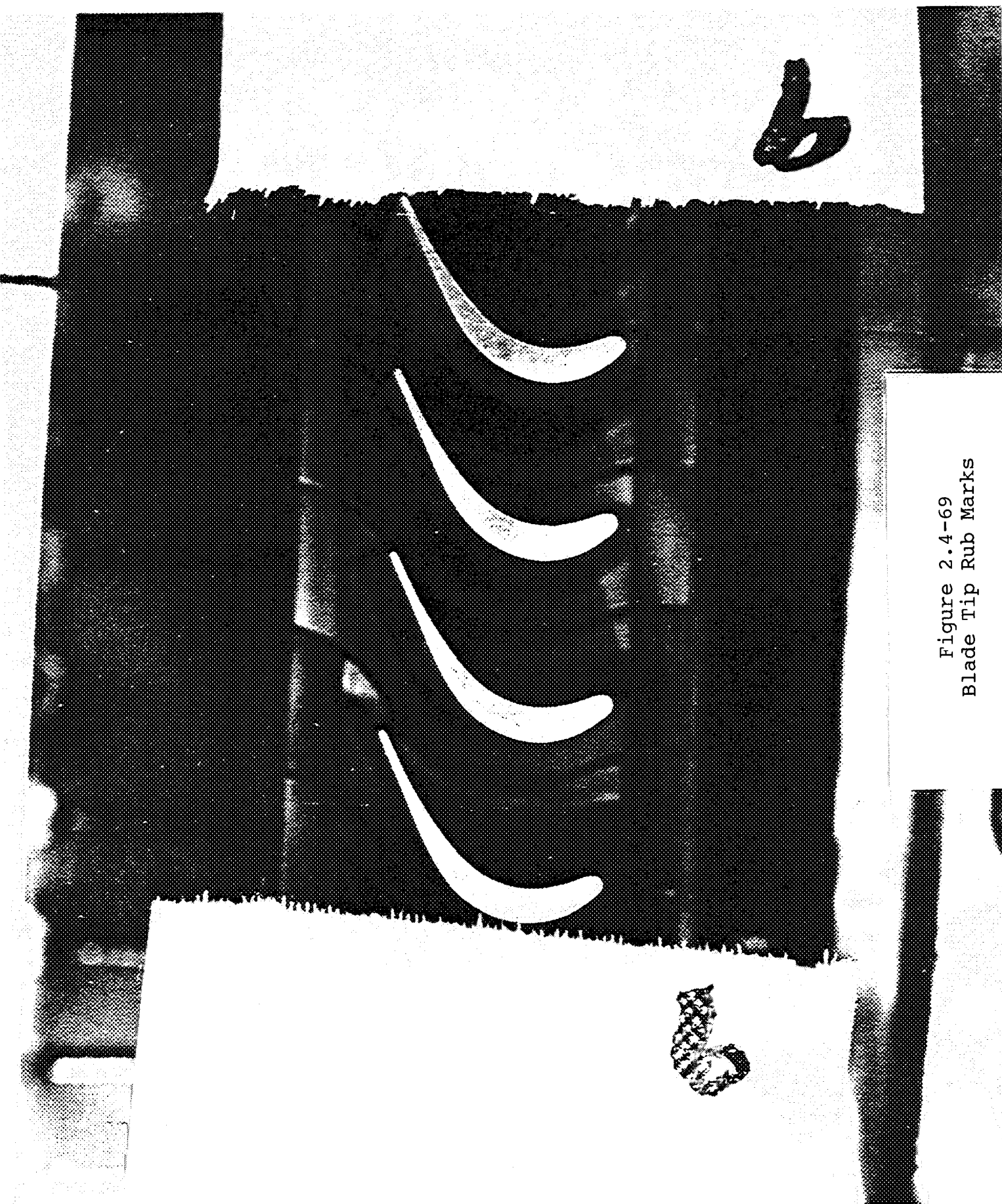


Figure 2.4-69
Blade Tip Rub Marks

2.4-82

ORIGINAL PAGE
COLOR PHOTOGRAPH

Tip Seal
From Rubbing Test

SSME Tip Seal

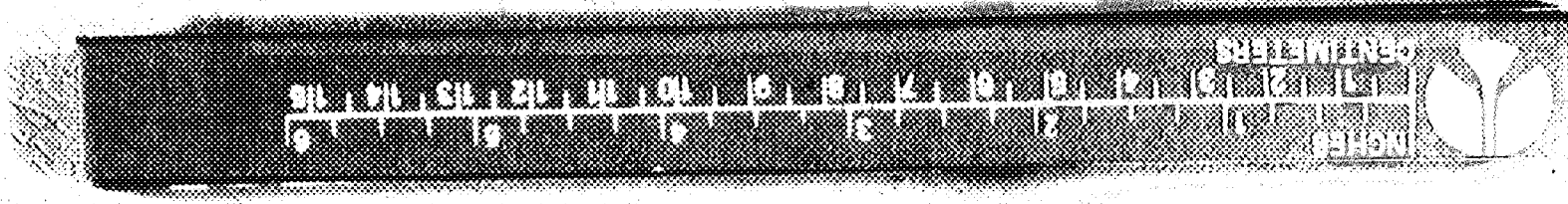
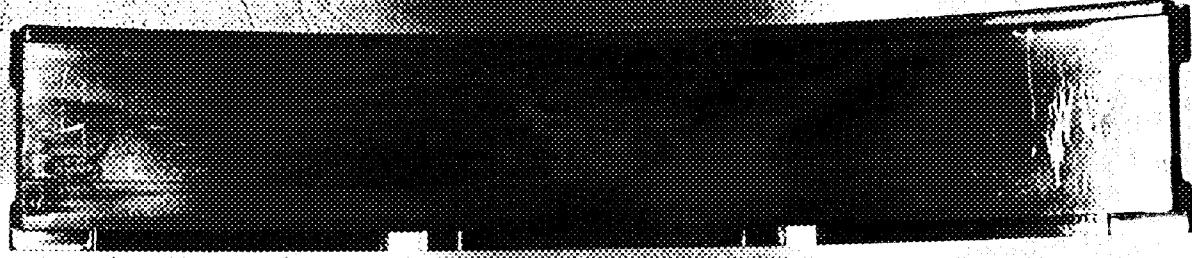
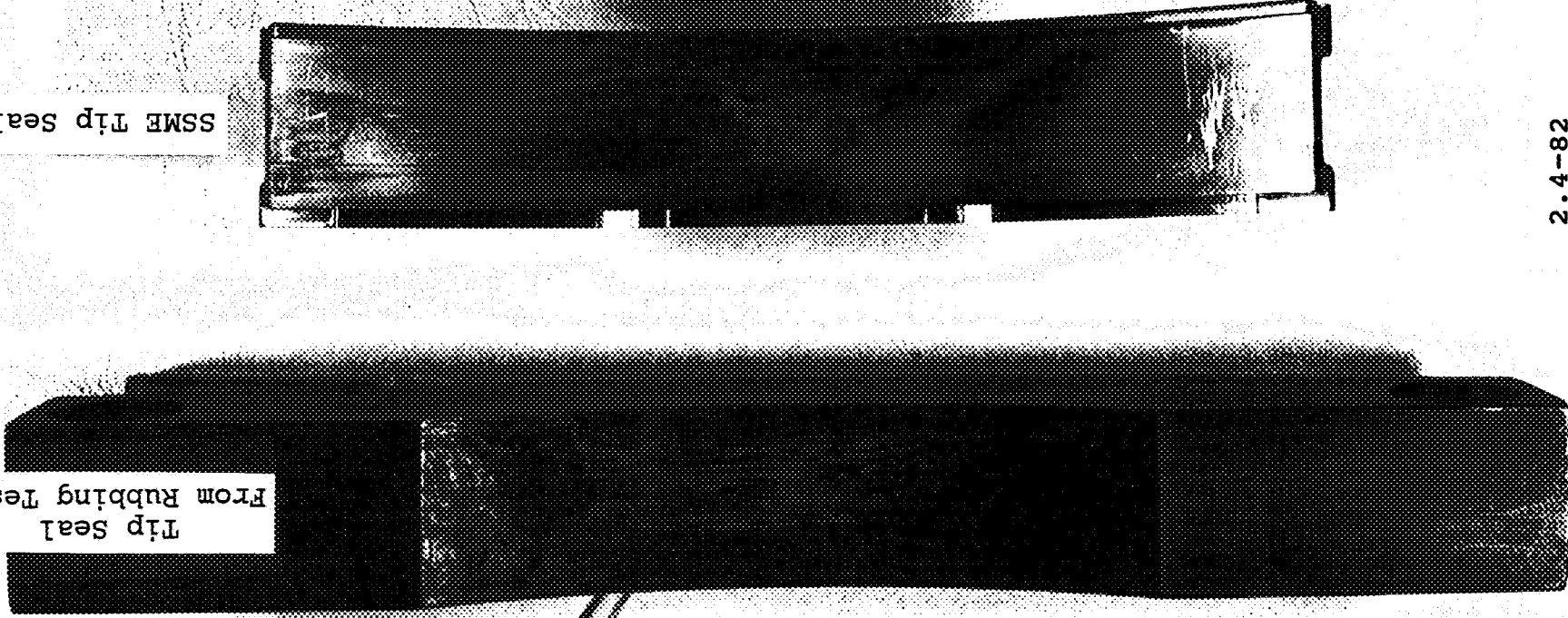


Figure 2.4-70
Comparison of Test Hardware Rub Pattern
with SSME Rub Pattern

Tip Seal
From Rubbing Test

2.4-83

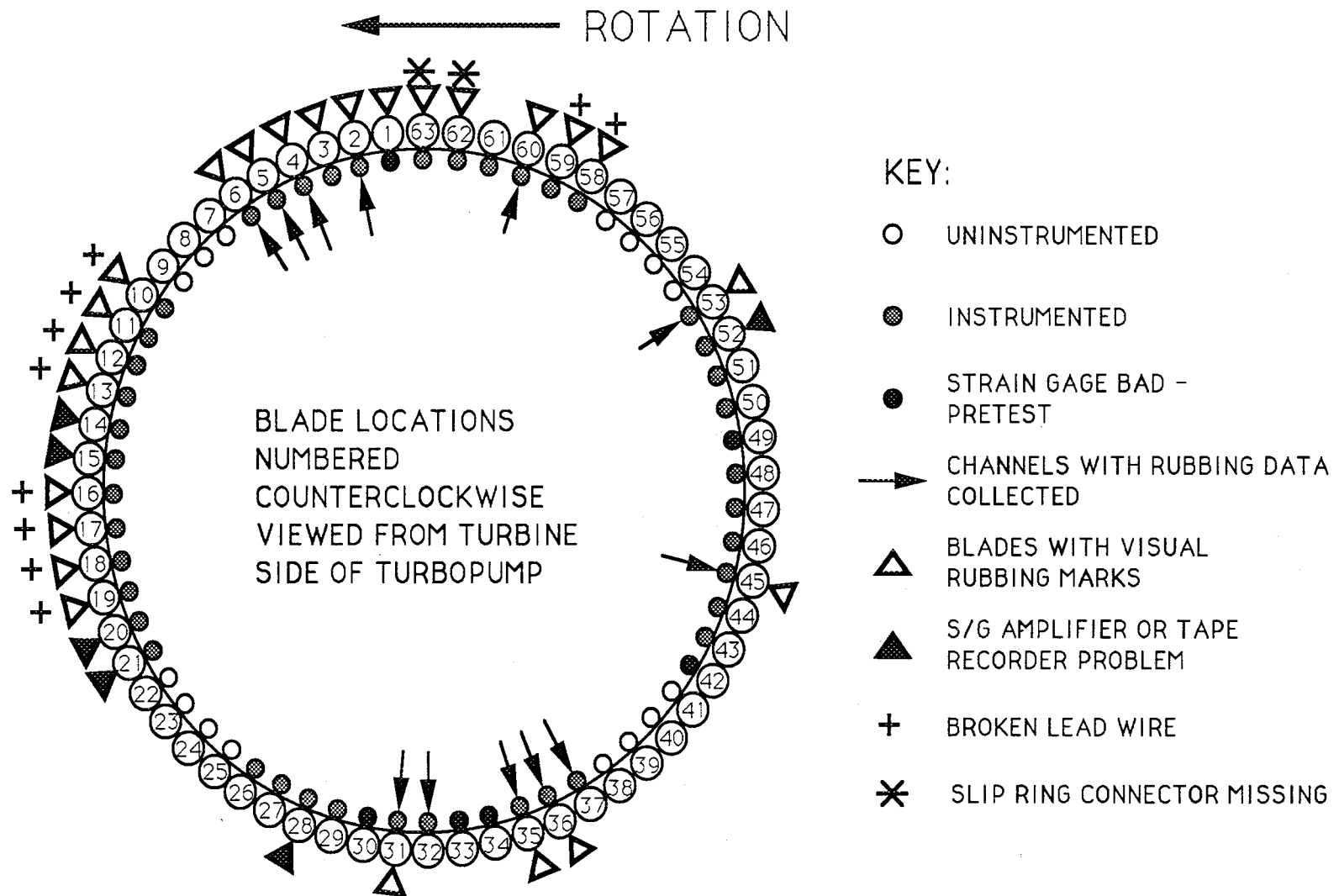
SSME Tip Seal

Figure 2.4-71
Comparison of Test Hardware Rub Pattern
with SSME Rub Pattern



Figure 2.4-72
Lead Wire Debonding

BLADE TIP RUBBING WHIRLIGIG MAP OF STRAIN GAGED BLADES



2.4-85

Figure 2.4-73 Correlation of Rubbing Inspection with Strain Data

2.5 TEST/ANALYSIS CORRELATION

As discussed in Section 2.1 the analysis portion of this study consisted of computing the dynamic response of a single blade subjected to a once per revolution half-sine pulse forcing function. Typical time-history response plots from the analysis are shown in Figures 2.5-1 and 2.5-2. As can be seen from the plots the character of the time histories is similar to the data of Figures 2.4-9 thru 2.4-17. The analysis predicts an initial rub-induced peak exactly as observed in the data followed by free vibration until the next rub and then a repeat of the cycle. During the free vibration decay the analysis shows predominantly first blade mode response while the data is not consistent in this respect. In some instances the data shows the decay to be entirely first mode while at other times it is the third mode or a combination of the first and third modes.

Although the analysis does not exactly match the free vibration portion of the rub cycle it does predict the important features of blade tip rubbing. The initial rub produced peak is shown in both the data and the analysis as the time at which the greatest stress occurs. This is clearly the most important aspect of rubbing and shows that the basic assumption of a once per revolution forcing function is valid.

A second objective of the testing was to verify the speed dependent behavior of the response due to blade tip rubbing. As shown in Figure 2.1-12 the analysis predicts a definite critical speed at which blade response will maximize. The testing was designed to prove this hypothesis by performing rubs at a variety of speeds. Testing was accomplished as planned, however only the first few rubs produced high amplitude strains. After the first two speed points the amplitudes reduced dramatically and remained at low levels on all subsequent rubs. This indicated a significant change in the behavior of the testor which cannot be attributed to speed effects (see discussion of Figure 2.4-8). One possible explanation is that the seal was "wearing in" as the test progressed thus providing a lower coefficient of friction and lower rub force.

Although the strain amplitude versus speed plots do not verify the speed dependent nature of blade tip rubbing the test data still can be used to predict it. Consulting the PSD plot of Figure 2.4-21 it can be seen that the response consists of a combination of vibration at the frequency of the discrete engine order forcing functions as well as vibration at the natural frequency of the blade. Notice that

the blade natural frequency at about 4545 Hz lies between the 8th and 9th engine order forcing functions. As the shaft speed changes the engine order forcing functions will shift accordingly but the natural frequency of the blade will remain nearly constant. The maximum response will occur when one of the engine order lines coincides with the natural frequency of the blade. For the blade of Figure 2.4-21 the 8N forcing function will excite this mode at 34090 rpm while the 9N forcing function will excite the mode at 30300 rpm. The testor was not run at speeds greater than 32700 so the high speed resonance was not excited. Rubbing was accomplished, however, at speeds very close to the 30300 rpm resonance with no amplitude peaking (Figure 2.4-8). It is obvious that this behavior should have been observed in the data had the setup not changed in some way during the course of the test.

It is difficult to compare amplitudes between the test and analysis because the magnitude of the friction force at the time of the rub is not known. Load cells were installed on the test article in an attempt to determine the friction force and normal load in an average sense but they all failed and no data was obtained. Nevertheless it is possible to determine the friction force necessary for the model to predict the stress amplitude seen in test.

The maximum peak-to-peak strain amplitude measured in the testing was 920 $\mu\text{in/in}$. This corresponds to a peak stress of 7820 psi assuming a uniaxial stress field with an elastic modulus of 17 million psi. As can be seen from the plot of Figure 2.5-1 the peak stress is shown as 1700 psi due to a 5 lb half sine pulse friction force. To generate a similar response at 7820 psi would require a peak friction force of 23 pounds. This magnitude seems entirely reasonable from a physical standpoint and could easily be generated in the test setup or in actual SSME operation. Therefore, given the proper friction force, the model adequately predicts rub-induced stresses.

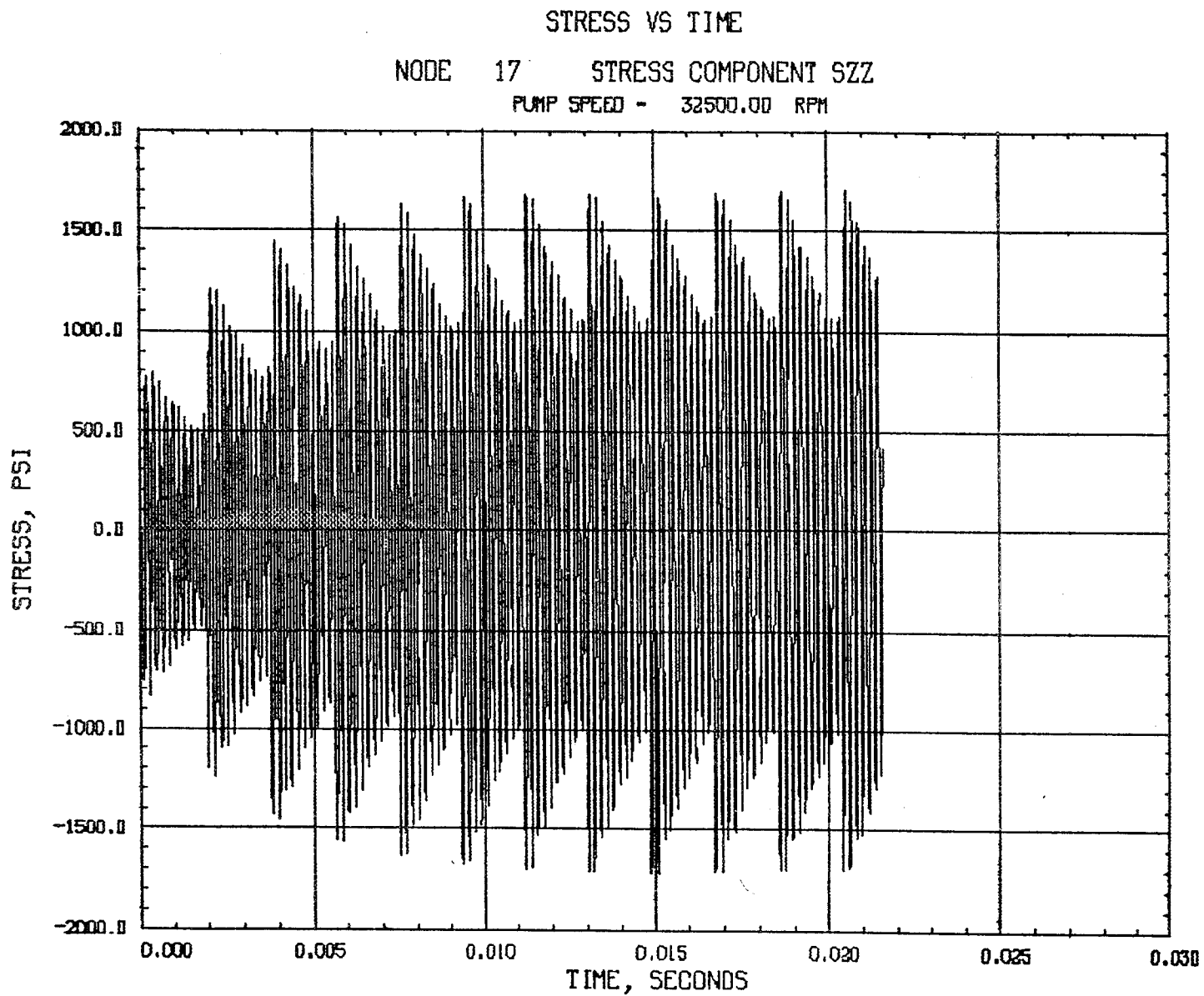


Figure 2.5-1
Stress Time-History Prediction
5 lb Peak Half-Sine Pulse

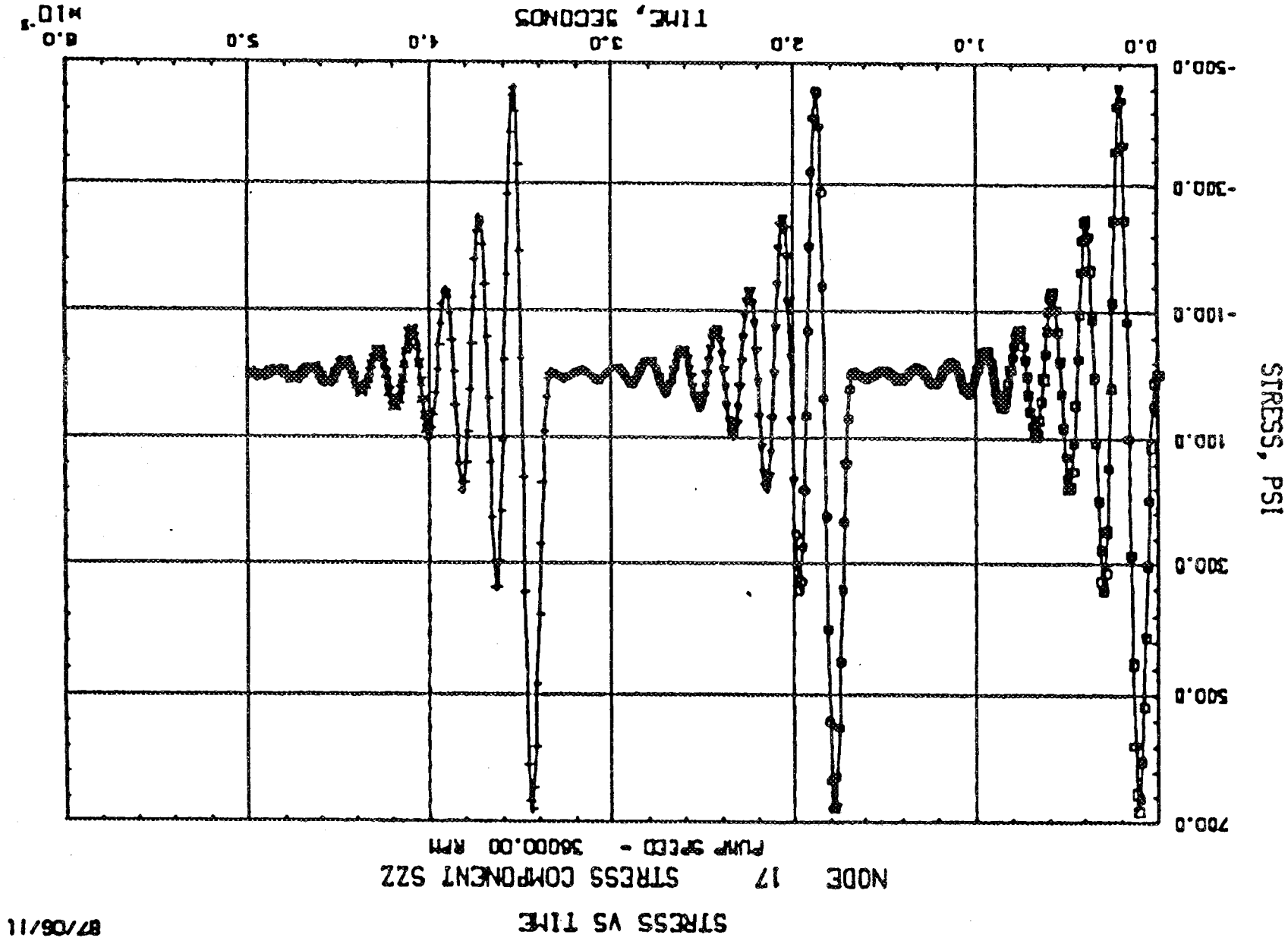


Figure 2.5-2
Stress Time-History Prediction
Typical Response During Several Rub Cycles

3.0 CONCLUSIONS AND RECOMMENDATIONS

3.1 CONCLUSIONS

The test and analysis results and presented herein support the following conclusions concerning blade tip rubbing.

1. Blade tip rubbing produces a stress time-history consisting of an initial rub-induced peak followed by a period of free vibration which decays until the next rub contact. The maximum stress in any single cycle always occurs during the initial peak.

2. The character of the free vibration portion of the rub cycle can be varied to a great extent. In some instances it is predominantly single mode vibration while in others it consists of multiple modes.

3. The frequency spectrum during rubbing consists of response at integer multiples of shaft speed as well as at the blade natural frequencies. Three of the first four blade modes were observed in the data.

4. Rub marks on the tip seal were similar to those found in SSME hardware after hot fire testing therefore the test adequately simulated SSME operation.

5. Maximum peak-to-peak strain observed during testing was 920 $\mu\text{in/in}$ which equates to a peak stress of 7820 psi. This stress level can be significant when combined with other operating stresses found in the SSME, however the period of the rub is of such short duration during a typical operational cycle that it is doubtful that much fatigue damage occurs due to this phenomenon.

6. A peak friction force of 23 pounds is necessary for the analysis and test stress amplitudes to coincide. This is entirely within the expected range of friction forces.

3.2 RECOMMENDATIONS FOR FURTHER WORK

Blade tip rubbing, in itself, has been adequately characterized by the testing and analysis presented in this report. Therefore we propose no new testing or analysis to better understand the tip rubbing phenomenon. This program has, however, resulted in the development of a new tool to

evaluate blade damping. As mentioned previously, the free vibration decay portion of the response can be used to determine blade damping. Since the blade responds in one or more natural modes of vibration during this decay the damping in each mode can be obtained by band pass filtering the signal and then using the log decrement technique. Unlike past whirligig testing where friction damper effectiveness was determined by comparison to an undamped blade, this type of testing can provide an actual modal value in percent of critical damping. In addition to providing a tool to measure the performance of friction dampers it can also serve to quantify the material damping available in integrally bladed disks (Blinks). Turbine disks of this type have been proposed as a cost cutting measure on future programs. The dynamic response characteristics of blisks are unknown at the present time and simply must be evaluated before design decisions can be made concerning their use in high energy turbomachinery.